Improving imaging and treatment of talar osteochondral defects

Kok, A.-C.

Publication date
2018
Document Version
Final published version
License
Other

[Link to publication](#)

IMPROVING IMAGING AND TREATMENT OF TALAR OSTEOCHONDRAL DEFECTS

Aimée Kok-Pigge

IMPROVING IMAGING AND TREATMENT OF TALAR OSTEOCHONDRAL DEFECTS

Aimée-Claire Kok-Pigge

Colophon

IMPROVING IMAGING AND TREATMENT OF TALAR OSTEOCHONDRAL DEFECTS

ACADEMISCH PROEFSCHRIFT

ter verkrijging van de graad van doctor
aan de Universiteit van Amsterdam
op gezag van de Rector Magnificus
prof. dr. ir. K.I.J. Maex
ten overstaan van een door het College van Promoties ingestelde commissie,
in het openbaar te verdedigen in de Agnietenkapel
op woensdag 17 januari 2018 om 14.00 uur
door Aimée-Claire Kok
geboren te Hilversum

Promotiecommissie:

Promoteres:	prof. dr. G.M.M.J. Kerkhoffs	AMC–UvA
	prof. dr. C.N. van Dijk	AMC–UvA
Co-promotor:	dr. ir. G.J.M. Tuijthof	Zuyd Hogeschool
Overige leden:	prof. dr. S.K. Bulstra	Rijksuniversiteit Groningen
	prof. dr. M. Maas	AMC–UvA
	prof. dr. C.J.F. van Noorden	AMC–UvA
	prof. dr. R.J. Oostra	AMC–UvA
	prof. dr. L.W. van Rhijn	Universiteit Maastricht
	prof. dr. D.B.F. Saris	Universiteit Utrecht

Faculteit der Geneeskunde
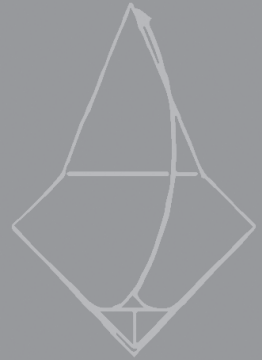
A smooth sea never made a skilful sailor

Table of contents

Chapter 1

INTRODUCTION AND OUTLINE
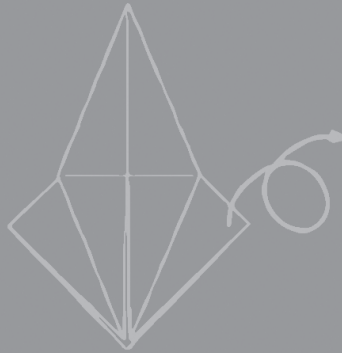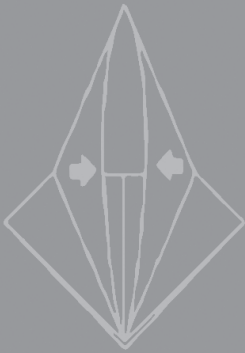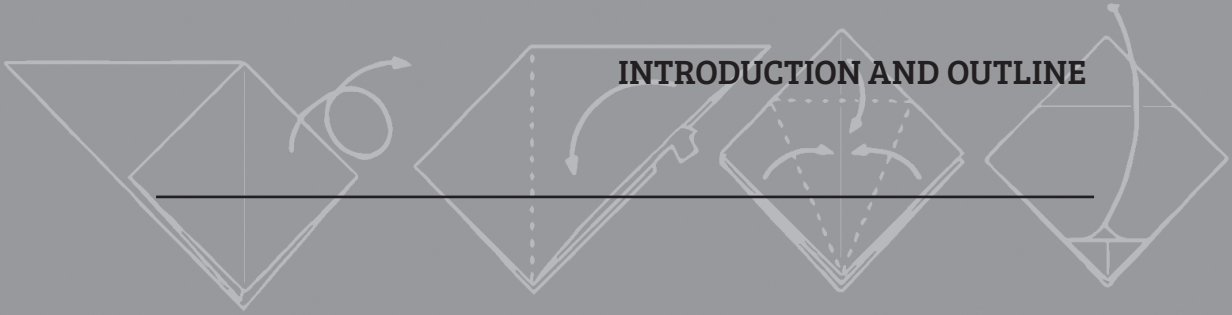
Background

An osteochondral defect is a lesion of the cartilage and the underlying subchondral bone of a joint (*Fig. 1.1*). It was first described for the ankle joint in 1922 [46], though the pathology itself has been studied in literature as early as 1738 [62].

Osteochondral defects of the talus (OCDT) are often caused by a traumatic event, such as a distortion [6] or an ankle fracture [41]. They are reported in more than 6% of the acute ankle sprains [9], up to 25% in chronic lateral ankle instability [23] and up to 50-73% of the acute ankle fractures [53, 75]. Secondary causes include degenerative disease, joint mal-alignment, metabolic abnormalities and avascular necrosis [63].

A typical OCDT patient is a 20-40 year old male reporting a traumatic event in the last year with complaints of deep ankle pain and swelling of the joint [101]. Ankle instability and locking are also often reported in literature [56]. In due time these OCDT can progress to ankle joint osteoarthritis with prolonged symptoms of pain and loss of joint function [59, 74].

The majority of the lesions in the talus involve both the superficial cartilage as well as the underlying bone [51]. Purely chondral lesions are less common. OCDT occur more often on the medial side of the talar dome where they are larger and deeper compared to their lateral counterpart [29].

Understanding difficulties in cartilage healing and repair

The ankle joint is covered by hyaline cartilage. This specific type of cartilage allows low-friction articulation and transmission of loads because of unique mechanical properties provided by a complex composition and structure (*Fig.1.2*)[80]. It is composed of chondrocytes in a dense extra-cellular matrix consisting mainly of
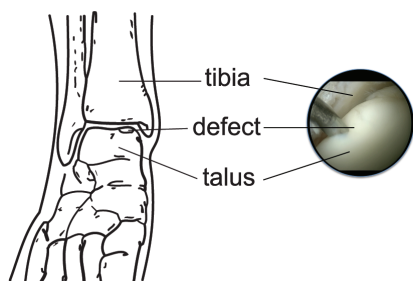
Figure 1.1. Schematic and arthroscopic image of an osteochondral defect of the medial talar dome
Damage of the cartilage layer and the underlying bone can be seen clearly on the right.

water, type II collagen and proteoglycans. Throughout the cartilage the composition and alignment of these various components is different, which creates three distinct zones: a superficial zone protecting against shear stresses, a transitional zone and a deep zone to resist major compression forces. When this structure is damaged, its complexity is not easily rebuilt which compromises the biomechanical properties.

Additionally, cartilage is an avascular tissue. It is supplied with nutrients through diffusion from the synovial fluid. This implies that, in case of cartilage damage, there is limited access to nutrients and the proliferating cells necessary for repair, such as mesenchymal stem cells [13, 77].
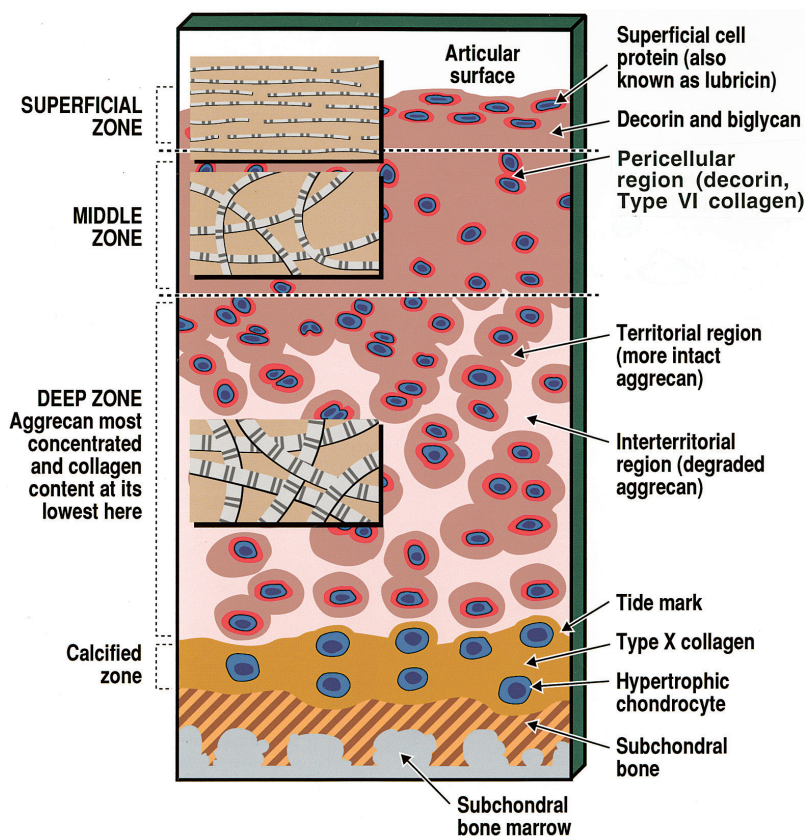
Figure 1.2. Graphic representation of the general structure of adult human articular cartilage.

It is composed of chondrocytes in a dense extra-cellular matrix consisting mainly of water, type II collagen and proteoglycans. There are three distinct zones: a superficial zone protecting against shear stresses, a transitional zone and a deep zone to resist major compression forces. The deep zone is connected to subchondral bone through a calcified layer. The insets show the differences in organization of collagen macrofibrils in the respective zones. Some special features of molecular content or properties also are indicated. *Re-printed with permission from Poole et al. (2001) [69].*

The combination of disabling complaints in an often active patient population and the limited intrinsic self-healing capacity make OCDT a challenging medical condition. Small defects show some spontaneous repair, in which the defect is covered with a fibrous like tissue. This fibrocartilage has inferior mechanical qualities due to its simpler structure and lower glycosaminoglycan content [13]. In larger defects, the repair tissue can become unstable and fails to fill the defect leading to prolonged pain, inflammatory reaction and possibly osteoarthritis.

The therapeutic challenge lies in developing strategies that either produce optimal repair tissue or near normal reconstruction of the defect using graft tissue with the aim to restore its original properties and provide pain relief. The last decade has known an exponential rise in publications on alternative treatment strategies ranging froxm various adaptions of existing techniques to entirely new treatments with tissue engineered products (*Fig. 1.3*, [21]). However, robust clinical studies showing consistent results are often lacking [56, 100]. Extensive knowledge of the cartilage repair process in vivo is essential to understand treatment outcome and optimize treatment algorithms for specific patient groups.

This thesis addresses a number of challenges in imaging, staging and treatment techniques that significantly contribute to our understanding of cartilage repair and the optimization of diagnostics and treatment of OCDT. In the next paragraphs the current practices and their specific challenges are discussed and subsequently the contents of this thesis is outlined further.
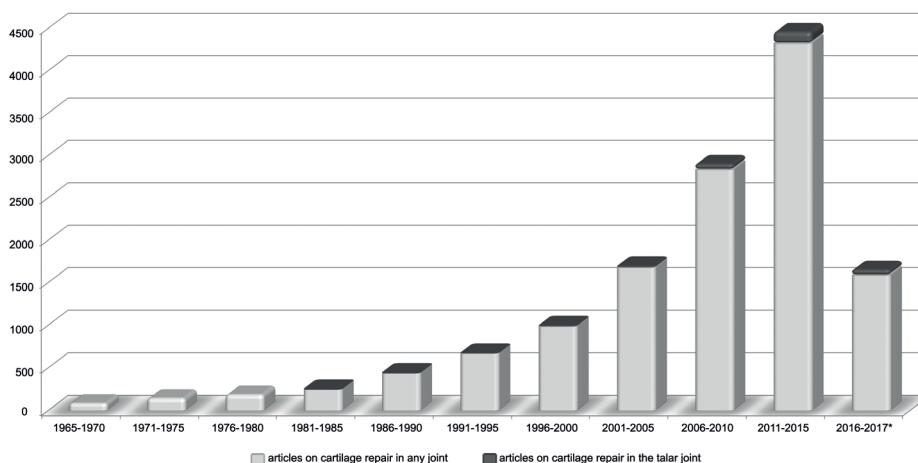
Figure 1.3. Growth in published articles on cartilage repair published (1966–2017)
*the article search for 2016-2017 was calculated from january 2016 to august 2017.
Source: PubMed and MedLine trend

Current practice in imaging patients with OCDT

The current diagnostic work-up for a patient starts with patient history and physical examination, distinguishing impingement from deep ankle pain due to an OCDT. Stability and ankle alignment are also noted. Thereafter, anteroposterior, mortise and lateral conventional radiographs of the ankle to determine the presence of an OCDT (*Fig. 1.4 A,B*)[5]. It also serves to identify both concomitant degenerative changes and the alignment of the ankle.

However, approximately 50% of OCDT are not identified on conventional radiographs and the defect size is often underestimated compared to CT [5, 92]. When a posterior defect is suspected an additional heel rise view improves detection [5, 84].

Additional imaging can provide better visualization of the dimensions and location of a lesion. In clinical practice, MRI and CT imaging are used with a good to excellent sensitivity and specificity for detecting OCDT (0.81 and 0.99 vs. 0.96 and 0.96 respectively) [5, 92]. CT and MRI image different aspects of a lesion.

Computed tomography (CT) uses three-dimensional X-ray imaging to create cross-sectional images of the ankle. Traditionally, is not able to image cartilage directly without additional intra-articular contrast [49]. It does accurately show the bony dimensions of a lesion, the integrity of the subchondral bone plate and presence of subchondral cysts (*Fig 1.4 C,D*) [55, 71]. This makes it particularly suited for lesions in the talus, which predominantly involve both cartilage and subchondral bone as compared to relative high prevalence of chondral lesions in other joints, such as the knee [51]. Also, it is argued that a painful OCDT inherently indicates bony involvement since the nerve endings are situated in the bone and not in the cartilage [24], making the subchondral bone an important structure to image. Finally, CT has been shown to be a useful pre-operative planning tool because surgeons can assess the available bone stock and plan the accessibility with an anterior arthroscopy [4].

Magnetic resonance imaging (MRI) uses a magnetic field and radio wave energy to compile cross-sectional images without radiation. MRI is suited for detecting bone bruises and gives detailed information on soft tissues, cartilage and the stability of a lesion (*Fig. 1.4 C,D,E,F*)[58]. MRI is also able to image small disruptions in the cartilage such as fissures. Traditionally, MRI does tend to overestimate the lesion size due to oedema [28]. Improvements in imaging resolution, dedicated ankle coils and additional sequences using T2- or PD-weighted fat suppression have improved these issues [3, 94]. Also, morphological features (such as integrity of the subchondral
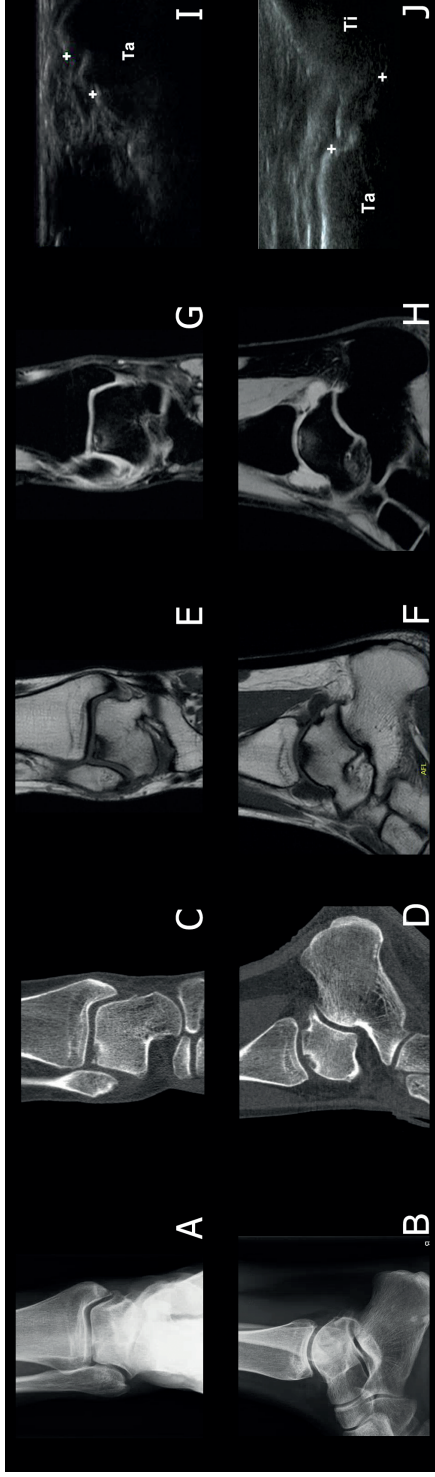
Fig.1.4. Examples from different imaging modalities for an OCDT of the lateral talar dome

Coronal views are presented in the top row and the corresponding sagittal views in the lower row. A and B: are conventional radiographs where the defect can be seen as a lytic discontinuation of the articular surface of the talar bone. C and D: CT scans showing the bony involvement of the OCDT. E and F: T1 MRI images suitable for assessment of the overlying cartilage, which can be seen as the hypodense line overlying the bone. G and H: T2 PD fat sat MRI images also showing bone oedema around the defect en between the loose fragment of the OCDT and the remaining talar bone. I and J: ultrasound views of an OCDT with the ankle full plantar flexion. The defect is marked between the two plus signs where a disruption of the talar surface can be seen. *Ta*: talus, *Ti*: tibia.

lamina or fibrillations) are more difficult to image compared to other joints because the cartilage in the ankle is very thin [76].

Imaging of longitudinal follow up of cartilage repair

To increase our understanding the effect treatments have on the repair tissue structure and cartilage quality we need to be able to meticulously monitor the repair process *in vivo* and over time.

The follow up of postoperative patients or those who are treated conservatively is routinely performed with the same modalities as discussed for diagnostics (radiographs, MRI, or CT), preferably at the lowest frequency that is clinically relevant. These modalities have several disadvantages when considering them for more extensive follow-up in research. Radiographs provide too little information, while subsequent CT scans are expensive, not primarily suited for assessing the cartilage repair tissue and generally increase the radiation burden. MRI is also an expensive and lengthy procedure. Ultrasound imaging does not have these limitations, but is not used traditionally to image bone or cartilage because of the limited penetration depth in bone. However, studies in osteoarthritis and rheumatology research have shown that ultrasound enables imaging of bone erosion and pathological changes in cartilage (*Fig1.4 D,E*) [34, 47, 64].

Another issue is that standard clinical imaging techniques study only the morphology of the repair tissue, looking at aspects such as integration into the adjacent cartilage or fibrillations and fissures. This is an indirect measure of the quality of the repair tissue. The golden standard for quality assessment is histological assessment [64], which assesses tissue composition in addition to morphology. However, histology is often reserved for *ex vivo* or animal studies due to its invasive nature.

Several experimental adaptions to CT and MRI imaging have been proposed in literature to indirectly image cartilage quality in patients. For CT this is done using intra-articular contrast [49]. For MRI, techniques such as T2 mapping or delayed gadolinium-enhanced MRI of cartilage (dGEMRIC) were developed [5]. While T2 mapping is related to water content and the reaction with collagen fibres in cartilage, dGEMRIC relies on glycosaminoglycan (GAG) content present in cartilage. Both water and GAG concentrations decrease with degeneration of cartilage. The advantage of T2 mapping over dGEMRIC and contrast CT is that it does not require intra-articular contrast and is performed in a single scanning session [36]. However, scanning times for T2 mapping are extensive and a standardized protocol is not yet available [26].

Several other advanced imaging techniques are not yet routinely applied in OCDT research. This thesis uses two of these techniques to ascertain their contribution to in-depth insight of the composition and quality of OCDT repair. The first is equilibrium partitioning of an ionizing contrast agent through a micro-CT (EPIC-micro CT). This technique using a negatively charged contrast agent, which distributes itself inversely between the negatively charged proteoglycan matrix, to estimate the GAG content of cartilage [65, 97]. By comparing attenuation ratios between healthy cartilage and repair tissue it is possible to determine the quality of cartilage repair tissue compared to healthy cartilage [98] (*Fig 8.4*). The second is Optical Coherence Tomography (OCT), which is a technique similar to ultrasound, but it uses near-infrared light to detect signs of degeneration of cartilage with good correlations to histopathology [18, 19](*Fig 3.1*). These techniques are pre-dominantly used in pre-clinical research [10, 99], cadaveric studies [18, 86] or in small clinical trials [19, 85]. Both techniques show good correlation with histology for osteoarthritis [18, 85], but have not been validated for cartilage repair tissue assessment [15, 85].

Quantifying OCDT and cartilage repair

In addition to visualization of OCDT and its repair process, measures are needed to compare treatment outcomes. This is facilitated by the use of classification systems. They can also aid in selecting the appropriate treatment for specific patients. There are multiple scoring systems available for each diagnostic technique to describe OCDT, which are briefly described in *Table 1.1*.

For postoperative imaging assessment of cartilage repair tissue using MRI and CT the presentation of results are generally mainly descriptive. Only one classification for MRI is broadly used: the Magnetic Resonance Observation of Cartilage Repair Tissue, MOCART [57]. There are two validated postoperative scores for arthroscopic assessment of repair tissue: The International Cartilage Repair Society (ICRS) cartilage repair assessment score [11] and the Oswestry arthroscopy score [79]. By contrast, there are numerous scores available for histology, five of which are validated scoring systems (*Fig. 1.5*). Recommendations have been published in an attempt to provide a guideline for the use for assessment systems [12, 42]. However, there is no true consensus on the golden standard yet [64].

Table 1.1. Frequently used classifications for OCDT grading for conventional radiographs, CT, MRI and arthroscopy.

Imaging modality	Conventional radiographs		CT		Arthroscopy		
Author/title	*Berndt and Harty (1959) [6]*	*Dore (1995) [27]*	*Ferkel (1990) [30]*	*Loomer (1993) [55]*	*Pritsch (1986) [70]*	*Cheng and Ferkel (1995) [16]*	*ICRS (2010) [38]*
Data	Biomechanical evaluation on 220 cadavers	169 talar lesions, based on three defect forms	50 lesions, adapted from Berndt and Harty	92 lesions, adapted from Berndt and Harty	24 lesions	18 lesions	Part of cartilage evaluation package. Designed for femoral lesions, but frequently used.
Stage 0		F form: Fracture					Normal cartilage
Stage I	Subchondral bone compression	Isolated fracture fragment with no modification of bone matrix, condensation of cyst	Cystic lesion	Subchondral bone compression	Intact cartilage surface	Smooth intact, but soft or ballotable cartilage	A: cartilage softening and superficial fibrillation B: superficial lacerations and fissures
Stage II	Partial separation of a fragment	O form: Osteonecrosis with sequestrum	A: Subchondral cyst with open communication with the talar dome B: Surface lesion, but non-displaced	Partial separation of a fragment	A: softening with remaining resilience B: loss of resilience / Soft overlying cartilage	Rough cartilage	Partial thickness cartilage lesions < 50% of cartilage depth

Imaging modality	Conventional radiographs	CT	Arthroscopy
	Detached, but undisplaced fragment		A: partial thickness cartilage lesions > 50% of cartilage depth B: down to calcified layer C: down to but not through the subchondral bone D: including blisters
Stage III	Underlying bone matrix comprises a radiolucent line of condensation associated with microcysts	Undisplaced fragment with lucency; Detached, but undisplaced fragment	Fibrillation or fissures; Frayed overlying cartilage
Stage IV	Displaced fragment; G form: Geode or bone cyst	Displaced fragment	Flap or exposed bone; Displaced fragment
Stage V	Radiolucent cystic aspect in body of bone with no free fragment or sequestrum	Subchondral cyst	Loose, undisplaced fragment
Stage VI			Displaced fragment

Imaging modality	MRI						
Author/ title	Dipaola (1991) [25]	Anderson (1989) [2]	Hepple (1999) [39]	University of Pittsburgh classification/ Taranow (1999) [83]	Mintz (2003) [61]	ICRS/Brittberg (2003) [12]	Griffith (2012) [35]
Data	4 talar and 6 femoral lesions	24 talar lesions	18 talar lesions	16 talar lesions Separate grading of cartilage and bone.	40 lesions Classification for MRI of the Cheng arthroscopy score	Review, adapted score for MRI from ICRS classification for arthroscopic cartilage repair. Designed for femoral lesions, but frequently used.	70 lesions Retrospective review
Stage 0					Normal cartilage	Normal cartilage	
Stage I	Thickening of articular cartilage and low signal on proton-density images	Articular cartilage damage only	Articular cartilage damage only	Subchondral impression or bone bruise	Hyperintense, but morphologically intact cartilage	A: cartilage softening and superficial fibrillation B: superficial lacerations and fissures	Bone marrow oedema or cystic change, without collapse of subchondral bone and without osteochondral junction separation
Stage II	Articular cartilage breached, low signal intensity rim behind fragment indicating fibrous attachment	Partial separation of the fragment. A: subchondral cyst	A: Cartilage injury with underlying fracture and surrounding bone oedema. B: Stage 2A without surrounding oedema	Subchondral cyst	Fibrillation or fissures, but not extending to bone	Partial thickness cartilage lesions < 50% of cartilage depth	Variable collapse of subchondral bone with osteochondral separation

Imaging modality	MRI						
Stage III	Articular cartilage breached, high signal changes behind fragment indicating synovial fluid between fragment and underlying subchondral bone	Unattached, undisplaced fragment	Detached, but undisplaced fragment	Partially separated, or detached but undisplaced fragment	Flap present or bone exposed	Partial thickness cartilage lesions > 50% of cartilage depth	Variable collapse of subchondral bone without osteochondral separation, with or without variable cartilage hypertrophy
Stage IV	Loose body	Displaced fragment	Detached and displaced fragment	Displaced fragment	Detached, but undisplaced fragment	Displaced fragment	Separation within or at edge of bone component
Stage V	Subchondral cyst formation		Displaced fragment		Displaced fragment		Complete detachment (unstable lesion)
Subgroups per stage				A: viable, intact cartilage B: breached nonviable cartilage			A: intact cartilage B: with cartilage fracture
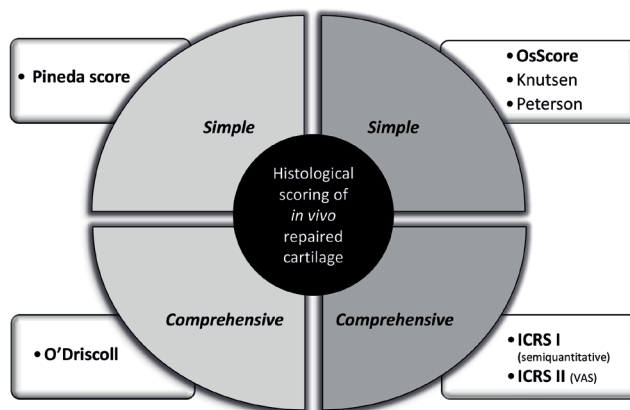
Figure 1.5. Scoring systems for histological analysis after in vivo cartilage repair
Validated scores are presented in bold. *Taken with permission from Rutgers et al. [73].*

Challenges in imaging and classification

Routine clinical imaging of OCDT is currently restricted to conventional X-ray, CT and MRI imaging. However, *in vivo* non-invasive advanced imaging techniques providing qualitative data could aid the physician in understanding treatment response. For research purposes, optimal imaging techniques for follow up and in-depth analysis are poorly defined. As noted above, there are numerous (experimental) suggestions for imaging and classification systems in literature. Many show overlapping items, but the complex nature of cartilage and cartilage repair creates just as much diversity in remaining parameters based on individual selection. Reproducible morphologic, quantitative and qualitative data is necessary that is comparable over time to explore the effect of new treatment techniques on repair. Uniform use of classification and scoring systems of the repair tissue is essential. Therefore, the challenge for clinical imaging lies in defining a minimal, non-invasive, set of useful imaging modalities and parameters that are clinically relevant, and a more extensive, ideally low-invasive, set for experimental research that include or correlate with histological quality.

Treatment patients with OCDT

Conservative treatment is generally reserved for children and patients with minor, early-onset symptoms or those who are unable or unwilling to undergo surgery [101]. Also, small, undisplaced lesions can cover spontaneously with fibrocartilage given rest [78] or cast immobilisation [8, 14, 43, 67] to unload the lesion to allow healing and prevent necrosis [101]. In literature only one retrospective study in adults exists, consisting of 26 patients, where the success rate was 62% [CI 43-78%]
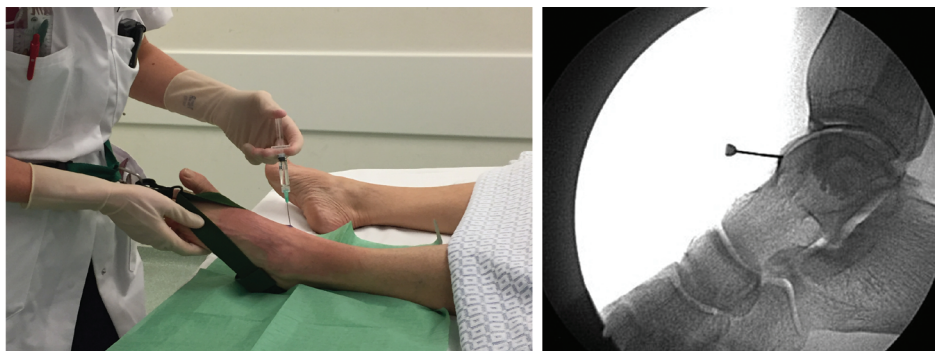
Figure 1.6. Intra-articular ankle infiltration
Left: Sterile infiltration into the joint. The use of a traction device is optional. Using a sterile band and the surgeons weight, the ankle joint can be put under traction [63]. *Right:* fluroscopy image of contrast agent being infiltrated into the ankle joint.

[78]. Available retrospective studies in children found good results in 39-92% of patients [40, 54]. Another retrospective study of 36 children in an OCDT referral centre showed that, while 86% required surgery after initial conservative treatment, the results for surgical treatment after primary conservative treatment are good [72]. It is therefore suggested that all OCDT except acute Berndt and Harty type IV lesions should be allowed a period of conservative treatment [6].

OCDT healing can be supported by intra-articular injections. Several types of injections are available, mainly hyaluronic acid ("viscosupplementation") [60], platelet rich plasma (PRP) [89], or mesenchymal stem cells [88]. The exact mechanisms of the beneficial effects are not completely clear. However, we will expand a little on the main mechanisms. Hyaluronic acid is a natural glycosaminoglycan that temporarily serves as a shock absorbing lubricant and encourages the synovium of the joint to produce more viscoelastic synovial fluid that restores the natural function of the fluid [57]. It is believed to be chondro-protective and anti-inflamatory, as well as analgesic [33, 82]. PRP promotes cartilage matrix synthesis and cell growth, while inhibiting catabolic effect [1, 31]. Both PRP and mesenchymal stem cells are thought to enhance cartilage repair by stimulating chondrogenic differentiation [1, 66].

An important, yet underappreciated, factor in treatment success with intra-articular infiltrations is the actual technique of injection. Previous literature has shown the rate of extra-articular injections is even up to 33% [7, 45]. Extra-articular placement will result in lack of efficacy while exposing the patient to possible adverse events, such as additional pain or inflammation [96]. Intra-articular placement can be verified by first injecting a contrast agent under fluoroscopy (*Fig. 1.6)*. However, this

introduces additional volume of fluid into the small joint and exposes the patient to a possible contrast-related reaction.

When non-operative treatment does not lead to satisfactory results, or when there is a symptomatic lesion with an unstable cartilage fragment, a number of surgical treatment options exist [32, 56, 91, 101]. Recent reviews for both primary and secondary defects have shown no true superior treatment for OCDT over others [21, 52]. The most predominant treatments are discussed below.

The mainstay of OCDT treatment in lesions smaller than 1.0-1.5 cm^2 is bone marrow stimulation or "microfracture" [17, 21, 32, 52, 56, 91, 101]. During an arthroscopic procedure, the subchondral bone is drilled or punctured with an arthroscopic awl to create microfracture holes [81]. The subsequent bleeding introduces mesenchymal stem cells located in the bone marrow to the defect and produces fibrocartilage. For smaller defects this can be enough to alleviate symptoms by sealing of the underlying bone and its exposed nerve endings [24]. The results of bone marrow stimulation in OCDT have been satisfactory in 61% up to 86% of the patients [20–22, 32, 52, 56, 91, 101].

In defects larger than 1,5 cm^2, the fibrocartilage layer produced by microfracture will generally be unstable and biomechanically inferior. These larger defects require techniques that are restorative, rather than reparative, aimed at regenerating stable hyaline-like type II cartilage. There are two types of restorative techniques based on their underlying strategy: introduction of harvested chondrocytes and implantation of an entirely new osteochondral unit.

Predominant techniques in the former category are autologous chondrocyte implantation, "ACI", and matrix-associated chondrocyte implantation, "MACI" [44, 95]. Success rates range from 78-93%[CI 45-98%] and 80-100% [CI 38-100%] respectively [21]. MACI has the advantage of not needing a donor site to harvest periosteal tissue to cover the defect because it uses a collagen membrane, unlike ACI. Both techniques require a two-stage treatment to harvest and replace the chondrocytes. Single step procedures include autologous matrix-induced chondrogenesis, "AMIC", in which spongiosa bone is placed in the defect and sealed with a collagen matrix [87], or autologous collagen-induced chondrogenesis, "ACIC", in which fibrin glue and a collagen matrix are used to fill the defect [93]. Success percentages range from 56-100% [CI 27-100%] [21].

Techniques implanting a new osteochondral unit predominantly include osteochondral autograft/allograft transfer system, "OATS" or "mosaicplasty" [37, 90], where osteochondral grafts are harvested and implanted into a debrided OCDT. Results show a 40-100% and 72-100% success rate respectively, with improvement on clinical outcome scores [21, 22, 56]. Disadvantages are the costs, up to 32% donor site morbidity when a graft is used, or the need for a second surgery [56].

Lastly, for lesions that are mainly subchondral with relatively intact cartilage, two additional treatments exist. Retrograde drilling aims to revascularize the subchondral bone and promote defect fill with new bone formation by non-transarticular drilling of the defect [83]. It is also an alternative for OCDT that are hard to reach using conventional arthroscopy. Success rates vary between 68% and 100 % [CI 49-100%] [21]. Secondly, a new surgical technique using a "lift, drill, fill and fix" concept stabilizes the overlying cartilage and the subchondral bone with a bioabsorbable screw after debridement of the defect[48], which preserves the hyaline cartilage and the congruency of the subchondral bone plate. Performing the procedure arthroscopically renders an arthrotomy with or without a malleolar osteotomy unnecessary [48].

Challenges in treatment

Similar to the analysis of current practice in imaging modalities, quite a large number of therapies are available. Many prognostic factors have been investigated to develop a treatment algorithm for OCDT. However, the results are often contradictory [50]. Possible explanations are the low level of evidence of the available studies [68] and the lack of consensus on diagnostic and scoring systems already mentioned earlier. However, it is also plausible that differences in operative technique execution, which is often underreported in literature, result in diversity in outcome. Or, formulated more positively: changing the technique could improve outcome.

Aim and outline of this thesis

This thesis aims to improve the chain of care for patients with OCDT. Firstly, by improving the imaging techniques to diagnose OCDT and to monitor ankle cartilage repair; secondly by optimizing currently used treatments. As mentioned throughout the introduction, the challenges are vast and large. This makes it impossible to address all issues in one thesis. Hence a number of specific issues have been selected that build on previous research and experience within our research group.

Part I: Improving pre-clinical imaging

It is imperative to have an in-depth understanding of the ankle cartilage healing process and the effects of specific interventions to cartilage tissue regeneration. The start is made in a pre-clinical research setting with establishing reliable, reproducible and representative methods to image and grade cartilage repair tissue.

An interesting question in this respect that remains to be answered is whether arthroscopic assessment of the repair tissue is related to the actual histological quality of the cartilage. This could allow intra-operative assessment without the need for a biopsy. Therefore, **Chapter 2** compares the ICRS arthroscopic cartilage repair assessment score, which is a conveniently concise scoring system, to the golden standard of histological analysis in a goat model. In **Chapter 3** we also use histology as reference, but compare it to Optical Coherence Tomography imaging to determine the usefulness of this advanced but relatively uninvasive pre-clinical imaging technique in gaining more extensive insight into the composition and quality of repair tissue of OCDT.

Part II: Improving clinical imaging

Continuing the quest to understand cartilage repair *in vivo*, the need arises to intensify clinical imaging for longitudinal monitoring at shorter intervals in time. This could provide new insights into the healing process and treatment response. As current diagnostic methods are unsuitable, we studied ultrasound imaging as a non-invasive, fast and affordable alternative. In **Chapter 4** the accuracy of ultrasound imaging of OCDT is first determined in a cadaveric study, followed by **Chapter 5**, which contains the assessment of the feasibility of using ultrasound imaging in patients with OCDT.

Part III: Optimizing treatment

While success rates of the predominant and established cartilage repair techniques are good, prognostic factors and reasons for failure are often unclear and contradictory. Descriptions of technique execution are underreported and under-investigated in literature. Critically examining the execution of these techniques could lead to a better understanding their failure and ways to adapt them for better results. **Chapter 6** presents a patient study comparing intra-articular infiltration with hyaluronic acid using a traction device to a conventional injection without traction to determine which method is more reliable.

Lastly, we study the effect of alterations in the first-line surgical therapy of bone marrow stimulation. This technique was chosen because of its wide spread popularity as a cheap, fast technique without donor site morbidity or need for two-stage surgery.

Chapter 7 contains a systematic review of the current literature on the variation in technique execution of bone marrow stimulation and whether it influences outcome. Finally, **Chapter 8** presents the results of an animal study that determined whether changing the geometry of microfracture holes influences healing of OCDT using a goat model.

References

1. Abrams GD, Frank RM, Fortier LA, Cole BJ. Platelet-rich plasma for articular cartilage repair. *Sports Med. Arthrosc*. 2013;21:213–9.

2. Anderson IF, Crichton KJ, Grattan-Smith T, Cooper RA, Brazier D. Osteochondral fractures of the dome of the talus. *J. Bone Joint Surg. Am*. 1989;71:1143–1152.

3. Barr C, Bauer JS, Malfair D, Ma B, Henning TD, Steinbach L, Link TM. MR imaging of the ankle at 3 Tesla and 1.5 Tesla: protocol optimization and application to cartilage, ligament and tendon pathology in cadaver specimens. *Eur. Radiol*. 2007;17:1518–1528.

4. Van Bergen CJ, Tuijthof GJ, Blankevoort L, Maas M, Kerkhoffs GM, Van Dijk CN. Computed tomography of the ankle in full plantar flexion: a reliable method for preoperative planning of arthroscopic access to osteochondral defects of the talus. *Arthroscopy*. 2012;28:985–992.

5. van Bergen CJ, Gerards RM, Opdam KT, Terra MP, Kerkhoffs GM. Diagnosing, planning and evaluating osteochondral ankle defects with imaging modalities. *World J. Orthop*. 2015;6:944–53.

6. Berndt A, Harty M. Transchondral fractures (osteochondritis dissecans) of the talus. *J. Bone Joint Surg. Am*. 1959;41–A:988–1020.

7. Bliddal H. Placement of intra-articular injections verified by mini air-arthrography. *Ann. Rheum. Dis.* 1999;58:641–643.

8. Blom JM, Strijk SP. Lesions of the trochlea tali. Osteochondral fractures and osteochondritis dissecans of the trochlea tali. *Radiol. Clin*. 1975;44:387–396.

9. Bosien WR, Staples OS RS. Residual disability following acute ankle sprains. *Bone Jt. Surg Am*. 1955;37:1237–1243.

10. Bouxsein ML, Boyd SK, Christiansen BA, Guldberg RE, Jepsen KJ, Müller R. Guidelines for assessment of bone microstructure in rodents using micro-computed tomography. *J. Bone Miner. Res.* 2010;25:1468–1486.

11. Brittberg M, Peterson L. Introduction of an articular cartilage classification. *ICRS Newsl.* 1998:5–8.

12. Brittberg M, Winalski CS. Evaluation of cartilage injuries and repair. *J Bone Jt. Surg Am*. 2003;85–A Suppl:58–69.

13. Buckwalter JA. Articular cartilage: injuries and potential for healing. *J Orthop Sport. Phys Ther*. 1998;28:192–202.

14. Canale ST, Belding RH. Osteochondral lesions of the talus. *J. Bone Joint Surg. Am*. 1980;62:97–102.

15. Cernohorsky P, Kok AC, Bruin DM de, Brandt MJ, Faber DJ, Tuijthof GJ, Kerkhoffs GM, Strackee SD, van Leeuwen TG. Comparison of optical coherence tomography and histopathology in quantitative assessment of goat talus articular cartilage. *Acta Orthop*. 2015;86:257–263.

16. Cheng M, Ferkel R, Applegate G. Osteochondral lesions of the talus: a radiologic and surgical comparison. In: *Oral presentation presented at: Annual Meeting of the American Academy of Orthopaedic Surgeons, New Orleans, LA*.

17. Choi WJ, Park KK, Kim BS, Lee JW. Osteochondral lesion of the talus: is there a critical defect size for poor outcome? *Am J Sport. Med*. 2009;37:1974–1980.

18. Chu CR. Arthroscopic Microscopy of Articular Cartilage Using Optical Coherence Tomography. *Am. J. Sports Med*. 2004;32:699–709.

19. Chu CR, Williams A, Tolliver D, Kwoh CK, Bruno 3rd S, Irrgang JJ. Clinical optical coherence tomography of early articular cartilage degeneration in patients with degenerative meniscal tears. *Arthritis Rheumatol*. 2010;62:1412–1420.

20. Chuckpaiwong B, Berkson EM, Theodore GH. Microfracture for Osteochondral Lesions of the Ankle: Outcome Analysis and Outcome Predictors of 105 Cases. *Arthroscopy*. 2008;24:106–112.

21. Dahmen J, Lambers KT, Reilingh ML, Bergen CJ Van. No superior treatment for primary osteochondral defects of the talus. *Knee Surgery, Sport. Traumatol. Arthrosc.* 2017.

22. Dekker TJ, Dekker PK, Tainter DM, Easley ME, Adams SB. Treatment of Osteochondral Lesions of the Talus: A Critical Analysis Review. *JBJS Rev.* 2017;5.

23. DIGiovanni BF, Fraga CJ, Cohen BE, Shereff MJ. Associated injuries found in chronic lateral ankle instability. *Foot ankle Int.* 2000;21:809–15.

24. van Dijk CN, Reilingh ML, Zengerink M, van Bergen CJ. Osteochondral defects in the ankle: Why painful? *Knee Surgery, Sport. Traumatol. Arthrosc.* 2010;18:570–580.

25. Dipaola JD, Nelson DW, Colville MR. Characterizing osteochondral lesions by magnetic resonance imaging. *Arthroscopy*. 1991;7:101–104.

26. Domayer SE, Apprich S, Stelzeneder D, Hirschfeld C, Sokolowski M, Kronnerwetter C, Chiari C, Windhager R, Trattnig S. Cartilage repair of the ankle: first results of T2 mapping at 7.0 T after microfracture and matrix associated autologous cartilage transplantation. *Osteoarthr. Cartil.* 2012;20:829–836.

27. Dore J, Rosset P. Lésions ostéochondrales du dôme astragalien. Étude multicentrique de 169 cas. *Ann Orthop Ouest*. 1995;27:146–91.

28. Elias I, Jung JW, Raikin SM, Schweitzer MW, Carrino JA, Morrison WB. Osteochondral lesions of the talus: change in MRI findings over time in talar lesions without operative intervention and implications for staging systems. *Foot Ankle Int*. 2006;27:157–166.

29. Elias I, Zoga AC, Morrison WB, Besser MP, Schweitzer ME, Raikin SM. Osteochondral lesions of the talus: localization and morphologic data from 424 patients using a novel anatomical grid scheme. *Foot Ankle Int*. 2007;28:154–161.

30. Ferkel R, Sgaglione N, Del Pizzo W. Arthroscopic treatment of osteochondral lesions of the talus: technique and results. *Orthop Trans.* 1990;14:172–173.

31. Fortier LA, Barker JU, Strauss EJ, McCarrel TM, Cole BJ. The role of growth factors in cartilage repair. In: *Clinical Orthopaedics and Related Research*.Vol 469.; 2011:2706–2715.

32. Giannini S, Vannini F. Operative treatment of osteochondral lesions of the talar dome: current concepts review. *Foot Ankle Int*. 2004;25:168–175.

33. Gormeli G, Karakaplan M, Gormeli CA, Sarikaya B, Elmali N, Ersoy Y. Clinical Effects of Platelet-Rich Plasma and Hyaluronic Acid as an Additional Therapy for Talar Osteochondral Lesions Treated with Microfracture Surgery: A Prospective Randomized Clinical Trial. *Foot ankle Int*. 2015;36:891–900.

34. Grassi W, Lamanna G, Farina A, Cervini C. Sonographic imaging of normal and osteoarthritic cartilage. *Semin Arthritis Rheum*. 1999;6:398–403.

35. Griffith JF, Yi Lau DT, Wai Yeung DK, Nar Wong MW. High-resolution MR imaging of talar osteochondral lesions with new classification. *Skeletal Radiol.* 2012;41:387–399.

36. Guermazi A, Alizai H, Crema MD, Trattnig S, Regatte RR, Roemer FW. Compositional MRI techniques for evaluation of cartilage degeneration in osteoarthritis. *Osteoarthr. Cartil.* 2015;23:1639–1653.

37. Hangody L, Kish G, Kárpáti Z, Szerb I, Udvarhelyi I, Modis L, Szerb I, Gaspar L, Dioszegi Z, Kendik Z. Mosaicplasty for the treatment of osteochondritis dissecans of the talus: two to seven year results in 36 patients. *Foot Ankle Int*. 2001;22:552–558.

38. Hauselmann HJ, Jakob RP, Levine D. ICRS Cartilage Injury Evaluation Package. *ICRS Cartil. Inj. Eval. Packag.* 2000:1–16.

39. Hepple S, Winson IG, Glew D. Osteochondral lesions of the talus: a revised classification. *Foot Ankle Int*. 1999;20:789–93.

40. Higuera J, Laguna R, Peral M, Aranda E, Soleto J. Osteochondritis dissecans of the talus during childhood and adolescence. *J. Pediatr. Orthop*. 1998;18:328–332.

41. Hintermann B, Regazzoni P, Lampert C, Stutz G, Gächter a. Arthroscopic findings in acute fractures of the ankle. *J. Bone Joint Surg. Br*. 2000;82:345–351.

42. Hurtig MB, Buschmann MD, Fortier LA, Hoemann CD, Hunziker EB, Jurvelin JS, Mcilwraith CW, Sah RL, Whiteside RA. Preclinical Studies for Cartilage Repair : Recommendations from the. 2012.

43. Huylebroek JF, Martens M, Simon JP. Transchondral talar dome fracture. *Arch. Orthop. Trauma. Surg*. 1985;104:238–241.

44. Johnson B, Lever C, Roberts S, Richardson J, McCarthy H, Harrison P, Laing P, Makwana N. Cell cultured chondrocyte implantation and scaffold techniques for osteochondral talar lesions. *Foot Ankle Clin*. 2013;18:135–150.

45. Jones A, Regan M, Ledingham J, Pattrick M, Manhire A, Doherty M. Importance of placement of intra-articular steroid injections. *BMJ*. 1993;307:1329–30.

46. Kappis M. Weitere beitrage zur traumatisch-mechanischen entstehung der spontanen knorpelablosüngen. *Deustche Zeitschler F Chir, 1922(171) p13-29*. 1922;171:13–29.

47. Keen HI, Conaghan PG. Usefulness of ultrasound in osteoarthritis. *Rheum Dis Clin North Am*. 2009;35:503–519.

48. Kerkhoffs GM, Reilingh ML, Gerards RM, de Leeuw PAJ. Lift, drill, fill and fix (LDFF): a new arthroscopic treatment for talar osteochondral defects. *Knee Surgery, Sport. Traumatol. Arthrosc*. 2016;24:1265–1271.

49. Kirschke JS, Braun S, Baum T, Holwein C, Schaeffeler C, Imhoff AB, Rummeny EJ, Woertler K, Jungmann PM. Diagnostic Value of CT Arthrography for Evaluation of Osteochondral Lesions at the Ankle. *Biomed Res. Int*. 2016;2016:3594253.

50. Kok AC, Dunnen S den, Tuijthof GJ, van Dijk CN, Kerkhoffs GM. Is Technique Performance a Prognostic Factor in Bone Marrow Stimulation of the Talus? *J. Foot Ankle Surg*. 2012;51:777–782.

51. Körner D, Gueorguiev B, Niemeyer P, Bangert Y, Zinser W, Aurich M, Walther M, Becher C, Ateschrang A, Schröter S. Parameters influencing complaints and joint function in patients with osteochondral lesions of the ankle—an investigation based on data from the German Cartilage Registry (KnorpelRegister DGOU). *Arch. Orthop. Trauma Surg*. 2017;137:367–373.

52. Lambers KT, Dahmen J, Reilingh ML, Bergen CJ Van. No superior surgical treatment for secondary osteochondral defects of the talus. *Knee Surgery, Sport. Traumatol. Arthrosc*. 2017.

53. Leontaritis N, Hinojosa L, Panchbhavi VK. Arthroscopically detected intra-articular lesions associated with acute ankle fractures. *J. Bone Joint Surg. Am*. 2009;91:333–9.

54. Letts M, Davidson D, Ahmer A. Osteochondritis dissecans of the talus in children. *J. Pediatr. Orthop*. 2003;23:617–625.

55. Loomer R, Fisher C, Lloyd-Smith R, Sisler J, Cooney T. Osteochondral lesions of the talus. *Am J Sport. Med*. 1993;21:13–19.

56. Looze CA, Capo J, Ryan MK, Begly JP, Chapman C, Swanson D, Singh BC, Strauss EJ. Evaluation and Management of Osteochondral Lesions of the Talus. *Cartilage*. 2017;8:19–30.

57. Marlovits S, Singer P, Zeller P, Mandl I, Haller J, Trattnig S. Magnetic resonance observation of cartilage repair tissue (MOCART) for the evaluation of autologous chondrocyte transplantation: Determination of interobserver variability and correlation to clinical outcome after 2 years. *Eur. J. Radiol*. 2006;57:16–23.

58. Marlovits S, Striessnig G, Resinger CT, Aldrian SM, Vecsei V, Imhof H, Trattnig S. Definition of perti-nent parameters for the evaluation of articular cartilage repair tissue with high-resolution magnetic resonance imaging. *Eur. J. Radiol.* 2004;52:310–319.

59. McCullough CJ, Venugopal V. Osteochondritis dissecans of the talus: the natural history. *Clin. Orthop. Relat. Res.* 1979:264–8.

60. Mei-Dan O, Maoz G, Swartzon M, Onel E, Kish B, Nyska M, Mann G. Treatment of osteochon-dritis dissecans of the ankle with hyaluronic acid injections: a prospective study. *Foot ankle Int.* 2008;29:1171–1178.

61. Mintz DN, Tashjian GS, Connell DA, Deland JT, O'Malley M, Potter HG. Osteochondral lesions of the talus: A new magnetic resonance grading system with arthroscopic correlation. *Arthroscopy.* 2003;19:353–359.

62. Monroe A. Part of the cartilage of the joint, separated and ossified. *Med. essays Obs.* 1738;IV:19.

63. O'Loughlin PF, Heyworth BE, Kennedy JG, Loughlin PF, Heyworth BE, Kennedy JG, Loughlin PF, Heyworth BE. Current concepts in the diagnosis and treatment of osteochondral lesions of the ankle. *Am. J. Sports Med.* 2010;38:392–404.

64. Orth P, Peifer C, Goebel L, Cucchiarini M, Madry H. Comprehensive analysis of translational osteo-chondral repair: Focus on the histological assessment. *Prog. Histochem. Cytochem.* 2015;50:19–36.

65. Palmer AW, Guldberg RE, Levenston ME. Analysis of cartilage matrix fixed charge density and three-dimensional morphology via contrast-enhanced microcomputed tomography. *Proc Natl Acad Sci U S A.* 2006;103:19255–19260.

66. Pelttari K, Steck E, Richter W. The use of mesenchymal stem cells for chondrogenesis. *Injury.* 2008;39:58–65.

67. Pettine KA, Morrey BF. Osteochondral fractures of the talus. A long-term follow-up. *J. Bone Joint Surg. Br.* 1987;69:89–92.

68. Pinski JM, Boakye LA, Murawski CD, Hannon CP, Ross KA, Kennedy JG. Low Level of Evidence and Methodologic Quality of Clinical Outcome Studies on Cartilage Repair of the Ankle. *Arthroscopy.* 2016;32:214–222.

69. Poole AR, Kojima T, Yasuda T, Mwale F, Kobayashi M, Laverty S. Composition and structure of articular cartilage: a template for tissue repair. *Clin. Orthop. Relat. Res.* 2001;1:S26–S33.

70. Pritsch M, Horoshovski H, Farine I. Arthroscopic treatment of osteochondral lesions of the talus. *J. Bone Joint Surg. Am.* 1986;68:862–865.

71. Reilingh ML, van Bergen CJ, Blankevoort L, Gerards RM, van Eekeren ICM, Kerkhoffs GM, van Dijk CN. Computed tomography analysis of osteochondral defects of the talus after arthroscopic debridement and microfracture. *Knee Surgery, Sport. Traumatol. Arthrosc.* 2016;24:1286–1292.

72. Reilingh ML, Kerkhoffs GM, Telkamp CJ, Struijs PA, van Dijk CN. Treatment of osteochondral defects of the talus in children. *Knee Surg. Sports Traumatol. Arthrosc.* 2014;22:2243–2249.

73. Rutgers M, van Pelt MJP, Dhert WJ, Creemers LB, Saris DB. Evaluation of histological scoring systems for tissue-engineered, repaired and osteoarthritic cartilage. *Osteoarthr. Cartil.* 2010;18:12–23.

74. Saltzman CL, Salamon ML, Blanchard GM, Huff T, Hayes A, Buckwalter JA, Amendola A. Epidemiol-ogy of ankle arthritis: report of a consecutive series of 639 patients from a tertiary orthopaedic center. *Iowa Orthop J.* 2005;25:44–46.

75. Saxena A, Eakin C. Articular talar injuries in athletes: results of microfracture and autogenous bone graft. *Am J Sport. Med.* 2007;35:1680–1687.

76. Schreiner MM, Mlynarik V, Zbyn S, Szomolanyi P, Apprich S, Windhager R, Trattnig S. New Technol-ogy in Imaging Cartilage of the Ankle. *Cartilage.* 2017;8:31–41.

77. Shapiro F, Koide S, Glimcher MJ. Cell origin and differentiation in the repair of full-thickness defects of articular cartilage. *J Bone Jt. Surg Am*. 1993;75:532–553.

78. Shearer C, Loomer R, Clement D. Nonoperatively managed stage 5 osteochondral talar lesions. *Foot Ankle Int*. 2002;23:651–654.

79. Smith GD, Taylor J, Almqvist KF, Erggelet C, Knutsen G, Garcia Portabella M, Smith T, Richardson JB, Portabella MG, Smith T, Richardson JB. Arthroscopic assessment of cartilage repair: a validation study of 2 scoring systems. *Arthroscopy*. 2005;21:1462–1467.

80. Sophia Fox AJ, Bedi A, Rodeo SA. The basic science of articular cartilage: structure, composition, and function. *Sports Health*. 2009;1:461–468.

81. Steadman JR, Rodkey WG, Rodrigo JJ. Microfracture: surgical technique and rehabilitation to treat chondral defects. *Clin Orthop Relat Res*. 2001:S362-9.

82. Strauss E, Schachter A, Frenkel S, Rosen J. The efficacy of intra-articular hyaluronan injection after the microfracture technique for the treatment of articular cartilage lesions. *Am. J. Sports Med*. 2009;37:720–726.

83. Taranow WS, Bisignani G a, Towers JD, Conti SF. Retrograde drilling of osteochondral lesions of the medial talar dome. *Foot ankle Int*. 1999;20:474–480.

84. Thompson JP, Loomer RL. Osteochondral lesions of the talus in a sports medicine clinic. A new radiographic technique and surgical approach. *Am. J. Sports Med*. 1984;12:460–463.

85. van Tiel J, Siebelt M, Reijman M, Bos PK, Waarsing JH, Zuurmond AM, Nasserinejad K, van Osch GJVM, Verhaar JAN, Krestin GP, Weinans H, Oei EHG. Quantitative in vivo CT arthrography of the human osteoarthritic knee to estimate cartilage sulphated glycosaminoglycan content: Correlation with ex-vivo reference standards. *Osteoarthr. Cartil*. 2016;24:1012–1020.

86. Van Tiel J, Siebelt M, Waarsing JH, Piscaer TM, Van Straten M, Booij R, Dijkshoorn ML, Kleinrensink GJ, Verhaar JAN, Krestin GP, Weinans H, Oei EHG. CT arthrography of the human knee to measure cartilage quality with low radiation dose. *Osteoarthr. Cartil*. 2012;20:678–685.

87. Valderrabano V, Miska M, Leumann A, Wiewiorski M. Reconstruction of osteochondral lesions of the talus with autologous spongiosa grafts and autologous matrix-induced chondrogenesis. *Am. J. Sports Med*. 2013;41:519–527.

88. Vannini F, Cavallo M, Ramponi L, Castagnini F, Massimi S, Giannini S, Buda RE. Return to Sports After Bone Marrow-Derived Cell Transplantation for Osteochondral Lesions of the Talus. *Cartilage*. 2017;8:80–87.

89. Vannini F, Di Matteo B, Filardo G. Platelet-rich plasma to treat ankle cartilage pathology - from translational potential to clinical evidence: a systematic review. *J. Exp. Orthop*. 2015;2:2.

90. VanTienderen RJ, Dunn JC, Kusnezov N, Orr JD. Osteochondral Allograft Transfer for Treatment of Osteochondral Lesions of the Talus: A Systematic Review. *Arthroscopy*. 2017;33:217–222.

91. Verhagen R a, Struijs P a, Bossuyt PM, van Dijk CN. Systematic review of treatment strategies for osteochondral defects of the talar dome. *Foot Ankle Clin*. 2003;8:233–42, viii–ix.

92. Verhagen RA, Maas M, Dijkgraaf MG, Tol JL, Krips R, van Dijk CN. Prospective study on diagnostic strategies in osteochondral lesions of the talus. Is MRI superior to helical CT? *J Bone Jt. Surg Br*. 2005;87:41–46.

93. Volpi P, Bait C, Quaglia A, Redaelli A, Prospero E, Cervellin M, Stanco D, de Girolamo L. Autologous collagen-induced chondrogenesis technique (ACIC) for the treatment of chondral lesions of the talus. *Knee Surg. Sports Traumatol. Arthrosc*. 2014;22:1320–1326.

94. Weber MA, Wunnemann F, Jungmann PM, Kuni B, Rehnitz C. Modern Cartilage Imaging of the Ankle. *Rofo*. 2017.

95. Wiewiorski M, Barg A, Valderrabano V. Autologous matrix-induced chondrogenesis in osteochondral lesions of the talus. *Foot Ankle Clin.* 2013;18:151–158.

96. Witteveen AGH, Giannini S, Guido G, Jerosch J, Lohrer H, Vannini F, Donati L, Schulz A, Scholl J, Sierevelt IN, van Dijk CN. A prospective multi-centre, open study of the safety and efficacy of hylan G-F 20 (Synvisc®) in patients with symptomatic ankle (talo-crural) osteoarthritis. *Foot Ankle Surg.* 2008;14:145–152.

97. Xie L, Lin AS, Levenston ME, Guldberg RE. Quantitative assessment of articular cartilage morphology via EPIC-microCT. *Osteoarthr. Cartil.* 2009;17:313–320.

98. Xie L, Lin ASP, Guldberg RE, Levenston ME. Nondestructive assessment of sGAG content and distribution in normal and degraded rat articular cartilage via EPIC-??CT. *Osteoarthr. Cartil.* 2010;18:65–72.

99. Xie T, Guo S, Zhang J, Chen Z, Peavy GM. Determination of characteristics of degenerative joint disease using optical coherence tomography and polarization sensitive optical coherence tomography. *Lasers Surg. Med.* 2006;38:852–865.

100. Yasui Y, Wollstein A, Murawski CD, Kennedy JG. Operative Treatment for Osteochondral Lesions of the Talus: Biologics and Scaffold-Based Therapy. *Cartilage.* 2017;8:42–49.

101. Zengerink M, Struijs PA, Tol JL, van Dijk CN. Treatment of osteochondral lesions of the talus: a systematic review. *Knee Surgery, Sport. Traumatol. Arthrosc.* 2010;18:238–246.
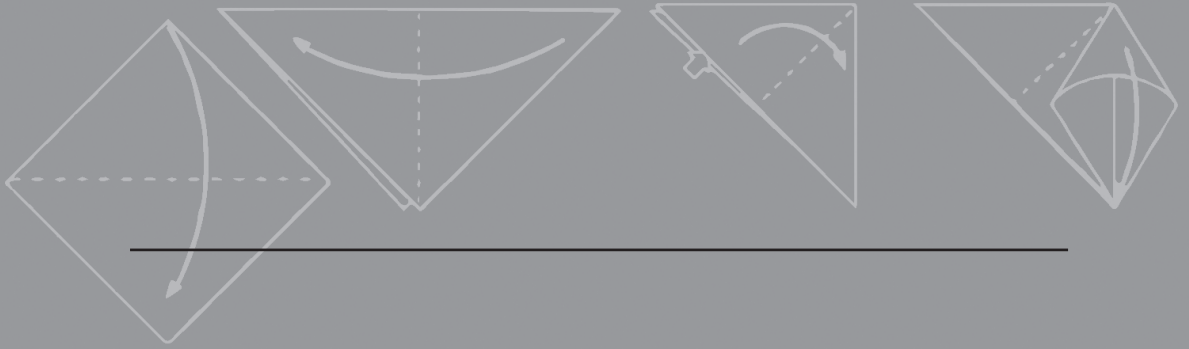
PART I

IMPROVING PRE-CLINICAL IMAGING
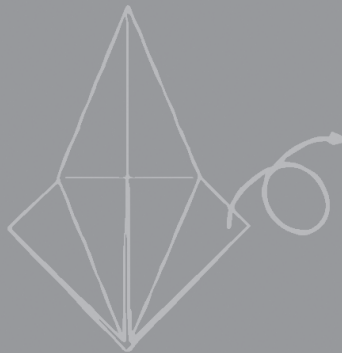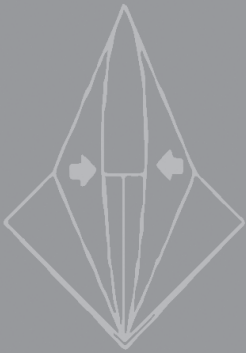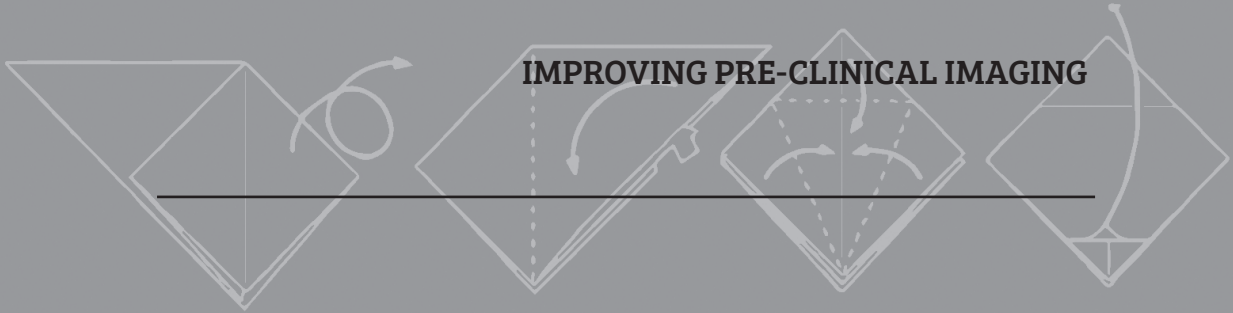
CHAPTER 2

Macroscopic ICRS Poorly Correlates with O'Driscoll Histological Cartilage Repair Assessment in a Goat Model

Aimée C. Kok
Christiaan J. van Bergen
Gabrielle J. M. Tuijthof
Mark N. Klinkenbijl
Cornelis J.F. van Noorden
C. Niek van Dijk
Gino M. M. J. Kerkhoffs
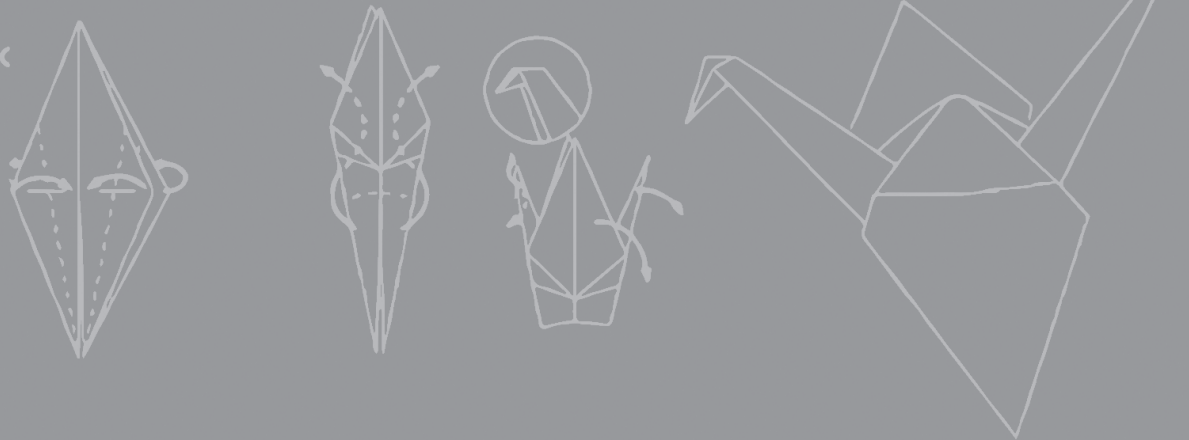
ABSTRACT

Background
The purpose of this research was to evaluate whether the macroscopic assessment of repair cartilage quality of talar osteochondral defects in a goat model using the ICRS score is in correspondence with histological assessment using the O'Driscoll histology score.

Materials and methods
32 caprine samples with 6 mm osteochondral defects treated with microfracture were analysed six months postoperatively using high-resolution digital images. Two observers independently scored the defects using the ICRS (0-12 points). Histological analysis was performed by one expert histologist using the O'Driscoll Score (0-24 points) on 5 µm slices stained with Masson Goldner and Safranin O. Total ICRS and O'Driscoll scores as well as sub items were compared using a Spearman correlation coefficient (p<0.05).

Results
The median ICRS for Observer 1 and 2 were 6.5 (range: 4-11) and 6.5 (range: 3-11). The median O'Driscoll score was 11.5 (range: 3-20). The correlation of the total ICRS scores and the O'Driscoll score was not significant, nor was the correlation of sub items (p>0.05).

Conclusion
This animal study suggests that isolated macroscopic ICRS assessment of cartilage repair tissue does not correlate well with histological assessment. Possible explanations may be limitations of surface assessment compared to analysis deeper into the tissue and the necessity of more elaborate macroscopic assessment including hypertrophy, colour, lesion size, location and degenerative status of the joint. Techniques that are more accurate, precise and reliable, such as histology, dGEMERIC and T2 mapping MRI, contrast enhanced CT or optical coherence tomography (OCT), should be considered as alternatives or at least as complimentary methods.

Introduction

Histological evaluation of cartilage repair tissue of after treatment of osteochondral defects is a longstanding and proven method for quality assessment with both qualitative and quantitative parameters [20]. Experimental animal studies often use histological analysis of the repair tissue after sacrifice of the animals [2, 6, 12, 14, 20, 21, 27, 33, 36]. In the case of clinical studies, a biopsy can be taken for histology [1, 16, 18]. Even though considered to be the gold standard, biopsies are usually not performed in a clinical setting because it destroys part of the repair tissue. In addition, the histological processing and subsequent analyses take time. This makes surgical intervention in 1 session with the assessment of the quality of repair based on the biopsy results not possible, necessitating a two-step procedure. Moreover, biopsies can only show the characteristics of that particular part of the lesion of which the biopsy was taken. Locational differences within the repair area are not detected. Furthermore, the quality of biopsy and the moment in follow-up of the acquisition affect the quality and result of the biopsy [10]. Therefore, histology of in vivo repaired tissue is generally restricted to a research setting, while in clinical practice, cartilage quality is assessed through imaging and intraoperative macroscopic evaluation by the surgeon [28].

Macroscopic assessment of the repair tissue during (second look) arthroscopy is used to assess the degree of defect fill, the aspect of repair tissue as well as its integration with adjacent cartilage after treatment [9]. It has shown to be associated with the clinical failure rate [22]. There are two validated grading systems in the literature that assess repair tissue quality during arthroscopy or open surgery, the Oswestry Arthroscopy Score (OAS) [34] and the International Cartilage Repair Society Cartilage Repair Assessment System (ICRS) [8]. Main components of both scores are the nature of the tissue (macroscopic appearance of the cartilage surface) and whether the repair tissue is satisfactory (the extent to which the original defect is filled with repair tissue and the integration of the repair tissue into the border zone). Both scores are used in the evaluation of human as well as animal repair tissue [26, 27, 30]. Other studies have reported satisfactory interobserver reliability and repeatability for both the ICRS and the OAS arthroscopic score with an ICC>0.7 and good correlation (Pearson's correlation coefficient, r=0.88; P<0.001). Cronbach's alpha was slightly better for the ICRS: 0.91 vs. 0.82 for the OAS [7, 34].

There is no data that compares the macroscopic scores and findings from the histological quality assessment scores. Therefore, it is unknown to which extent these macroscopic scores correlate with the histological reference standard. A good correlation would strengthen diagnosis and evaluation based on arthroscopic assessment

instead of histology, whereas a poor correlation would indicate that the score is insufficient for objective cartilage repair tissue assessment. The aim of this study was to evaluate the correlation of the macroscopic ICRS score to a histological score of repaired cartilage. The hypothesis was that the ICRS corresponds moderately with histological analysis, because the ICRS evaluates the surface of osteochondral defects whereas histology also assesses deeper tissue layers.

Materials and methods

Materials

32 caprine samples of treated osteochondral defects treated were analysed six months postoperatively. The samples were retrieved from a study investigating the healing response of artificially created talar osteochondral defects of sixteen goats treated with microfracture [23]. The study protocol was approved by the local Animal Welfare Committee (protocol number ORCA102287). A 6 mm diameter osteochondral defect was drilled in the tali of both hind legs using a posterolateral surgical approach. In the same surgical session, the goats received microfracture treatment using microfracture awls. The animals were allowed to directly bear weight postoperatively. The goats were sacrificed after a follow-up of 24 weeks, after which the tali were extracted and photographed in multiple directions using a high resolution digital camera (Panasonic Lumix, Kadoma, Japan).

The tali were cut into 20 mm × 20 mm blocks around the defect over the entire depth of the talus. The samples were embedded in Methylmetacrylate and 5 μm sections were cut at approximately a quarter and at the centre of each defect. Haematoxylin and Eosin (general staining), Safranin-O (GAG content) and Masson Goldner (Collagen) staining were performed on multiple sections for each location. Representative slices of both locations were selected for cartilage quality assessment. Macroscopic scoring: The photographs of the samples were collected, blinded and randomized using a computer program. Two orthopaedic surgeons skilled in ankle arthroscopy (GK,MK) scored the high-resolution photographs individually using the ICRS score. The ICRS score consists of three items: degree of defect repair, integration of the border zone and macroscopic appearance that are each scored 0 to 4 (Table 1). The total score (ranging from 0-12) is categorized in 1 of 4 grades (normal, nearly normal, abnormal and severely abnormal) [8].

Histologic scoring

Thirty histological sections were available per sample. All were scanned for quality of processing and staining. Selected histological sections were scored by one expert histologist (RvN) using the O'Driscoll histology score [31]. A recent review provides an overview of the existing histological scoring systems [14]. Both the O'Driscoll score [31] and the Pineda score [32] met our requirements of applicability for the assessment of cartilage repair and available validation for animal studies [29]. The O'Driscoll score was used because of its extensiveness. The score by O'Driscoll contains 4 main categories and sub items, which gives a total score of a maximum of 24 points [31].

Statistical analysis

To test our hypothesis, the validity of the ICRS was determined by calculating the interobserver variability and the correlation between the O'Driscoll score and the ICRS. A sample size of 32 had 80% power to detect a minimum level of correlation of 0.4 (moderate correlation based on the definition of Landis and Koch [25]) with a 0.05 two-sided significance. A correlation above 0.4 was considered to be of possible significance, since both Landis c.s. and Fleiss c.s. define a correlation below 0.4 as only poor to fair [15, 25]. For the ICRS to be a reliable tool for cartilage repair assessment a less than moderate correlation coefficient is not desired. Due to skewed distributions and outliers, non-parametric Spearman's correlation coefficients were calculated between the total O'Driscoll and ICRS scores, as well as between specific subsets. The subsets were chosen selected on the basis of the related themes of the scored items: Macroscopic appearance (ICRS) and Surface regularity (O'Driscoll score); and Integration to border zone (IRCS) and Bonding to the adjacent cartilage (O'Driscoll score). A p<0.05 was considered significant.

Results

ICRS

The median ICRS score was 6.5 (range 4-11) for Observer 1 and 6.5 (range (3-11) for Observer 2 (*Table 2.1*). The defects were classified mainly as a grade II (nearly normal, n=10 and n=15 for Observer 1 and 2, respectively), or a grade III (abnormal, n=22 and n=16 for Observer 1 and 2, respectively). Only Observer 2 classified one defect as grave IV (severely abnormal). The inter-observer agreement was 50% with a κ of 0.4 (p<0.001) for the total ICRS score. The agreement for the sub items was higher.

Table 2.1: Summary of the ICRS score.

		Observer 1 (n=)	Observer 2 (n=)
Degree of defect repair	In level with surrounding cartilage	16	14
	75% repair of defects depth	14	14
	50% repair of defects depth	2	3
	25% repair of defects depth	0	1
	0% repair of defects depth	0	0
Integration to border zone	Complete integration with surrounding cartilage	0	0
	Demarcating border < 1mm	5	7
	3/4 of graft integrated, 1/4 with a notable border >1mm	5	8
	1/2 of graft integrated with surrounding cartilage, 1/2 with a notable border > 1mm	22	17
	No contact to 1/4 of graft integrated with surrounding cartilage	0	0
Macroscopic appearance	Intact smooth surface	2	2
	Fibrillated surface	5	6
	Small, scattered fissures or cracks	9	8
	Several small, or few but large fissures	16	16
	Total degeneration of grafted area	0	0
Median total ICRS score (range)		**6.5 (4-11)**	**6.5 (3-11)**
ICRS Grade	Grade I (normal)	0	0
	Grade II (nearly normal)	10	15
	Grade III (abnormal)	22	16
	Grade IV (severely abnormal)	0	1

Sub item scores, total score and grading according to the ICRS are given.

Histology

The median O'Driscoll score of the samples was 11.5 (range 3-20, *Table 2.2*). All defects were predominantly filled with fibrous tissue, with diminished Safranin-O staining and with large collagen structures visible using polarized light microscopy. The variety in surface appearance and structural integrity was substantial (*Table 2.2* and *Figure 2.1*).

Table. 2.2: Summary and dispersion of the O'Driscoll score per sub item and total score.

Characteristics		Number of samples
Nature of predominant tissue		
	Hyaline articular cartilage	0
Cellular morphology	Incompletely differentiated mesenchyme	17
	Fibrous tissue or bone	15
	Normal or nearly normal	1
	Moderate	11
Safranin-O staining of the matrix	Slight	14
	None	6
Structural characteristics		
	Smooth and intact	3
	Superficial horizontal lamination	12
Surface regularity	Fissures 25-100 % of the thickness	13
	Severe disruption, including fibrillation	4
	Normal	0
Structural integrity	Slight disruption, including cysts	16
	Severe disintegration	16
	100 % of adjacent cartilage	6
Cartilage Thickness	50-100% of adjacent cartilage	12
	0-50% of adjacent cartilage	14
	Bonded at both ends of graft	23
Bonding to the adjacent cartilage	Bonded at one end, or partially at both ends	7
	Not bonded	2
Freedom from cellular changes of degeneration		
	Normal cellularity	9
	Slight hypocellularity	13
Hypocellularity	Moderate hypocellularity	19
	Severe hypocellularity	1
	No clusters	23
Chondrocyte clustering	<25 % of the cells	8
	25-100 % of the cells	1
Freedom from degenerative changes in adjacent cartilage		
	Normal cellularity, no clusters, normal staining	14
	Normal cellularity, mild clusters, moderate staining	6
	Mild or moderate hypocellularity, slight staining	12
	Severe hypocellularity, poor or no staining	0
Median total O'Driscoll score		11.5 (range 3-20)

Correlations

The Spearman's rank correlation coefficient of the average total ICRS score for either observers or the O'Driscoll score was not significant (Observer 1: ρ=-0.004, p=0.98, 95% CI=0.40-0.37, Observer 2: ρ=-0.132, p=0.47, 95% CI=0.53-0.29, *Figure 2.3*). Likewise, the correlations were not statistically significant for the specific subsets of macroscopic appearance (ICRS) and surface regularity (O'Driscoll score) or for the subset integration to border zone (IRCS) and bonding to the adjacent cartilage (O'Driscoll score) (*Table 2.3*).
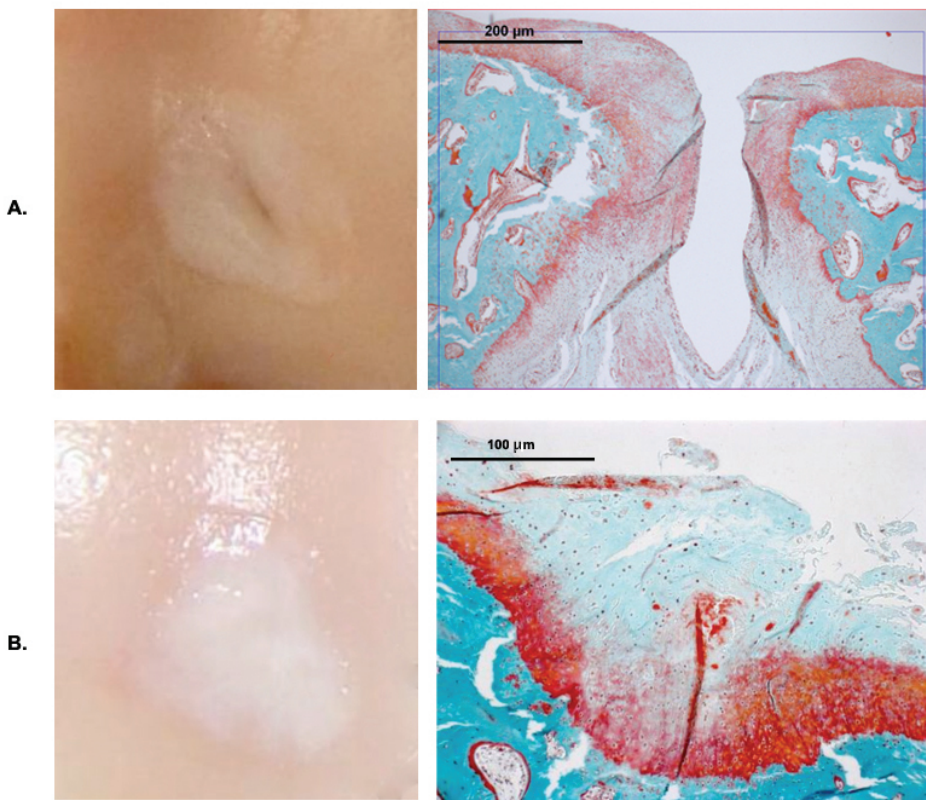
Figure 2.1: correlation between macroscopy and histology.
Two different situations are shown demonstrating the clear correlation between the macroscopic image (*left*) and the corresponding histological slice (*right*) when there is a large superficial disturbance, and the difficulty with assessing cartilage repair tissue in a sample with a smooth surface. *A.* Sample with an evident large cleft visible both macroscopically (*left*) and on the Safranin-O histological slice (*right, 50x magnification*). *B.* Sample that was scored as "nearly normal" by the ICRS (*left*), but that shows hypocellularity and structural irregularities on the Masson Goldner slice causing much lower O'Driscoll histological score (*right, 100x magnification*).
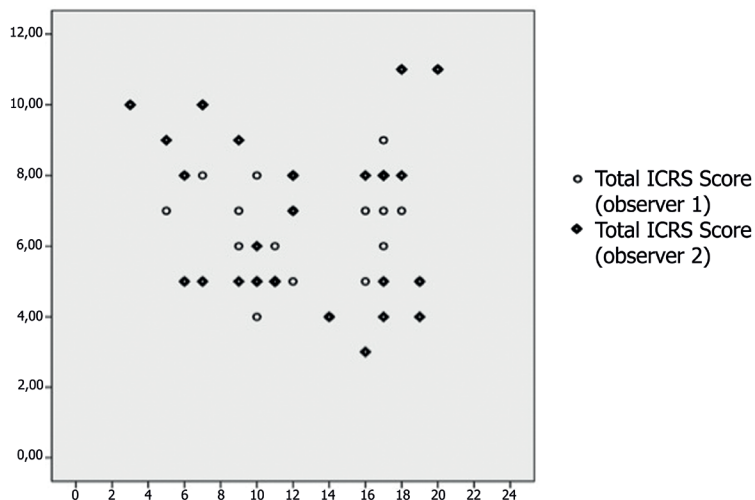
Figure 2.2: Scatter plot of the O'Driscoll score and the ICRS score.
Results from Observer 1 and Observer 2 show the lack of correlation (ρ:-0.004, p=0.98, 95% CI -0,40 - 0,37 and ρ:-0.132, p=0.547, 95% CI -0,53 - 0,29, respectively).

Table 2.3: Interobserver agreement for the 2 observers of the ICRS score and correlations between the O'Driscoll score and the IRCS.

Interobserver agreement			
Subitem ICRS	%	k	p-value
Degree of defect repair	0.84	0.73	<0.001
Integration to border zone	0.81	0.66	<0.001
Macroscopic appearance	0.71	0.57	<0.001
Total ICRS score	0.50	0.39	<0.001

Correlations (Spearman's rho)						
	Observer 1			Observer 2		
Total O'Driscoll score vs. total ICRS score	-0.004	p=0.98	95% CI: -0.40 – 0.37	-0.132	p=0.47	95% CI: -0.53 – 0.29
"Bonding to the adjacent cartilage" (ODS) vs. "Integration to border zone" (ICRS)	-0.61	p=0.74	95% CI: -0.44 – 0.31	-0.38	p=0.83	95% CI: -0.34 – 0.35
"Surface regularity" (ODS) vs. "Macroscopic appearance" (ICRS)	-0.22	p=0.22	95% CI: -0.53 - 0.14	-0.33	p=0.86	95% CI: -0.39 – 0.34

Discussion

The aim of this study was to assess the correlation between the macroscopic cartilage repair tissue assessment using the ICRS score and the histological assessment using the O'Driscoll score after microfracture treatment of talar osteochondral defects in a goat model. Our hypothesis was that the scores would correlate moderately, however, no significant correlation was found between both scores.

45

Macroscopic ICRS Poorly Correlates with O'Driscoll Histological Cartilage Repair Assessment in a Goat Model | **CHAPTER 2**

Strengths of this study are the use of a validated goat model, two surgeons with extensive clinical experience with arthroscopic cartilage repair, as well as an expert histologist familiar with cartilage repair histology. However, the number of samples was limited and the average quality of the fibrous repair tissue did not cover the full range of the O'Driscoll score (range 3-20 vs. 0-24). These two factors may at least in part have contributed the absence of a correlation. Also, the macroscopic scoring was not performed in vivo, but by means of post mortem photographs. Although this is a method that is frequently used in a variety of studies for macroscopic scoring of cartilage [3, 7, 19], it does not allow the freedom of assessment from all angles as in vivo arthroscopy does. Lastly, the study was designed to detect a correlation larger than 0.4, because a correlation smaller than this was considered to be clinically irrelevant. A more subtle correlation could be present between the scores or sub items.

Apart from limitations in the study design, several characteristics of the ICRS score may also have affected the lack of correlation. Firstly, only extreme structural disorganizations such as large clefts can be registered by the macroscopic score (*Figure 2.1A*), whereas subtle structural differences, such as smaller fissures or cysts hidden from the macroscopic surface (*Figure 2.1B*), are not detected. This leads to over-estimation of the quality of repair tissue by macroscopic assessment compared to histological measures (*Figure 2.2*).

Secondly, the lack of correlation could be explained by the introduction of individual judgement in the ICRS score, because both the degree of defect fill and measurement of the demarcating border require the observer to determine quantitative values based on individual estimations. It could be possible that repeated individual scoring results in a different score. Previous articles did not specify the degree of experience with the ICRS scoring of the observers, but one article did show a significant increase in inter observer agreement after two months training [30]. Whether this also influences the correlation to histology remains to be investigated.

Thirdly, the ICRS does not allow the observer to report graft hypertrophy, nor does it include the colour aspect of the defect. Both items have been discussed in literature to be of relative importance and are included in the Oswestry Arthroscopy scale. However, we were not able to detect a colour difference as used by the OAS (pearly hyaline like, white fibrous tissue, yellow bone) between our samples with a good or a poor O'Driscoll score, since all were more or less white fibrous tissue. Moreover, the O'Driscoll score assesses the borders in one plane and is location dependent, while the ICRS score takes the entire defect rim into consideration and judges the percentage of the rim that is attached. This explanation is supported by the fact

that no correlation was found between the sub item scores for the integration of the repair tissue into the border zone.

The results indicate that despite the satisfactory inter observer reliability found previously, ICRS scoring may not be an accurate manner to determine cartilage or repair quality during arthroscopy. Arthroscopy also allows for assessment of multiple domains such as the size of the lesion and the general state of degeneration of the joint. Since these are all features that influence the healing or possible deterioration of cartilage defects, these items could be added in the score to make the ICRS scoring more accurate [4, 13, 17].

For research purposes, alternatives of histology that are more accurate, precise and reliable should be considered, such as dGEMERIC and T2 mapping MRI, contrast enhanced CT or optical coherence tomography (OCT) [24]. These techniques are also applied more and more in clinical practice and according to the increasing amount of literature of these advanced techniques image parameters correlate highly with cartilage quality [5, 11, 35, 37].

In conclusion, this animal study suggests that isolated macroscopic assessment of the quality of cartilage repair tissue of talar osteochondral defects treated with micro fracture using the ICRS score has a poor correlation with histological analysis. Possible explanations may be found in the limitations of surface assessment compared to analysis deeper into the tissue and the necessity of more elaborate macroscopic assessment including hypertrophy, colour, lesion size, location and degenerative status of the joint.
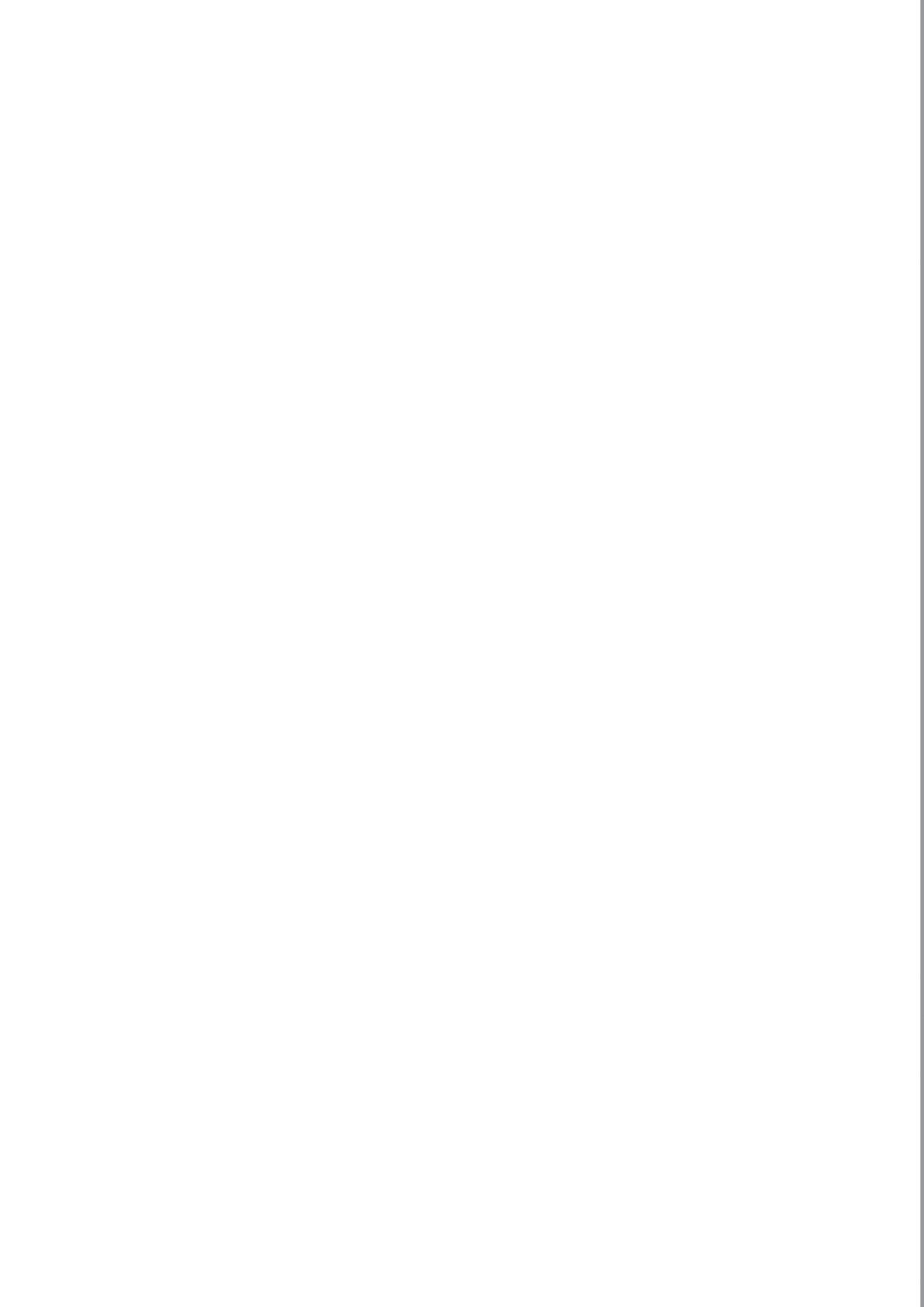
Acknowledgements

48

CHAPTER 2 | Macroscopic ICRS Poorly Correlates with O'Driscoll Histological Cartilage Repair Assessment in a Goat Model

References

1. Adachi N, Deie M, Nakamae A, Ishikawa M, Motoyama M, Ochi M. Functional and radiographic outcome of stable juvenile osteochondritis dissecans of the knee treated with retroarticular drilling without bone grafting. *Arthroscopy*. 2009;25:145–152.

2. Aroen A, Heir S, Loken S, Engebretsen L, Reinholt FP. Healing of articular cartilage defects. An experimental study of vascular and minimal vascular microenvironment. *J Orthop Res*. 2006;24:1069–1077.

3. Batiste DL, Kirkley A, Laverty S, Thain LM, Spouge AR, Holdsworth DW. Ex vivo characterization of articular cartilage and bone lesions in a rabbit ACL transection model of osteoarthritis using MRI and micro-CT. *Osteoarthr. Cartil.* 2004;12:986–996.

4. Becher C, Driessen A, Hess T, Giuseppe U, Nicola L, Longo UG, Maffulli N, Thermann H, Giuseppe U, Nicola L. Microfracture for chondral defects of the talus: maintenance of early results at midterm follow-up. *Knee Surg Sport. Traumatol Arthrosc*. 2010;18:656–663.

5. Bekkers JEJ, Bartels LW, Benink RJ, Tsuchida AI, Vincken KL, Dhert WJ, Creemers LB, Saris DB. Delayed gadolinium enhanced MRI of cartilage (dGEMRIC) can be effectively applied for longitudinal cohort evaluation of articular cartilage regeneration. *Osteoarthr. Cartil.* 2013;21:943–949.

6. Blackburn WD, Chivers S, Bernreuter W, Blackburn Jr. WD, Chivers S, Bernreuter W. Cartilage imaging in osteoarthritis. *Semin Arthritis Rheum*. 1996;25:273–281.

7. van den Borne MPJ, Raijmakers NJH, Vanlauwe J, Victor J, de Jong SN, Bellemans J, Saris DB. International Cartilage Repair Society (ICRS) and Oswestry macroscopic cartilage evaluation scores validated for use in Autologous Chondrocyte Implantation (ACI) and microfracture. *Osteoarthr. Cartil.* 2007;15:1397–1402.

8. Brittberg M, Peterson L. Introduction of an articular cartilage classification. *ICRS Newsl.* 1998:5–8.

9. Brittberg M, Winalski CS. Evaluation of cartilage injuries and repair. *J Bone Jt. Surg Am*. 2003;85–A Suppl:58–69.

10. Brun P, Dickinson SC, Zavan B, Cortivo R, Hollander AP, Abatangelo G. Characteristics of repair tissue in second-look and third-look biopsies from patients treated with engineered cartilage: relationship to symptomatology and time after implantation. *Arthritis Res Ther*. 2008;10:R132.

11. Cernohorsky P, Kok AC, Bruin DM de, Brandt MJ, Faber DJ, Tuijthof GJ, Kerkhoffs GM, Strackee SD, van Leeuwen TG. Comparison of optical coherence tomography and histopathology in quantitative assessment of goat talus articular cartilage. *Acta Orthop*. 2015;86:257–263.

12. Chevrier A, Hoemann CD, Sun J, Buschmann MD. Chitosan-glycerol phosphate/blood implants increase cell recruitment, transient vascularization and subchondral bone remodeling in drilled cartilage defects. *Osteoarthr. Cartil.* 2007;15:316–327.

13. Chuckpaiwong B, Berkson EM, Theodore GH. Microfracture for Osteochondral Lesions of the Ankle: Outcome Analysis and Outcome Predictors of 105 Cases. *Arthroscopy*. 2008;24:106–112.

14. Delle Sedie A, Riente L, Bombardieri S. Limits and perspectives of ultrasound in the diagnosis and management of rheumatic diseases. *Mod Rheumatol*. 2008;18:125–131.

15. Fleiss JL, Levin B, Paik MC. The Measurement of Interrater Agreement. In: *Statistical Methods for Rates and Proportions*. John Wiley & Sons, Inc.; 2004:598–626.

16. Giannini S, Buda R, Grigolo B, Bevoni R, Di Caprio F, Ruffilli A, Cavallo M, Desando G, Vannini F. Bipolar fresh osteochondral allograft of the ankle. *Foot Ankle Int*. 2010;31:38–46.

17. Giannini S, Vannini F. Operative treatment of osteochondral lesions of the talar dome: current concepts review. *Foot Ankle Int*. 2004;25:168–175.
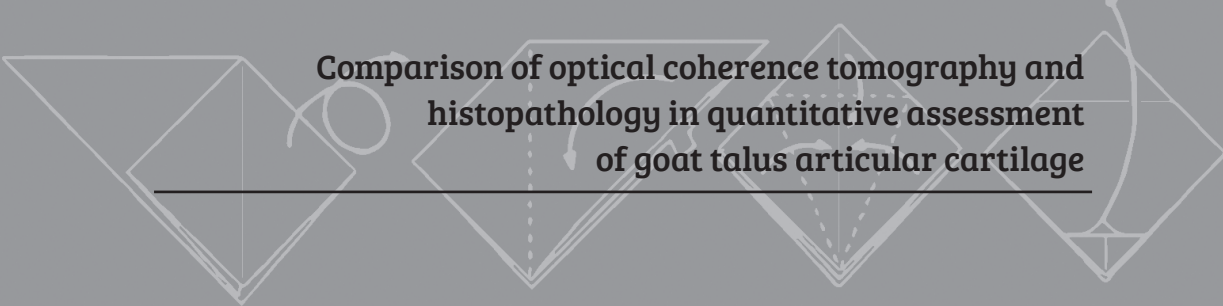
18. Gikas PD, Morris T, Carrington R, Skinner J, Bentley G, Briggs T. A correlation between the timing of biopsy after autologous chondrocyte implantation and the histological appearance. *J Bone Jt. Surg Br*. 2009;91:1172–1177.

19. Hattori K, Ikeuchi K, Morita Y, Takakura Y. Quantitative ultrasonic assessment for detecting microscopic cartilage damage in osteoarthritis. *Arthritis Res. Ther.* 2005;7:R38–R46.

20. Hoemann C, Kandel R, Roberts S, Saris DB, Creemers L, Mainil-Varlet P, Methot S, Hollander a. P, Buschmann MD, Hoemann C. Roberts S., Saris D.B.F., Creemers L., Mainil-Varlet P., Methot S., (...), Buschmann M.D. KR. International cartilage repair society (ICRS) recommended guidelines for histological endpoints for cartilage repair studies in animal models and clinical trials. *Cartilage*. 2011;2:153–172.

21. Jackson DW, Lalor PA, Aberman HM, Simon TM. Spontaneous repair of full-thickness defects of articular cartilage in a goat model. A preliminary study. *J Bone Jt. Surg Am*. 2001;83–A:53–64.

22. Knutsen G, Drogset JO, Engebretsen L, Grontvedt T, Isaksen V, Ludvigsen TC, Roberts S, Solheim E, Strand T, Johansen O, Grøntvedt T, Isaksen V, Ludvigsen TC. A randomized trial comparing autologous chondrocyte implantation with microfracture. Findings at five years. *J Bone Jt. Surg Am*. 2007;89:2105–2112.

23. Kok AC, Tuijthof GJ, Den Dunnen S, Van Tiel J, Siebelt M, Everts V, Van Dijk CN, Kerkhoffs GM. No effect of hole geometry in microfracture for talar osteochondral defects. *Clin. Orthop. Relat. Res.* 2013;471:3653–3662.

24. Kokkonen HT, Jurvelin JS, Tiitu V, Töyräs J. Detection of mechanical injury of articular cartilage using contrast enhanced computed tomography. *Osteoarthr. Cartil.* 2011;19:295–301.

25. Landis JR, Koch GG. The measurement of observer agreement for categorical data. *Biometrics*. 1977;33:159–174.

26. Lee KB, Bai LB, Yoon TR, Jung ST, Seon JK. Second-look arthroscopic findings and clinical outcomes after microfracture for osteochondral lesions of the talus. *Am. J. Sports Med.* 2009;37 Suppl 1:63S–70S.

27. Milano G, Sanna Passino E, Deriu L, Careddu G, Manunta L, Manunta A, Saccomanno MF, Fabbriciani C. The effect of platelet rich plasma combined with microfractures on the treatment of chondral defects: an experimental study in a sheep model. *Osteoarthr. Cartil.* 2010;18:971–980.

28. Mithoefer K, Mcadams T, Williams RJ, Kreuz PC, Mandelbaum BR. Clinical efficacy of the microfracture technique for articular cartilage repair in the knee: an evidence-based systematic analysis. *Am J Sport. Med*. 2009;37:2053–2063.

29. Moojen DJ, Saris DB, Auw Yang KG, Dhert WJ, Verbout AJ. The correlation and reproducibility of histological scoring systems in cartilage repair. *Tissue Eng*. 2002;8:627–634.

30. Nakamura T, Sekiya I, Muneta T, Hatsushika D, Horie M, Tsuji K, Kawarasaki T, Watanabe A, Hishikawa S, Fujimoto Y, Tanaka H, Kobayashi E. Arthroscopic, histological and MRI analyses of cartilage repair after a minimally invasive method of transplantation of allogeneic synovial mesenchymal stromal cells into cartilage defects in pigs. *Cytotherapy*. 2012;14:327–338.

31. O'Driscoll SW, Keeley FW, Salter RB. Durability of regenerated articular cartilage produced by free autogenous periosteal grafts in major full-thickness defects in joint surfaces under the influence of continuous passive motion. A follow-up report at one year. *J. Bone Joint Surg. Am.* 1988;70:595–606.

32. Pineda S, Pollack A, Stevenson S, Goldberg V, Caplan A. A semiquantitative scale for histologic grading of articular cartilage repair. *Acta Anat*. 1992;143:335–340.

33. Simon TM, Aberman HM. Cartilage regeneration and repair testing in a surrogate large animal model. *Tissue Eng Part B Rev*. 2010;16:65–79.

34. Smith GD, Taylor J, Almqvist KF, Erggelet C, Knutsen G, Garcia Portabella M, Smith T, Richardson JB, Portabella MG, Smith T, Richardson JB. Arthroscopic assessment of cartilage repair: a validation study of 2 scoring systems. *Arthroscopy*. 2005;21:1462–1467.

35. Smith TO, Drew BT, Toms AP, Donell ST, Hing CB. Accuracy of magnetic resonance imaging, magnetic resonance arthrography and computed tomography for the detection of chondral lesions of the knee. *Knee Surgery, Sport. Traumatol. Arthrosc.* 2012;20:2367–2379.

36. Verhagen RA, Maas M, Dijkgraaf MG, Tol JL, Krips R, van Dijk CN. Prospective study on diagnostic strategies in osteochondral lesions of the talus. Is MRI superior to helical CT? *J Bone Jt. Surg Br*. 2005;87:41–46.

37. Watanabe A, Boesch C, Anderson SE, Brehm W, Mainil Varlet P. Ability of dGEMRIC and T2 mapping to evaluate cartilage repair after microfracture: a goat study. *Osteoarthr. Cartil.* 2009;17:1341–1349.
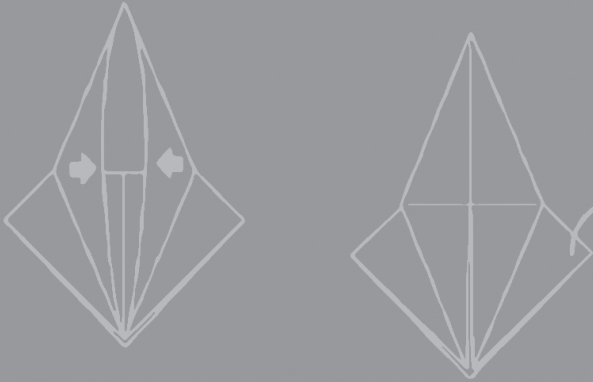
CHAPTER 3

Comparison of optical coherence tomography and histopathology in quantitative assessment of goat talus articular cartilage

Paul Cernohorsky
Aimée C. Kok
D. Martijn de Bruin
Martin J. Brandt
Dirk J. Faber
Gabrielle J. Tuijthof
Gino M. Kerkhoffs
Simon D. Strackee
Ton G. van Leeuwen
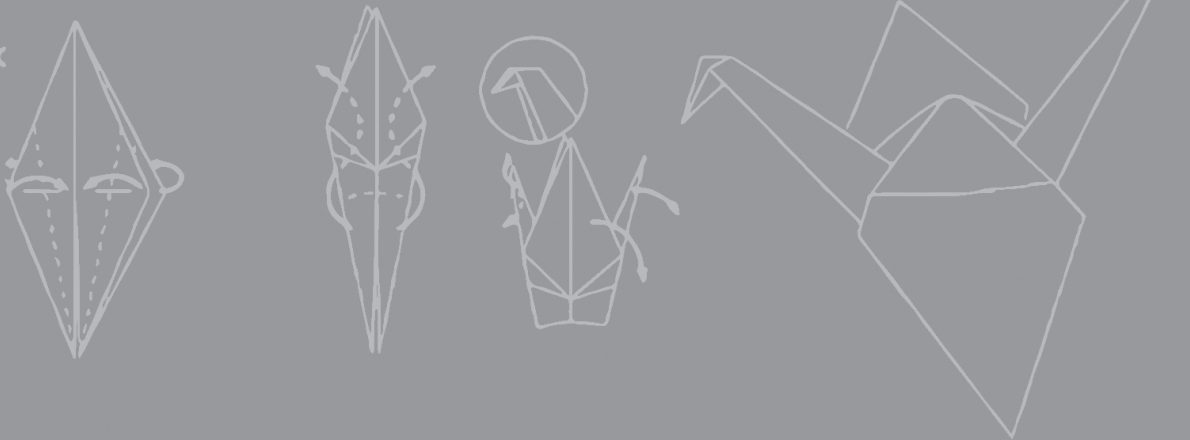
Abstract

Background
Optical coherence tomography (OCT) is a light-based imaging technique suitable for depiction of thin tissue layers such as articular cartilage. Quantification of results and direct comparison with a reference standard is needed to confirm the role of OCT in cartilage evaluation.

Materials and methods
Goat talus articular cartilage repair was assessed quantitatively with OCT and compared with histopathology using semi-automated analysis software. Osteochondral defects were created centrally in goat tali with subsequent healing over 24 weeks. After sacrifice, the tali were analysed using OCT and processed into histopathology slides. Cartilage thickness, repair tissue area, and surface roughness were measured. Also, light attenuation coefficient measurements were performed to assess differences in the properties of healthy tissue and repair tissue.

Results
Intra-class correlation coefficients for resemblance between the two techniques were 0.95 ($p < 0.001$) for thickness, 0.73 ($p = 0.002$) for repair tissue area, and 0.63 ($p = 0.015$) for surface roughness. Light attenuation differed significantly between healthy cartilage (8.2 (SD 3.9) mm^{-1}) and repair tissue (2.8 (SD 1.5) mm^{-1}) ($p < 0.001$).

Conclusion
Compared to histopathology as the standard reference method, OCT is a reproducible technique in quantitative analysis of goat talus articular cartilage, especially when assessing cartilage thickness and to a lesser extent when measuring repair tissue area and surface roughness. Moreover, differences in local light attenuation suggest measurable variation in tissue structure, enhancing the clinical applicability of quantitative measurements from cartilage OCT images.

Introduction

Within the diagnostic work-up of degenerative disease in small joints, imaging techniques such as conventional radiographs, computed tomography (CT), and magnetic resonance imaging (MRI) are unable to accurately depict thin cartilage layers in clinical diagnostics.

Optical coherence tomography (OCT) can detect damage to articular cartilage [6, 10], and at an earlier stage compared to macroscopic evaluation during arthroscopy [8, 24]. OCT is analogous to ultrasound, but uses near-infrared light rather than sound to produce high-resolution, cross-sectional images with limited depth penetration (typically up to 2 mm). Relatively recently, the use of OCT in cartilage imaging in large joints such as the knee has been reported [8, 24]. Also, animal models [1, 2, 13, 15, 17, 19, 21, 23] and in vitro studies [3, 11] have been used to assess the feasibility of OCT in imaging of osteoarthritic cartilage. A strong correlation was found between the grade of degenerative changes seen on OCT and results of macroscopic evaluation during knee arthroscopy in humans (r = 0.85) [10]. This correlation was also seen when using a histopathology grading scale (r = 0.98) [8].

In contrast to imaging of the relatively thick cartilage layers of the knee joint (> 2 mm) [2, 9, 10, 24], OCT of thin cartilage layers in small joints [1, 2, 6, 13, 15, 17, 19, 21, 23] allows the possibility of depicting the cartilage-bone interface, enabling cartilage thickness measurements. Also, the use of the OCT signal attenuation as a function of depth (µOCT) has discriminative capabilities when assessing tissue structure in urology [5] and gynaecology [22]. The application of similar parameters using the back reflection of light was demonstrated in OCT of horse articular cartilage [21]. Recently, the use of fiber-optic OCT was demonstrated in minimally invasive imaging of trapeziometacarpal articular cartilage [6], paving the way for clinical application during arthroscopy. Thus, OCT remains a promising technique for in situ evaluation of cartilage damage in patients with osteoarthritis in small joints of the wrist or ankle.

Using a goat model in this study, we optimized conditions for the best achievable one-to-one co-localization between 3D OCT images and histopathology, which has not been described before. Here we describe a direct comparison between OCT and histopathology in assessment of the clinically valuable parameters cartilage thickness, repair tissue area, and surface roughness. To reliably assess these parameters simultaneously, we developed custom-made semi-automated analysis software. In addition, quantification of the OCT signal using µoct was performed on all cartilage OCT samples to assess differences between healthy cartilage and repair tissue.

Materials and methods

Subjects and surgical procedure

The study protocol was approved by the animal welfare committee of the Academic Medical Center, University of Amsterdam (ORCA102287). Eleven female Dutch milk goats were used. All goats were four years of age with a mean weight of 71 (SD 11) kg. To ensure assessment of both healthy tissue and cartilage-like repair tissue during quantitative analysis, osteochondral defects with a diameter of 6.0 mm and a depth of 3.0 mm were created in the tali of the hind legs. Under general anaesthesia, an incision was made on the lateral side of the Achilles tendon, exposing the talus [3, 11]. Using a cannulated drill guide, the osteochondral defects were drilled centrally in the surface of the talus under continuous rinsing with 0.9% NaCl. The joint capsule, subcutaneous tissue, and skin were closed with absorbable sutures. Postoperatively the goats were allowed normal weight bearing and were followed up daily without any restrictions on food or exercise. The goats were killed after 24 weeks. The tali were cut into 20 × 20 mm blocks, marking the ventral side of the saw plane. Samples were fixed in 4% formaldehyde and dehydrated in ethanol in preparation for further histological processing.

Optical coherence tomography

OCT images were acquired with a commercially available 50-kHz swept source OCT system (Santec Inner Vision 2000) with an optical depth (z-axis) resolution of ~10 µm and lateral (x/y-axis) resolution of ~40 µm, operating at a central wavelength of 1.300 nm with a bandwidth of 120 nm. Cartilage samples were placed on a translation platform in a small petri dish. The OCT scan unit was vertically mounted and focused by moving it towards and from the sample, in order to optimize OCT imaging depth sensitivity. Conceding that there were height differences in the talar articular surface, care was taken to place the surface of the samples at a perpendicular overall angle to the OCT signal beam. Then, 3D OCT datasets were acquired, focusing on the centre of the osteochondral defect, producing cross-sectional images perpendicular to the labelled ventral saw plane. Dimensions of the datasets were 400 (z, depth) × 300 (x, length) pixels over 300 (y, width) slices, distributed over a 2.7 (z, refractive index = 1.4 for cartilage) × 12 (x) × 12 (y) mm^3 scanned area, resulting in a digital sampling resolution of 10 × 40 × 40 µm^3, equivalent to the optical resolution of the system. Raw data were converted to TIFF stacks and calibrated to the appropriate scale. Amira software (version 4.5; Visage Imaging, San Diego, CA) was used for 3D visualization of the datasets.

Histopathology

After OCT scanning, the fixed and dehydrated samples were embedded in methyl methacrylate (MMA). Before sectioning into slices, the previously marked ventral saw plane was re-identified. Samples were placed in the microtome with the marked saw plane perpendicular to the cutting blade. The (regenerated) osteochondral defect was visually located and 5-µm slices were produced halfway through the defect. The slices were stained with hematoxylin and eosin for general cell morphology and identification of cartilage tissue, and visually inspected using light microscopy. Then the slices were scanned using a slide scanner at 4× magnification. Images from scanned slices were converted to TIFF format and calibrated to the appropriate scale.

Matching of OCT with histology

From each talus, one histopathology slide clearly depicting the central part of the osteochondral defect was selected for analysis. Where possible, slides with distinct features were selected in order to facilitate matching with corresponding OCT images. From a 300-slice 3D OCT dataset, one OCT B-scan was selected for analysis after agreement on matching of structural visual parameters with similar visual parameters in previously selected histopathology slides (*Figure 3.1*).

Analysis of OCT and histological data

For quantitative analysis, the parameters cartilage thickness, repair tissue area, and surface roughness were chosen since they provide distinct and (clinically) relevant information about the condition of the articular cartilage. For reproducible measurements, custom-made image analysis software was developed, written as a Java plugin for the open-source image processing software package Fiji. The software incorporates edge detection for identification of the articular surface and assisted drawing of auxiliary lines used for calculation of the three descriptive parameters (*Figure 3.2*). For edge detection in both the OCT images and the histopathology images, a median filter was applied. Then a starting (z-) coordinate was chosen, after which the next x-point was found as the maximum of the first derivative of the intensity versus depth in a band around the previous z-value. After smoothing in the x-direction, the final edge was constructed. Auxiliary lines were constructed by manually placing five points (in orange) on the normal-appearing cartilage interface, top and bottom, on both sides of the defect. The points were fitted with a fourth-degree polynomial to extrapolate the expected cartilage layer through the osteochondral defect. The top line (in blue) represented the expected trajectory of the articular cartilage top surface when disregarding the osteochondral defect. The bottom auxiliary line (in green) represented the expected transitional zone between cartilage and subchondral bone when disregarding the osteochondral defect. Measured cartilage thickness

was defined as the mean thickness of the articular cartilage layer outside the boundaries of the osteochondral defect identified, representing a measurement of healthy articular cartilage thickness in mm. Cartilage repair tissue area was defined as the area marked by the bottom auxiliary line (in green), the detected edge (in pink), and the lateral boundaries of the osteochondral defect (in red), in mm^2. Surface roughness was defined as the root mean square of the distance between the top auxiliary line (in blue) and the detected edge (in pink), restricted by the lateral boundaries of the osteochondral defect (in red). For determination of intra-observer variability, all semi-automated analyses were repeated five times by the same observer for every OCT and histopathology image, at intervals of at least one week.

To correct for learning effects of the observer, the last three measurements for each image were used for analysis. Agreement between these measurements was calculated using Spearman's correlation. OCT signal attenuation measurements were performed as described previously [12]. The attenuation per mm^{-1} (μoct) was calculated using an exponential decay model on the OCT signal amplitude curve as a function of depth after correction for setup-specific calibration parameters [4]. These corrections are needed in order to take into account the effects of the point-spread function of the optics in the sample arm [14] and the roll-off of the OCT sensitivity with depth. The "healthy cartilage" and "repair tissue" regions were readily identified for analysis of the other quantitative parameters (thickness, repair tissue area, and surface roughness). A region with vertical boundaries at least 400–600 μm apart (10–15 A-lines), to ensure averaging over enough data points, was therefore chosen for attenuation measurements from each predefined region. For the horizontal boundaries, in healthy cartilage, measurements were taken from the air-to-tissue interface (blue lines in *Figure 3.2*) to the cartilage-bone interface (green lines in *Figure 3.2*). In repair tissue, measurements were taken from the air-to-tissue interface (pink lines in *Figure 3.2*) to the location of the lower fitted boundary line (green lines in *Figure 3.2*). In all cases, care was taken to select a measurement area with an apparently homogeneous OCT signal to give the most reliable attenuation fit.

Statistics

2D plots with linear correlation fit were constructed for direct comparison of OCT values and histopathology values regarding the three parameters measured. The slope and goodness of fit (r) of the correlation lines were determined. Since two different methods of measurement (OCT and histopathology) were used, Bland-Altman plots were constructed to show the differences between measurements. To determine agreement between measurements in the OCT and histopathology groups, the intra-class correlation coefficient (ICC) was calculated.

An ICC value of 0 indicated poor agreement, between 0 and 0.20 slight agreement, between 0.20 and 0.40 fair agreement, between 0.40 and 0.60 moderate agreement, between 0.60 and 0.80 substantial agreement, and between 0.80 and 1.00 indicated near-perfect agreement. Paired t-tests were used to assess the differences in attenuation measurements between healthy cartilage and repair tissue. Any p-values < 0.05 were considered statistically significant. Statistical analyses were performed using GraphPad Prism 5 and SPSS 19.

Results

22 tali were scanned using the Santec OCT system. The 3D OCT datasets acquired clearly showed the osteochondral defect, located centrally in the scans (*Figure 3.1*). On all OCT scans, similar image characteristics were observed and identification of the cartilage layer and the transitional zone between articular cartilage and subchondral bone was achieved. A distinct dark banding pattern on the cartilage-bone interface was discerned in normal-appearing cartilage; this was not visible in the OCT sections containing the osteochondral defect (indicated by green arrows in *Figure 3.1*).

Regarding the histopathology, hematoxylin and eosin stained slides were obtained from all 22 tali. Visual inspection of the articular surface and the site of the osteochondral defect was performed using light microscopy. Care was taken to achieve an accurate match between OCT and histopathology. By visual inspection, a good match was achieved in thirteen cases (*Figure 3.2A*). However, in nine cases only a fair match was found between OCT and histopathology, resulting in differences between the parameters measured (*Figure 3.2B*). For all the measurements taken into account for analysis, both on OCT and histopathology, inter-observer correlation coefficients were > 0.97, showing reproducibility of measurements. All the results obtained for the three parameters (cartilage thickness, repair tissue area, and surface roughness) by the two modalities are depicted in *Figure 3.3* (scatter plots) and *Figure 3.4* (Bland-Altman plots). Exemplary measurements from a good match and a fair match are highlighted in green and red, respectively. When assessing cartilage thickness in the x-y plots, the slope of the regression line was 0.71 (r = 0.93, Pearson's correlation).

Attenuation coefficients were measured for all 22 samples, in both healthy cartilage and repair tissue. A difference in attenuation coefficient was observed between the healthy cartilage group (8.2 (SD 3.9) mm^{-1}) and the repair tissue group (2.8 (SD 1.5) mm^{-1}) (p < 0.001). The difference in attenuation denotes a local difference in tissue characteristics and structure.
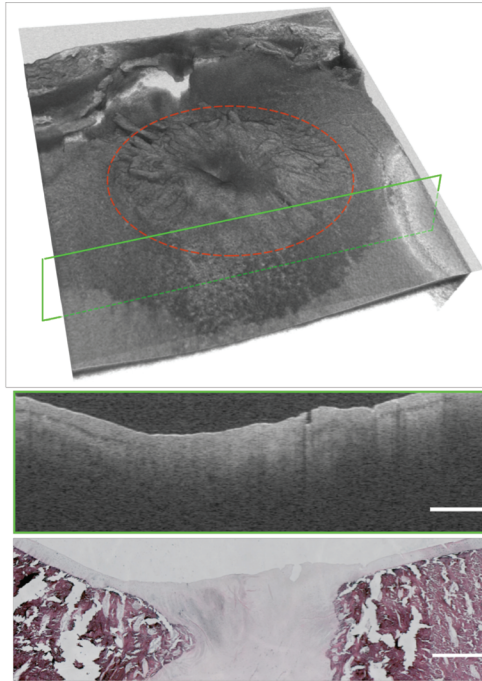
Figure 3.1: View of a typical matched OCT and histology slice dataset

A 3D overview of the 300 slice single OCT slice is shown (*top*). A single OCT slice and the matched histopathology slide are also shown (*bottom*). The site of the osteochondral defect is marked in red and the location of the OCT slide is marked with a green frame. Landmark properties such as small fissures (*white arrow*) and the transitional zone between cartilage and subchondral zone (*green arrows*) are identified in both modalities.
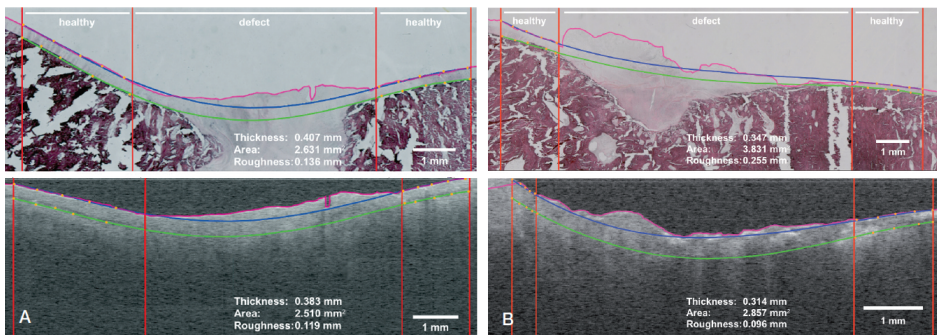
Figure 3.2: examples of matches between histopathology and OCT

A. Good match between histopathology and OCT. Auxiliary lines were created by the analysis software. The pink line represents edge detection. The top and bottom boundaries of the cartilage layer with extrapolation through the osteochondral defect are shown with the blue and green lines, respectively. The vertical red lines mark the location of healthy cartilage and the (start of the) osteochondral defect. Thickness is defined as the average distance between the blue and green line in healthy tissue regions. Area is computed from the area bounded by the pink line and green line in the defect region. Roughness is defined as the root-mean-square distance between the pink line and the blue line in the defect region. *B. Fair match between OCT and histopathology.* This produces noticeable differences in the parameters repair tissue area and surface roughness. Definitions of the parameters are explained above and in the text.

With a calculated ICC of 0.95 (95% CI: 0.87–0.98, p < 0.001), agreement between OCT and histopathology regarding thickness measurement was considered to be near-perfect. For repair tissue area, the slope of the regression fit was 0.55 (r = 0.57). With a calculated ICC of 0.73 (95% CI: 0.34–0.87, p = 0.002), agreement between OCT and histopathology when assessing repair tissue area was deemed substantial. For surface roughness, the slope of the regression line was 0.69 (r = 0.48). With a calculated ICC of 0.63 (95% CI: 0.10–0.84, p = 0.02), agreement between OCT and histopathology when assessing surface roughness was substantial.
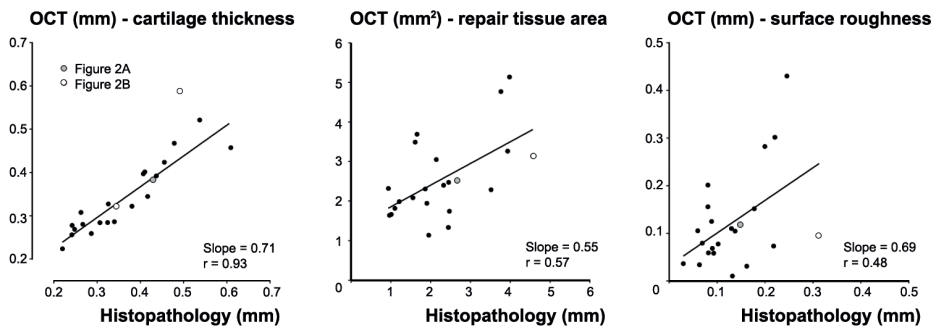
Figure 3.3: Graphical comparison between OCT and histopathology (x-y plot).
The figure depicts measurements of the quantitative parameters cartilage thickness, repair tissue area, and surface roughness, with fitted linear regression lines. Measurements from a good match between OCT and histopathology (*A*) and a fair match (*B*) are shown in green and red, respectively.
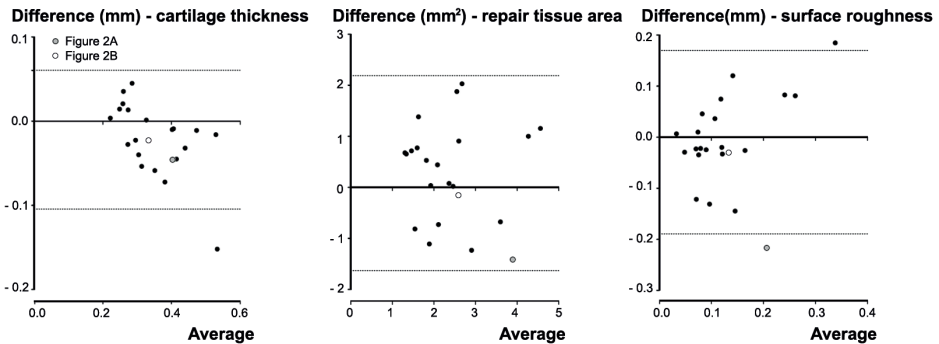
Figure 3.4: Bland–Altman plots showing the differences between the two methods of measurement.
The dashed lines represent the 95% limits of agreement. The good match from *Figure 3.3A* is shown in green and the fair match from *Figure 3.2B* is shown in red.

Discussion

To our knowledge, this is the first report of a direct quantitative comparison of 3D OCT and histopathology in imaging of articular cartilage using semi-automated software with a surface detecting algorithm that calculates the three parameters cartilage thickness, repair tissue area, and surface roughness simultaneously. Identification of measurement parameters that are clinically relevant is important for the development of OCT as a clinical diagnostic technique when directed at degenerative joint disease such as osteoarthritis. Since in osteoarthritis, loss of thickness and quality of cartilage are important diagnostic features, thickness appears to be an important parameter to be able to measure accurately. When considering cartilage quality, this is less straightforward since it is a parameter that is difficult to quantify. However, fibrillation of the cartilage surface is a known degenerative feature in the development of osteoarthritis, and was chosen as a relevant parameter to measure. Regarding repair tissue area, measurement of areas of distinct tissue types (for clinical purposes) can help to establish whether there is disease. Since osteochondral defects were created in a standardized procedure, we considered it feasible to attempt to measure its area on a (2D) cross-sectional slice as a precursor to 3D cartilage volume measurements in future. Our findings show that OCT provided information similar to that from histopathology when we assessed selected quantitative parameters in goat articular cartilage tissue. Previously, structural analysis of articular cartilage has been performed on histopathology alone [18] or OCT alone [8], and cartilage thickness has been compared between OCT and histopathology in a rabbit model [13]. Moreover, Han et al. found a near-perfect correlation in thickness measurements between OCT and histopathology (r= 0.96). More recently, better intra- and inter-observer agreement was found when using OCT (69% and 44%, respectively) than when using arthroscopy (57% and 32%, respectively) in assessment of cartilage damage based on the International Cartilage Repair Society (ICRS) grading system [16]. Comparisons have also been made between OCT and ultrasound using parameters such as roughness-, reflection-, and backscattering coefficients for both modalities [21], with similar levels of agreement. Also, OCT has shown to be an accurate imaging technique for thickness measurements in thin (tissue) layers [4].

Our custom-devised software enabled standardized and partially automated analysis that was applicable to the two different imaging modalities (OCT and histopathology). Intra-observer agreement was measured to be more than 0.90 for all three parameters, showing the reliability of the measurement method and software. The ICC for comparison between the two groups showed at least substantial agreement in all parameters, and near-perfect agreement for the parameter thickness. Although

this means good agreement between OCT and histopathology for cartilage thickness, it also shows to a certain extent the fallibility of the model for measurement of the parameters repair tissue area and surface roughness. Differences measured are partly attributable to a degree of tearing and wrinkling of the tissue slides that will occur during histological processing with a microtome. Moreover, the OCT-derived thickness is linearly dependent on the assumed refractive index, i.e. a lower refractive index would lead to greater measured thickness. Even though the refractive index of most highly scattering tissues is around 1.4 (SD 0.1) [20], the exact value for processed specimens such as those in our study is unknown, and it may well be slightly different.

A dark banding pattern was seen at the cartilage-bone interface on the OCT images. Banding patterns have been seen on cartilage OCT images, especially when using polarization sensitive OCT (PS-OCT) [11]. They may well be caused by birefringence due to differences in local collagen fiber orientation, which has been described before using polarized light [7]. Further studies using a PS-OCT system are needed to measure the polarization properties of cartilage tissue.

The present study revealed that a direct quantitative comparison between OCT and histopathology was not exemplary for the parameters repair tissue area and surface roughness. In general, when comparing tissue structures from 2D histopathology slides to a selected slice from a 3D OCT dataset, accurate matching is crucial for reliable measurements. Small changes in orientation of the slides compared to the OCT scans may have occurred during matching, mainly as a result of histological processing, inevitably leading to minor differences in measurement.

Clinical implications
The value of OCT compared to the information from histopathology slides suggests an important (clinical) advantage. Regions of interest are investigated more easily on OCT, since orientation of the images is no longer an issue that should be taken into account. Also, in our study, accurate perpendicular alignment of the OCT camera with respect to the sample ensured the largest (3D) field of view possible. For clinical application and using fibre optic OCT, a flexible, sideward-looking OCT probe would permit easier (and more natural) perpendicular placement of the OCT beam in relation to the sample, automatically correcting for this alignment issue.

Previous reports have shown virtually perfect correlations between quantitative measurements in 2D OCT and histopathology. Oddly, we did not succeed in replicating the same level of correlation using 3D OCT. Since small differences in

63

Comparison of optical coherence tomography and histopathology in quantitative assessment of goat talus articular cartilage | **CHAPTER 3**

sub-millimetre measurements appear to be inevitable, an accurate description of the methods of matching between OCT and histopathology is important—as is extraction of quantitative parameters.

Modern, non-invasive imaging techniques such as highfield-strength MRI (HF-MRI) may provide new insights in the development of osteoarthritis. However, development of dedicated HF-MRI cartilage sequences (at 5 or 7 Tesla) is slow— and to our knowledge, not yet fit for clinical practice. More conventional field strengths (1.5 and 3 Tesla) lack signal-to-noise ratio and spatial resolution to accurately depict the thin cartilage layers that are the subject of the present study. While the development of HF-MRI is very inspiring and clinical application would be a major contribution to the field, until such time, the development of high-resolution optical techniques such as in situ OCT for clinical cartilage imaging may enhance our understanding of the aetiology and progression of disease. Moreover, in contrast to non-invasive imaging such as MRI, OCT can be used hands-on by the surgeon during operative procedures such as arthroscopy.

When light attenuation was assessed, a significant difference was found between healthy cartilage and repair tissue. This shows that healthy cartilage and repair tissue (as we defined it in this study) have distinct optical properties causing the observed differences in attenuation, although it is as yet unknown which (cellular) components in cartilage tissue play the main role. Differences in light attenuation will have to be confirmed by morphological differences in local tissue structure in future studies. However, the attenuation coefficient as a quantifiable measure of pathology in degenerative joint disease greatly enhances the value of OCT as a non-destructive diagnostic technique.

Finally, OCT has already been shown to be able to monitor disease in an animal osteoarthritis model [1]. In addition, the feasibility of in situ cartilage measurements in a small wrist joint has been demonstrated [6], making quantification of structures from cartilage OCT images a valuable addition to clinical disease monitoring in osteoarthritis of small joints. In summary, the combination of high-resolution non-destructive imaging, percutaneous access for in situ measurements using fibre optic OCT, hands-on use by the attending physician, and the quantitative information that the OCT signal can provide could make OCT a very promising technique for clinical imaging of small-joint osteoarthritis in the near future.

References

1. Adams SB, Herz PR, Stamper DL, Roberts MJ, Bourquin S, Patel NA, Schneider K, Martin SD, Shortkroff S, Fujimoto JG, Brezinski ME. High-resolution imaging of progressive articular cartilage degeneration. *J. Orthop. Res.* 2006;24:708–15.

2. Bear DM, Szczodry M, Kramer S, Coyle CH, Smolinski P, Chu CR. Optical coherence tomography detection of subclinical traumatic cartilage injury. *J. Orthop. Trauma.* 2010;24:577–82.

3. van Bergen CJ, Kerkhoffs GM, Marsidi N, Korstjens CM, Everts V, van Ruijven LJ, van Dijk CN, Blankevoort L. Osteochondral Defects of the Talus: A Novel Animal Model in the Goat. *Tissue Eng. Part C. Methods.* 2013;19.

4. de Bruin DM, Bremmer RH, Kodach VM, de Kinkelder R, van Marle J, van Leeuwen TG, Faber DJ. Optical phantoms of varying geometry based on thin building blocks with controlled optical properties. *J. Biomed. Opt.* 2010;15:25001.

5. Bus MTJ, Muller BG, de Bruin DM, Faber DJ, Kamphuis GM, van Leeuwen TG, de Reijke TM, de la Rosette JJMCH. Volumetric In-Vivo Visualization of Upper Urinary Tract Tumors Using Optical Coherence Tomography: A Pilot Study. *J. Urol.* 2013.

6. Cernohorsky P, de Bruin DM, van Herk M, Bras J, Faber DJ, Strackee SD, van Leeuwen TG. In-situ imaging of articular cartilage of the first carpometacarpal joint using co-registered optical coherence tomography and computed tomography. *J. Biomed. Opt.* 2012;17:60501.

7. Changoor A, Nelea M, Méthot S, Tran-Khanh N, Chevrier A, Restrepo A, Shive MS, Hoemann CD, Buschmann MD. Structural characteristics of the collagen network in human normal, degraded and repair articular cartilages observed in polarized light and scanning electron microscopies. *Osteoarthr. Cartil.* 2011;19:1458–1468.

8. Chu CR. Arthroscopic Microscopy of Articular Cartilage Using Optical Coherence Tomography. *Am. J. Sports Med.* 2004;32:699–709.

9. Chu CR, Izzo NJ, Irrgang JJ, Ferretti M, Studer RK. Clinical diagnosis of potentially treatable early articular cartilage degeneration using optical coherence tomography. *J. Biomed. Opt.* 2007;12:51703.

10. Chu CR, Williams A, Tolliver D, Kwoh CK, Bruno 3rd S, Irrgang JJ. Clinical optical coherence tomography of early articular cartilage degeneration in patients with degenerative meniscal tears. *Arthritis Rheumatol.* 2010;62:1412–1420.

11. Drexler W, Stamper D, Jesser C, Li X, Pitris C, Saunders K, Martin S, Lodge MB, Fujimoto JG, Brezinski ME. Correlation of collagen organization with polarization sensitive imaging of in vitro cartilage: Implications for osteoarthritis. *J. Rheumatol.* 2001;28:1311–1318.

12. Faber DJ, van der Meer FJ, Aalders MCG, van Leeuwen TG. Quantitative measurement of attenuation coefficients of weakly scattering media using optical coherence tomography. *Opt Express.* 2004;12:4353–4365.

13. Han C. Analysis of rabbit articular cartilage repair after chondrocyte implantation using optical coherence tomography. *Osteoarthr. Cartil.* 2003;11:111–121.

14. Van Leeuwen TG, Faber DJ, Aalders MC. Measurement of the axial point spread function in scattering media using single-mode fiber-based optical coherence tomography. *IEEE J. Sel. Top. Quantum Electron.* 2003;9:227–233.

15. Liu B, Vercollone C, Brezinski ME. Towards improved collagen assessment: Polarization-sensitive optical coherence tomography with tailored reference arm polarization. *Int. J. Biomed. Imaging.* 2012;2012.

65

Comparison of optical coherence tomography and histopathology in quantitative assessment of goat talus articular cartilage | **CHAPTER 3**

16. Niemelä T, Virén T, Liukkonen J, Argüelles D, te Moller NCR, Puhakka PH, Jurvelin JS, Tulamo R-M, Töyräs J. Application of optical coherence tomography enhances reproducibility of arthroscopic evaluation of equine joints. *Acta Vet. Scand.* 2014;56:3.

17. Pan Y, Li Z, Xie T, Chu CR. Hand-held arthroscopic optical coherence tomography for in vivo high-resolution imaging of articular cartilage. *J. Biomed. Opt.* 2003;8:648–54.

18. Pastoureau PC, Hunziker EB, Pelletier JP. Cartilage, bone and synovial histomorphometry in animal models of osteoarthritis. *Osteoarthr. Cartil.* 2010;18.

19. Saarakkala S, Wang S-Z, Huang Y-P, Zheng Y-P. Quantification of the optical surface reflection and surface roughness of articular cartilage using optical coherence tomography. *Phys. Med. Biol.* 2009;54:6837–6852.

20. Tearney GJ, Brezinski ME, Bouma BE, Hee MR, Southern JF, Fujimoto JG. Determination of the refractive index of highly scattering human tissue by optical coherence tomography. *Opt. Lett.* 1995;20:2258.

21. Virén T, Huang YP, Saarakkala S, Pulkkinen H, Tiitu V, Linjama A, Kiviranta I, Lammi MJ, Brünott A, Brommer H, Van Weeren R, Brama PAJ, Zheng YP, Jurvelin JS, Töyräs J. Comparison of ultrasound and optical coherence tomography techniques for evaluation of integrity of spontaneously repaired horse cartilage. *J. Med. Eng. Technol.* 2012;36:185–192.

22. Wessels R, de Bruin DM, Faber DJ, van Boven HH, Vincent AD, van Leeuwen TG, van Beurden M, Ruers TJM. Optical coherence tomography in vulvar intraepithelial neoplasia. *J. Biomed. Opt.* 2012;17:116022.

23. Xie T, Xia Y, Guo S, Hoover P, Chen Z, Peavy GM. Topographical variations in the polarization sensitivity of articular cartilage as determined by polarization-sensitive optical coherence tomography and polarized light microscopy. *J. Biomed. Opt.* 2008;13:54034.

24. Zheng K, Martin SD, Rashidifard CH, Liu B, Brezinski ME. In vivo micron-scale arthroscopic imaging of human knee osteoarthritis with optical coherence tomography: comparison with magnetic resonance imaging and arthroscopy. *Am. J. Orthop. (Belle Mead. NJ).* 2010;39:122–125.

PART II
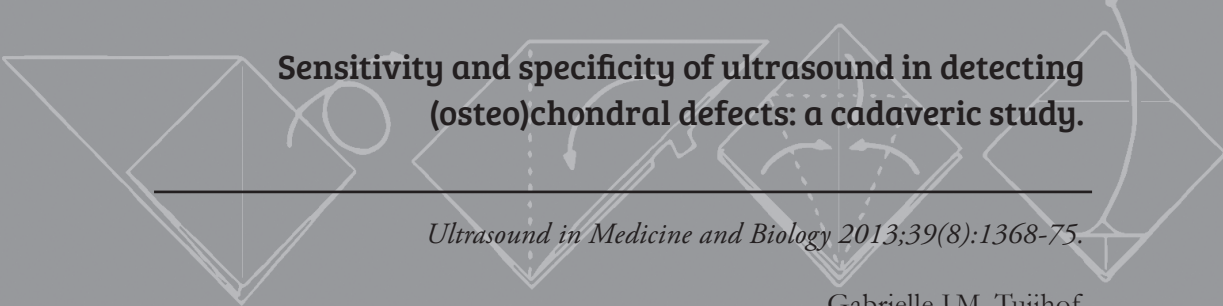
IMPROVING CLINICAL IMAGING
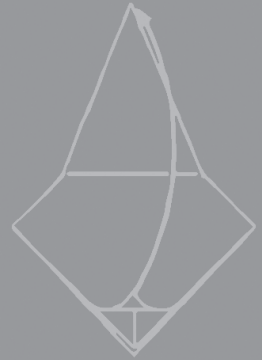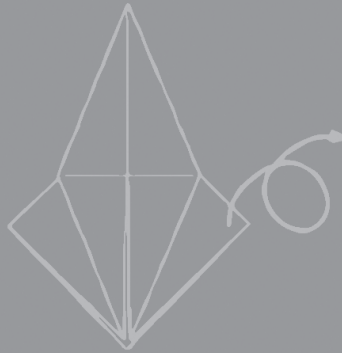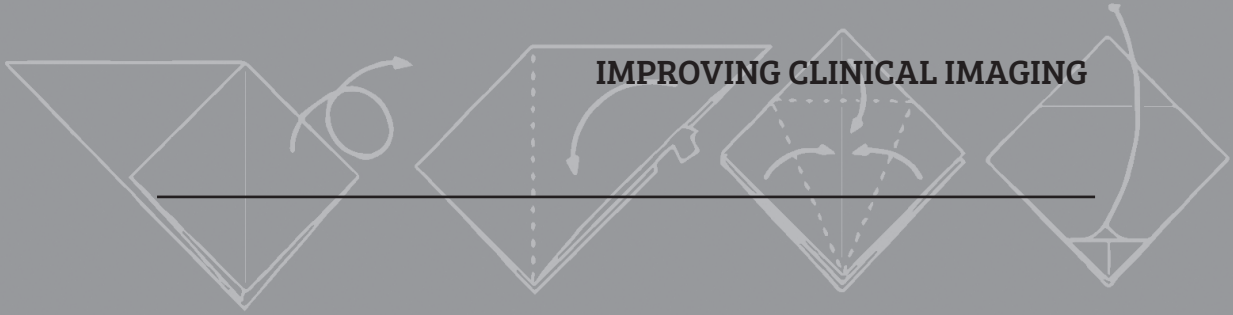
CHAPTER 4

Sensitivity and specificity of ultrasound in detecting (osteo)chondral defects: a cadaveric study.

Gabrielle J.M. Tuijhof
Aimée C. Kok
Maaike P. Terra
Juri F.A. Aaftink
Geert J. Streekstra
C. Niek van Dijk
Gino M.M.J. Kerkhoffs

Abstract

Background
The long-term prognosis of cartilage lesions evolving into an eroding subchondral bone defect is not known. Longitudinal monitoring using ultrasound could assist in overall understanding. The aim of the work described in this article was to determine the feasibility of using ultrasound to detect small (osteo-)chondral defects.

Materials and methods
On the anterior talar surface of ten human cadaveric ankles, at most four defects were arthroscopically created: two pure chondral defects 3 and 1.5 mm in diameter and two osteochondral defects 3 and 1.5 mm in diameter. All ankles were examined by two observers, and their ultrasound observations were validated using computed tomography scans and photographs.

Results
Overall sensitivity was 96% for observer 1 and 92% for observer 2, and specificity for both observers was 100%. 68% and 79% of defect sizes were within relevant limits of agreement (20.2 ± 1.0 mm), respectively.

Conclusion
Ultrasound imaging has the potential to detect small (osteo-)chondral defects located within visible areas.

Introduction

A chondral or an osteochondral defect (OCD) is described as the separation of a fragment of cartilage without or with damage to the underlying subchondral bone [15]. OCDs of the talus (OCDT) can be the result of sustained trauma like ankle sprains, possibly with remaining lateral instability or ankle and distal fibular fractures. These defects cause impairment because of deep joint pain, limited range of motion, stiffness, catching, locking and swelling [28]. Eventually they contribute to premature development of osteoarthritis [7, 19, 23], which is associated with disability. Systematic reviews have reported clinical success rates up to 86% for surgical treatment of OCDT [15, 28], achieved predominantly with arthroscopic debridement and drilling. The therapy failures cannot be contributed solely to patient characteristics, because the exact mechanism underlying the cartilage healing process after arthroscopic microfracturing is not fully understood [4, 26]. The long-term prognosis of untreated focal (osteo-)chondral defects is unknown.

Longitudinal monitoring of OCDT in patients at short intervals could contribute to the overall understanding of the mechanisms of cartilage pathogenesis and healing and eventually be used to optimize treatment. As normal radiographs are unsuitable for diagnosis of OCDT, additional scans are frequently obtained using magnetic resonance imaging (MRI) [5, 18] or computed tomography CT [17]. Both modalities serve as gold standards for imaging OCDT in the ankle joint [27]. However, they are less suited for longitudinal monitoring of patients at short intervals, because of ionizing radiation (CT) or timely image acquisition and limited availability (MRI). On-going developments in ultrasound, its true non-invasiveness and its cost-effectiveness [21] make it a valuable alternative candidate [14]. With respect to ultrasound imaging of cartilage and bony structures, recent studies have reported: (i) its clinical importance in detecting bone erosion [11, 20]; (ii) its potential to visualize an estimated minimum of 50% of the talar cartilage surface when the foot is in maximum plantar flexion [2] (approximately 80% of all OCDT are located in this area of the surface [8]; and (iii) guidelines to identify pathologic changes in cartilage and bone [10, 14].

In vitro studies on porcine and human knee specimens have indicated that ultrasound can be used to detect and grade OCDT from 4 mm in diameter accurately and reliably [6] also in a semi-clinical simulated setting [19]. The present study extended this research, focusing on the monitoring of patients suspected of having a talar OCD who do not receive surgical treatment in the acute phase of onset, as this could provide insight into the natural healing capacity of cartilage. This requires the detection of relatively small defects (smaller than 0.4 mm in diameter) in the ankle joint.

The additional challenge is that talar cartilage is on average twice as thin as knee joint cartilage [24], which might hamper the visibility of small lesions. Thus, the aim of this feasibility study was to determine the diagnostic capacity of ultrasound in detecting the presence or absence of particularly small chondral and osteochondral defects in the talus using a human ankle cadaver model.

Methods

Defect preparation

The following considerations were used to determine which defect types and sizes were to be studied. The theoretically smallest detectable defect size was derived from the wavelength, which was calculated by dividing the speed of sound in soft tissue (1540 m/s [13]) by the scanning frequency (10 MHz or higher). This gives a rough theoretical estimate of ultrasound scanner resolution of 0.15 mm. If noise is accounted for, this implies that the smallest detectable size is around 0.5 mm. From a clinical point of view, the size of the smallest osteochondral defects (called fissure) is unknown [18]. On the basis of MRI findings that describe the presence of fissures running perpendicular through the cartilage surface [18] and a mean cartilage thickness of approximately 1 mm [24], the smallest clinical fissure was estimated to be 1 mm in diameter. In a pilot study, the number of defects that could be created on the anterior talar surface and the types and sizes of the defects were determined using ultrasound equipment (T3000, 12L5-V linear probe, Terason Ultrasound, Burlington, MA, USA) and eight inexperienced observers. They were medical students who had no prior experience in ultrasound imaging. Before beginning the pilot study, the observers were allowed to practice for 5 minutes on a cadaver bone covered with muscle and skin. The observers were asked to detect six OCDT of 4 mm depth and three diameters (0.8, 1.7 and 4 mm) created on each talar surface of two cadaver ankles (12 OCD in total). This revealed that an OCD 4 mm in diameter could be detected with 90% sensitivity, which implied that 29 of 32 attempts indicated the presence of such an OCD.

Table 4.1: created conditions

Condition	Type of defect	Diameter	Disler grade [6]
Condition 0	no defect		
Condition 1	chondral	3 mm	2
Condition 2	osteochondral	3 mm	4
Condition 3	chondral	1.5 mm	2
Condition 4	osteochondral	1.5 mm	4

The size of the OCD could be determined without systematic error and with significant moderate reliability (ICC = 0.6, with a 95% confidence interval 0.4–0.8). On the basis of these estimations, and the fact that experienced observers would be used in this study, five conditions were defined (*Table 4.1*).

Defects were made via an anterior arthroscopic ankle approach (by G.M.M.J.K.) to mimic the clinical setting as closely as possible. This allowed normal ultrasound examination with intact soft tissue overlying the talus (*Fig. 4.1*). Ten fresh formerly frozen human cadaver ankles were accessed with routine arthroscopic equipment via the anteromedial and lateral portals [16]. Permission from the Medical Ethical Committee of the Academic Medical Centre in Amsterdam was not needed to use these cadavers. After inspection of the talar surface, up to four conditions were created in random order. There were five ankles with four conditions, four with three conditions and one with two conditions, for a total of 34 conditions. The defects were drilled manually under arthroscopic vision in a more or less horizontal line running from medial to lateral. After irrigation of the joint, the portals were sutured to prevent air from flowing into the joint.

Study design
Two observers—one experienced skeletal radiologist (M.P.T.) and one orthopaedic resident trained in ultrasound imaging of the ankle joint (A.C.K.)— performed the ultrasound evaluation blinded for number, location and type of defect.
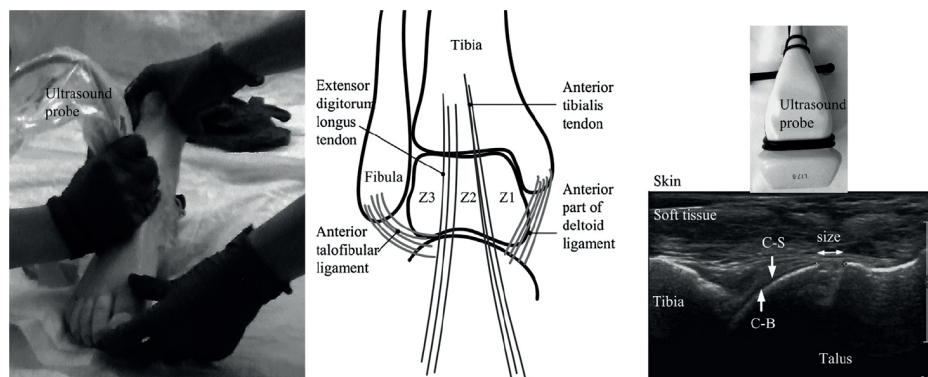
Figure. 4.1: study design
Left: Cadaver ankle positioned in plantar flexion with the ultrasound probe oriented in the sagittal plane. *Middle*: Frontal view of ankle joint showing the ligaments and tendons that form the three zones for localization on the anterior talar surface (Z1–Z3). *Right*: Ultrasound image recorded in the sagittal plane. C-B: cartilage-bone interface, C-S: cartilage-soft tissue interface, size: measurement of defect size between maximum interruptions of the C-B interface.

A state-of-the-art scanner was used (iU22 x Matrix Ultrasound System, Philips, Eind-hoven, The Netherlands) equipped with a 17-MHz linear array transducer (L17–5, Philips) and operated at standard musculoskeletal settings including a focus depth between 2.5 and 3.5 cm, a gain of 49% and a dynamic range of 70 dB. The observers were asked to determine the presence of defects and, on detection, to localize their position and grade (chondral vs. osteochondral) and size them. Each ankle was held in maximum plantar flexion to expose the anterior part of the talar surface (*Fig. 4.1*) [2]. As an aid in localization, the exposed ankle surface was divided into three zones as described in part by Elias et al. [8] (*Fig. 4.1*).

In practice, the three medial to lateral zones were identified by ligaments and ten-dons overlying the talar surface: zone 1 running from the anterior deltoid ligament to the lateral border of the tibialis anterior tendon; zone 2 running from lateral border of the tibialis anterior tendon to the medial border of the extensor digitorum longus tendon; and zone 3 running from the medial border of the extensor digi-torum longus tendon to the anterior talofibular ligament. The extensor digitorum longus tendon had not yet split into multiple branches at the level used to determine the zones. After identification of these anatomic landmarks, the actual observa-tions started. The observer inspected the talar surface and, on detecting a defect, localized it guided by the landmarks. As not all ankles exhibited all four defects, the observers were instructed not to image a certain zone as defined above (*Fig. 4.1*). In this way they remained blind to the number and type of defects to expect in each ankle. Subsequently, the observer graded the defect as chondral or osteochondral according to the guidelines suggested by Disler et al. and Grassi et al. [1, 6]. A defect was graded chondral if the ultrasound image revealed only discontinuation at the cartilage-soft tissue interface and damaged underlying cartilage (*Fig. 4.1*). A defect was graded osteochondral if disruptions were present at the cartilage-soft tissue and cartilage-bone interfaces (*Fig. 4.1*). Finally, the size of the defect was measured in the sagittal plane with the probe placed at an angle perpendicular to the underlying bone surface (*Fig. 4.1*). The image plane exhibiting the maximum defect size was determined and stored. The measurement tool provided by the ultrasound scanner was used to measure the straight distance from the most posterior point where the cartilage–bone or cartilage–soft tissue interface was first interrupted to the most anterior point of the interruption (*Fig. 4.1*). The complete protocol was repeated for all defects found in all 10 ankles by both observers.

Data processing and statistical analysis
To confirm the location, grade and size of the defects, CT scans of the cadaveric ankles, as well as photographs of the dissected talar surfaces, were obtained. CT

images were acquired on a Philips Brilliance 64 scanner (collimation 64 x 0.625 mm, pitch 0.875, tube voltage 120 kV, tube charge 400 mAs, voxel size 0.5 x 0.5 x 0.33 mm). Defect locations having a bony component were identified by an independent researcher (J.F.A.A.) on CT scans using the free software package ImageJ [22]. Defects were graded osteochondral if the CT scan revealed the slightest damage to bone; all other defects were graded chondral. Defect size was measured in the sagittal CT slice. A similar protocol was used to confirm the location of the chondral defect in photographs of dissected tali and to measure defect sizes vertically in the frontal plane.

The main outcome measures were the sensitivity and specificity of ultrasound in detecting the presence or absence of defects. These consisted of the percentage of conditions 1–4 correctly identified and the percentage of condition 0 correctly identified, respectively. For each observer, the percentage of correctly graded defects—osteochondral defects (conditions 2 and 4) and chondral defects (conditions 1 and 3)—and the percentage of correctly localized defects were determined as fractions of the total number of defects detected per observer. Agreement between defect size measurements made using ultrasound and measurements made from references values derived from CT scans and photographs, per observer, was visualized by constructing a Bland–Altman plot [3]. This rather strict method tends to reject rather than falsely accept the new clinical measurement method. To qualify for this analysis, only measurements of correctly identified and graded defects were included. We stated that ultrasound measurements are clinically as suitable as reference measurements if the differences are within the limits of agreement, χ_{diff} $\pm 2SD_{diff}$ (-0.2 x 1.0 mm), as reported by Mathiesen et al. [19]. Finally, the intra-class correlation coefficient (ICC) was determined to reflect inter-observer variation using the classification of Fleiss et al. [9], and a paired t-test was performed to identify the presence or absence of a systematic error between observers.

Results

Of the 40 conditions planned, 34 could be created, because in four ankles significant deterioration or lesions were found on arthroscopic inspection; in one ankle a defect of condition 3 could not be found on inspection of the dissected talus; and in one ankle a defect of condition 4 was accidentally created underneath another condition and was excluded.

After verification with CT scans and photographs, this resulted in 16 osteochondral defects, ten chondral defects and eight instances of no defect. *Figures 4.2* and *4.3*

are representative images of an osteochondral defect (condition 4) and a chondral defect (condition 1) that were correctly identified, graded, localized and sized with their corresponding reference images for comparison. Note the close resemblance of the bony contours in the CT slice and ultrasound images. The cartilage-soft tissue and cartilage-bone interfaces are both clearly disrupted in *Figure 4.2*, which indicates the presence of an osteochondral defect, whereas only the cartilage-soft tissue interface is disrupted in *Figure 4.3*, which indicates the presence of a chondral defect.

Sensitivity was 96% and 92% for observers 1 and 2, respectively, and specificity was 100% for both (*Table 4.2*). Both observers missed chondral defects (one vs. two). Overall correct grading of the defects was 92% for observer 1 and 79% for observer 2. Both observers graded two osteochondral defects incorrectly as chondral, one of which was the same defect (*Table 4.3*). Note that observer 2 tended to grade
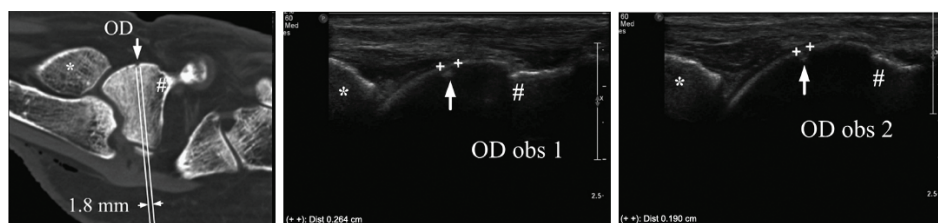
Figure 4.2: Representative example of a 1.5-mm-diameter grade 4 osteochondral defect (OD) as described by Disler et al. (2000) (condition 4)
Top: Reference CT slice in the sagittal plane. *Centre*: Ultrasound image of observer 1 ("obs 1") indicating the presence (*white arrow*) and size (#) of the defect. *Bottom*: Ultrasound image of observer 2 ("obs 2") indicating the presence (*white arrow*) and size (#) of the defect. The asterisk indicates the distal part of the tibia in all images.
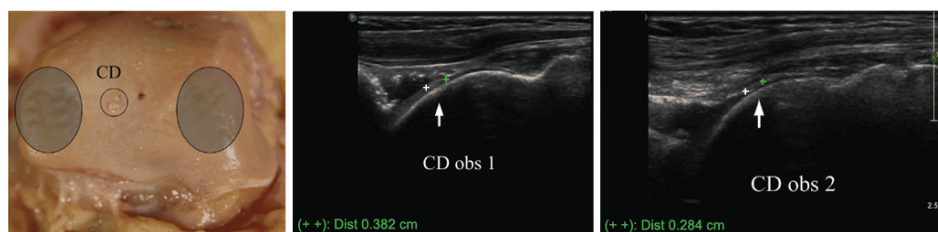
Figure 4.3: Representative example of a pure 3-mm-diameter grade 2 chondral defect (CD) as described by Disler et al. (2000) (condition 1)
Top: Reference digital photograph of dissected in the frontal plane. This talus had two regions where cartilage had already deteriorated (*ovals*). Chondral damage is indicated by the small circle. *Centre*: Ultrasound image of observer 1 ("obs 1") indicating the presence (*white arrow*) and size (#) of the defect. *Bottom*: Ultrasound image of observer 2 ("obs 2") indicating the presence (*white arrow*) and size (#) of the defect.

Table 4.2. Sensitivity and specificity for all conditions per observer

Item	Total number	Observer 1	Observer 2
		Sensitivity	
Conditions 1–4	26	25 (96%)	24 (92%)
		Specificity	
Condition 0	8	8 (100%)	8 (100%)

Table 4.3. Number and percentage of correct grading of defects for all conditions identified*

Condition	Number of conditions identified		Number of conditions graded correctly	
	Observer 1	Observer 2	Observer 1	Observer 2
Conditions 1–4	25	24	23 (92%)	19 (79%)
Conditions 2 and 4	16	16	14 (88%)	14 (88%)
Conditions 1 and 3	9	8	9 (100%)	5 (63%)
			Number of conditions located correctly	
Conditions 1–4			24 (96%)	23 (96%)

* Grading was either osteochondral (conditions 2 and 4, total = 16) or chondral (conditions 1 and 3, total = 10). Additionally, the number and percentage of correct localizations of a defect were determined using the three zones (*Fig. 4.1*).

chondral defects as osteochondral, which is expressed as a lower percentage of correct grading (*Table 4.3*). Both observers correctly localized all but one identified defect, which was the same one for both observers (*Table 4.3*). The mean size of all identified defects measured by observer 1 was 3.6 mm (SD = 1.2 mm), and that by observer 2 was 3.4 mm (SD = 1.0 mm). The mean for reference measurements was 3.6 mm (SD = 1.4 mm). The t-test indicated the absence of a systematic error between the observers (mean: -0.1 mm, 95% CI: -0.6 to 0.5 mm).

According to the Bland–Altman plot for observer 1, the limits of agreement ranged from -2.5 to 2.8 mm (*Fig. 4.4*), with two measurements outside this range. In the plot for observer 2, the limits of agreement ranged from -2.4 to 0.9 mm, with one measurement outside this range (*Fig. 4.4*). Subanalysis of osteochondral defects alone indicated a decrease in the limits of agreement: -1.4 to 2.0 mm for observer 1 and -1.5 to 1.5 mm for observer 2. Compared with the clinically accepted limits of agreement (-0.2 ±1.0 mm), one-third (observer 1) and one-fifth (observer 2) of all measurements fell outside this range (*Fig. 4.4*). Inter-observer variation for a single measurement was moderate (ICC 0.5), but the ICC increased to 0.7 when only osteochondral defects were analysed.
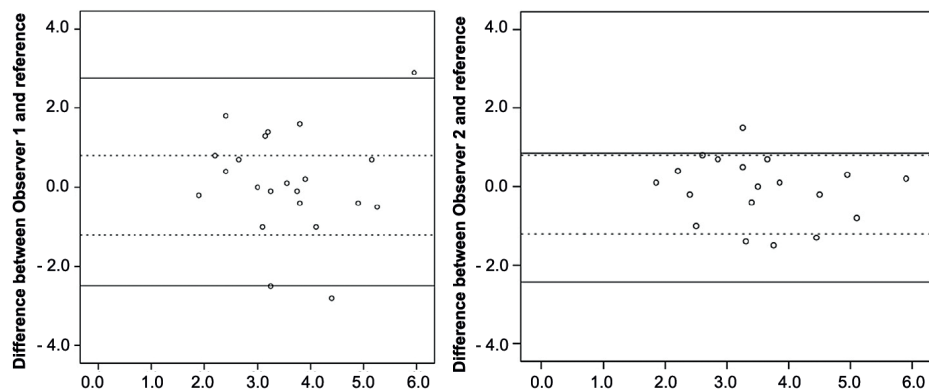
Figure 4.4: Bland–Altman plots of the difference between observer and reference values for defect size versus mean of defect sizes measured by observer on ultrasound images and references values measured on CT scans and photographs.

The limits of agreement ($\chi_{diff} \pm 2SD_{diff}$) for observer 1 are 0.1 ± 2.6 mm, and those for observer 2 are 20.8 ± 1.6 mm as indicated by the continuous lines. The clinically acceptable limits of agreement, as reported by Mathiesen et al. (2004), range from 21.2 to 0.8 mm (**dotted lines**).

Discussion

This study found that ultrasound is capable of identifying the presence or absence of small cartilage defects with or without bony involvement (*Tables 4.2 and 4.3*). Sensitivity and specificity are equally high, as described by Disler et al. [6], and the two observers disagreed on the presence versus absence of only one defect. This result is promising, because compared with that in Disler et al. [6], the defect size in this study was smaller, the talar cartilage surface was almost twice as thin as that of the knee and ultrasound observations were performed on cadaveric human ankles having intact overlying tissue to mimic a realistic clinical setting.

Apparently, disruption of the cartilage-soft tissue and cartilage–bone interfaces is a strong indicator of damage (*Figures 4.2 and 4.3*) and is minimally influenced by cartilage thickness and defect size.

The use of overlying tendons and ligaments to divide the cartilage surface into three zones was useful both for the observers to orient themselves and to prevent double identification of defects and for the researchers to match the reference images to the ultrasound images (*Figures 4.2 and 4.3*). Overall this resulted in 96% correct localizations. The defect grading was good, but less consistent than that reported by Mathiesen et al. [19]. In particular, observer 2 was challenged to grade chondral defects correctly. This can be partially explained by the method of defect creation, which did not allow for precise depth control of the defects as presented

by Mathiesen et al. [19]. This resulted in grade 3 (Disler et al. [6]) lesions running up to the cartilage-bone interface.

Defects were measured without systematic error and exhibited reasonable limits of agreement. Our reliability is moderate in comparison to other studies in which measurement of defect size or cartilage thickness was performed on ultrasound images [6, 11, 25]. However, our overall limits of agreement were twice as large as those reported by Mathiesen et al. [19].

For ultrasound to qualify for longitudinal monitoring, defect grading and accuracy and reliability of sizing should be high so that changes can be detected over time. As there is no indication of the actual accuracy required, the first step would to improve the method to achieve the highest accuracy possible, which can be achieved, as our study protocol had limitations. First, the defects created under the arthroscopic approach were slightly larger than the original drill head diameter, and in some cases, their alignment was slightly angulated to the bone surface. This increased resemblance to actual clinical practice, where patients do not present with perfect circular defects. For comparative analysis, the defect sizes measured on the reference images were taken. Second, sub-analysis of the osteochondral defect measurements alone revealed a higher ICC and smaller limits of agreement approaching those of Mathiesen et al. [19]. This indicates that measurements of talar defects in ultrasound images correspond highly to measurements in sagittal CT slices. As positioning the bones in the photographs in a sagittal plane would not allow defect size measurement, their orientation differed, which possibly introduced variation in the measurements. The use of MRI or CT arthrography could increase the accuracy of measurement of chondral defects, as these modalities can visualize cartilage surfaces, whereas CT cannot. Third, the total number of samples in this study was smaller than those in the other studies, which possibly increased the influence of outliers. The number of conditions was further decreased by the failure to create six conditions. Additionally, the cadavers were elderly persons, who, in general, have thinner cartilage than the intended patient group of relatively young and active adults. Fourth, our study protocol differed in essential aspects from those of the other studies [6, 19, 25], so an adequate power analysis could not be done. Finally, as this is a relatively new indication, the observers could benefit from intensive training. Evidence exists that intensive training results in high inter-observer agreement rates for the detection of bone erosions in patients with rheumatoid arthritis [11].

This study is of clinical importance, because it encourages further research on the applicability of ultrasound to longitudinal monitoring of OCDT. Of course, it must be

noted that ultrasound still has the major drawback of not being able to visualize the complete talar surface [10, 14, 21]. This requires careful selection of patients who have a defect in the visible talar surface area. In addition to the proposed measures to increase accuracy and reliability, image processing tools can be applied complementarily to discriminate subtle change in the course of time. An example is the image filter that is based on 2-D Log-Gabor filters and phase symmetry, results for which have been promising in small bony fractures [12].

Ultrasound imaging is said to be highly user dependent and to provide images that are more difficult to interpret compared with radiography, CT or MRI [10, 14, 21]. This feasibility study supports earlier findings [6, 11, 19, 25] that high observer reliability can be achieved for imaging pathology of cartilage and bone contours. Additionally, Figures 4.2 and 4.3 indicate high resemblance between ultrasound and CT images, which suggests that proper choice of recognizable imaging planes could decrease the difficulty of interpretation. In conclusion, this feasibility study has yielded the first results supporting the development of a protocol for longitudinal monitoring of patients at short intervals.

Acknowledgements

References

1. Backhaus M, Burmester GR, Gerber T, Grassi W, Machold KP, Swen WA, Wakefield RJ, Manger B. Guidelines for musculoskeletal ultrasound in rheumatology. *Ann. Rheum. Dis.* 2001;60:641–9.

2. Van Bergen CJ, Tuijthof GJ, Blankevoort L, Maas M, Kerkhoffs GM, Van Dijk CN. Computed tomography of the ankle in full plantar flexion: a reliable method for preoperative planning of arthroscopic access to osteochondral defects of the talus. *Arthroscopy.* 2012;28:985–992.

3. Bland JM, Altman DG. Cronbach's alpha. *BMJ.* 1997;314:572.

4. van Dijk CN, Reilingh ML, Zengerink M, van Bergen CJ. Osteochondral defects in the ankle: Why painful? *Knee Surgery, Sport. Traumatol. Arthrosc.* 2010;18:570–580.

5. Dipaola JD, Nelson DW, Colville MR. Characterizing osteochondral lesions by magnetic resonance imaging. *Arthroscopy.* 1991;7:101–104.

6. Disler DG, Raymond E, May DA, Wayne JS, McCauley TR. Articular Cartilage Defects: In Vitro Evaluation of Accuracy and Interobserver Reliability for Detection and Grading with US1. *Radiology.* 2000;215:846–851.

7. Elias I, Jung JW, Raikin SM, Schweitzer MW, Carrino JA, Morrison WB. Osteochondral lesions of the talus: change in MRI findings over time in talar lesions without operative intervention and implications for staging systems. *Foot Ankle Int.* 2006;27:157–166.

8. Elias I, Zoga AC, Morrison WB, Besser MP, Schweitzer ME, Raikin SM. Osteochondral lesions of the talus: localization and morphologic data from 424 patients using a novel anatomical grid scheme. *Foot Ankle Int.* 2007;28:154–161.

9. Fleiss JL, Levin B, Paik MC. The Measurement of Interrater Agreement. In: *Statistical Methods for Rates and Proportions.* John Wiley & Sons, Inc.; 2004:598–626.

10. Grassi W, Lamanna G, Farina A, Cervini C. Sonographic imaging of normal and osteoarthritic cartilage. *Semin Arthritis Rheum.* 1999;6:398–403.

11. Gutierrez M, Filippucci E, Ruta S, Salaffi F, Blasetti P, di Geso L, Grassi W. Inter-observer reliability of high-resolution ultrasonography in the assessment of bone erosions in patients with rheumatoid arthritis: Experience of an intensive dedicated training programme. *Rheumatology.* 2011;50:373–380.

12. Hacihaliloglu I, Abugharbieh R, Hodgson AJ, Rohling RN. Bone Surface Localization in Ultrasound Using Image Phase-Based Features. *Ultrasound Med. Biol.* 2009;35:1475–1487.

13. Halliwell M. A tutorial on ultrasonic physics and imaging techniques. *Proc. Inst. Mech. Eng. H.* 2010;224:127–142.

14. Keen HI, Conaghan PG. Usefulness of ultrasound in osteoarthritis. *Rheum Dis Clin North Am.* 2009;35:503–519.

15. Kok AC, Dunnen S den, Tuijthof GJ, van Dijk CN, Kerkhoffs GM. Is Technique Performance a Prognostic Factor in Bone Marrow Stimulation of the Talus? *J. Foot Ankle Surg.* 2012;51:777–782.

16. de Leeuw PAJ, van Sterkenburg MN, van Dijk CN. Arthroscopy and endoscopy of the ankle and hindfoot. *Sports Med. Arthrosc.* 2009;17:175–84.

17. Loomer R, Fisher C, Lloyd-Smith R, Sisler J, Cooney T. Osteochondral lesions of the talus. *Am J Sport. Med.* 1993;21:13–19.

18. De Maeseneer M, Shahabpour M, Van Roy P, Pouders C. MRI of cartilage and subchondral bone injury. A pictorial review. *JBR-BTR organe la Société R. Belge Radiol. / orgaan van K. Belgische Ver. voor Radiol.* 2008;91:6–13.

19. Mathiesen O, Konradsen L, Torp-Pedersen S, Jorgensen U, Jørgensen U. Ultrasonography and articular cartilage defects in the knee: an in vitro evaluation of the accuracy of cartilage thickness and defect size assessment. *Knee Surg Sport. Traumatol Arthrosc*. 2004;12:440–443.

20. McNally EG. Ultrasound of the small joints of the hands and feet: Current status. *Skeletal Radiol*. 2008;37:99–113.

21. Parker L, Nazarian LN, Carrino JA, Morrison WB, Grimaldi G, Frangos AJ, Levin DC, Rao VM. Musculoskeletal imaging: medicare use, costs, and potential for cost substitution. *J Am Coll Radiol*. 2008;5:182–188.

22. Rasband WS. ImageJ. *1997-2011*. 2011.

23. Saltzman CL, Salamon ML, Blanchard GM, Huff T, Hayes A, Buckwalter JA, Amendola A. Epidemiology of ankle arthritis: report of a consecutive series of 639 patients from a tertiary orthopaedic center. *Iowa Orthop J*. 2005;25:44–46.

24. Shepherd DE, Seedhom BB. Thickness of human articular cartilage in joints of the lower limb. *Ann Rheum Dis*. 1999;58:27–34.

25. Spannow AH, Pfeiffer-Jensen M, Andersen NT, Stenbøg E, Herlin T, Rheumatology P, Spannow AH, Pfeiffer-Jensen M, Andersen NT, Stenbøg E, Herlin T. Inter -and intraobserver variation of ultrasonographic cartilage thickness assessments in small and large joints in healthy children. *Pediatr. Rheumatol. Online J*. 2009;7:12.

26. Steadman JRJ, Briggs KKK, Rodrigo JJJ, Kocher MS, Gill TJ, Rodkey WG. Outcomes of microfracture for traumatic chondral defects of the knee: average 11-year follow-up. *Arthroscopy*. 2003;19:477–484.

27. Verhagen RA, Maas M, Dijkgraaf MG, Tol JL, Krips R, van Dijk CN. Prospective study on diagnostic strategies in osteochondral lesions of the talus. Is MRI superior to helical CT? *J Bone Jt. Surg Br*. 2005;87:41–46.

28. Zengerink M, Struijs PA, Tol JL, van Dijk CN. Treatment of osteochondral lesions of the talus: a systematic review. *Knee Surgery, Sport. Traumatol. Arthrosc*. 2010;18:238–246.

CHAPTER 5

Feasibility of ultrasound imaging of osteochondral defects in the ankle: a clinical pilot study.

Aimée C. Kok
Maaike P. Terra
Sebastian Muller
Christian Askeland
C. Niek van Dijk
Gino M.M.J. Kerkhoffs
Gabrielle J.M. Tuijhof
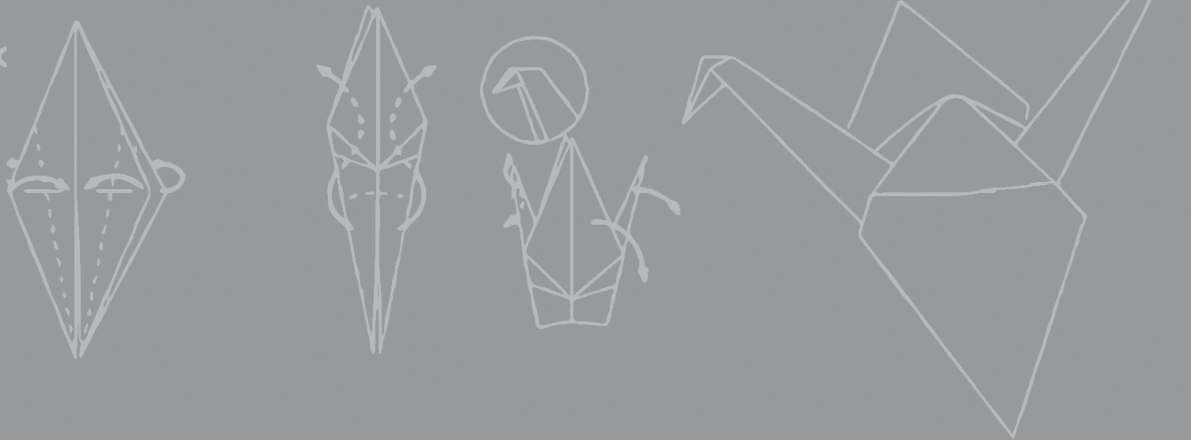
Abstract

Background
Talar osteochondral defects (OCDT) are imaged using magnetic resonance imaging (MRI) or computed tomography (CT). For extensive follow-up, ultrasound might be a fast, non-invasive alternative that images both bone and cartilage.

Aim
In this study the potential of ultrasound, as compared with CT, in the imaging and grading of OCDT is explored.

Methods
On the basis of prior CT scans, nine ankles of patients without OCDT and nine ankles of patients with anterocentral OCDT were selected and classified using the Loomer CT classification. A blinded expert skeletal radiologist imaged all ankles with ultrasound and recorded the presence of OCDT.

Results
Similar to CT, ultrasound revealed typical morphologic OCDT features, for example, cortex irregularities and loose fragments. Cartilage disruptions, Loomer grades IV (displaced fragment) and V (cyst with fibrous roof), were visible as well.

Conclusion
This study encourages further research on the use of ultrasound as a follow-up imaging modality for OCDT located anteriorly or centrally on the talar dome.

Introduction

The ankle is the second most predominant joint vulnerable to osteochondral defects (OCDT), exceeded only by the knee in prevalence [34]. Compared with defects seen in the knee, talar OCDT are usually smaller and more commonly involve bone [15, 30]. In general, OCDT have poor intrinsic healing potential because of the lack of vascularization of the cartilage, which leads to early development of osteoarthritis [11, 33].

Although there has been substantial research on cartilage regeneration in vitro [14, 21, 38], few studies have investigated cartilage tissue regeneration in vivo. Longitudinal monitoring of patients with OCDT at short intervals could contribute to this knowledge and assist in the formulation of patient-specific treatment algorithms.

The diagnostic techniques currently used for localization, sizing, grading and follow-up of OCDT are computed tomography (CT) [29, 31], magnetic resonance imaging (MRI) [20, 40] and arthroscopy [18, 27]. The suitability of these modalities for longitudinal follow-up varies, because of either the ionizing load (CT), the lengthy acquisition times (MRI) or the invasive nature of the procedure (intra-articular contrast is required to image cartilage with CT and arthroscopy).

Although ultrasound (US) has not been the preferred imaging modality for diagnosis of OCDT, its inherent characteristics qualify it for longitudinal monitoring. It is a non-invasive, cost-effective, fast and easily accessible technique in both experimental and clinical settings [37]. Recent studies have reported the ability of ultrasound to image abnormalities involving cartilage and the bony cortex in early and late-stage rheumatoid arthritis [4, 5, 16, 22, 23, 26]. Also, in vitro and in vivo US studies have been performed to determine structural bone quality, osteoporosis and nasal fractures [1, 28, 32].

The visibility of talar OCDT within reach of ultrasound is dictated by the over-projection of the tibia. Previous research on the suitability of lesions for anterior ankle arthroscopy has indicated that lesions in the posterior half of the talus do not appear in plantar flexion [3]. Therefore, only anterior and central lesions are within the scope of ultrasound examination, representing 70%–90% of all OCDT in the ankle [6, 12, 29, 34].

The goal of our study was to determine the feasibility of ultrasound for the visualization and grading of talar OCDT. To our knowledge, this is the first study to investigate

the feasibility of using ultrasound to image OCDT in a clinical setting and to image a group representative of patients with talar OCDT.

Methods

This study was approved by the medical ethics committee of the Academic Medical Centre (METC 2011_276). Eighteen patients were included. General inclusion criteria were: age below 18, single-ankle pathology without surgical treatment for OCDT and a CT scan of the ankle joint in the preceding two years. For each patient, we had a CT scan acquired either in full plantar flexion or in a neutral position. Nine patients were included with an osteochondral defect in the anterior or central zone, expected to be visualized using ultrasound. This was either determined by protrusion of the defect from beneath the tibia either in the full plantar flexion CT scan or in the neutral position CT scan using the guideline that the anterior 50% of the talar dome will protrude from beneath the tibia in full plantar flexion [3]. Nine additional patients who did not have an OCDT in the anterior talar dome served as negative controls. After receipt of a signed informed consent, the patient underwent a short physical examination to measure the degree of ankle flexion and to determine whether there were visible signs of ankle pathology, such as swelling and scars. The patient was instructed to fully plantarflex the ankle by placing the foot on the examination bench and moving backward while keeping the sole of the foot on the bench. The maximum degree of plantarflexion was measured and recorded using a goniometer. Patients were instructed not to discuss any specifics concerning their complaints or disease.

Computed tomography protocol

Computed tomography scans were acquired during regular clinical assessment of ankle complaints according to the clinical protocol of our institution (*Table 5.1*) with a Philips MX8000 Multidetector scanner (Philips Medical Systems Eindhoven, The Netherlands). Presence or absence of an OCDT was determined by different clinical radiologists unaware of the study, as part of routine clinical care. The defects were scored according to the classification of Loomer et al. [29]. This is a validated classification that uses bony aspects of a lesion to divide it into one of five grades: sub-chondral compression (grade I), partial osteochondral fracture (grade II), un-displaced complete osteochondral fracture (grade III), complete fracture with a displaced fragment (grade IV) and radiolucent defect with an intact roof (grade V). To estimate the location of the defect, the talus was divided into three equal zones: medial, central and lateral [12].

Table 5.1. Ultrasound and computed tomography settings*

Ultrasound		Computed tomography	
Parameter	Setting	Parameter	Setting
Frequency	17 MHz	Gantry tilt (degrees)	0
Depth	3.0 cm	Field of view (mm)	120
Gain	49%	Slice thickness (mm)	0.6
Frame rate	High	Increment (mm/rotation)	0.3
Frames per second	30	Image matrix	512 x 512
Dynamic range	70 dB	(row x column, isotrope volume)	
Persistence	2	Pitch	1.400
Clarity	High	Rotation time	1 s
		Resolution	High
		Radiation dose (mAs/slice)	160
		Reconstruction filter setting	E

* For the investigations, an iU22 xMatrix ultrasound scanner with a 17-5 MHz broadband linear array medical transducer and a MX8000 Multidetector computed tomography scanner were used (all Philips Medical Systems Eindhoven, The Netherlands).

Ultrasound protocol

After ensuring the ankle was in full plantar flexion and a neutral in-eversion position, an experienced musculoskeletal radiologist (M.T.) performed the ultrasound investigation using an iU22 xMatrix scanner (Philips Medical Systems) with a 17-5 MHz broadband linear array transducer (Philips Medical Systems) (*Table 5.1*).

The presence or absence of an OCDT was recorded based on the 2-D US images during the examination. Relevant US images were stored on digital video to allow comparison with the CT images. On detection, OCDT were localized and classified as osteochondral or chondral. In our study, chondral lesions at ultrasonography were defined as having a poorly visualized and blurred outer border of the cartilage, loss of cartilage transparency and/or increased echogenicity reflecting structural modification (*Fig. 5.1, II*). An osteochondral lesion was defined as a chondral lesion with subchondral flattening and/or disruption of the subchondral margin (*Fig. 5.1, IV*). Although chondral lesions cannot be observed with CT, their presence was documented to verify if the morphologic aspects described in ex vivo results are comparable to these in vivo results and whether ultrasound is able to image any type of defect [7, 10, 13, 16, 26, 37]. The osteochondral defects were used for comparison to the CT scan. Details on this protocol were presented earlier [39]. The talus was divided into three zones using the ankle tendons as an anatomic reference (*Fig. 5.2*).

Data analysis

The ability to detect OCDT with ultrasound was determined with CT diagnosis as the reference standard. Detection of an OCDT with ultrasound was considered correct if it was indicated as such in the same zone as on the CT scan. Because of the lack of an ultrasound classification system for OCDT, we considered as correct all ultrasound images that revealed a visible OCDT in the positive patient group with Loomer grades II–V. Loomer grade I was excluded, as this type of lesion has no superficial signs of disruption and, therefore, is not visible with ultrasound because of the limited penetration of ultrasound into bone [36]. Subsequently, a one on-one descriptive sub-analysis of the positive patient group was performed to describe the morphologic features on ultrasound images that are characteristic of the different Loomer grades of OCDT.

Results

One patient in the anterior OCDT group did not appear for the exam and was excluded. The eight remaining patients had a primary anterior or central OCDT as confirmed by CT. Patient characteristics were similar for both groups (*Table 5.2*). Ultrasound revealed the presence of an OCDT in seven patients (*Table 5.3*). Two chondral lesions were seen during the ultrasound exam. Five of the eight possibly detectable defects were detected with ultrasound (*Fig. 5.1*). Six of nine negative control patients were diagnosed by ultrasound as negative. Two of the false-positive ultrasound diagnoses were described as chondral lesions, which we were unable to objectify with the CT scans because they were acquired without intra-articular contrast and therefore not able to image cartilage.

Table 5.2. Patient characteristics

	OCD group	*Negative control group*	
Sex (male:female)	4:4	3:6	ns
Age (years)	41 (32–58)	47 (33–65)	ns
Side (right:left)	5:3	6:3	ns
Plantar flexion (degrees)	35 (20–45)	30 (15–45)	ns
Nature of pathology	Primary lesion (n = 8)	Subtalar OCD (n = 1)	
	Lateral (n = 1)	Posterior OCD (n = 3)	
	Medial (n=7)	Talonavicualr arthrosis (n = 1)	
		Peroneus longus rupture (n = 1)	
		Retrocalcaneal bursitis (n = 1)	
		No pathology on CT (n = 2)	

OCD: osteochondral defect; ns: no significant difference between groups.
All averages are presented as median (range).
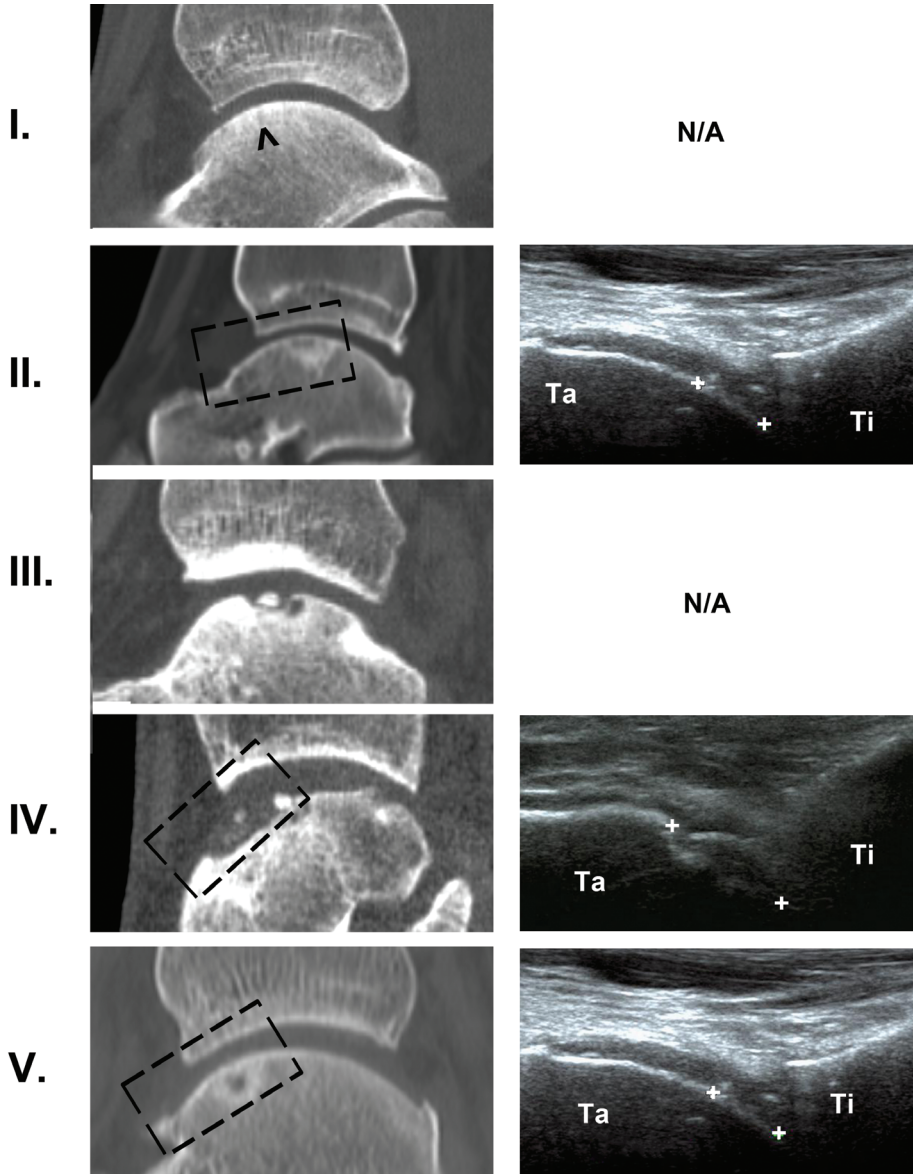
Figure 5.1. Comparison between computed tomography (CT) and ultrasound (US) images sorted on the basis of the Loomer classification.

I. Grade I (subchondral impression, arrowhead) was not visible on US. *II.* Grade II (incomplete fracture) was visualized as a disruption of the cartilage. *III.* Grade III (complete un-displaced fracture) was not visible. *IV.* Grade IV (complete displaced fracture) appeared as disruption of both cartilage and bone. *V.* Grade V (cyst with a fibrous roof) appeared as disruption of the cartilage with a pronounced shadow in the talar bone. *Ti: tibia, Ta: talus.*
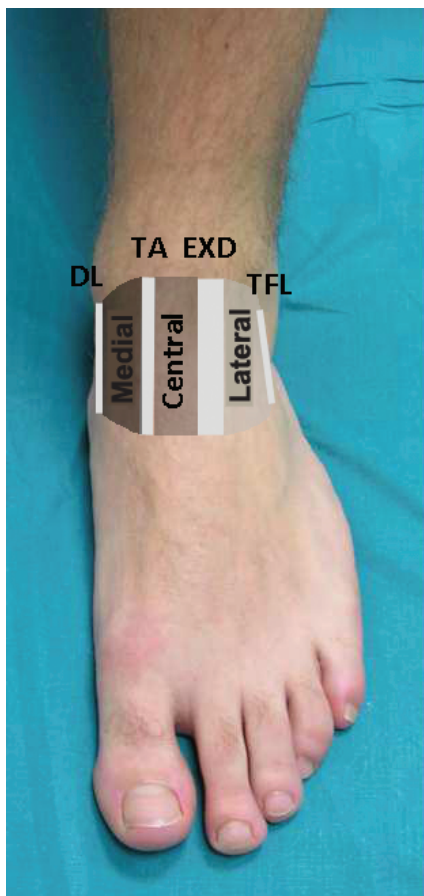
Figure 5.2 (left): Three zones are used to identify the location of the defects on ultrasound

The medial zone is defined by the anterior deltoid ligament medially and the lateral border of the tibialis anterior. The central zone is defined by the lateral border of the tibialis anterior and the medial border of the extensor digitorum longus tendon. The lateral zone is defined by the lateral border of the extensor digitorum longus tendon and the anterior talofibular ligament. *DL: deltoid ligament, TA: tibialis anterior, EXD: extensor digitorum, TFL: talofibular ligament.*
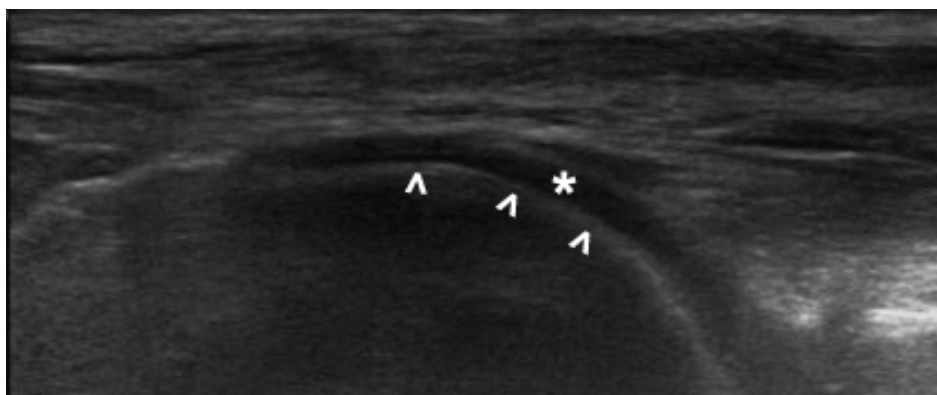
Figure 5.3 (below): Representative ultrasound image of the talus with the cartilage

The cartilage is represented by a hypo-echoic band (*) between the hyper-echoic line representing the osteochondral junction of the talus (*arrowheads*) below and the soft tissue above.

Table 5.3. Results of computed tomography and ultrasound examinations

CT scan			Corresponding ultrasound exam	
		n=	Positive (n=)	Negative (n=)
Osteochondral defects		**8**	**5**	**3**
Loomer grade				
I	Sub-chondral compression	1	-	1
II	Incomplete fracture	1	1	-
III	Un-displaced OCD	1	-	1
IV	Displaced OCD	3	2	1
V	Fibrous roof	2	2	-
No osteochondral defect		**9**	**4***	**6**

* Of which two chondral defects were undetectable with CT

Discussion

This article describes the findings of our clinical pilot study set up to determine the ability of ultrasound to image OCDT for future use in longitudinal follow-up of surgically treated OCDT. It was found that healthy and smooth cartilage, as well as chondral disruption and bone loss, were identified, indicating that ultrasound can differentiate between healthy cartilage and chondral and osteochondral defects.

On ultrasound images, cartilage was seen as a hypo-echoic band between the hyper-echoic line (osteochondral junction) below and the soft tissue above (*Fig. 5.3*). This band exhibits sharp margins when the probe is placed perpendicular to the talar surface. Damage to the cartilage had aspects similar to those previously reported in the knee in earlier ex vivo studies [7, 10, 13, 16, 26, 37]: narrowing of the hypo-echoic band with disruptions in the sharp edges and more hyper-echoic patches with blurring.

For osteochondral defects, the hyper-echoic line beneath the cartilage representing the osteochondral junction is disrupted (*Fig. 5.1, IV*). Cartilage thinning could also be detected as an indicator of degenerative arthropathy [25]. Talar cartilage is thinner than knee cartilage and the joint is more congruent [35], but the hyper-echoic zone and its relation to the surrounding bone and soft tissue appear similar to those of the femoral condyles as described by Iagnocco et al. [24] and Hammer and Terslev [17].

When ultrasound images were compared with CT images, the typical features of OCDT were recognizable in both modalities, such as an irregular bone cortex and loose fragments (*Fig. 5.1*). Also, for orientation purposes, it is convenient that the US images can be recorded in the sagittal plane, similar to sagittal CT images.

Our present results suggest that specific defect types are more suitable for follow-up with ultrasound than others. Subchondral depression and bone oedema (Loomer grade I) were not detected (*Fig. 5.1, I*). This is due to the limited penetration of ultrasound into bone [36]. An additional difficulty with these lesions is that the overlying cartilage is not affected, unlike more advanced stages of chondral pathology that could raise the suspicion of a lesion. Additional patients with depression of the subchondral bone would have to be imaged in future studies to determine the use of ultrasound for this type of lesion. In grade II incomplete fractures, ultrasound might not reveal very clear disruption of the osteochondral junction yet, because it is partially intact. But chondral disruptions in the cartilage above might indicate a defect, as was the case with the included lesion in this category (*Fig. 5.1, II*). Loomer grade III lesions with a partially resorbed un-displaced fragment were expected to exhibit a fissure between the stable rim of the adjacent cartilage and the fragment.

Based on the theoretical resolution that is achieved by ultrasound, such a fissure should be detectable if larger than 1.5 mm [39]. However, this was not seen in the one un-displaced fragment included in our study. Further research should explore the feasibility of using US to image these un-displaced fractures, focusing special attention on subtle differences of the osteochondral junction at the rim of the defect where the fissure can be expected. Displaced osteochondral fractures (Loomer grade IV) in the anterior half of the talus were visible on ultrasound in two of three patients (*Fig. 5.1, IV*). Fibrous defects with an intact roof were detected in both included cases (grade V) (*Fig. 5.1, V*). The last two types of lesions are indicated for surgery in both the acute and chronic phases [9, 29]. In pre-operative follow-up, it is clinically important to know when a smaller defect progresses into these operable stages or remains stable. Postoperatively, it is desirable to assess the fill grade of these defects with repair tissue [2]. Based on the results of the present study, we expect ultrasound to be able to provide suitable imaging for longitudinal monitoring of anterior OCDT. Because both chondral disruptions and disruptions of the osteochondral junction are visualized, ultrasound is also expected to detect progression of a chondral lesion into a deeper osteochondral lesion over time based on the presence or absence of disruption of the osteochondral junction.

A strength of this study was that a blinded observer diagnosed and recorded the defects following a standard protocol tested in a previous study [39]. Also, in addition to the initial exam, videos of the diagnostic process allowed in-depth post hoc analyses of the localization of the proposed defects and comparison of the ultrasound images with the CT scans.

The study also had limitations. Because of the small sample size in this feasibility study, our results are descriptive in nature. We were not able to calculate a reliable sensitivity or specificity. However, in our previous human cadaveric study, we obtained high sensitivity, specificity and inter-observer agreement for detection of artificially created ø 3to 15-mm cartilage defects [39]. The accuracy that can be achieved and which factors influence this accuracy remain to be investigated in a larger clinical study. For example, in one study the minimal cartilage thickness in the lateral femoral condyle was significantly over-estimated because the lateralization of the patella in flexion limited the field of view. Also, measurements made on transverse ultrasound scans that revealed a smaller part of the cartilage than the longitudinal scans agreed less with MRI than the longitudinal scans (Yoon et al. 2008). Which part of the talar surface is visualized using ultrasound and whether this surface area influences measurements as in the knee remain unknown.

The present study allowed us to examine different types of natural osteochondral defects, but we were not able to establish any differences in appearance based on aetiology. A study using ultrasound during arthroscopy did reveal differences in ultrasound magnitude between traumatic and atraumatic defects [19].

Another issue arose from using CT as the reference standard; in our centre, we prefer CT scans to MRI in the diagnostic and pre-operative workup of talar OCDT, because the cause of the symptomatic deep ankle pain in OCDT lies in the defect in the subchondral bone layer, not the aneural cartilage. This subchondral layer is visualized by CT [8], but it also implies that chondral disruptions seen on the ultrasound exam could not be validated. For this, MRI would be the appropriate reference.

A general limitation of using ultrasound to image the talar dome lies in the fact that not the entire talar dome can be imaged, making ultrasound unsuitable as a primary diagnostic tool. However, for easily accessible (post-operative) longitudinal follow-up, anterior and central defects could be followed at short intervals using the initial diagnostic CT or MRI scan as a reference.

In summary, this clinical pilot study indicates that cartilage disruptions, OCDT with a displaced fragment and lesions with a fibrous aspect should be visible on ultrasound when located in the anterior or central part of the talar dome, with a similarity in visualization to CT.

Acknowledgements

References

1. Ardeshirpour F, Ladner KM, Shores CG, Shockley WW. A preliminary study of the use of ultrasound in defining nasal fractures: Criteria for a confident diagnosis. *Ear, Nose Throat J.* 2013;92:508–512.

2. Van Bergen CJ, de Leeuw PAJ, van Dijk CN. Treatment of osteochondral defects of the talus. *Rev Chir Orthop Reparatrice Appar Mot.* 2008;94:398–408.

3. Van Bergen CJ, Tuijthof GJ, Blankevoort L, Maas M, Kerkhoffs GM, Van Dijk CN. Computed tomography of the ankle in full plantar flexion: a reliable method for preoperative planning of arthroscopic access to osteochondral defects of the talus. *Arthroscopy.* 2012;28:985–992.

4. Blackburn WD, Chivers S, Bernreuter W, Blackburn Jr. WD, Chivers S, Bernreuter W. Cartilage imaging in osteoarthritis. *Semin Arthritis Rheum.* 1996;25:273–281.

5. Castriota-Scanderbeg A, De Micheli V, Scarale MG, Bonetti MG, Cammisa M. Precision of sonographic measurement of articular cartilage: inter- and intraobserver analysis. *Skelet. Radiol.* 1996;25:545–549.

6. Choi WJ, Park KK, Kim BS, Lee JW. Osteochondral lesion of the talus: is there a critical defect size for poor outcome? *Am J Sport. Med.* 2009;37:1974–1980.

7. Delle Sedie A, Riente L, Bombardieri S. Limits and perspectives of ultrasound in the diagnosis and management of rheumatic diseases. *Mod Rheumatol.* 2008;18:125–131.

8. van Dijk CN, Reilingh ML, Zengerink M, van Bergen CJ. Osteochondral defects in the ankle: Why painful? *Knee Surgery, Sport. Traumatol. Arthrosc.* 2010;18:570–580.

9. Van Dijk CN, Scholte D. Arthroscopy of the ankle joint. *Arthroscopy.* 1997;13:90–96.

10. Disler DG, Raymond E, May DA, Wayne JS, McCauley TR. Articular Cartilage Defects: In Vitro Evaluation of Accuracy and Interobserver Reliability for Detection and Grading with US1. *Radiology.* 2000;215:846–851.

11. Elias I, Jung JW, Raikin SM, Schweitzer MW, Carrino JA, Morrison WB. Osteochondral lesions of the talus: change in MRI findings over time in talar lesions without operative intervention and implications for staging systems. *Foot Ankle Int.* 2006;27:157–166.

12. Elias I, Zoga AC, Morrison WB, Besser MP, Schweitzer ME, Raikin SM. Osteochondral lesions of the talus: localization and morphologic data from 424 patients using a novel anatomical grid scheme. *Foot Ankle Int.* 2007;28:154–161.

13. Fessell DP, Vanderschueren GM, Jacobson JA, Ceulemans RY, Prasad A, Craig JG, Bouffard JA, Shirazi KK, van Holsbeeck MT. US of the ankle: Technique, anatomy, and diagnosis of pathologic conditions. *Radiographics.* 1998;18:325–340.

14. Fortier LA, Barker JU, Strauss EJ, McCarrel TM, Cole BJ. The role of growth factors in cartilage repair. In: *Clinical Orthopaedics and Related Research.*Vol 469.; 2011:2706–2715.

15. Gobbi A, Francisco RA, Lubowitz JH, Allegra F, Canata G. Osteochondral lesions of the talus: randomized controlled trial comparing chondroplasty, microfracture, and osteochondral autograft transplantation. *Arthroscopy.* 2006;22:1085–1092.

16. Grassi W, Lamanna G, Farina A, Cervini C. Sonographic imaging of normal and osteoarthritic cartilage. *Semin Arthritis Rheum.* 1999;6:398–403.

17. Hammer HB, Terslev L. Role of ultrasound in managing rheumatoid arthritis. *Curr. Rheumatol. Rep.* 2012;14:438–444.

18. Hangody L, Kish G, Kárpáti Z, Szerb I, Udvarhelyi I, Modis L, Szerb I, Gaspar L, Dioszegi Z, Kendik Z. Mosaicplasty for the treatment of osteochondritis dissecans of the talus: two to seven year results in 36 patients. *Foot Ankle Int.* 2001;22:552–558.
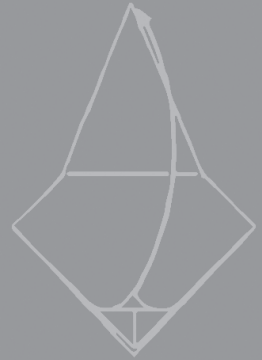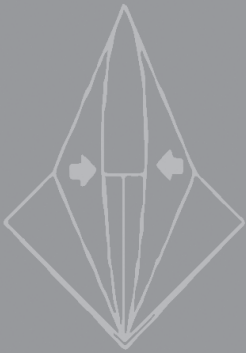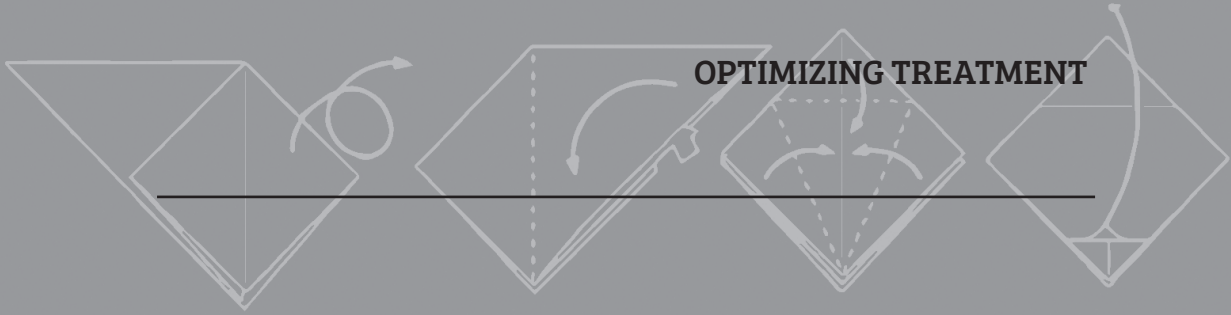
19. Hattori K, Kumai T, Takakura Y, Tanaka Y, Ikeuchi K. Ultrasound evaluation of cartilage damage in osteochondral lesions of the talar dome and correlation with clinical etiology: a preliminary report. *Foot Ankle Int*. 2007;28:208–213.

20. Hayter C, Potter H. Magnetic resonance imaging of cartilage repair techniques. *J Knee Surg*. 2011;24:225–240.

21. Hildner F, Albrecht C, Gabriel C, Redl H, van Griensven M. State of the art and future perspectives of articular cartilage regeneration: a focus on adipose-derived stem cells and platelet-derived products. *J Tissue Eng Regen Med*. 2011;5:e36-51.

22. Hodler J, Resnick D. Current status of imaging of articular cartilage. *Skelet. Radiol*. 1996;25:703–709.

23. Iagnocco A, Meenagh G, Riente L, Filippucci E, Delle Sedie A, Scire CA, Ceccarelli F, Montecucco C, Grassi W, Bombardieri S, Valesini G. Ultrasound imaging for the rheumatologist XXIX. Sonographic assessment of the knee in patients with osteoarthritis. *Clin Exp Rheumatol*. 2010;28:643–646.

24. Iagnocco A, Rheumatology A. Best Practice & Research Clinical Rheumatology Imaging the joint in osteoarthritis : a place for ultrasound ? *Best Pract. Res. Clin. Rheumatol.* 2010;24:27–38.

25. Karvonen RL, Negendank WG, Teitge RA, Reed AH, Miller PR, Fernandez- Madrid F. Factors affecting articular cartilage thickness in osteoarthritis and aging. *J. Rheumatol.* 1994;21:1310–1318.

26. Keen HI, Conaghan PG. Usefulness of ultrasound in osteoarthritis. *Rheum Dis Clin North Am*. 2009;35:503–519.

27. Lee KB, Bai LB, Yoon TR, Jung ST, Seon JK. Second-look arthroscopic findings and clinical outcomes after microfracture for osteochondral lesions of the talus. *Am. J. Sports Med.* 2009;37 Suppl 1:63S–70S.

28. Lee KI. Correlations of linear and nonlinear ultrasound parameters with density and microarchitectural parameters in trabecular bone. *J. Acoust. Soc. Am.* 2013;134:EL381-6.

29. Loomer R, Fisher C, Lloyd-Smith R, Sisler J, Cooney T. Osteochondral lesions of the talus. *Am J Sport. Med*. 1993;21:13–19.

30. Magnussen RA, Dunn WR, Carey JL, Spindler KP. Treatment of Focal Articular Cartilage Defects in the Knee A Systematic Review. *Clin Orthop Relat Res*. 2008;466:952–962.

31. O'Loughlin PF, Heyworth BE, Kennedy JG, Loughlin PF, Heyworth BE, Kennedy JG, Loughlin PF, Heyworth BE. Current concepts in the diagnosis and treatment of osteochondral lesions of the ankle. *Am. J. Sports Med.* 2010;38:392–404.

32. Pluskiewicz W, Adamczyk P, Drozdzowska B, Pyrkosz A, Halaba Z. Quantitative ultrasound and peripheral bone densitometry in patients with genetic disorders. *Ultrasound Med. Biol.* 2006;32:523–528.

33. Saltzman CL, Salamon ML, Blanchard GM, Huff T, Hayes A, Buckwalter JA, Amendola A. Epidemiology of ankle arthritis: report of a consecutive series of 639 patients from a tertiary orthopaedic center. *Iowa Orthop J*. 2005;25:44–46.

34. Saxena A, Eakin C. Articular talar injuries in athletes: results of microfracture and autogenous bone graft. *Am J Sport. Med*. 2007;35:1680–1687.

35. Shepherd DE, Seedhom BB. Thickness of human articular cartilage in joints of the lower limb. *Ann Rheum Dis*. 1999;58:27–34.

36. Smith J, Finnoff JT. Diagnostic and interventional musculoskeletal ultrasound: part 2. Clinical applications. *PM R*. 2009;1:162–177.

37. Spannow AH, Pfeiffer-Jensen M, Andersen NT, Stenbøg E, Herlin T, Rheumatology P, Spannow AH, Pfeiffer-Jensen M, Andersen NT, Stenbøg E, Herlin T. Inter -and intraobserver variation of ultrasonographic cartilage thickness assessments in small and large joints in healthy children. *Pediatr. Rheumatol. Online J.* 2009;7:12.

38. Spiller KL, Maher SA, Lowman AM. Hydrogels for the repair of articular cartilage defects. *Tissue Eng. Part B. Rev*. 2011;17:281–99.

39. Tuijthof GJ, Kok AC, Terra MP, Aaftink JFA, Streekstra GJ, van Dijk CN, Kerkhoffs GM. Sensitivity and specificity of ultrasound in detecting (osteo)chondral defects: A cadaveric study. *Ultrasound Med. Biol.* 2013;39:1368–1375.

40. Welsch G, Mamisch T, Domayer SE, Dorotka R, Kutscha-Lissberg F, Marlovits S, White LM, Trattnig S. Cartilage T2 assessment at 3-T MR imaging: in vivo differentiation of normal hyaline cartilage from reparative tissue after two cartilage repair procedures--initial experience. *Radiology*. 2008;247:154–161.
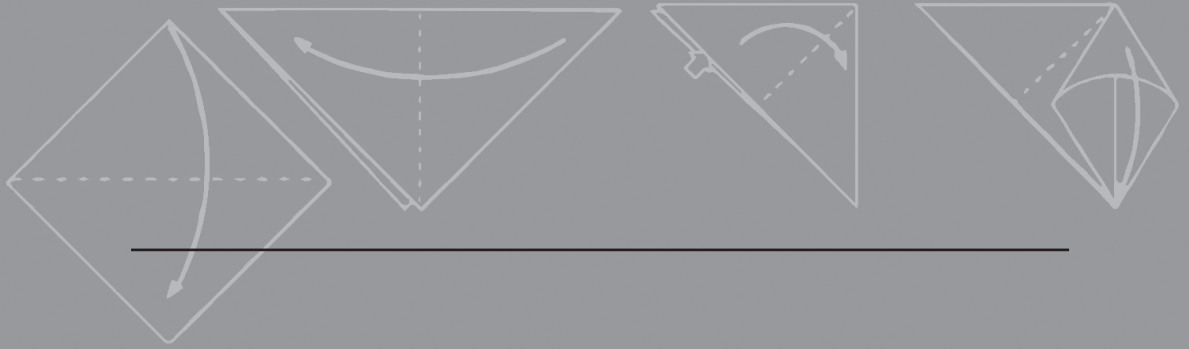
Feasibility of ultrasound imaging of osteochondral defects in the ankle: a clinical pilot study. | **CHAPTER 5**

PART III

CHAPTER 6

**The optimal injection technique for the osteoarthritic ankle:
A randomized, cross-over trial.**

Angelique Witteveen
Aimée C. Kok
Inger N. Sierevelt
Gino M.M.J. Kerkhoffs
C. Niek van Dijk
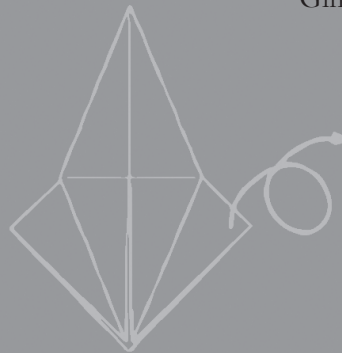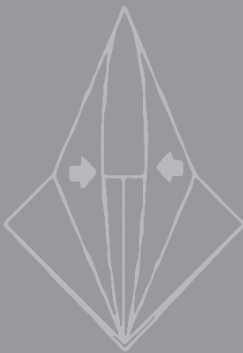
Abstract

Background
To optimize the injection technique for the osteoarthritic ankle in order to enhance the effect of intra-articular injections and minimize adverse events.

Methods
Randomized cross-over trial. Comparing two injection techniques in patients with symptomatic ankle osteoarthritis. Patients received an injection with hyaluronic acid using either one of the techniques. Four weeks later the second injection was given using the other technique. Primary outcome was the failure rate of the injection.

Results
Seventy patients fulfilled the study. The failure rate for both injection techniques was 24%. Forty-one patients in the traction group and thirty-nine in the group without traction experienced treatment related local adverse events. Other secondary outcomes did not show any difference between injection techniques.

Conclusions
There is no significant difference comparing the two injection methods regarding any of our formulated outcome measures. The use of contrast-aided fluoroscopy for injecting the severe osteoarthritic ankle can be advised at all times.

Introduction

Hyaluronic acid and steroid injections are nowadays frequently used as part of the conservative treatment for the osteo-arthritic joint [12]. Adverse reactions besides poor efficacy of hyaluronic acid are mainly contributed to extra-articular placements [1, 5, 20]

Osteoarthritis might stiffen the joint and osteophytes might block the way of the needle, which will make injecting the joint even more difficult. We treat patients with hyaluronic acid injections for more than ten years now. Patients experienced a lot of different adverse events and a variable result in efficacy of hyaluronic acid [20, 21]. This made us curious about how effective we are, injecting our patients intra-articularly. Two methods of injecting are used in our clinic; one using the injection technique that is commonly used for the ankle joint and one using a traction device that is commonly used for ankle arthroscopy [15, 18]. The traction device is believed to open up the joint, which might facilitate the injection [15]

An optimization of the injection technique could possibly enhance the efficacy of our intra articular injections and minimize the amount of adverse events. The primary aim of this study was to investigate the accuracy of intra-articular injections in the osteo-arthritic ankle joint using the traction device compared to the injection technique that is commonly used for the ankle joint [15, 18]. The secondary aim was to investigate the differences in the ease of the procedure, adverse events and patient reported outcomes.

Methods

Study design

This study was designed as a randomized cross-over trial with two treatment moments. Patients were recruited from our outpatient clinic. The patient's suit-ability was assessed and they were informed about the study. Written, informed consent was obtained from each patient prior to enrolment in the study. After sign-ing the informed consent, patients were randomized to one of two groups: group I first received an injection using the traction device, followed by an injection without traction a month later. Group II received the injection without traction followed by the injection with the traction device. The dosing schedule was based on our study of the safety and efficacy of hylan G-F 20 (Synvisc®) in patients with symptomatic ankle (talo-crural) osteoarthritis [20]. This study showed it is safe and effective to repeat the injection, in case of insufficient pain relief, after 1, 2 or 3 months. It was

therefore decided, in order to test both injection techniques, to offer each patient two injections with one month interval.

Injections were placed by one of the orthopaedic surgeons (AW) according to a standardized protocol. For randomization, an online randomization program (www. randomizer.org) was used. Due to the clear differences in treatment modalities, neither patients nor the treating surgeon (AW) could be blinded. The study protocol, patient information and patient consent form were approved by the internal review board (Medical Ethical Committee of the Academic Medical Center, Amsterdam).

Patient population
The study was open to patients of either gender presenting with osteoarthritic pain in the ankle ('study ankle') at our outpatient clinic, above 18 years of age in a general good health. Criteria for inclusion were: a clinical diagnosis of primary or secondary ankle OA confirmed by X-ray. Each X-ray was scored for the severity of osteoarthritis according to the van Dijk et al. scale [8]. An indication for a hyaluronic acid injection was made at clinic visit by the orthopaedic surgeon. Exclusion criteria were: no knowledge of the Dutch language or not able to understand the study protocol; patients who were allergic to contrast (Visipaque®); oral or parenteral anticoagulant therapy; clinically significant venous or lymphatic stasis in the study leg (oedema); patients with related hypersensitivities to avian protein or any components of hyaluronan-based injection devices; concomitant inflammatory arthropathy; any history of, or active skin infection at the injection site; any significant chronic skin disorder at the injection site; symptomatic peripheral vascular disease; women who were pregnant or nursing, or women of childbearing potential not using a medically acceptable form of birth control.

Treatment
Both injections (with and without the traction device) were placed through the anteromedial portal of the ankle joint as described for ankle arthroscopy using strict aseptic administration technique [17] Before the HA injection was performed, 0.5–1 ml of lidocaine (1%) was used subcutaneous as local analgesic. Intra-articular placement of the needle was assumed if no resistance was felt when injecting some local anaesthetic into the joint. A small amount (0.5–1 ml) of contrast fluid (Visipaque®) was injected by switching the syringe while holding the needle in place to determine the position of the needle on fluoroscopy. The X-ray beam was directed laterally. If the position was correct any fluid or effusion present in the joint was removed prior to the injection of 2 ml of hyaluronic acid (Fermathron®). If the position was not correct the needle was relocated and a small amount of additional contrast fluid injected until the position was found to be correct on X-ray.
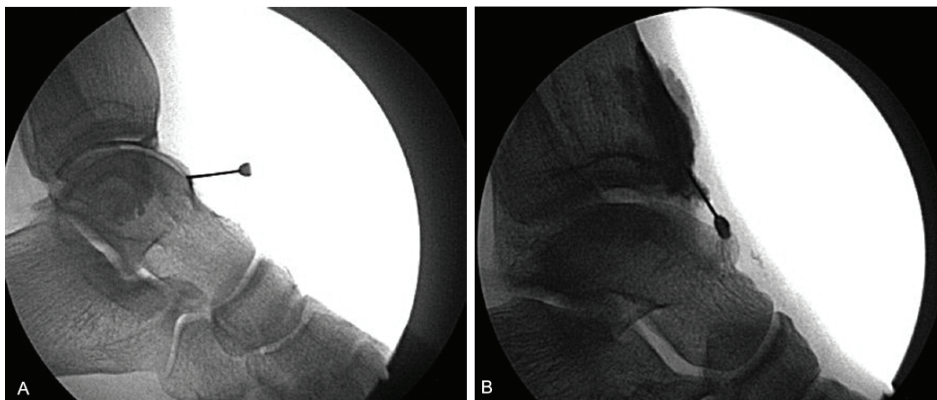
Figure 6.1. Intra- and extra-articular infiltration of the ankle in a lateral X ray
(A) Contrast fluid inside the joint (success); (B) contrast fluid outside the joint (failure).

In case of an injection with traction, the non-invasive ankle distraction device was applied after marking the injection site on the skin. Traction was applied after initial insertion of the needle after which the injection protocol was followed as would be in the injection without traction. The amount of traction was the same as in normal ankle arthroscopy and was applied for less than 1 minute. The second injection was performed by the same experienced physician who had administered the first injection (AW). This was done in the same manner using the other technique. Patients were allowed immediate full weight bearing when tolerated, but were advised not to perform any sport activities within two days after the injection.

Outcome measures
The primary outcome was the intra-articular needle positioning. The accuracy of the injection was determined by fluoroscope. The location of the injected contrast was registered as either inside (success) or outside (failure) the joint (*Fig. 6.1*).

Secondary outcomes were:
- Ease of procedure defined as the amount of relocations of the needle needed by the orthopaedic surgeon to assume that the needle was in the joint.
- The surgeon was asked how she experienced the injection procedure; this was registered in smooth, normal, difficult, extremely difficult.
- Adverse events (AEs), for each injection procedure the type, location and duration of each local adverse event was recorded together with the amount and type of rescue medication used by the patient to resolve these events. All patients were contacted by telephone one week after each injection to make inquiries for adverse events. In case of an adverse event this was repeated weekly until the adverse event resolved.

- The severity of any side effect experienced was registered using the 4-point scale, labelled as no side effects, mild (easily tolerated, caused minimal discomfort and did not interfere with everyday activities), moderate (caused sufficient discomfort to interfere with normal everyday activities), or severe (incapacitating and prevented normal everyday activities).
- Patient reported outcomes: pain during the injection; after each injection procedure each patient was asked to express the pain during the injection on a VAS score (0–100, 0 mm being no pain and 100 being extreme pain).
- Preference of injection technique; after the two injections each patient was asked which method he/she preferred and the reason why.

Statistical analysis

Sample size calculation was based on the primary end point (success rate). A difference of 20% of failure rates between the two methods was considered clinical relevant. Based on a power of 80% a two-sided alpha of 0.05, a sample size of 70 patients was needed. Statistical analysis was performed using SPSS 19.0 (IBM, Illinois, 2011). Due to skewed distributions, data were described as medians and ranges for continuous variables. Categorical outcomes were described as frequencies and percentages.

Prior to the main analysis in which the difference between the two injection modalities was evaluated, the presence of a carryover effect and a period effect was assessed. A carry-over effect implies that the effect of the first injection was still present when the patient received the second injection. This was assessed by analysing the difference in success rate between the two moments by use of a McNemar test. The sequence (period) effects consider whether the impact of the injection was different when the order of the injections was changed. The period effect was assessed by comparing the difference in success rate between the two injection modalities in group I to the difference in success rate between the two injection modalities in group II, by use of a Mann–Whitney U test.

For the secondary continuous or ordinal outcomes (VAS, degree of difficulty, amount of injections), the carry-over effect was assessed by analysing the difference between the first and the second injection using a Wilcoxon signed ranks test. The period effect was assessed by analysing the absolute difference between injections with and without traction between group I and II using Mann–Whitney U test. If a carry-over effect or period effect was present, the results of the second injection period were discarded from the analysis and only described per period.

For the main comparison of the two injection techniques, the difference in success rate between the two injection modalities was analysed using a McNemar test. Continuous and ordinal outcomes were analysed using a Wilcoxon signed ranks test. In case of period and carry over effects, non-paired chi-squared and Mann–Whitney U tests were performed for only the first injection group. Correlations between continuous and ordinal outcome measures were calculated by use of Spearman correlation coefficients. Significance level of <0.05 was considered statistically significant.

Results

Patient population
Seventy from 72 randomized patients fulfilled the study (*Fig. 6.2*). This group consisted of 40 male and 30 female patients (*Table 6.1*). Due to logistic reasons eight patients received the injection in inverse order and therefore changed injection groups (*Fig. 6.2*). Finally, 27 (38%) patients had a primary injection with traction first and 43 (62%) without traction.

Two patients in each group withdrew, both had a grade 2 Osteoarthritis (OA) (*Fig. 6.2*). One female patient withdrew after an easy intra-articular injection with traction, due to persisting pain after the injection, which lasted 14 days. This was graded as a severe adverse event. The other, male patient had an injection without traction, which ended up being extra-articular. This patient sustained a possible allergic reaction after the injection (swelling and severe pain), lasting a couple of days and resolving with pain medication. It was graded as a moderate adverse event. This patient was advised not to receive a second injection.

Since this is a cross-over study only patients that received both injections could be analysed statistically, therefore the results of these two patients were discarded from the analysis. However, since these patients had to withdraw because of the occurrence of adverse events, their first injections were analysed for these events. *Table 6.2* shows the success rate of the injections in both techniques. The success rate in both the traction group and the group without traction was 76%. An analysis was carried out of the first and last 15 patients to estimate the effect of a learning curve. Of the first 15 patients who were injected, 2/15 (13%) injections with traction were extra-articular compared to 5/15 (33%) without traction. Of the last 15 patients who were subjected to both injections, 2/15 (13%) of the injections in both the traction group and the group without traction were extra-articular. No significant learning curve was found (p = 0.32).

Table 6.1. Baseline demographics of included patients

	Total population	Group I	Group II
		traction-without traction	without traction-traction
	N=70	N=27	N=43
Gender			
Male	40 (57%)	16 (59%)	24 (56%)
Female	30 (43%)	11 (49%)	19 (44%)
Age, median (range)	45.0 (18-68 years)	43.7 (18-68 years)	48.0 (19-68 years)
Side			
Right	38 (54%)	13 (48%)	25 (58%)
Left	32 (46%)	14 (52%)	18 (42%)
Osteoarthritis grade (Van Dijk)			
Grade 1	1 (1%)	1 (4%)	0 (0%)
Grade 2	58 (83%)	21 (78%)	37 (86%)
Grade 3	11 (16%)	5 (18%)	6 (14%)

Ease of procedure

No significant difference was found in the amount of attempts to place the needle into the joint between both techniques (p = 0.18) (*Table 6.2*). There was no significant difference in how either injection procedure was perceived by the orthopaedic surgeon (p = 0.57) (*Table 6.2*). No significant relationship was found between the grade of osteoarthritis, the amount of attempts to get into the joint and how the injection was perceived by the surgeon with and without traction (0.24 < p < 0.94).

Adverse events

Forty-one patients (58%) experienced one or more adverse events after an injection with traction (*Table 6.3*). Ten injections were extra-articular, there was no difference between the type of adverse events between the extra-articular group and the intra-articular group. Most adverse events were mild or moderate in severity and resolved by itself or by walking on crutches for several days or taking pain medication (acetaminophen or NSAIDs) for a short period of time (less than three days). Thirty-nine patients (55%) experienced one or more adverse events after the injection without traction, eight were extra-articular. There was no difference between the type of adverse events between the extra-articular group and the intra-articular group (*Table 6.3*).

All adverse events resolved in a similar manner as mentioned above. Both groups had five patients that experienced severe adverse events. One of them was the patient that had to withdraw, as reported earlier. These adverse events consisted of the same type of events as the mild and moderate group and they resolved in the same way as mentioned above (*Table 6.3*).
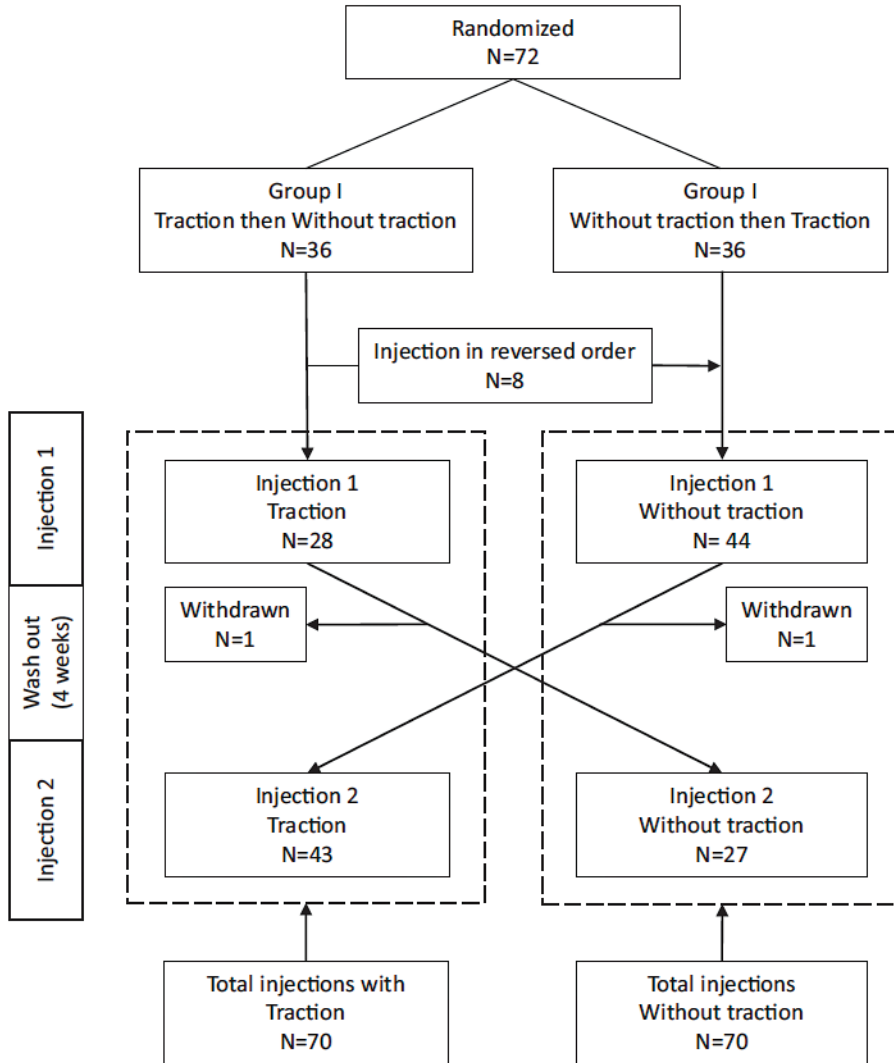
Figure 6.2. Composition of the two injection groups.

Patient reported outcomes

Pain during the injection

Due to the presence of a significant period effect and carry over effect ($p < 0.01$) concerning the VAS pain score of the patients, the results of the second injection were discarded from the analysis. The pain caused by the first injection was not significantly different between the injections with traction (median 7, range 0–80) and without traction (median 12, range 0– 64, $p = 0.88$) (*Table 6.4*). Grade 2 scored

Table 6.2. Success rate, ease of procedure and number of attempts until the surgeon was satisfied with the needle position.

	Injection with traction	Injection without traction
	N=70	N=70
Success rate of injections	53/70 (76%)	53/70 (76%))
Ease of procedure		
Smooth	13	16
Normal	40	36
Difficult	12	14
Extremely difficult	5	4
Number of attempts	2 (1–8)	2 (1–8)

Table 6.3. Types and severity of adverse events perceived after the injection.

	Injection with traction			Injection without traction		
Severity of AE	41/71 patients (58%)			39/71 patients (55%)		
	Mild N=20	Moderate N=16	Severe N=5	Mild N=25	Moderate N=9	Severe N=5
Types of adverse events and their frequency						
Pain	8	12	5	15	5	4
Swelling	7	9	3	11	5	3
Stiffness	0	2	0	0	1	1
Redness	1	3	0	0	0	0
Other (cold, warm, instability)	5	2	0	2	3	0
Total	**21**	**28**	**8**	**28**	**14**	**8**

a significantly lower median VAS score of 9.5 (range: 0–64) compared to median 49 (2–60) for grade 3 concerning the injections without traction (p = 0.03). For the injections with traction the difference between grade 2 (median 5 (0–80)) and grade 3 (median 21 (5–75) was not statistically significant (p = 0.18).

Preference for either technique

Patients were asked if they had a preference for either technique. Twenty-one (30%) answered no, twenty-six (37%) preferred without traction and twenty-three (33%) preferred traction.

Discussion

The present study evaluated the accuracy, the ease of the procedure, adverse events and patient reported outcomes of intra-articular injections in the osteo-arthritic ankle joint using a traction device compared to the injection technique without

Table 6.4. Patient reported outcome: pain (VAS 0-100 mm) perceived during the injection

	Group I				Group II			
	Injection 1 traction		*Injection 2 without traction*		*Injection 1 without traction*		*Injection 2 traction*	
	N	*VAS, median (range)*	*N*	*VAS, median (range)*	*N*	*VAS, median (range)*	*N*	*VAS, median (range)*
Total	**N=28**	**7 (0–80)**	**N=27**	**16 (0–70)**	**N= 44**	**12 (0–64)**	**N=43**	**32 (0–81)**
Van Dijk osteoarthritis grade								
Grade 1	N=1	0			N=0	n/a		
Grade 2	N=22	5 (0–80)		n/a*	N=38	9.5 (0–64)		n/a*
Grade 3	N=5	21 (5–75)			N=6	49 (2–60)		

*Due to the presence of a significant period effect and carry over effect (p < 0.01) concerning the VAS pain score of the patients, the results of the second injection were discarded from the analysis.

traction that is commonly used in the ankle joint. No optimal technique could be identified. Both injection techniques showed the same amount of failure rates (*Table 6.2*), 17/70 patients (24%). Due to the fact that joint opening could facilitate the intra-articular positioning of the needle we expected a higher success rate using the traction method. Different kinds of traction devices (invasive and non-invasive) are known to open up the ankle joint in patients under general and spinal anaesthesia. Joint opening up to 4.7 mm was described using an invasive distractor, a non-invasive distractor (the same as we used) created a joint opening of 4.3 mm in patients under anaesthesia [3, 15]. Most of these were not suffering from osteoarthritis. Dowdy used a non-invasive distractor to examine 7 healthy volunteers, with 14 ankles. He measured, under permanent direct lateral fluoroscopically imaging, an increase from 3.1 ± 0.5 mm to a mean of 4.2 ± 0.6 mm [9]. We did not examine the joint space opening in this study. The arthritic joint might open up less, which is a possible explanation for the same amount of failure rate.

The same five patients were initially injected extra-articular in both groups. Four had a grade 2 ankle OA (van Dijk scale) and one a grade 3. One of these grade 2 patients had a large osteophyte in the front of his ankle, which was clearly visible on the lateral X-ray. The grade 3 patients had a very stiff ankle with a fixed plantar flexion of 10°. A lot of these injections would have been placed extra-articular, if not for con-trast aided fluoroscopic control. Taking into account that patients in our study suffer from osteoarthritis, our failure rate is somewhat more positive than the failure rate Jones et al. showed; 24% vs. 33% [11]. However, our failure rate is still substantial and it seems advisable, in order to prevent failure of the injection in clinical practice, that more successful injection techniques will be investigated. Several suggestions have been made in literature to test placement of intra-articular injections using some alternative form of additional imaging. Bliddal et al. suggested fluoroscopically

controlled mini-air arthrography [5], Glattes et al. hypothesized that a small amount of air added to an intra-articular knee injection can confirm accurate placement by a squishing sound when moving the knee [10]. In both studies the placement was also verified by post-injection radiographs. Secondly, ultrasound guided injections are suggested in literature, however these injections have only been evaluated on cadaver feet without osteoarthritis [13, 16]. The added value of these alternative modalities remains to be investigated. At this moment, the best way to inject the ankle joint is still with the aid of fluoroscopy. If fluoroscopy is not available, the use of a traction device can potentially increase the success rate. The results of our small sub analysis showed an improvement of 20% (33% to 13%) of the amount of intra articular injections in the last 15 patients compared to the first 15 patients whereas the amount remained the same for the injections with traction (13%). However, this difference was not significant (p = 0.32).

Despite the fact we know all our injections ended up being intra-articular, we still have a considerable amount of adverse events (*Table 6.3*). Hyaluronic acid was only injected after we proved that the contrast fluid was intra-articular. We certainly were critical and decided to register every unwanted side effect, which might not be the case in other studies. Hyaluronic acid in itself is known to induce temporary benign side effects like pain, swelling, warmth [2, 6, 7, 19]. We have seen this before during our own research as well [20, 21]. Possibly higher molecular weight hyaluronic acid induces more side effects [6]. Fermathron, which we used, is a long chain molecule with a weight between 0.5 and 1.8 x 10^6 Da, this is considered a low molecular weight. At this point no clear explanation has been found for the relatively high incidence of adverse events [2, 14, 19, 22].

As for patient reported outcomes, patients were more painful at the second injection than at the first, hence the carry-over effect. This is a phenomenon we frequently observe in our daily practice. Possibly this is created by the injected hyaluronic acid at the first time-point. An injection of hyaluronic acid stimulates hyalocytes to produce larger chains of hyaluronic acid. These hyalocytes are synovial-lining cells. The stimulated synovial membrane might be painful on injection [4]. Patients with severe osteoarthritis (grade 3) seem to tolerate traction better, however it is only a small group of 11 patients (*Table 6.4*), so no real conclusions can be drawn. They indicated less pain compared to an injection without traction. However, these patients perceived more pain during either injection compared to the patients with grade 2 osteoarthritis (58 patients). An explanation for the preference for traction in severe osteoarthritis can be sought in the discomfort that will be created compress-ing osteophytes and irritated synovium by dorsiflexion of the ankle in the case of an

injection without traction, but again since this is just a small amount of patients no absolute recommendations can be made.

Conclusions
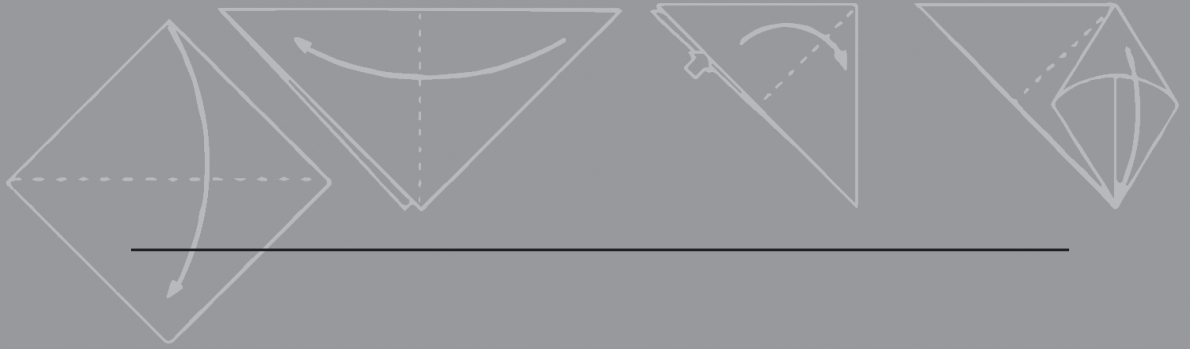
There is no significant difference between the two injection methods regarding any of our formulated outcome measures. Considering the substantial amount of possible extra articular injections prior to fluoroscopic control with both techniques, the use of contrast-aided fluoroscopy for injecting the ankle with severe osteoarthritis, anterolateral or anteromedial osteophytes is advisable.

References

1. Abate M, Schiavone C, Salini V. Hyaluronic acid in ankle osteoarthritis: Why evidence of efficacy is still lacking? *Clin. Exp. Rheumatol.* 2012;30:277–281.

2. Adams ME, Lussier AJ, Peyron JG. A risk-benefit assessment of injections of hyaluronan and its derivatives in the treatment of osteoarthritis of the knee. *Drug Saf.* 2000;23:115–30.

3. Albert J, Reiman P, Njus G, Kay DB, Theken R. Ligament strain and ankle joint opening during ankle distraction. *Arthrosc. J. Arthrosc. Relat. Surg.* 1992;8:469–473.

4. Balazs EA, Denlinger JL. Viscosupplementation: A new concept in the treatment of osteoarthritis. In: *Journal of Rheumatology*.Vol 20.; 1993:3–9.

5. Bliddal H. Placement of intra-articular injections verified by mini air-arthrography. *Ann. Rheum. Dis.* 1999;58:641–643.

6. Chang KV, Hsiao MY, Chen WS, Wang TG, Chien KL. Effectiveness of intra-articular hyaluronic acid for ankle osteoarthritis treatment: A systematic review and meta-analysis. *Arch. Phys. Med. Rehabil.* 2013;94:951–960.

7. Cohen MM, Altman RD, Hollstrom R, Hollstrom C, Sun C, Gipson B. Safety and efficacy of intra-articular sodium hyaluronate (Hyalgan) in a randomized, double-blind study for osteoarthritis of the ankle. *Foot ankle Int.* 2008;29:657–663.

8. Van Dijk CN, Scholte D. Arthroscopy of the ankle joint. *Arthroscopy*. 1997;13:90–96.

9. Dowdy PA, Watson B V, Amendola A, Brown JD. Noninvasive Ankle Distraction: Relationship Between Force, Magnitude of Distraction, and Nerve Conduction Abnormalities. *Arthroscopy*. 1996;12:64–69.

10. Glattes RC, Spindler KP, Blanchard GM, Rohmiller MT, Mccarty EC, Block J. A Simple, Accurate Method to Confirm Placement of Intra-articular Knee Injection. *Am. J. Sports Med.* 2002;32:1029–1031.

11. Jones A, Regan M, Ledingham J, Pattrick M, Manhire A, Doherty M. Importance of placement of intra-articular steroid injections. *BMJ*. 1993;307:1329–30.

12. Kalunian K. Nonpharmacologic therapy of osteoarthritis. *UpToDate*. 2012.

13. Khosla S, Thiele R, Baumhauer JF. Ultrasound guidance for intra-articular injections of the foot and ankle. *Foot ankle Int.* 2009;30:886–890.

14. Moskowitz RW. Hyaluronic acid supplementation. *Curr. Rheumatol. Rep.* 2000;2:466–71.

15. Niek Van Dijk C, Verhagen RAW, Tol HJL. Resterilizable noninvasive ankle distraction device. *Arthrosc. - J. Arthrosc. Relat. Surg.* 2001;17:1–5.

16. Reach JS, Easley ME, Chuckpaiwong B, Nunley J a. Accuracy of ultrasound guided injections in the foot and ankle. *Foot ankle Int.* 2009;30:239–242.

17. Schuman L, Struijs PA, Dijk CN Van. Arthroscopic treatment for osteochondral defects of the talus. *J Bone Jt. Surg Br*. 2002;84:364–368.

18. Tallia AF, Cardone DA. Diagnostic and therapeutic injection of the ankle and foot. *Am. Fam. Physician*. 2003;68:1356–1362.

19. Waddell DD. The tolerability of viscosupplementation: low incidence and clinical management of local adverse events. *Curr. Med. Res. Opin.* 2003;19:575–580.

20. Witteveen AGH, Giannini S, Guido G, Jerosch J, Lohrer H, Vannini F, Donati L, Schulz A, Scholl J, Sierevelt IN, van Dijk CN. A prospective multi-centre, open study of the safety and efficacy of hylan G-F 20 (Synvisc®) in patients with symptomatic ankle (talo-crural) osteoarthritis. *Foot Ankle Surg.* 2008;14:145–152.

21. Witteveen AGH, Sierevelt IN, Blankevoort L, Kerkhoffs GM, van Dijk CN. Intra-articular sodium hyaluronate injections in the osteoarthritic ankle joint: Effects, safety and dose dependency. *Foot Ankle Surg.* 2010;16:159–163.

22. Wright KE, Maurer SG, Di Cesare PE. Viscosupplementation for osteoarthritis. *Am. J. Orthop. (Belle Mead. NJ).* 2000.

The optimal injection technique for the osteoarthritic ankle: A randomized, cross-over trial. | **CHAPTER 6**

CHAPTER 7

Is technique performance a prognostic factor in bone marrow stimulation of the talus?

Aimée C. Kok
Steven den Dunnen
Gabrielle J.M. Tuijthof
C. Niek van Dijk
Gino M.M.J. Kerkhoffs
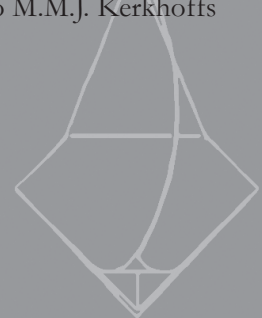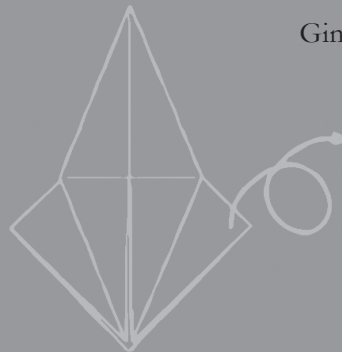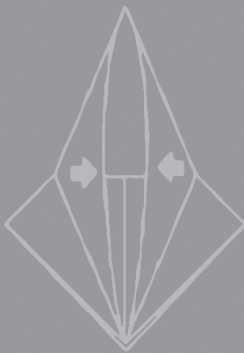
Abstract

Background
Although results of bone marrow stimulation in osteochondral defects of the talus (OCDT) have been satisfactory, the technique performance has not yet been subjected to review as a prognostic factor.

Aim
The aim of this systematic review is to determine whether variation within technique influences outcome of bone marrow stimulation for OCDT.

Methods
Electronic databases were searched for articles on OCDT treated with bone marrow stimulation techniques, providing a technique description. Six articles on microfracture were included (198 patients). Lesion size averaged 0.9 cm^2 to 4.5 cm^2, and follow-up varied from 2 to 6 years.

Results
Key elements were removal of unstable cartilage, hole depth variation between 2 and 4 mm until bleeding or fat droplets occurred, and a distance between the created holes of 3 to 4 mm. The success rate (excellent/good results by any clinical outcome score) was 81%. There is a vast similarity in the technique with similar outcomes as in previous general reviews; therefore, variation in technique as currently described in the literature does not seem to influence the outcome of bone marrow stimulation for OCDT.

Conclusion
Whether the instruments used or the hole depth and geometry influence clinical outcome remains to be determined. Microfracture is safe and effective for OCDTs smaller than 15 mm. However, in this review, only 81% of patients obtained satisfactory results. Larger clinical trials are needed with clearly defined patient groups, technique descriptions, and reproducible outcome measures to provide insight in the specific indications and the preferred technique of bone marrow stimulation.

Introduction

An osteochondral defect is a lesion involving articular cartilage and subchondral bone often caused by a traumatic event. Osteochondral lesions of the talus (OCDT) are reported in more than 6% of acute ankle sprains [8, 40], up to 25% in chronic lateral ankle instability [15], and up to 50% of acute ankle fractures [41]. Symptoms are deep ankle pain on weight bearing and prolonged joint swelling. When conservative treatment does not lead to satisfactory results, arthroscopic debridement and bone marrow stimulation are simple and cost-effective operative treatments with a lower morbidity rate and a faster return to activity than open surgery [9, 14, 19, 41, 49]. Bone marrow stimulation is performed during arthroscopy by drilling the subchondral bone [1, 31, 38] or by using an arthroscopic awl to create microfracture holes [2, 46]. The subsequent bleeding induces an intrinsic healing process involving mesenchymal stem cells located in bone marrow, which results in fibrocartilage formation in the defect [44].

The results of bone marrow stimulation in OCDT have been satisfactory in 61% and up to 86% of patients [48, 49]. Recent studies in both the talus and the knee joint have analysed the influence of possible prognostic factors, such as lesion size [14, 20], location [14, 43], age [14, 30, 46], or body weight [20, 25] to account for the rate of therapy failure, but many results are contradictory and remain inconclusive [14, 33].

To our knowledge, there are no studies or reviews that have taken the specific operative technique of bone marrow stimulation into account. Because it is an invasive procedure, it is important to investigate the execution of the technique and the possible effects of its variation on the outcome [12, 45]. This includes the choice for either drilling or using an awl, because differences in biological reaction between drilling and the use of an awl have been observed in animal studies because of heat necrosis and impacted bone fragments [10, 12]. Also, we believe that paying greater attention to each separate step in the bone marrow stimulation procedure is important because each step has a different biological significance. This will be discussed in greater detail in the methods section.

The primary aim of this systematic review was to analyse the technique variation of bone marrow stimulation for treatment of osteochondral defects of the talus. Our hypothesis was that there is variation in the key steps of the technique performance with the key steps defined as debridement, introduction of the holes, and confirmation of adequate bleeding. We expected variation in the extent of debridement, instruments used, and dimensions and dispersion of the holes, as well as introduction of additional steps to the procedure. This allowed us to determine whether the technique itself is a prognostic factor for treatment outcome.

124

CHAPTER 7 | Is technique performance a prognostic factor in bone marrow stimulation of the talus?

Materials and Methods

Electronic databases (Cochrane Central Register of Controlled Trials, MEDLINE, EMBASE [classic]) were used for searching for clinical studies on microfracture or debridement and drilling published between 1946 and September 2010. Search terms for title and abstract were "microfracture," "subchondral drilling," "subchondral arthroplasty," (also as MeSH term), or "Pridie drilling." The references of eligible articles were screened by hand for additional articles.

Full-text articles with original patient groups were included when a clear description of the type of bone marrow stimulation treatment and details on the technique were given. Descriptive articles without patient groups, animal studies, articles on microfracture outcomes without a clear description of the technique, and case reports were excluded. All English, Dutch, German, French, and Italian articles were included (*Fig. 7.1*).

All articles were independently screened by two reviewers (A.K. and S.D.) by title and abstract. If the article was possibly eligible or the nature of the article was unclear, the full text was consulted. Any disagreement on inclusion or exclusion between the reviewers was resolved by discussion. Third-party adjudication was not necessary.

The level of evidence was assessed by both reviewers using the Levels of Evidence for Primary Research Question Chart of the Centre for Evidence-Based Medicine
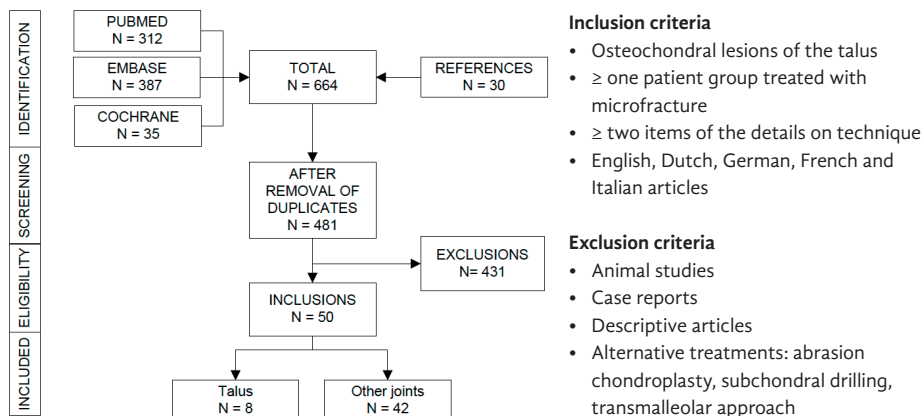
Figure 7.1. Flow chart outlining the article selection process
From the 664 identified articles, 50 articles remained after screening the title and abstract for eligibility and duplicate removal. In 42 articles the bone marrow stimulation was performed on other joints (the knee, the hip, the shoulder or the hallux). Six studies used awls to perform bone marrow stimulation. The remaining two studies used drilling with K wires. We excluded these two studies from further review because of a large risk of selection bias.

(Oxford, UK) as adapted by the Journal of Bone and Joint Surgery [3]. Included articles were scored on each of the items displayed in *Table 7.2*.

The included articles were scored on the key elements of the technique, which were taken from the original article by Steadman et al [46], based on the key features to elicit the biological reaction that should take place. Sufficient debridement of the lesion is the first of the essential steps in this technique, first described by Magnuson [34]. Debridement of loose flaps prevents residual tissue to hamper the development of repair tissue. In addition to this mechanical factor, the removal can also decrease the inflammatory response within the joint that is caused by the damaged tissue. Debridement can decrease symptoms, but will not prevent the deterioration of the lesion [28]. Additional procedures at this stage are first the removal of the calcified tissue, if the base of the lesion has calcified. Removing this calcified layer first will improve the bonding of the repair tissue [18]. The preparation of a perpendicular rim creates a stable and defined defect that is surrounded by healthy cartilage as a solid scaffold for the repair tissue. The formation of repair tissue is induced by the introduction of pluripotent mesenchymal stem cells from the subchondral vascular bone marrow. Defects that do not involve the subchondral bone plate and the boundary between the cartilage and the bone are secluded from this pool. This is the reason that abrasion of the base of the lesion alone is likely to not induce healing of the lesion [26, 36]. Also, it is known that pure chondral defects do not show intrinsic healing, because the subchondral bone plate is still intact. By penetrating the subchondral bone plate, an access is created, whether this is with an awl or by drilling. Too extensive debridement of the subchondral bone creates a risk of bone overgrowth and a thinner repair cartilage.

When placing the holes, it is important to leave sufficient space between the holes to prevent the intermediate bone from becoming unstable [35]. Also, the depth of the holes should be ample because shallow holes will not bleed and thus do not cause an influx of mesenchymal stem cells.

PASW Statistics 18.0.5 (IBM Corporation, Somers, NY) was used for data collection and analysis. Participants were patients with osteochondral defects of the talus who were treated by means of debridement and subsequent microfracture or subchondral drilling after failure of conservative therapy. Diagnosis was made by clinical evaluation and confirmed by conventional radiograph, MRI, and/or CT scan. The ankle joint was free of concomitant diseases, such as osteoarthritis, rheumatic arthritis, and associated injuries. Failure rate was defined as the necessity of reoperation because of persistent complaints, and/or a score below 70 points using the American Orthopaedic Foot and Ankle Society's Ankle Hindfoot Score (AOFAS-AHS). When there

CHAPTER 7 | Is technique performance a prognostic factor in bone marrow stimulation of the talus?

126

Table 7.1. Characteristics of the patient groups that received bone marrow stimulation of the included articles

Author/Year of publication	Level of evidence	Cases (ankles)	M:F	Age in years (range)	Follow-up in months (range)	Cases lost to follow-up	Lesion size in cm²	% traumatic	Location lesion (N=, %)							
									Medial			Lateral			Central	Medial and lateral
									Anterior	Central	Posterior	Anterior	Central	Posterior		
Becher et al. 2010	Level IV	45	25:20	40 (16-74)	70 (16-115)	6	0.5 – 2,0	69%	|------30 (67%)------|			|------11 (24%)------|		-	4 (9%)
Choi et al. 2009	Level III	51	37:14	35 (13-66)	44 (16-70)	0	1 (0.3-2.3)	n/a	9 (18%)	18 (35%)	12 (24%)	6 (12%)	6 (12%)	-	-	-
Gobbi et al. 2006	Level II	9 (10)	6:3	24 (17-28)	53 (24-119)	0	4,5 (1,5-8)§	n/a	|------3 (30%)------|			|------7 (70%)------|		-	-
Guo et al. 2010	Level IV	32	26:6	22 (12-52)	32 (12-59)	4	11.6 ± 3.5§	n/a	|------27 (84%)------|			|------5 (16%)------|		-	-
Lee et al. 2010	Level IV	35	27:8	35 (17-50)	33 (21-48)	0	0.9 (0.6–1.4)	86%	|------29 (83%)------|			|------6 (17%)------|		-	-
Saxena et al. 2007	Level IV	26	18:8	36 (18-44)	32* (24-55)	0	n/a	n/a	9 (34%)	3 (12%)	-	12 (46%)	-	1 (4%)	1 (4%)	-
Weighted average				**33 (12-74)**			**0.3 – 4.5**			**67%**			**27%**			

*study characteristics of the whole patient populations, including other study groups.
§ Two studies only included patients with either lesions smaller or larger than 1,5 cm².

Table 7.2. Summary of the bone marrow stimulation technique as described in the included articles

Items in the treatment performance were based on the original article by Steadman et al [46]. In all studies, synovectomy or debridement was performed. Several additional recommendations or remarks were made by the authors. Two studies referred directly to the original article by Steadman et al. in the technique description.

Article	Instrument	Dimensions	Dispersion	Debridement	Check	Technique and Additional Remarks
Becher et al. 2010	Arthroscopic awl	2–4 mm deep	3 to 4 mm apart	Limited synovectomy	Fat droplets	n/a
Choi et al. 2009	Microfracture awl	Multiple perforations perpendicular to the joint surface	n/a	Removal of cartilage cap and excision of the lesion	n/a	Referring to Steadman et al. Abrasion arthroplasty in case of loss of subchondral bone until a stable, smooth articular surface was created.
Gobbi et al. 2006	Microfracture awl	Multiple perforations perpendicular to the joint surface	3 to 4 mm apart	Unstable chondral fragments, calcified layer	Fat droplets and blood	Referring to Steadman et al.
Guo et al. 2010	Microfracture awl	Approximately 4 mm deep	n/a	Yes	Bleeding	n/a
Lee et al. 2010	Arthroscopic awl	3–4 mm deep	3 to 4 mm apart	All unstable cartilage and fibrous tissues	Fat droplets and blood	Sharp, perpendicular margins. Peripheral to centre in a spiral pattern with different angles.
Saxena et al. 2007	Chondropick	n/a	n/a	Yes	n/a	Caution to leave the subchondral bone plate intact.

were different therapies performed in one study, data were extracted of the bone marrow stimulation groups only. In the event that articles did not provide the data necessary for our analysis, the missing data were requested by correspondence with the authors.

A total of 664 articles were found (*Fig. 7.1*). Four hundred thirty-one articles were excluded for the following reasons: the article was not about microfracture in the sense of a therapy for osteochondritis dissecans (N=217), did not contain a technique description (N=52), was an abstract or congress report (N=20), was a descriptive article (N=116), was an animal study (N=16), or was an additional duplicate (N=10). Fifty articles on bone marrow stimulation met the inclusion criteria for further review. Forty-two articles concerned joints other than the ankle. The eight articles concerning osteochondral defects of the talus are reviewed here (*Table 7.1*). Six studies used awls to perform bone marrow stimulation. The remaining two studies used drilling with Kirschner wires [24]. We excluded these two studies from further review because we felt the results would run a large risk of bias because of the small number of studies.

Results

One randomized controlled trial, two prospective, and three retrospective case series were included (*Table 7.1*). The six included articles summarize the outcome of a total of 198 patients (199 ankles). Study size varied from 9 (10 ankles) to 51 patients, with a weighted average age of 34 (range: 13 to 74) years. The average follow-up varied from 2 to 6 years. The average of lesion size per study varied from 0.9 cm^2 to 4.5 cm^2. Two studies only included patients with either lesions smaller [32] or larger than 1.5 cm^2 [21]. In total, medial lesions were more prevalent than lateral lesions (70% and 27%, respectively). The remaining lesions were either centrally located or "kissing" lesions running from medial to lateral.

Technique

Technique descriptions in the different articles showed much similarity on the provided details of the bone marrow stimulation technique (*Table 7.2*). In all studies, synovectomy or debridement was performed. Hole depth was either 2 to 4 mm deep or not specified [17, 24, 41]. The distance between the holes, mentioned in three studies [5, 21, 32], was consistently between 3 and 4 mm.

Authors from four studies visualized bleeding or fat droplets from the subchondral bone to confirm adequate treatment of the defect [5, 21, 22, 32]. Several additional

recommendations were made: the preparation of a perpendicular rim to prevent the blood clot from detaching [32], complete and careful removal of the calcified layer on top of the subchondral plate [21] without damaging it [5], making holes perpendicular to the surface [13, 21], and the sequence of the holes [32]. Two studies referred directly to the original article by Steadman et al [46] in the technique description [13, 21].

Clinical Outcome

Because of the heterogeneity of the studies, meta-analysis was not performed. Weighted averages were calculated from the clinical outcome scores and failure rates with respect to the number of procedures performed in the studies. The most prevalent outcome scale was the AOFAS-AHS [29], which was used in five studies [13, 21, 22, 32, 41]. The improvement on the last follow-up was significant in all studies (weighted average preoperative: 63, range 34 to 72; weighted average postoperative: 89, range 84 to 94). The visual analogue scale (VAS) [39] scores were used in three studies [5, 22, 32] (*Table 7.3*). VAS score for pain decreased from 6.8 (range 6.5 to 7) to 2.3 (range 2 to 2.51). Five studies divided the primary outcome into categories (excellent, good, moderate, poor) to evaluate the success rate of the procedure (4,32,34−36) (*Table 7.3*).

In total, 81% of the patients reached excellent to good results (range 66% to 96%), 13% retrieved a moderate result (range 2% to 29%), and the remaining 6% (range 0% to 10%) were considered a poor result. In the case of the AOFAS-AHS, "excellent" corresponded with an end score of > 90, "good" corresponded with a score between 80 and 90, "moderate" (or "fair") corresponded with a score between 70 and 80, and a "poor" outcome was defined as a score below 70 or a failure of the therapy.

Failure Rate and Complications

The weighted average failure rate was 6% (range 0% to 19%, 13 out of 193 procedures; *Table 7.3*). In case of failure, bone marrow stimulation was performed again or a secondary therapeutic procedure was used, such as cartilage grafts, an ankle arthrodesis, or ankle prosthesis. Failure occurred on average 2 to 3 years after the initial surgery. The only reported complication was persistent pain after 24 months in one bilateral case [21]. Five studies reported no complications [5, 13, 22, 32, 41].

Prognostic Factors

Age or sex did influence the treatment outcome significantly in four and two studies, respectively. Anterior lesions had better clinical results in two studies when compared with central or posterior lesions [22, 41]. Anterior-medial lesions resulted

CHAPTER 7 | Is technique performance a prognostic factor in bone marrow stimulation of the talus?

130

Table 7.3. Available preoperative and postoperative VAS and AOFAS scores in the microfracture studies

The categorical clinical outcome in the scoring system is shown (excellent, good, moderate, and poor) and the failure rate is presented as a percentage of the respective patient group*

Article	VAS		AOFAS		Scoring system	Overall clinical outcome				Failure
	Pre-operative	Post-operative	Pre-operative	Post-operative		Excellent %	Good %	Moderate %	Poor %	N= /total (%)
Becher et al. 2010	6.5	2.4 P < .001	NA	NA	HHS	49	31	10	10	4/39 (10%)
Choi et al. 2009		NA	63 ± 17	87 ± 8 P < .001	AOFAS	29	37	29	5	2/51 (5%)
Gobbi et al. 2006		NA	34	84 P < .001	AOFAS		NA			1/10 (10%)
Guo et al. 2010	7,0 ± 1,4	2,5 ± 2,5 P < .001	72 ± 4	89 ± 11 P < .001	AOFAS	|-----87-----|		3	10	6/32 (19%)
Lee et al. 2010	7 (5-8)	2 (0-5) P < .05	63 (52-77)	90 (73-100) P < .05	AOFAS	46	43	11	0	0/35 (0%)
Saxena et al. 2007		NA	55 ± 8	94 ± 6 P < .001	AOFAS	74	22	2	2	0/26 (0%)
Weighted average (range)	**6.8 (6.5-7)**	**2.3 (2-2.5)**	**63 (34-72)**	**89 (84-94)**		**81%**		**13%**	**6%**	**6%**

Weighted averages were calculated based on the size of the patient groups per article. AOFAS: American Orthopaedic Foot and Ankle Society score; HHS: Hannover Scoring System; VAS: visual analogue scale.

in better AOFAS-AHS scores when compared with lateral lesions (44 vs. 56) and a faster return to activities (14 vs. 18 to 20 weeks). This was not seen with lesions located on the medial side of the talus [41]. Two studies show two separate prognostic factors that are not mentioned in the other four studies. Becher et al [5] found that degenerative chondral defects result in lower Hannover Scoring System (HSS) scores than traumatic osteochondral defects (60 vs. 86, p < .001) and VAS scores. The explanation would be that in osteochondral defects without signs of joint degeneration the cartilage around the defect is intact, whereas in degenerative lesions caused by posttraumatic loss of joint cartilage thickness in the presence of existing degenerative joint disease, the condition of the surrounding cartilage will also be inferior.

There are several prognostic factors that show conflicting results. Body mass index (BMI) was found to have a lower clinical outcome in patients with a BMI above 25 kg/m^2 on the HSS (84 vs. 75) and the VAS scores for pain (1.6 vs. 3.0), with 18 patients below and 27 patients above 25 kg/m^2 [5]. Lee et al found no difference with 21 patients below 25 kg/m2, but a smaller amount of patients above 25 kg/m^2 (N=14).

Lastly, symptoms present more than one year resulted in lower scores for clinical outcome (AOFAS 86 vs. 93, p < .05) [32]. However, another study showed no significant influence of symptom duration [13].

Discussion

The aim of this systematic review was to determine whether variation in the technique influences the outcome of bone marrow stimulation in OCDT. It is shown that there is a high level of similarity in the descriptions of the technique performance. Unstable cartilage is removed; 2 to 4 mm deep holes are made with a distance of 3 to 4 mm between the holes and perpendicular to the surface in a spiral pattern from the outer rim to the centre of the defect. Additionally, a perpendicular rim is prepared to prevent the blood clot from detaching, and the calcified layer on top of the subchondral plate is completely but carefully removed.

An important difference between our study and that of previous reviews is that we selected articles specifically based on the description of the essential steps of the bone marrow stimulation technique. The high level of consistency in the disclosed details of the technique in our review does not allow for further analysis of the effect of different surgical techniques as a prognostic factor for outcome. However,

it does show the clinical outcome of a consistent treatment strategy that is performed with specific attention drawn to the correct dimensions and placement of the microfracture holes. It provides insight into the possible influence of the correct effectuation of the microfracture technique on the variability of outcome with bone marrow stimulation. The characteristics of the study population are similar to those of studies that did not use this inclusion criterion (age, male/female ratio, length of follow-up, lesion size and location [16], aetiology [4, 31, 37, 40]. Also, the 81% success rate in our review was comparable with the success rates reported in previous reviews and studies: 81% [4, 42], 87% [48], and 85% [47, 49], although obviously the experience and skills of the surgeon would influence outcome.

Because of the nature of the technique and the biological response it aims to elicit, it is vital that the key elements of the technique are accurately executed. However, recent literature suggests that the nature of the key elements as defined in the method section might be more delicate than the current guidelines advise, for example, 2 vs. 4 mm drill holes resulted in a different outcome in a recent animal study [11]. This has yet to be investigated in clinical studies.

Also, there is a difference in mechanism between the use of a microfracture awl and the drilling of a Kirschner wire. Both methods are arthroscopic procedures and are therefore relatively minimally invasive. The flexible Kirschner wire allows for drilling in different angles in a high congruent joint like the ankle. The rigid, angled awls allow for treatment "around the corner" and a better control for creating holes at the desired depth and perpendicular to the surface [6, 7], but these are difficult to use in posterior defects and hold the risk of damaging the tibial edge by wedging the instrument if used with too much force. There are no large comparative clinical studies available that compare drilling with microfracture. In the initial eligible studies, two different bone marrow stimulation techniques were used: the drilling of Kirschner wires or the use of an awl to puncture the subchondral plate. The first was described in only two studies and was excluded because of the risk of selection bias [17, 24]. However, both studies on drilling did indicate less satisfactory results compared with the included microfracture studies. This might be explained by the small amount of studies and the use of different outcome questionnaires. Both drilling studies used several different scoring systems and were not comparable. In Ferkel et al [17], the AOFAS postoperative score was 84 (range 34 to 100) and lesions were evaluated according to the grading on arthroscopy. This resulted in significant differences in clinical outcome between the lesions with intact cartilage (Cheng-Ferkel grade A-C) and those with (partially) detached cartilage (Cheng-Ferkel grade D-E).

Aside from microfracture and drilling, there is a vast amount of other surgical treatment options that use a different approach (retrograde drilling, bone marrow stimulation using a transmalleolar approach), or a different technique to elicit bleeding (abrasion arthroplasty) or that use grafts (osteochondral autograft transplantation, autologous chondrocyte implementation). It was not within the scope of this review to investigate the technique of these other treatment modalities for primary OCDT. Bone marrow stimulation is still the preferred treatment for primary OCDT [49], and although several attempts have been made to provide an algorithm for the choice of treatment, there is a lack of high-quality comparative studies to determine the appropriate treatment for each individual patient based on patient characteristics, lesion type, and other prognostic factors. When synthesizing these possible prognostic factors, we were confronted with several conflicting results in the current literature. A BMI < 25 kg/m^2 [5, 32], anterior lesions [13, 22, 41], duration of symptoms less than one year [13, 32], and traumatic aetiology [5, 13] showed better clinical results in some articles, but were insignificant in others.

Also, because we needed to exclude many articles based on the lack of a technique description, the number of studies that investigate a particular prognostic factor is very limited. Hence, we were unable to formulate any strong conclusions because of a lack of power.

However, there were two results that followed from our analysis. First, in two studies a larger lesion size negatively influenced outcome in the patient cohort, but did not provide data on the microfracture group only [13, 22]. However, Choi et al did report that in the patient cohort receiving either microfracture or abrasion arthroplasty, lesions smaller than 1.5 cm^2 showed significantly higher AOFAS scores at 48-month follow-up and a 90% good to excellent result, compared with 20% in lesions with a larger surface area. Two studies included only patients with lesions either smaller or larger than 1.5 cm^2 [21, 32]. Outcome was not comparable, but failure rates were 0% and 10%, respectively. Considering that lesion size is often overestimated or underestimated [42], the use of a grading system is a valid alternative. Adequate measurement of lesion dimensions is important to determine the appropriate therapeutic intervention for OCDT [23, 27].

Second, it has been previously suggested that advanced age is considered a relative contraindication [46] because of the diminished quality of bone and limited revalidation possibilities [30]. This review contains five articles with patients more than 50 years of age and up into the seventh decade, with four showing no differences in

clinical outcome between patients younger than 50 years of age and those older [5, 13, 22, 32].

This review has limitations. Because of the selection criteria, only 6 studies were included, with a relatively small number of patients. The majority of articles were retrospective case series with limited statistical analysis. The articles that were excluded for this review showed a similar quality. The lack of strong evidence is a known problem in the literature for treatment osteochondral defects in the talus [33]. In our opinion, this not only shows the need for higher quality studies, but also underlines the necessity to supply more information on the exact nature of the intervention to improve reproducibility and allow for in-depth comparison of study groups in surgical interventions.

In conclusion, there is a large degree of similarity described in the literature in regard to bone marrow stimulation in the treatment of osteochondral lesions of the talus. Microfracture is a safe and effective therapy for OCDT with a diameter smaller than 15 mm. The percentage of total success of bone marrow stimulation of this defined and homogenous treatment procedure as defined by any clinical outcome score was 81%, which shows persistent improvement on an average follow-up of 70 months up to 14 years in one study. The failure rate was 6%. However, whether the instruments used or the hole depth and geometry influence clinical outcome remains to be determined in clinical studies because these have not yet been investigated.

Larger, randomized clinical trials with homogeneous patient groups, an adequate description of the surgical intervention(s), elaborate lesion description and grading, and reproducible outcome measures would provide the opportunity to construct a founded theory for the indication for the use of bone marrow stimulation and prognostic factors. This would be valuable in the pre-selection of patients, which would increase the success rate by referring patients who have a high risk of treatment failure with another therapy regimen.

References

1. Alexander AH, Lichtman DM. Surgical Treatment of Transchondral Talar-Dome Fractures (Osteochondritis Dissecans): Long-Term Follow-up. *J Bone Jt. Surg Am*. 2008;62:646–652.

2. Alford JW, Cole BJ. Cartilage restoration, part 2: techniques, outcomes, and future directions. *Am. J. Sports Med.* 2005;33:443–60.

3. Anon. The Journal of Bone and Joint Surgery Instructions for Authors. Available at: http:// www.jbjs. org/public/instructionsauthors.aspx#LevelsEvidence. Accessed July 1, 2011.

4. Baker CL, Morales RW, Baker C.L. J, Morales RW. Arthroscopic Treatment of Transchondral Talar Dome Fractures: A Long-term Follow-up Study. *Arthroscopy*. 1999;15:197–202.

5. Becher C, Driessen A, Hess T, Giuseppe U, Nicola L, Longo UG, Maffulli N, Thermann H, Giuseppe U, Nicola L. Microfracture for chondral defects of the talus: maintenance of early results at midterm follow-up. *Knee Surg Sport. Traumatol Arthrosc*. 2010;18:656–663.

6. Van Bergen CJ, de Leeuw PAJ, van Dijk CN. Treatment of osteochondral defects of the talus. *Rev Chir Orthop Reparatrice Appar Mot*. 2008;94:398–408.

7. Bhosale AM, Richardson JB. Articular cartilage: Structure, injuries and review of management. *Br. Med. Bull.* 2008;87:77–95.

8. Bosien WR, Staples OS RS. Residual disability following acute ankle sprains. *Bone Jt. Surg Am*. 1955;37:1237–1243.

9. Buckwalter JA. Articular cartilage: injuries and potential for healing. *J Orthop Sport. Phys Ther*. 1998;28:192–202.

10. Chen H, Chevrier A, Hoemann CD, Sun J, Ouyang W, Buschmann MD. Characterization of subchondral bone repair for marrow-stimulated chondral defects and its relationship to articular cartilage resurfacing. *Am. J. Sports Med.* 2011;39:1731–1740.

11. Chen H, Hoemann CD, Sun J, Chevrier A, McKee MD, Shive MS, Hurtig M, Buschmann MD. Depth of subchondral perforation influences the outcome of bone marrow stimulation cartilage repair. *J Orthop Res*. 2011;29:1178–1184.

12. Chen H, Sun J, Hoemann CD, Lascau-Coman V, Ouyang W, McKee MD, Shive MS, Buschmann MD. Drilling and microfracture lead to different bone structure and necrosis during bone-marrow stimulation for cartilage repair. *J Orthop Res*. 2009;27:1432–1438.

13. Choi WJ, Park KK, Kim BS, Lee JW. Osteochondral lesion of the talus: is there a critical defect size for poor outcome? *Am J Sport. Med*. 2009;37:1974–1980.

14. Chuckpaiwong B, Berkson EM, Theodore GH. Microfracture for Osteochondral Lesions of the Ankle: Outcome Analysis and Outcome Predictors of 105 Cases. *Arthroscopy*. 2008;24:106–112.

15. DIGiovanni BF, Fraga CJ, Cohen BE, Shereff MJ. Associated injuries found in chronic lateral ankle instability. *Foot ankle Int.* 2000;21:809–15.

16. Elias I, Zoga AC, Morrison WB, Besser MP, Schweitzer ME, Raikin SM. Osteochondral lesions of the talus: localization and morphologic data from 424 patients using a novel anatomical grid scheme. *Foot Ankle Int*. 2007;28:154–161.

17. Ferkel RD, Zanotti RM, Komenda GA, Sgaglione NA, Cheng MS, Applegate GR, Dopirak RM. Arthroscopic treatment of chronic osteochondral lesions of the talus: long-term results. *Am. J. Sports Med.* 2008;36:1750–1762.

18. Frisbie DD, Trotter GW, Powers BE, Rodkey WG, Steadman JR, Howard RD, Park RD, McIlwraith CW. Arthroscopic subchondral bone plate microfracture technique augments healing of large chondral defects in the radial carpal bone and medial femoral condyle of horses. *Vet. Surg. VS Off. J. Am. Coll. Vet. Surg.* 1999;28:242–255.

19. Giannini S, Ruffilli A, Pagliazzi G, Mazzotti A, Evangelisti G, Buda R, Faldini C. Treatment algorithm for chronic lateral ankle instability. *Muscles. Ligaments Tendons J.* 2014;4:455–60.

20. Giannini S, Vannini F. Operative treatment of osteochondral lesions of the talar dome: current concepts review. *Foot Ankle Int.* 2004;25:168–175.

21. Gobbi A, Francisco RA, Lubowitz JH, Allegra F, Canata G. Osteochondral lesions of the talus: randomized controlled trial comparing chondroplasty, microfracture, and osteochondral autograft transplantation. *Arthroscopy.* 2006;22:1085–1092.

22. Guo Q, Hu Y, Jiao C, Yu C, Ao Y. Arthroscopic treatment for osteochondral lesions of the talus: analysis of outcome predictors. *Chin. Med. J. (Engl).* 2010;123:296–300.

23. Han SH, Lee JW, Lee DY, Kang ES. Radiographic changes and clinical results of osteochondral defects of the talus with and without subchondral cysts. *Foot ankle Int.* 2006;27:1109–1114.

24. Hunt SA, Sherman O. Arthroscopic treatment of osteochondral lesions of the talus with correlation of outcome scoring systems. *Arthroscopy.* 2003;19:360–367.

25. Japour C, Vohra P, Giorgini R, Sobel E. Ankle arthroscopy: follow-up study of 33 ankles--effect of physical therapy and obesity. *J Foot Ankle Surg.* 1996;35:199–209.

26. Johnson LL. Arthroscopic abrasion arthroplasty: a review. *Clin. Orthop. Relat. Res.* 2001:S306-17.

27. Jung HG, Carag JA V, Park JY, Kim TH, Moon SG. Role of arthroscopic microfracture for cystic type osteochondral lesions of the talus with radiographic enhanced MRI support. *Knee Surgery, Sport. Traumatol. Arthrosc.* 2011;19:858–862.

28. Kim HK, Moran ME, Salter RB. The potential for regeneration of articular cartilage in defects created by chondral shaving and subchondral abrasion. An experimental investigation in rabbits. *J Bone Jt. Surg Am.* 1991;73:1301–15.

29. Kitaoka HB, Alexander IJ, Adelaar RS, Nunley JA, Myerson MS, Sanders M. Clinical rating systems for the ankle-hindfoot, midfoot, hallux, and lesser toes. *Foot ankle Int.* 1994;15:349–353.

30. Kreuz PC, Erggelet C, Ph D, Steinwachs MR, Ph D, Krause SJ, Lahm A, Ph D, Niemeyer P, Ghanem N, Uhl M, Ph D, Südkamp N, Ph D, Able T. Is Microfracture of Chondral Defects in the Knee Associated With Different Results in Patients Aged 40 Years or Younger? *Arthroscopy.* 2006;22:1180–1186.

31. Kumai BYT, Takakura Y, Higashiyama I, Tamai S, Kumai T, Takakura Y, Higashiyama I, Tamai S. Arthroscopic Drilling for the Treatment of Osteochondral Lesions of the Talus. *J Bone Jt. Surg Am.* 1999;81:1229–1235.

32. Lee KB, Bai LB, Chung JY, Seon JK. Arthroscopic microfracture for osteochondral lesions of the talus. *Knee Surg Sport. Traumatol Arthrosc.* 2010;18:247–253.

33. Loveday D, Clifton R, Robinson A. Interventions for treating osteochondral defects of the talus in adults. *Cochrane Database Syst Rev.* 2010:CD008104.

34. Magnussen RA, Dunn WR, Carey JL, Spindler KP. Treatment of Focal Articular Cartilage Defects in the Knee A Systematic Review. *Clin Orthop Relat Res.* 2008;466:952–962.

35. Mithoefer K, Williams RJ, Warren RF, Potter HG, Spock CR, Jones EC, Wickiewicz TL, Marx RG. Chondral resurfacing of articular cartilage defects in the knee with the microfracture technique. Surgical technique. *J. Bone Joint Surg. Am.* 2006;88 Suppl 1:294–304.

36. Nakajima H, Goto T, Horikawa O, Kikuchi T, Shinmei M. Characterization of the cells in the repair tissue of full-thickness articular cartilage defects. *Histochem. Cell Biol.* 1998;109:331–338.

37. Ogilvie-Harris DJ, Sarrosa EA. Arthroscopic treatment after previous failed open surgery for osteochondritis dissecans of the talus. *Arthroscopy.* 1999;15:809–812.

38. Parisien JS. Arthroscopic treatment of osteochondral lesions of the talus. *Am J Sport. Med.* 1986;14:211–217.

39. Revill SI, Robinson JO, Rosen M, Hogg MI. The reliability of a linear analogue for evaluating pain. *Anaesthesia*. 1976;31:1191–1198.

40. Robinson D, Nevo Z. Articular cartilage chondrocytes are more advantageous for generating hyaline-like cartilage than mesenchymal cells isolated from microfracture repairs. *Cell Tissue Bank*. 2001;2:23–30.

41. Saxena A, Eakin C. Articular talar injuries in athletes: results of microfracture and autogenous bone graft. *Am J Sport. Med*. 2007;35:1680–1687.

42. Schäfer D, Boss A, Hintermann B. Accuracy of arthroscopic assessment of anterior ankle cartilage lesions. *Foot Ankle Int*. 2003;24:317–20.

43. Schimmer RC, Dick W, Hintermann B. The role of ankle arthroscopy in the treatment strategies of osteochondritis dissecans lesions of the talus. *Foot Ankle Int*. 2001;22:895–900.

44. Shapiro F, Koide S, Glimcher MJ. Cell origin and differentiation in the repair of full-thickness defects of articular cartilage. *J Bone Jt. Surg Am*. 1993;75:532–553.

45. Slabaugh MA, Hess DJ, Bajaj S, Farr J, Cole BJ. Management of Chondral Injuries Associated With Patellar Instability. *Oper. Tech. Sports Med*. 2010;18:115–122.

46. Steadman JR, Rodkey WG, Rodrigo JJ. Microfracture: surgical technique and rehabilitation to treat chondral defects. *Clin Orthop Relat Res*. 2001:S362-9.

47. Tol JL, Struijs PA, Bossuyt PM, Verhagen RA, van Dijk CN. Treatment strategies in osteochondral defects of the talar dome: a systematic review. *Foot ankle Int*. 2000;21:119–126.

48. Verhagen R a, Struijs P a, Bossuyt PM, van Dijk CN. Systematic review of treatment strategies for osteochondral defects of the talar dome. *Foot Ankle Clin*. 2003;8:233–42, viii–ix.

49. Zengerink M, Struijs PA, Tol JL, van Dijk CN. Treatment of osteochondral lesions of the talus: a systematic review. *Knee Surgery, Sport. Traumatol. Arthrosc*. 2010;18:238–246.
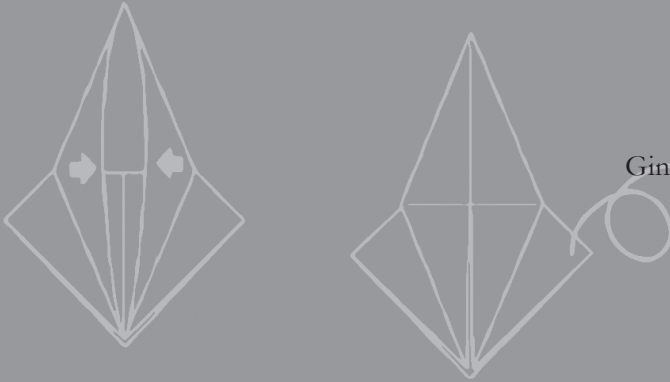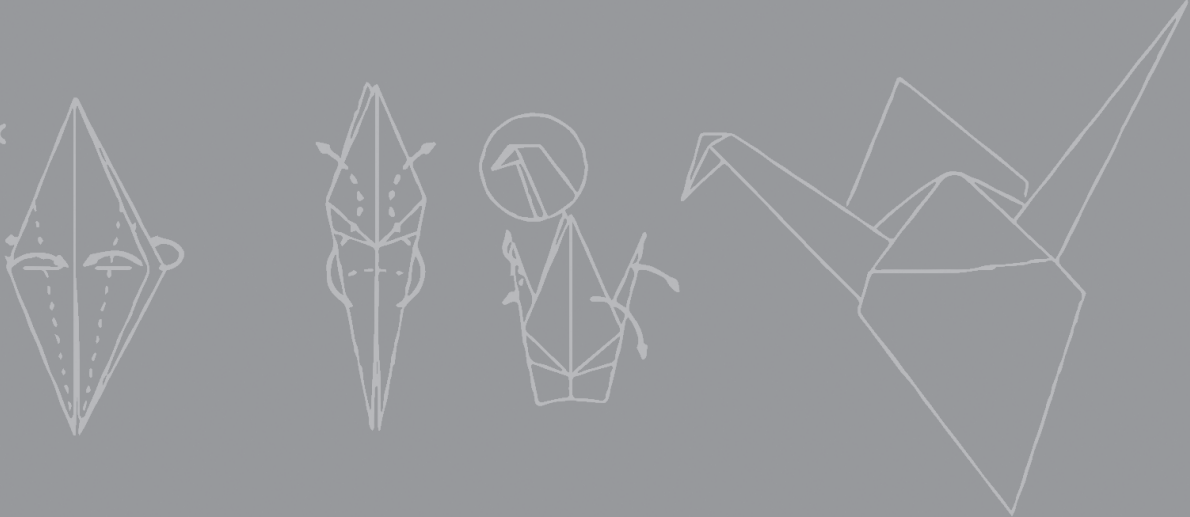
CHAPTER 8

No effect of hole geometry in microfracture for talar osteochondral defects

Aimée C. Kok
Gabrielle J. M. Tuijthof
Steven den Dunnen
Jasper van Tiel
Michiel Siebelt
Vincent Everts
C. Niek van Dijk
Gino M. M. J. Kerkhoffs

Abstract

Background
Debridement and bone marrow stimulation is an effective treatment option for patients with talar osteochondral defects. However, whether surgical factors affect the success of microfracture treatment of talar osteochondral defects is not well characterized.

Aim
We hypothesized (i) holes that reach deeper into the bone marrow-filled trabecular bone allow for more hyaline-like repair; and (ii) a larger number of holes with a smaller diameter result in more solid integration of the repair tissue, less need for new bone formation, and higher fill of the defect.

Methods
Talar osteochondral defects that were 6 mm in diameter were drilled bilaterally in 16 goats (32 samples). In eight goats, one defect was treated by drilling six 0.45 mm diameter holes in the defect 2 mm deep; in the remaining eight goats, six 0.45 mm diameter holes were punctured to a depth of 4 mm. All contralateral defects were treated with three 1.1 mm diameter holes 3 mm deep, mimicking the clinical situation, as internal controls. After 24 weeks, histologic analyses were performed using Masson-Goldner/Safranin-O sections scored using a modified O'Driscoll histologic score (scale 0–22) and analysed for osteoid deposition. Before histology, repair tissue quality and defect fill were assessed by calculating the mean attenuation repair/healthy cartilage ratio on Equilibrium Partitioning of an Ionic Contrast agent (EPIC) micro CT (µCT) scans. Differences were analysed by paired comparison and Mann-Whitney U tests.

Results
Significant differences were not present between the 2 mm and 4 mm deep hole groups for the median O'Driscoll score (p = 0.31) and the median of the µCT attenuation repair/healthy cartilage ratios (p = 0.61), nor between the 0.45-mm diameter and the 1.1-mm diameter holes in defect fill (p = 0.33), osteoid (p = 0.89), or structural integrity (p = 0.80).

Conclusions
The results indicate that the geometry of microfracture holes does not influence cartilage healing in the caprine talus. Bone marrow stimulation technique does not appear to be improved by changing the depth or diameter of the holes.

Introduction

Debridement and bone marrow stimulation is a simple, cost-effective operative treatment for osteochondral defects with lower morbidity and faster return to activity than open cartilage restoration surgery [7, 8, 14, 16, 44, 53]. Systematic reviews have shown a current clinical success percentage of 86%. The affect of patient and defect specific prognostic factors such as lesion size [14, 16], location [14, 45], age [14, 24, 48], or body weight [15, 22] is inconclusive owing to the absence of well-designed prospective studies [22, 23]. The exact mechanisms of the healing process are unknown, which makes prediction of clinical outcome difficult [41, 51].

There is little, and only experimental, research on whether improvements in surgical technique can enhance the healing process of damaged cartilage surfaces. One animal study suggests that the depth of subchondral perforation influences the degree of fill and quality of repair tissue [9]. Other research indicates that there is a difference in bone structure and degree of bone necrosis between drilling and microfracture [11, 34].

A recent systematic literature review showed a large degree of similarity in current surgical techniques for microfracture [23], including use of K-wires [2, 26, 36] or awls [48], removal of unstable cartilage, hole depth between 2 and 4 mm until bleeding or fat droplets occur, and hole spread with a distance of 3 to 4 mm. These recommendations are similar to the originally presented technique by Steadman et al. [48]. Additional recommendations are creation of a stable rim, placement of the holes perpendicular to the surface, and removal of the calcified layer at the base of the defect [12, 17, 27]. To the best of our knowledge, there are no published studies regarding whether hole size or distance between the defects influences the degree and quality of the repair tissue.

The aim of our study was to determine the influence of hole geometry, when performing microfracture treatment in the talus, on the quality of the repair cartilage and the filling grade of the defect in a goat model. We formulated two hypotheses: (i) holes that reach deeper into the bone marrow-filled trabecular bone result in better quality repair tissue; and (ii) a larger number of holes with a smaller diameter result in a more solid integration of the repair tissue, less need for new bone formation, and higher fill of the defect.

Materials and Methods

Sixteen female Dutch milk goats (Capra hircus sana), 4 years of age, with an average weight of 69 kg (range 44–86 kg), were used in this study. Screening for pregnancy and disease was performed before entering the trial. The goats were kept in group-housing starting one week before and continuing until one week after surgery to minimize stress. The number of goats was determined from a sample size calculation performed using a power of 90% and two-sided significance level of 5% between groups. A 10% SD of the histology score was described by O'Driscoll et al. [32]; therefore, a minimal effect of 15% was considered clinically significant [4, 25]. Our study protocol was approved by the local animal welfare committees (ORCA102287).

Talar defects are predominantly osteochondral defects, unlike the knee where chondral defects most often are seen [3, 12, 14, 19, 50]. The primary surgical treatment for both is microfracture [7, 53]. To best represent the clinical situation, we created an osteochondral talar defect. The dimensions of the created defect depth and diameter and the distance between the microfracture holes in this study were scaled down using the respective ratio between a critical-size osteochondral defect in the human (15 mm diameter) and in the smaller goat talus (6 mm diameter) [12, 21]. Therefore, defect depth was 3 mm, reaching just underneath the sub chondral bone plate [13] but sufficiently shallow to avoid pre-emptive spontaneous bleeding (*Fig. 8.1*). One defect in each goat served as a reference mimicking standard clinical microfracture dimensions: three holes of 1.1 mm diameter and 3 mm deep (*Table 8.1*). The contralateral defect served to test our hypotheses. To investigate the effect of microfracture hole depth, this defect was treated with microfracture awls penetrating only the subchondral bone plate (2 mm) in half of the goats, whereas in the other half, the holes reached the centre of the talus (4 mm) (*Table 8.1*). To determine the effect of the microfracture hole diameter and number, the contralateral defects of the goats were treated with six holes of 0.45-mm diameter, keeping the total treatment surface area constant (*Table 8.1*).

All operative procedures were performed in a standardized manner by the first author (ACK), one experienced orthopaedic surgeon (GMK), and an assistant (*Appendix 8A.1*). A posterolateral surgical approach was used to access the talus [6]. Through a 6 mm diameter cannulated drill guide, the osteochondral defect was drilled in the tali of both hind legs perpendicular to the talar surface under continuous cooling with saline. The defect was placed at the centre of the talar dome as designated by one surgeon for all goats. After debridement, the goats were treated according to a randomization scheme (*Table 8.1; Fig. 8.1*) using custom-made surgical templates.

Table 8.1. Treatment group specifications

Number of specimens	Talus	Number of holes	Diameter	Depth
8 goats (16 defects)	Randomized talus (8 defects)	6	0.45 mm	2 mm
	Contralateral talus (8 defects)	3	1.1. mm	3 mm
8 goats (16 defects)	Randomized talus (8 defects)	6	0.45 mm	4 mm
	Contralateral talus (8 defects)	3	1.1. mm	3 mm
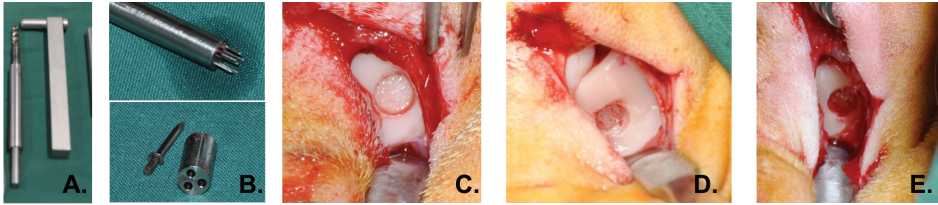
Figure 8.1A–E: Surgical technique
A 6-mm diameter osteochondral defect was drilled in the talus of both hind legs. In the same session, one defect subsequently was treated with six 0.45-mm diameter puncture holes of either 2 mm or 4 mm depth. The contralateral defect was treated with three puncture holes made by a 0.045- (1.1 mm diameter) K-wire capped to a depth of 3 mm to simulate the dimensions of the current clinically applied microfracture awls. *A.* The customized drill guide was designed to create a 3-mm deep defect. *B.* The microfracture tools used to standardize the diameter and distance between the holes are shown. *C.* The 6-mm diameter, 3-mm depth created defect was made without bleeding from the defect before treatment. *D.* The defect was treated with six 0.45-mm diameter holes with punctuate bleeding from the holes. *E.* The contralateral defect was treated with three holes of 0.045 K-wires (1.1 mm diameter).

The joint capsule and subcutaneous tissue were closed with interrupted 2-O absorbable sutures and the skin was closed with an absorbable continuous intracutaneous suture. The animals were encouraged to perform immediate weight bearing and were transferred to a farm off-site after primary wound closure to complete follow-up under daily observation with neither food nor exercise restriction. After 24 weeks, the goats were euthanized. All tali were collected, photographed, and stored at 4o C in phosphate-buffered saline 1% with aspartic, serine, and cysteine proteases inhibitors (complete ULTRA Mini Tablets; Roche Diagnostics Corporation, Indianapolis, IN, USA).

To compare the microscopic quality of the repair tissue between the 2 mm and the 4 mm groups, histologic analysis was performed. Second, osteoid formation and repair tissue integration were compared in the 1.1 mm and 0.45 mm diameter groups to establish any differences in integration and bone formation between these groups. All tali were cut into 20 9 20-mm blocks around the defect, leaving the entire depth of the talus intact. The blocks were fixed in 4% formaldehyde in a 0.1 mol/L phosphate buffer, dehydrated, and embedded in methylmethacrylate. At a quarter into

and at the centre of the defect, 5 µm slices were sectioned and stained alternately with hematoxylin and eosin, Safranin-O, and Masson-Goldner trichrome. Collagen fibres were examined using polarized light to assess the structure of the repair tissue. Hyaline cartilage will show organization of the fibres, whereas fibrous tissue does not.

To quantify our cartilage quality assessment, a modified form of the score described by O'Driscoll et al. was used (*Appendix 8A.2*) [32]. The original score by O'Driscoll et al. contains four main categories: nature of predominant tis sue, structural characteristics, freedom from cellular changes of degeneration, and freedom from degenerative changes of the adjacent cartilage, which give a maximum total score of 24 points. The subitem cartilage thickness was not scored, because the repair tissue in the defects was never thinner than the healthy cartilage surrounding the defects. Therefore, a maximum of 22 points could be scored in this study. Each sample was scored twice with a one month interval by one blinded observer (ACK). Differences between the scores at the two times were resolved by an experienced histologist (VE). The entire defect was represented by an average O'Driscoll score, which was calculated using the values at a quarter and at the centre of the defect.

To quantitatively assess glycosaminoglycan (GAG) content [37], sections from the centre of the defect were stained with Safranin-O without any counterstaining and digitally analysed using a Leica microscope (Leica, Wetzlar, Germany) with a 518-nm wavelength filter and evaluated using imaging software [40]. The normalized average Safranin-O intensity (SOI) ratio of the repair tissue compared with the healthy reference cartilage region in the same sections then was calculated. A ratio close to one suggests a cartilage quality of the repair tissue close to that of healthy cartilage.

Osteoid formation was assessed on regular slices using the Masson-Goldner sections from the centre and categorized into three groups: (1) no osteoid formation; (2) slight, less than 20% of the defect; or (3) substantial osteoid formation, greater than 20% of the defect.

Repair tissue integrity was quantified by a subitem of the O'Driscoll score into three categories: (1) full integration; (2) slight disruptions including cysts; or (3) severe disruptions.

To compare the quality of the repair tissue between the 2-mm and 4-mm deep groups, a non contrast-enhanced micro-CT scan (µCT) and an equilibrium partitioning of an ionic contrast agent (EPIC) through µCT (EPIC-µCT) scan were acquired

of each entire talus using an µCT scanner (Skyscan1076; Skyscan, Kontich, Belgium) [35, 52] before histologic analysis. The EPIC-µCTwas acquired after the tali had been saturated for 24 hours in a 40% Hexabrix 360 dilution (Guebet BV, Gorinchem, The Netherlands) [52]. The following scan settings were used: isotropic voxel size of 18 µm; voltage of 70 kV; current of 111 µA; 0.5-mm aluminium filter; and 198° with a 0.4° rotation step. Using Skyscan analysis software (Skyscan), a normalized attenuation (grey value) ratio was calculated between a region of cartilage repair tissue and a region of healthy cartilage on the opposite side of the talus. A normalized attenuation ratio close to one indicates that the quality of the repair tissue is close to that of healthy cartilage.

To compare the effect on repair tissue volume between the 4 mm and 2 mm deep holes the cartilage repair tissue volume was determined as a percentage of the total tissue volume of a three-dimensional volume of 8 x 8 x 8-mm around the centre of the defect. Two observers (ACK, SdD) individually determined the repair tissue volume using image software [40], and disagreements between the observers were solved by discussion resulting in a single value per sample (*Fig. 8.2*).

All surgical wounds healed without infection. Two complications occurred after surgery: one temporary pressure neuropathy of the peroneal nerve, which sub sided completely within 12 hours, and one persistent swelling of both hind legs causing impeded mobilization. Supportive treatment was given using cooling gel. One goat was terminated early at 22 weeks follow-up for a bilateral front hoof problem causing

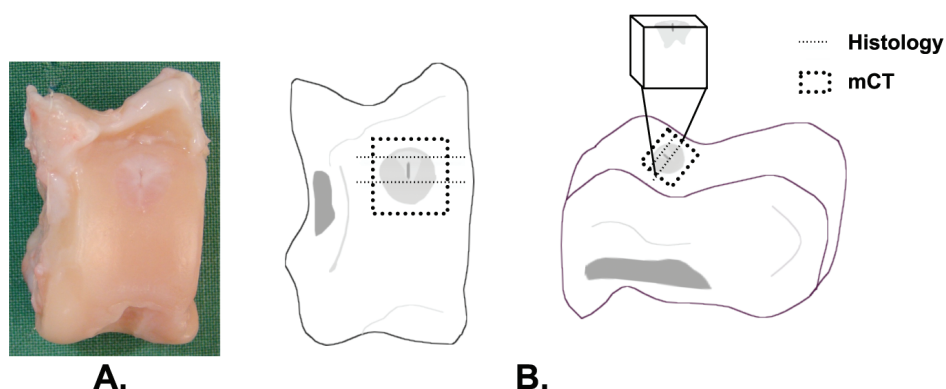**Figure 8.2A-B: regions of interest for µCT and histological analysis**
(A) A photograph of the talus with the treated defect is shown. (*B*) Schematic representations of the same talus in the cranial (*left*) and lateral (*right*) views show the two locations of histologic analysis (*dotted lines*) and the 8 x 8 x 8-mm region of interest in the µCT of which the percentage of repair tissue area was calculated.
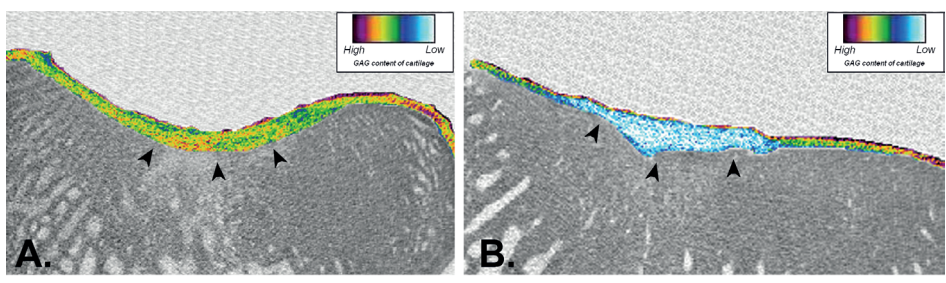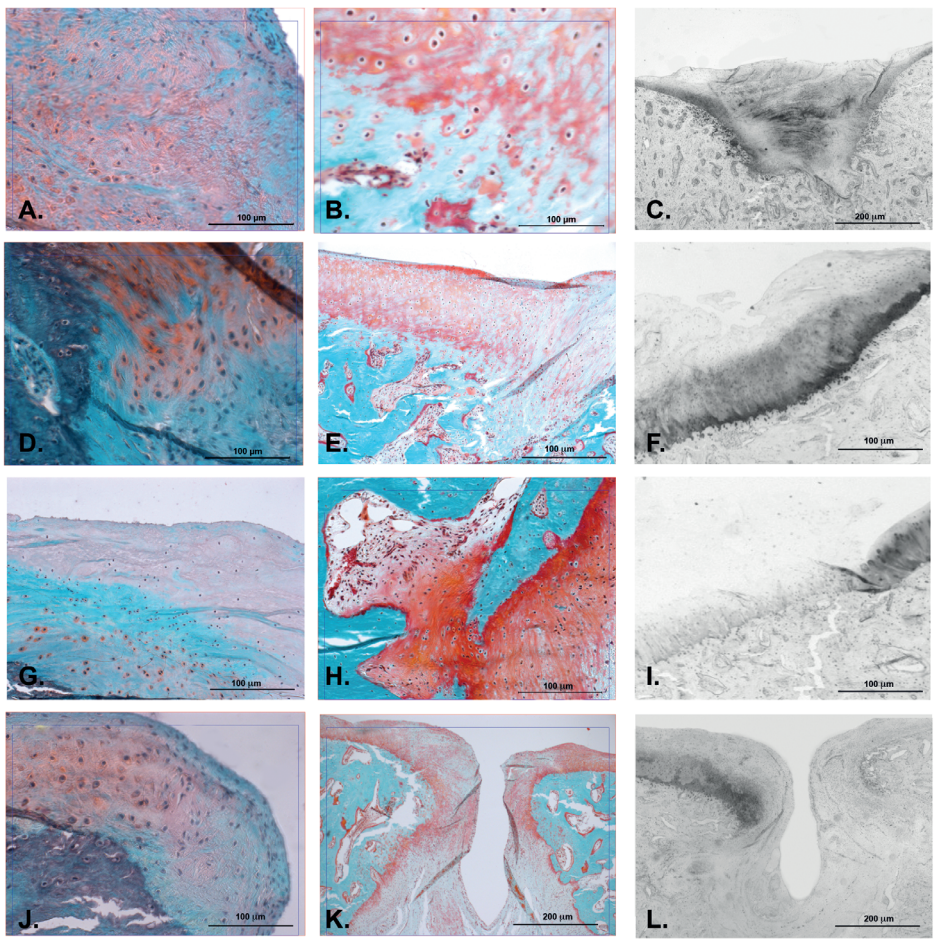
Figure 8.3A–L: Histological examples of a best (A-C), moderate (D-F) and poor result (G-I) including a moderate result with a large cleft (J-L).

Best case result with (*A*) moderate Safranin-O staining with evenly distributed GAG (*original magnification, 9400*x), (*B*) Masson-Goldner staining with little osteoid formation (*original magnification, 9200*x); and (*C*) Safranin-O without counterstains used for digital Safranin-O intensity with moderate staining and evenly distributed GAGs, and a smooth surface without disruptions or cysts in the repair tissue.

A moderate result is shown with (*D*) Safranin-O staining with patches of moderate staining and also unstained tissue (*original magnification, 9400*); (*E*) Masson-Goldner staining with several osteoid isles visible underneath the repair tissue (*black arrows*) (*original magnification, 9200*); (*F*) Safranin-O without counterstains showing patches of moderate staining and also unstained tissue for the same sample. Overall, the staining is less than the healthy tissue *(* = repair tissue, white arrow = adjacent cartilage*)*, and the repair tissue has not bonded to the healthy tissue (*black arrow*).

A worst case result is shown with (*G*) Safranin-O staining with a strong zonal distribution of Safranin-O and an irregular surface (*original magnification, 9400*x); (*H*) Masson-Goldner staining with large osteoid formations (*original magnification, 9200*x); and (*I*) Safranin-O without counterstains used for digital Safranin-O intensity (*SOI*), with a large difference in SOI between the repair tissue staining are shown *(* = repair tissue; white arrow = adjacent cartilage*)*. The repair tissue has not bonded to the adjacent cartilage (*black arrow*).

(*J*) Safranin-O staining of a sample with a cleft in the center shows similar results to the moderate case with moderate Safranin-O staining (*original magnification, 9400x*). (*K*) A few osteoid isles can be seen on the sample with Masson-Goldner staining (*original magnification, 9200x*). (*L*) There was uneven Safranin-O distribution and detachment of the healthy cartilage on the Safranin-O without counterstains digital analysis.

Figure 8.4A–B: Two samples of EPIC-µCT images

The arrows indicate the repair tissue site in the cartilage. (*A*) The contrast influx is close to that of the adjacent cartilage, indicating a relatively similar GAG content. This results in an attenuation ratio (repair tissue: healthy reference) close to 1. (*B*) In this sample the attenuation ratio is lower owing to the low attenuation in the repair tissue caused by the lower negative change density.

Table 8.2. Results per depth group

Results are presented as median values with ranges between brackets.

	2 mm			4 mm			Difference between groups
	Randomized talus	Control	Difference	Randomized talus	Control	Difference	
MODS	12.5 (10.8–15.3)	12.0 (9.0–13.0)	1.3 (-1.25–4.3)	11.5 (9.8–16.0)	12.6 (11.5–14.3)	-0.9 (-4.3–2.0)	2.4* (p = 0.04)
SOI ratio	1.8 (1.4–2.7)	1.7 (1.1–4.7)	0.2 (-3.0–1.3)	1.5 (0.9–2.4)	1.4 (1.0–2.3)	0.2 (1.2–0.5)	0 (NS)
µCT attenuation ratio	1.6 (1.5–1.8)	1.6 (1.4–1.7)	0.01 (-0.2–0.4)	1.6 (1.3–2.1)	1.5 (1.3–1.8)	0.03 (0.3–0.8)	0.02 (NS)

Difference between 2-mm and 4-mm groups is significant (p = 0.04); MODS: modified O'Driscoll score; SOI: Safranin-O intensity ratio; NS: not significant (p>0.05).

walking difficulty and pain. There were no apparent problems with the hind legs. The last two weeks at the end of the follow-up period were expected to have had minimal influence on the overall healing tendency. Therefore, these tali were included for analysis. All other 15 goats completed follow-up without difficulty.

The modified O'Driscoll scores including subitems, attenuation ratios, and repair tissue volume percentages from the EPIC-µCT, the Safranin-O intensity ratios, and the osteoid formation categories were analysed nonparametrically as a result of skewed distribution of the data and the small sample sizes. Paired analysis between the experimental and control sides of each goat was performed to decrease the influence of repair variability between the goats. In addition, the differences between the talus treated with the experimental treatment and the contralateral talus were calculated per goat using Mann-Whitney U tests (p = 0.05). The EPIC-µCT attenuation ratios correlated significantly with the SOI ratio for the experimental groups (r^2 = 0.5; p = 0.05) and the control defects (r^2 = 0.7; p = 0.006). In one µCTof the 2 mm group, an artefact was seen on the defect. This sample and its matching control were excluded for this specific analysis.

Results

We found no clinically significant relationship between repair tissue quality and the depth of microfracture holes. The median difference in the modified O'Driscoll score between the treatment and control legs per goat per group was 1.3 (range: -1.3 to 4.3) for the 2 mm group and -0.9 (range: -4.3 to 2.0) for the 4 mm group (*Table 8.2*). This difference was statistically significant (p = 0.04). All sections contained predominantly fibrous cartilage repair tissue with diminished Safranin-O staining

Table 8.3. Results per diameter group

Diameter	Ø 0.45 mm	Ø 1.1 mm	Difference
Structural integrity (O'Driscoll Score)			
Normal	1 (6%)	4 (25%)	
Slight disruption	10 (63%)	9 (36%)	NS
Severe disruption	5 (31%)	3 (19%)	
Osteoid formation			
None	1 (6%)	2 (13%)	
Moderate	8 (50%)	8 (50%)	NS
Severe	7 (44%)	6 (38%)	
Repair tissue volume (%)			
Median (Range)	23% (10-40%)	29% (10-75%)	-3% (NS)

NS: not significant (p>0.05).

and disorganized collagen structures on polarized light microscopy. The majority of the defect surfaces showed smooth surfaces (18 samples; *Fig. 8.3*). One goat in the 2 mm group had large residual defects with a cleft in the centre in both tali (*Fig. 8.3*). No cause could be identified from the operation or the postoperative period. Thirteen samples showed progressive hypocellularity near the surface in a zonal distribution compared with deeper zones near the sub chondral bone plate (six controls, three in the 2 mm group and four in the 4 mm group; *Fig. 8.3*).

Digital analysis of the Safranin-O intensity showed five samples in the control group and two in the 4 mm experimental group with uniform Safranin-O distribution with moderate staining. The other defects showed only patches of staining (*Fig. 8.3*). The difference in SOI ratio per goat per group was the same, 0.2, for the 2 mm and the 4 mm groups. This was not significant (*Table 8.2*). No significant difference was present between the attenuation ratio of the 2 mm group (range: -0.2 to 0.4) or the 4 mm group (range: 0.0 to 0.8) (*Table 8.2*). In all scans the repair tissue was largely saturated with the contrast agent (average grey value 84/255, 33%) indicating a relatively low GAG content, compared with the relatively low saturation (average grey value 53/255, 21%), indicating high GAG content for the healthy adjacent cartilage (*Fig. 8.4*).

We also found no relationship between defect fill or repair tissue integrity between the 2 mm and 4 mm groups. On histology, the O'Driscoll score subitem ''structural integrity'' was not significantly different between the 2 mm and 4 mm groups nor was the osteoid formation (*Table 8.3*). Six samples showed severe disruption of tissue integrity, evenly distributed over both experimental groups and the control

groups (*Fig. 8.3*). No significant difference was present in repair tissue volume on the EPIC-μCT scans (range: 10%–75%; *Table 8.3*).

Discussion

The aim of our study was to determine the effect of depth and diameter of holes created with microfracture bone marrow stimulation on repair tissue quality and the filling grade of the defect. We found that hole depth and hole diameter did not influence the defect fill or the structural integrity of repair tissue. To our knowledge, there are no previous comparative studies that have investigated hole diameter to compare with these results.

Our study has some limitations. Despite the efforts to standardize the protocol, a large variation was present in quality of repair tissue and defect fill even though we used a sample size calculation that was based on previous studies [4, 6, 25, 31]. The variation might be because the goats were not restricted in mobilization causing some goats to mobilize at a different pace [1]. However, signs of disturbed healing resulting from too fast or hampered mobilization (e.g., limping, swelling) were not seen. In addition, there was a large range in weight in our animals (range: 47–90 kg). However, this proved to be attributable to two outliers, whereas 14 of 16 goats weighed 60 to 80 kg.

The results of repair response compared with non-weight bearing locations (e.g., the trochlea), which correspond to less hyaline repair tissue [20]. Additionally, talar cartilage is known to be stiffer and denser with a higher GAG and lower water content [49]. This changes the physical properties of the cartilage and its response to cyclic loading. Further clinical research is needed to investigate whether the biomechanical differences also might influence the healing response, clinical outcome, and controversial prognostic factors in the two most predominantly used joints for bone marrow stimulation [29, 46]. This should be taken into account when applying our results to the knee, especially because we used an animal model to answer our research question. Extrapolating results from an animal study to a clinical situation should be done cautiously.

In many cartilage studies smaller, mainly rabbit models have been used [8, 11, 13, 46]. We chose a goat model because this allows creation of larger defects (6 mm in diameter) that do not heal spontaneously [21]j. In addition, the two outliers were similar to those of the other goats. We do not expect this to have influenced our

results, because the literature is controversial regarding the effect of weight on the outcome of microfracture [5, 23, 27].

Another limitation is the use of the smaller joint (the ankle) rather than the knee. This limited the extremes in microfracture hole depth between the treatment groups in the current study. All other animal studies used the knee [11, 21, 28, 46, 47]. The maximum depth for the microfracture holes in the talus was 4 mm when using a 3 mm deep osteochondral defect and without penetrating the centre of the talus. Other studies used depths between 2 and 6 mm [10, 11, 28]. In addition, the knee is connected to a shaft bone containing a large reserve of bone marrow [38], whereas the talus is dependent on the external vascular supply and the cells present in the trabecular bone [39]. These differences might have limited the number of cells that could be recruited from deeper areas. However, the talus is a more congruent joint and such a confined space might protect the blood clot from detaching during initial weight bearing. Immediate weight bearing on the defects also could have enhanced cortical and trabecular bone structure of the goat is similar to human bone and the proportion of cartilage to subchondral bone [13, 47]. In addition, some studies had a shorter follow-up (range: 1–56 days) [10, 11, 47], which is less analogous to the clinical situation. Clinical studies of the ankle use a follow-up period that generally ranges from several months to years [5, 12, 18, 26, 27, 29, 44, 53].

Concerning our first hypothesis, the differences we observed in terms of the O'Driscoll score for cartilage repair were on the border of statistical significance favouring 2 mm deep holes over 4 mm deep holes, but did not reach the threshold of 15% defined elsewhere as clinically significant [43, 47]. A study using a rabbit model indicated that deeper compared with shallower drilling (6 mm versus 2 mm) elicited a cartilage repair tissue with a more hyaline character in the repair matrix [10]. We did not find this in our study. The predominantly fibrous repair tissue that we observed was similar to that in other cartilage repair studies using the microfracture technique [8, 28, 53]. This also caused a considerable saturation level of the repair tissue in the EPIC-μCT of the repair tissue, resulting from the relatively low GAG content. More subtle zonal differences in the repair tissue as seen in the Safranin-O slices remained undetected. Further research is needed to determine the right saturation protocol of fibrous tissue to enhance the potential of EPIC-μCT analysis of cartilage repair tissue.

Concerning our second hypothesis, no differences were found between 0.45 mm diameter microfracture holes and 1.1 mm diameter holes in the "structural integrity" subitem of the O'Driscoll score, repair tissue volume, or osteoid formation (*Table 8.3*). Another study also used the O'Driscoll score to assess 6-mm diameter defects

in goats treated with subchondral drilling (mean score: 11.3; SD 8.7) [28]. A couple studies reported limited bonding to the subchondral bone and adjacent cartilage and only 30% to 50% defect fill [8, 28]. The modified O'Driscoll score in our study was higher and all samples showed good bonding to the subchondral bone, bonding to the adjacent cartilage on at least one side, and higher overall defect fill (*Fig. 8.3; Table 8.3*).

The study has several strengths. First, a high level of standardization was achieved by the use of specifically designed surgical templates to minimize variation in hole diameter, depth, and hole dispersion. Second, the minimally invasive approach decreased the operative burden on the animal and reduced the chance of postoperative complications. Third, the animals were used as their own controls to compensate for the high variability between goats. A control group with an untreated defect was deemed an unnecessary increase of used animals, because previous studies have shown the significant lack of healing of these defects [6, 28]. Fourth, samples were analysed according to the guidelines for cartilage assessment in animal studies [20]. For cartilage assessment, the modified O'Driscoll score was used [32] because it is validated in animal models [30, 42]. Supporting the modified O'Driscoll score, two semiautomatic quantitative techniques were used as an internal reference: μCT and digital Safranin-O analysis. The use of μCT also offered a three-dimensional volume in which bone and cartilage repair could be assessed in the entire defect.

Using these tools and approaches, we found no clinically significant difference in the cartilage repair tissue quality or degree of defect fill of talar osteochondral defects treated with different sized microfracture holes or holes with different depths.

References

1. Adams MA. The mechanical environment of chondrocytes in articular cartilage. *Biorheology*. 2006;43:537–545.

2. Alexander AH, Lichtman DM. Surgical Treatment of Transchondral Talar-Dome Fractures (Osteochondritis Dissecans): Long-Term Follow-up. *J Bone Jt. Surg Am*. 2008;62:646–652.

3. Aroen A, Heir S, Loken S, Engebretsen L, Reinholt FP. Healing of articular cartilage defects. An experimental study of vascular and minimal vascular microenvironment. *J Orthop Res*. 2006;24:1069–1077.

4. Beardmore AA, Brooks DE, Wenke JC, Thomas DB. Effectiveness of local antibiotic delivery with an osteoinductive and osteoconductive bone-graft substitute. *J Bone Jt. Surg Am*. 2005;87:107–112.

5. Becher C, Driessen A, Hess T, Giuseppe U, Nicola L, Longo UG, Maffulli N, Thermann H, Giuseppe U, Nicola L. Microfracture for chondral defects of the talus: maintenance of early results at midterm follow-up. *Knee Surg Sport. Traumatol Arthrosc*. 2010;18:656–663.

6. van Bergen CJ, Kerkhoffs GM, Marsidi N, Korstjens CM, Everts V, van Ruijven LJ, van Dijk CN, Blankevoort L. Osteochondral Defects of the Talus: A Novel Animal Model in the Goat. *Tissue Eng. Part C. Methods*. 2013;19.

7. Van Bergen CJ, de Leeuw PAJ, van Dijk CN. Treatment of osteochondral defects of the talus. *Rev Chir Orthop Reparatrice Appar Mot*. 2008;94:398–408.

8. Buckwalter JA. Articular cartilage: injuries and potential for healing. *J Orthop Sport. Phys Ther*. 1998;28:192–202.

9. Chen H, Chevrier A, Hoemann CD, Sun J, Ouyang W, Buschmann MD. Characterization of subchondral bone repair for marrow-stimulated chondral defects and its relationship to articular cartilage resurfacing. *Am. J. Sports Med*. 2011;39:1731–1740.

10. Chen H, Hoemann CD, Sun J, Chevrier A, McKee MD, Shive MS, Hurtig M, Buschmann MD. Depth of subchondral perforation influences the outcome of bone marrow stimulation cartilage repair. *J Orthop Res*. 2011;29:1178–1184.

11. Chen H, Sun J, Hoemann CD, Lascau-Coman V, Ouyang W, McKee MD, Shive MS, Buschmann MD. Drilling and microfracture lead to different bone structure and necrosis during bone-marrow stimulation for cartilage repair. *J Orthop Res*. 2009;27:1432–1438.

12. Choi WJ, Park KK, Kim BS, Lee JW. Osteochondral lesion of the talus: is there a critical defect size for poor outcome? *Am J Sport. Med*. 2009;37:1974–1980.

13. Chu CR, Szczodry M, Bruno S. Animal models for cartilage regeneration and repair. *Tissue Eng Part B Rev*. 2010;16:105–115.

14. Chuckpaiwong B, Berkson EM, Theodore GH. Microfracture for Osteochondral Lesions of the Ankle: Outcome Analysis and Outcome Predictors of 105 Cases. *Arthroscopy*. 2008;24:106–112.

15. Giannini S, Ruffilli A, Pagliazzi G, Mazzotti A, Evangelisti G, Buda R, Faldini C. Treatment algorithm for chronic lateral ankle instability. *Muscles. Ligaments Tendons J*. 2014;4:455–60.

16. Giannini S, Vannini F. Operative treatment of osteochondral lesions of the talar dome: current concepts review. *Foot Ankle Int*. 2004;25:168–175.

17. Gobbi A, Francisco RA, Lubowitz JH, Allegra F, Canata G. Osteochondral lesions of the talus: randomized controlled trial comparing chondroplasty, microfracture, and osteochondral autograft transplantation. *Arthroscopy*. 2006;22:1085–1092.

18. Hangody L, Kish G, Kárpáti Z, Szerb I, Udvarhelyi I, Modis L, Szerb I, Gaspar L, Dioszegi Z, Kendik Z. Mosaicplasty for the treatment of osteochondritis dissecans of the talus: two to seven year results in 36 patients. *Foot Ankle Int*. 2001;22:552–558.

19. Hjelle K, Solheim E, Strand T, Muri R, Brittberg M. Articular cartilage defects in 1,000 knee arthroscopies. *Arthroscopy*. 2002;18:730–734.

20. Hoemann C, Kandel R, Roberts S, Saris DB, Creemers L, Mainil-Varlet P, Methot S, Hollander a. P, Buschmann MD, Hoemann C. Roberts S., Saris D.B.F., Creemers L., Mainil-Varlet P., Methot S., (…), Buschmann M.D. KR. International cartilage repair society (ICRS) recommended guidelines for histological endpoints for cartilage repair studies in animal models and clinical trials. *Cartilage*. 2011;2:153–172.

21. Jackson DW, Lalor PA, Aberman HM, Simon TM. Spontaneous repair of full-thickness defects of articular cartilage in a goat model. A preliminary study. *J Bone Jt. Surg Am*. 2001;83–A:53–64.

22. Japour C, Vohra P, Giorgini R, Sobel E. Ankle arthroscopy: follow-up study of 33 ankles--effect of physical therapy and obesity. *J Foot Ankle Surg*. 1996;35:199–209.

23. Kok AC, Dunnen S, Tuijthof GJ, van Dijk CN, Kerkhoffs GM. Is technique performance a prognostic factor in bone marrow stimulation of the talus? *J Foot Ankle Surg*. 2012;51:777–782.

24. Kreuz PC, Erggelet C, Ph D, Steinwachs MR, Ph D, Krause SJ, Lahm A, Ph D, Niemeyer P, Ghanem N, Uhl M, Ph D, Südkamp N, Ph D, Able T. Is Microfracture of Chondral Defects in the Knee Associated With Different Results in Patients Aged 40 Years or Younger? *Arthroscopy*. 2006;22:1180–1186.

25. Kruyt MC, Dhert WJ, Oner FC, van Blitterswijk CA, Verbout AJ, de Bruijn JD. Analysis of ectopic and orthotopic bone formation in cell-based tissue-engineered constructs in goats. *Biomaterials*. 2007;28:1798–1805.

26. Kumai BYT, Takakura Y, Higashiyama I, Tamai S, Kumai T, Takakura Y, Higashiyama I, Tamai S. Arthroscopic Drilling for the Treatment of Osteochondral Lesions of the Talus. *J Bone Jt. Surg Am*. 1999;81:1229–1235.

27. Lee KB, Bai LB, Chung JY, Seon JK. Arthroscopic microfracture for osteochondral lesions of the talus. *Knee Surg Sport. Traumatol Arthrosc*. 2010;18:247–253.

28. Lind M, Larsen A, Clausen C, Osther K, Everland H. Cartilage repair with chondrocytes in fibrin hydrogel and MPEG polylactide scaffold: an in vivo study in goats. *Knee Surg Sport. Traumatol Arthrosc*. 2008;16:690–698.

29. Loveday D, Clifton R, Robinson A. Interventions for treating osteochondral defects of the talus in adults. *Cochrane Database Syst Rev*. 2010:CD008104.

30. Moojen DJ, Saris DB, Auw Yang KG, Dhert WJ, Verbout AJ. The correlation and reproducibility of histological scoring systems in cartilage repair. *Tissue Eng*. 2002;8:627–634.

31. Newton PO, Lee SS, Mahar AT, Farnsworth CL, Weinstein CH. Thoracoscopic multilevel anterior instrumented fusion in a goat model. *Spine (Phila Pa 1976)*. 2003;28:1614–9; discussion 1620.

32. O'Driscoll SW, Keeley FW, Salter RB. Durability of regenerated articular cartilage produced by free autogenous periosteal grafts in major full-thickness defects in joint surfaces under the influence of continuous passive motion. A follow-up report at one year. *J. Bone Joint Surg. Am*. 1988;70:595–606.

33. O'Driscoll SW, Marx RG, Beaton DE, Miura Y, Gallay SH, Fitzsimmons JS. Validation of a simple histological-histochemical cartilage scoring system. *Tissue Eng*. 2001;7:313–320.

34. Orth P, Goebel L, Wolfram U, Ong MF, Graber S, Kohn D, Cucchiarini M, Ignatius A, Pape D, Madry H. Effect of subchondral drilling on the microarchitecture of subchondral bone: analysis in a large animal model at 6 months. *Am J Sport. Med*. 2012;40:828–836.

35. Palmer AW, Guldberg RE, Levenston ME. Analysis of cartilage matrix fixed charge density and three-dimensional morphology via contrast-enhanced microcomputed tomography. *Proc Natl Acad Sci U S A*. 2006;103:19255–19260.

36. Parisien JS. Arthroscopic treatment of osteochondral lesions of the talus. *Am J Sport. Med*. 1986;14:211–217.

37. Pastoureau P, Leduc S, Chomel A, De Ceuninck F. Quantitative assessment of articular cartilage and subchondral bone histology in the meniscectomized guinea pig model of osteoarthritis. *Osteoarthr. Cartil.* 2003;11:412–423.

38. Pittenger MF, Mackay AM, Beck SC, Jaiswal RK, Douglas R, Mosca JD, Moorman MA, Simonetti DW, Craig S, Marshak DR. Multilineage potential of adult human mesenchymal stem cells. *Science (80-.).* 1999;284:143–147.

39. Prasarn ML, Miller AN, Dyke JP, Helfet DL, Lorich DG. Arterial anatomy of the talus: a cadaver and gadolinium-enhanced MRI study. *Foot Ankle Int.* 2010;31:987–993.

40. Rasband WS. ImageJ. *1997-2011*. 2011.

41. Redman SN, Oldfield SF, Archer CW. Current strategies for articular cartilage repair. *Eur Cell Mater.* 2005;9:23–32.

42. Rutgers M, van Pelt MJP, Dhert WJ, Creemers LB, Saris DB. Evaluation of histological scoring systems for tissue-engineered, repaired and osteoarthritic cartilage. *Osteoarthr. Cartil.* 2010;18:12–23.

43. Saris DB, Dhert WJ, Verbout AJ. Joint homeostasis. The discrepancy between old and fresh defects in cartilage repair. *J Bone Jt. Surg Br.* 2003;85:1067–1076.

44. Saxena A, Eakin C. Articular talar injuries in athletes: results of microfracture and autogenous bone graft. *Am J Sport. Med.* 2007;35:1680–1687.

45. Schimmer RC, Dick W, Hintermann B. The role of ankle arthroscopy in the treatment strategies of osteochondritis dissecans lesions of the talus. *Foot Ankle Int.* 2001;22:895–900.

46. Shapiro F, Koide S, Glimcher MJ. Cell origin and differentiation in the repair of full-thickness defects of articular cartilage. *J Bone Jt. Surg Am.* 1993;75:532–553.

47. Simon TM, Aberman HM. Cartilage regeneration and repair testing in a surrogate large animal model. *Tissue Eng Part B Rev.* 2010;16:65–79.

48. Steadman JR, Rodkey WG, Rodrigo JJ. Microfracture: surgical technique and rehabilitation to treat chondral defects. *Clin Orthop Relat Res.* 2001:S362-9.

49. Treppo S, Koepp H, Quan EC, Cole AA, Kuettner KE, Grodzinsky AJ. Comparison of biomechanical and biochemical properties of cartilage from human knee and ankle pairs. *J Orthop Res.* 2000;18:739–748.

50. Widuchowski W, Widuchowski J, Trzaska T. Articular cartilage defects: study of 25,124 knee arthroscopies. *Knee.* 2007;14:177–182.

51. Williams Iii RJ, Brophy RH. Cartilage repair procedures: clinical approach and decision making. *Instr Course Lect.* 2008;57:553–561.

52. Xie L, Lin AS, Levenston ME, Guldberg RE. Quantitative assessment of articular cartilage morphology via EPIC-microCT. *Osteoarthr. Cartil.* 2009;17:313–320.

53. Zengerink M, Struijs PA, Tol JL, van Dijk CN. Treatment of osteochondral lesions of the talus: a systematic review. *Knee Surgery, Sport. Traumatol. Arthrosc.* 2010;18:238–246.

Appendix 8A.1.
Substances used during operative treatment and euthanasia

1. General anesthesia
10 mg/kg ketamine (Alfasan International BV, Woerden, The Netherlands)

1.5 mg atropine (Centrafarm Services BV, Etten-Leur, The Netherlands)

10–20 mg etomidate intravenously (B. Braun Melsungen AG, Melsungen, Germany) on effect per goat

250 μg fentanyl bolus intravenous injection (Hameln pharmaceuticals gmbh, Hameln, Germany) and repetition based on heart rate

15 mg midazolam bolus injection intravenously (Dormicum; Roche Nederland BV, Woerden, The Netherlands) and repetition on heart rate

1%–2.0% isoflurane (Nicholas Piramal Limited, London, UK) per inhalation

2. Epidural injection
0.1 mg/kg morphine in 4 mL NaCl 0.9%

3. Postoperative pain medication
One 75-μg/hour Duragesic patch (Janssen Cilag BV, Tilburg, The Netherlands)

0.02 mg/kg meloxicam subcutaneously once daily, 5 days maximum

4. Euthanasia
10 mg/kg ketamine (Alfasan International BV)

1.5 mg atropine (Centrafarm Services BV)

10 mg xylazine intramuscularly (Sedazine1; ASTfarma, Oudewater, The Netherlands)

20 mg/kg pentobarbital natrium intravenously (Euthasol 20%; ASTfarma)

Appendix 8A.2
Modified O'Driscoll score as used in this article

| Characteristics		Points
Nature of predominant tissue		
	Hyaline articular cartilage	4
Cellular morphology	Incompletely differentiated mesenchyme	2
	Fibrous tissue or bone	0
	Normal or nearly normal	3
	Moderate	2
Safranin-O staining of the matrix	Slight	1
	None	0
Structural characteristics*		
	Smooth and intact	3
Surface regularity	Superficial horizontal lamination	2
	Fissures 25 to 100 % of the thickness	1
	Severe disruption, including fibrillation	0
	Normal	2
Structural integrity	Slight disruption, including cysts	1
	Severe disintegration	0
	Bonded at both ends of graft	2
Bonding to the adjacent cartilage	Bonded at one end, or partially at both ends	1
	Not bonded	0
Freedom from cellular changes of degeneration		
	Normal cellularity	3
	Slight hypocellularity	2
Hypocellularity	Moderate hypocellularity	1
	Severe hypocellularity	0
	No clusters	2
Chondrocyte clustering	<25 % of the cells	1
	25-100 % of the cells	0
Freedom from degenerative changes in adjacent cartilage		
	Normal cellularity, no clusters, normal staining	3
	Normal cellularity, mild clusters, moderate staining	2
	Mild or moderate hypocellularity, slight staining	1
	Severe hypocellularity, poor or no staining	0

* The subitem ''Thickness of repair tissue'' was left out because all repair tissue was always thicker than the adjacent cartilage and therefore could not be scored accurately (published with permission from O'Driscoll et al [33]
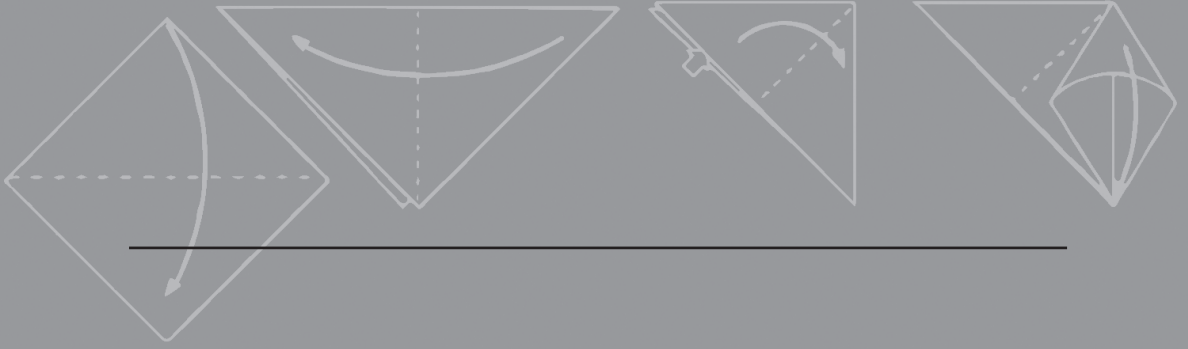
PART IV

GENERAL DISCUSSION AND SUMMARY
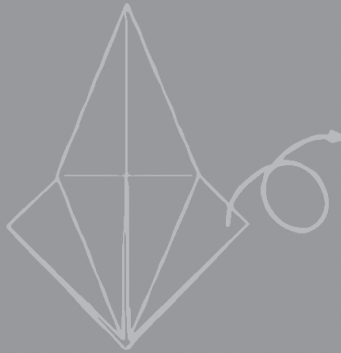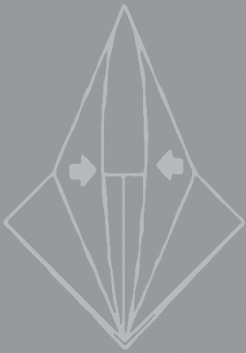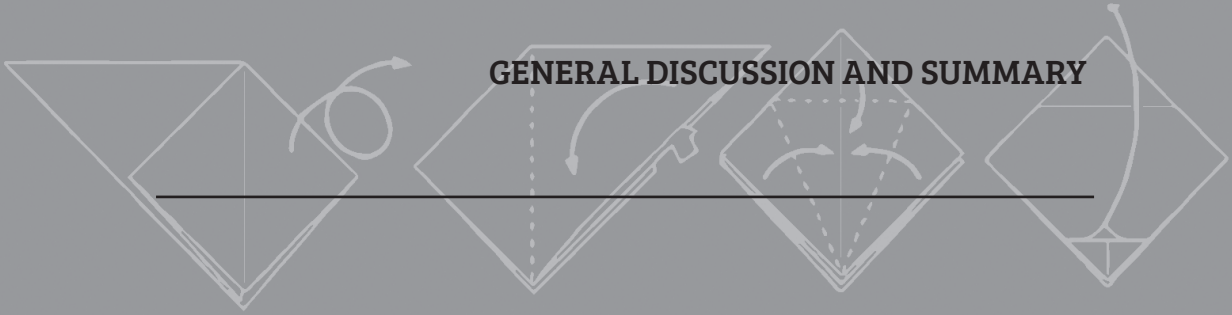
General discussion

Cartilage repair is a complex process, which still is not fully understood [31, 50]. Meticulous monitoring of treatment effects on the repair process will aid our understanding. Important prerequisites in this respect are reliable imaging modalities for both diagnostics and monitoring, as well as uniform scoring systems to compare results. To date, there is no consensus in literature with respect to the use of imaging or scoring systems [46]. This thesis addresses relevant issues in imaging, staging and therapeutic techniques to improve the diagnostics and treatment of OCDT.

Part I: Optimizing pre-clinical imaging

Optimizing the pre-clinical imaging of repair tissue will contribute to more reliable, comparable research data. To reach a consensus on pre-clinical imaging modalities and scoring systems in the future, the controversies in this field as well as alternatives were explored.

Macroscopic vs. structural assessment

The theoretical advantage of macroscopic assessment of repair cartilage quality is obvious: its non-invasive easy use allows a surgeon performing an arthroscopy to instantly judge the quality of tissue without the need for a biopsy. However, it is shown in **chapter 2** that macroscopic scoring of cartilage repair provides an insufficient representation of the repair tissue quality because it is solely dependent on superficial morphological data whereas the golden standard, histological assessment, allows qualitative and structural in-depth assessment as well. Currently, it is unclear whether macroscopic scoring alone can achieve equally reliable assessment as histology [4]. Possibly the accuracy of macroscopic assessment can be improved by a more elaborate analysis including additional parameters such as hypertrophy, colour, response to palpation, lesion size, location and degenerative status of the joint [42].

Until we establish whether a reliable macroscopic scoring system can be achieved, advanced imaging techniques such as Optical Coherence Tomography (OCT), as studied in **chapter 3,** could bridge the gap. OCT is a fibre optically based imaging technique suited for arthroscopy [43] and has been used in imaging meniscal tears and cartilage degeneration [9, 40]. The imaging depth is limited to approximately 2 mm [5], which is sufficient to reach the subchondral bone plate in the talus since the talar cartilage thickness is around 1.4 mm [6]. Since OCT can be applied arthroscopically and without the need for a biopsy it allows relatively non-invasive measurement of more in-depth parameters, such as repair tissue depth and fissures or surface

indentations, which are known to be relevant in repair tissue assessment [4]. Based on validated microscopic scoring systems, other interesting characteristics to study are structural integrity (including subchondral cysts) and bonding of the repair tissue to the adjacent cartilage [38, 51]. To our knowledge OCT has not been used in assessment of OCDT imaging, OCDT repair or even the ankle in general. Future research should investigate whether OCT is suitable for this purpose and then used to aid in the development of a non-invasive score. When comparing OCT imaging to histology it should be taken into consideration that our *ex vivo* study has shown the importance of accurate co-localisation of OCT and histological slices for reliable matching and comparison. Other studies have shown good results with 3D histology, which uses a reference cutting plane and dense histological sampling [1].

Sample size and quantification

This thesis touches several sensitive points in the development of a validated assessment scheme. There are two essential conclusions. Firstly, in order to include the entire spectrum of possible results of repair tissue quality, an extensive number of samples is needed. Especially in *in-vivo* studies where not all confounding factors can be controlled, such as weight bearing in goats for example, study methods should be designed specifically to achieve a large variety in results (**chapter 2**). However, in concordance with the 3R principles of animal studies (replacement, reduction, refinement) it might prove impossible to design a prospective study with sufficient subjects and the use of retrospective data from other studies should be considered (**chapter 3**). Perhaps the rise of big data analysis techniques can play a role in facilitating this process.

Secondly, semi-quantitative scoring will benefit from automated assessment, such as in our studies in **chapter 3 and 8**. Though semi-quantitative scoring suggests a higher degree of accuracy (e.g. as more or less than 50%) than non-quantitative scoring, it is highly dependent on the interpretation of the observer and thereby subject to a significant learning curve [38]. In other fields automated assessment is used for objectification with higher correlations than visual assessment [37]. It would be incredibly valuable to explore the possibilities of complete automated assessment, since many current scoring items allow quantification. The challenge lies in correlating those results with clinically relevant differences.

Part II: Improving clinical imaging

Chapters 4 and 5 have shown that ultrasound is a viable imaging technique for longitudinal follow up of anterior and centrally located OCDT in patients at short

intervals in time [19, 26]. Several practical directions and recommendations for the future can be made based on this thesis.

In full plantar flexion the tibial bone still covers the posterior part of the talus; the tibial bone inhibits ultrasound waves and thereby imaging of the posterior talar cartilage surface. Therefore, ultrasound is not suited for defects on the posterior aspect of talar dome [3]. Similarly, the tibial superposition also limits the area of the talar dome that can be accessed with anterior ankle arthroscopy. Current pre-operative planning uses a plantar CT scan to determine whether a central OCDT clears the tibial bone in plantar flexion to determine the accessibility with anterior ankle arthroscopy. Recent studies have shown that the visible anterocentral area of the talus with ultrasound coincides with the area accessible with anterior ankle arthroscopy [2]. This could make ultrasound a useful tool in the pre-operative planning to determine whether a lesion can be treated using anterior arthroscopy without the need of an additional plantar CT scan.

The results of our studies also justify further steps to explore the use of ultrasound to gain more *in-vivo* insight in the cartilage repair process. Based on the combined experience from our studies and literature, we expect ultrasound to be able to detect every predominant morphological feature presented in various OCDT and repair tissue classification systems for other imaging modalities such as defect fill, surface regularity, and integration into the adjacent cartilage [22, 35]. Future research will have to determine to what degree cartilage repair tissue changes are detectable before we consider ultrasound for post-operative follow up. There are two possible applications of ultrasound in this respect: non-invasive morphological ultrasound imaging using the conventional probes and a more invasive ultrasound imaging of acoustic properties of cartilage using experimental probes which require direct contact with the cartilage.

As for non-invasive use in clinical practice, we propose using a standardized protocol. Since ultrasound is highly observer dependent this will be essential when considering it for comparative longitudinal follow up [6,7,20]. An adapted imaging protocol is presented in the appendix based on our experience (**Appendix 9A.1**). Also, the use of 3D tracked imaging (as used in **chapter 5**, fig. 9.1) would be a significant contribution to the reproducibility because of read-back options and one-on-one location retrieval between different exams [21].

As for quantitative ultrasonic assessment of cartilage, it has been shown in previous literature that the ultrasound signal correlates with cartilage thickness and structural properties including cartilage integrity in osteoarthritis [21, 29, 33, 34].

Converting ultrasonic echoes into wavelet maps allows analysis of the maximum magnitude and echo duration, which in turn have been shown to correlate with quantitative cartilage indices. This allows successful detection of microscopic changes [17, 21]. Ultrasonic palpation gives information on cartilage stiffness and relaxation times in case of compression and indentation to allow *in vivo* biomechanical testing [48].

The invasive nature of this technique currently puts quantitative ultrasound more in the realm of pre-clinical imaging. The challenge lies in developing a non-invasive system what will allow *in vivo* assessment. Our study group is currently designing this by combining acoustic wave generation, mechanical loading and ultrasonic sensing to quantify cartilage damage within the Vibrant Vision project under a new STW grant. Current testing of biomechanical behaviour of cartilage requires require complex *ex vivo* set ups with cylindrical samples made to fit the testing machine, taken from their surrounding articular cartilage potentially changing the water flow

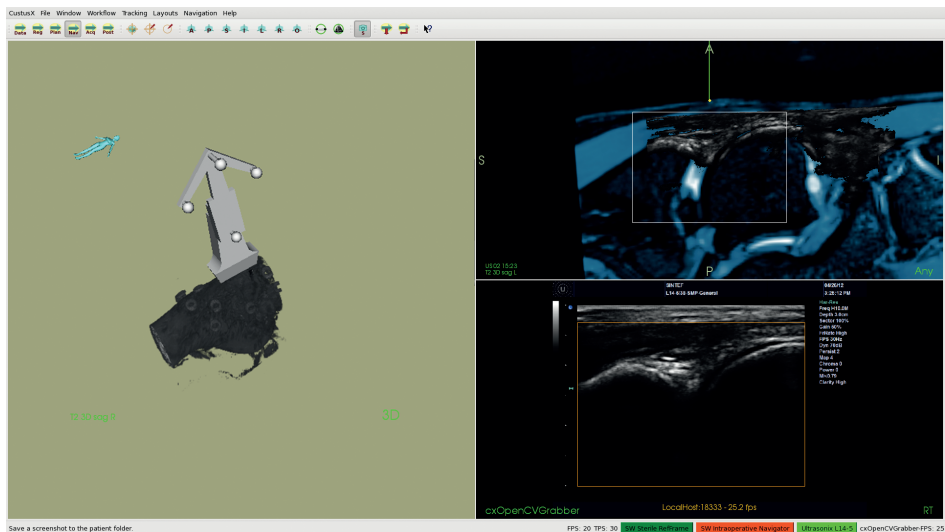**Figure 9.1 Location retrieval of ultrasound images using 3D tracking**
3D tracking is used to co-localise CT images (blue) and ultrasound images (black and white) using Custus X. *Left*: ultrasound probe projection on the reconstructed 3D ultrasound volume, *Top right*: sagittal CT image (blue) with ultrasound image overlay after registration of both volumes, *Bottom right*: original ultrasound image of the talar dome.

and collagen fibre structure and therefore the biomechanical behaviour. Proving a tool for *in vivo* mechanical assessment could change this for both joint and vertebral disc research.

Maybe this degree of detail will prove too advanced for routine clinical practice. However, in case of thin cartilage such as the ankle where cartilage stiffness differences are less outspoken, it could aid the surgeon with an objective measure of cartilage quality and locate subchondral defects with an intact cartilage surface.

Part III: Optimizing treatment

In literature, clinical results and prognostic factors of OCDT treatment techniques are often contradictory and inconclusive due to factors such as low level of evidence, small patient groups and heterogeneity of the study methods and patient populations [11, 45]. This thesis has shown that the effect of technique detail is underreported and we implore researchers to investigate adaptations of existing treatment options and aid in designing a patient and defect specific treatment algorithm.

Infiltration technique

In **chapter 6** we presented a cross-over patient study that investigates the accuracy of intra-articular injections in the osteo-arthritic ankle joint with or without the use of a traction device. While the study was performed on patients with arthritis and not OCDT, infiltrations with hyaluronic acid are often used in patients with OCDT with or without concomitant arthritis as well [36]. No significant differences were found between the two techniques, but it should be noted that the substantial amount of possible extra-articular injections corresponds with previous literature [24]. It is advisable to use imaging during injection, especially with severe osteoarthritis, anterior osteophytes or less experienced surgeons. Traditionally, contrast-aided fluoroscopy is used for this type of imaging. However, considering the results presented in previous research [27, 52], and **chapters 4 and 5**, ultrasound could serve as an alternative without the burden of radiation or the use of a contrast-agent. This could significantly reduce the amount of extra-articular injections and increase successful therapeutic agent delivery while preventing exposure to unnecessary adverse events.

If adequate infiltration is safeguarded, the next research question to be answered is which agent to use, both as solitary treatments and as supplemental agents to surgical treatment. Recently several high level clinical studies have been published providing positive results for microfracture with the addition hyaluronic acid [49]

and platelet rich plasma [18] with lower pain scores and higher functional outcome. Further research will need to provide long term follow up in larger cohorts to establish whether these augmentations prove useful in the long term.

Microfracture technique

In **chapter 7** it was shown that specific technique descriptions were often lacking in current literature. If a description was given, it often was comparable to the technique as presented in the original article by Steadman [53]. The majority of included articles were retrospective case series with limited statistical analysis and a relatively small number of patients. The articles that were excluded for this review showed a similar quality. A recent review concluded there has been no improvement in level of evidence based medicine practice for microfracture in recent years and results have remained highly variable [16].

In our opinion, essential improvements would have to be established to improve this current impasse. Future studies should not only include precise information on their methods, but also data on possible prognostic factors (such as lesion size, patient related factors and postoperative regimen), use a sound methodology and uniform grading systems, and provide standardized outcome measurements. A validated imaging and scoring evaluation guideline for OCDT is therefore warranted. Such a scheme is already available for the knee in the form of the ICRS cartilage evaluation package for the knee [22], which holds a standardized work-up using validated questionnaires, defect type, location and treatment registration, and postoperative assessment scores. This could serve as an example for a similar package for the ankle. However, the selection of imaging modalities and matching scoring systems would have to be made from the many available options (as illustrated in the introduction of this thesis) in a way that carries broad consensus.

The necessity of more high-level therapeutic studies with standardized homogeneous methods including detailed technique descriptions is evident. However, designing clinical studies using a more standardized approach can be challenging. We expect technique variation to be unavoidable to some extent due to factors such as limited access to central-posterior defects using the current rigid instruments [14] or irregular defects. This could result in cartilage damage due to wedging of the instruments and unstandardized distribution of the microfracture holes. Possible ways to improve these problems are the adaption of the current surgical tools or the use of an animal model in which practical factors can be controlled more (such as choosing an easily accessible defect location). This thesis utilizes both these strategies.

To improve the current rigid surgical tools for microfracture our research group initiated the "hydrochipper' project. Its aim is to create a more flexible arthroscopic microfracture tool that at the same time could provide a standardized microfracture pattern. Water jet cutting is used instead of the conventional microfracture awls or drills to achieve more control over the distribution of the holes while using a flexible device. Water jet has been used in various surgical fields for cutting, such as in tonsillectomies [32] and hepatectomies [55]. It has also been suggested for peri-prosthetic interface cutting in revision surgery [28]. While straightforward cutting through cortical bone and accurate drilling to a limited depth in trabecular bone are very different in terms of device demands, the proof of concept *ex vivo* studies have shown promising results in terms of accuracy and reproducibility [13, 14]. We expect a more standardized treatment using this technique because depth, geometry and direction perpendicular to the cartilage surface can be controlled by using one flexible water jet head that makes several holes in one jetting session. In addition, water jet is able to produce holes as small as 0.3 mm in diameter, which we hypothesised would cause less damage to the subchondral bone providing a better scaffold for the repair tissue.

However, our animal study in **chapter 8** showed no difference between small diameter and larger diameter holes using conventional tools (0.45 mm vs. 1.1 mm). Interestingly, another study published in two separate articles found a significantly better quality repair with smaller holes (1.0 mm vs. 1.8 mm) in full thickness chondral defects in sheep femoral defects [15, 41]. But these results are not truly comparable considering the established differences between various animal models, as well as between the ankle and the knee joint [10, 23]. Also, our model used osteochondral defects and our large holes were about the same size as the small holes in the aforementioned study by Eldracher et al. and Orth et al. [15, 41]. Our study used the conventional microfracture awls, because a suitable water jet device was not yet available. It would be interesting to compare water jet microfracture to the conventional awls to see whether this produces a different repair tissue. Still unpublished data of a second animal study using water jet in chondral defects of the goat talus has shown no significant adverse events, but since animal studies are not directly applicable to human pathology, patient studies are imperative in the future.

Based on the best available evidence, microfracture is an established, simple and financially favourable technique with low morbidity for patients. The current indications for microfracture are relatively narrow since it is generally accepted that it only produces a stable tissue in small OCDT [7, 11]. It is also broadly stated that since it does not produce hyaline like cartilage the long-term results could deteriorate and

show progression to osteoarthritis [30, 31]. However, using microfracture combined with other techniques to improve the stability and quality of the repair tissue, such as with additives or a biomimetic scaffold gel, has not been explored extensively yet. Herein lies another possible option for optimization.

There are several prospective RCTs available on the use of hyaluronic acid and PRP with microfracture. Görmeli et al. compared a single injection with hyaluronic acid, PRP and saline after microfracture treatment in 40 patients with OCDT smaller than 15 mm. Follow-up up to two years showed significantly better VAS and AOFAS scores in the PRP and hyaluronic acid group compared to the control saline group [18]. The overall satisfaction rate at one year however was still rather low: fully or partially satisfied total scores were 85% for PRP, 86% for hyaluronic acid, and 77% in the control group. Several other prospective RCT studies compared either PRP or hyaluronic acid to microfracture alone with similar results [12, 20]. So, while either PRP or hyaluronic acid might improve results of microfracture, a number of patients remain with complaints. This could be due to insufficient effect of the compound, wrong infiltration technique or inadequate selection of patient and lesion characteristics.

We firmly believe that it is imperative to design patient specific treatment algorithm with careful consideration of defect characteristics. Possibly suitable alternatives for one indication should be investigated in comparable patient groups. Currently, there does not seem to be a difference between chondral and osteochondral defects in terms of treatment outcome [25, 44, 47]. However, in our opinion OCDT treatment should not be differentiated for affected tissue, but by affected structural component and size. Also, the primary or secondary nature should be established and treated as a different entity due to the differences in mechanism of injury and healing potential [39]. Following this reasoning, it should be determined whether small, superficial defects benefit from injected additives, such as hyaluronic acid or PRP. More substantial defects involving different structural components (such as deep defects) or that are inherently unstable (larger defects) could benefit from guided regeneration. Relatively superficial but larger defects could be treated using biomimetic scaffolds [8, 54] to improve repair tissue integration and stability, while large deep defects could be reconstructed using directly implanted substitutes (such as TOPIC). The challenge lies in defining if and where simple additives suffice, and where extensive reconstructive treatment is necessary.
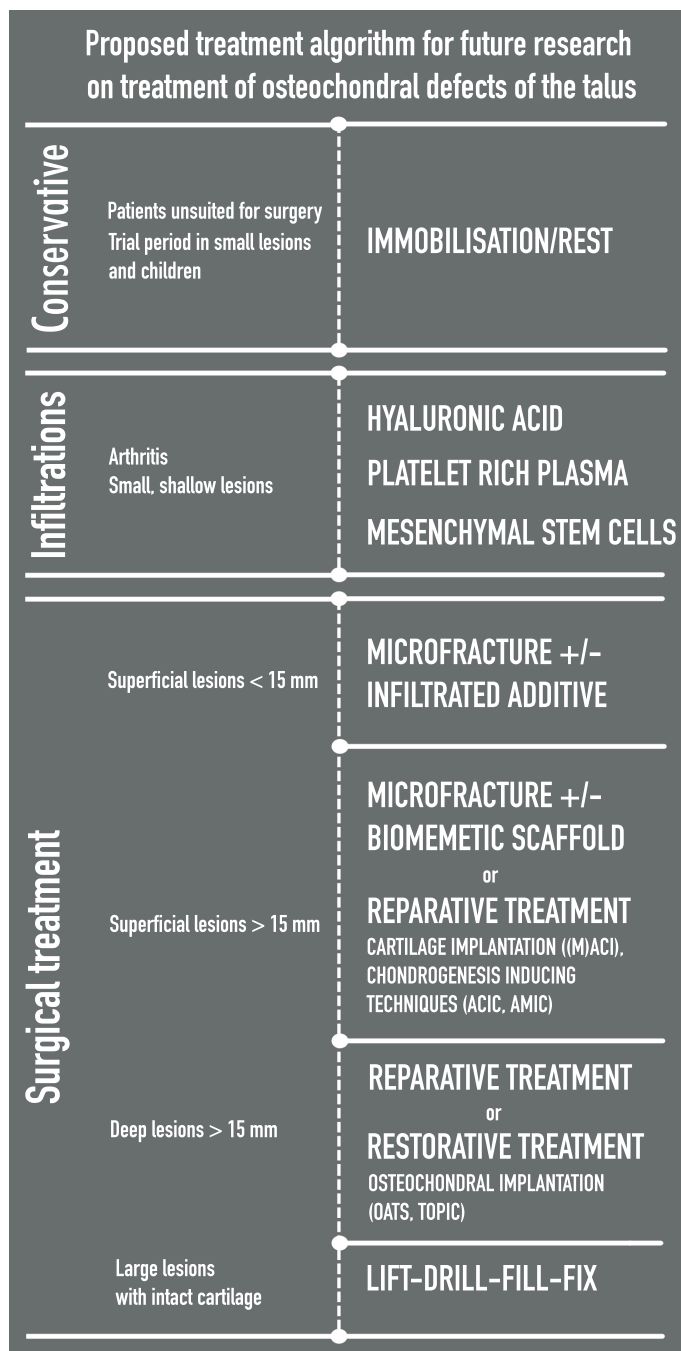
Fig. 9.2 Suggested treatment algorithm as a guideline for future research and treatment
This algorithm takes into consideration OCDT size, structural nature of a defect, previous treatment and patient characteristics. Possibly suitable alternatives for one indication should be investigated in comparable patient groups using methodically sound research methods.

Conclusion

This thesis contains various research modalities such as basic science, literature review, cadaveric experiments, and *in vivo* animal and patient studies dedicated to optimizing existing imaging and treatment techniques for OCD of the talus.

Based on the results of these studies presented in this thesis we conclude the following:

- There is need for a guideline outlining which imaging techniques and validated imaging scoring systems can be used in diagnostic assessment of OCDT and repair tissue after treatment.
- Advanced techniques that have proven useful in other fields can be considered for imaging OCDT repair to increase our understanding of the cartilage repair process. Optical Coherence Tomography for example can assess cartilage thickness and surface morphology without biopsy with good correlation with histology.
- Ultrasound imaging is feasible as a cheaper, less invasive alternative for extensive follow up for anterior and central OCLT. Future research will concentrate on its usefulness in clinical imaging of repair tissue and on quantitative ultrasonic assessment of cartilage quality.
- Intra-articular infiltration in the ankle benefits from imaging using either conventional fluoroscopy or ultrasound by decreasing the amount of unintended extra-articular injections.
- Detailed descriptions of the microfracture technique are often lacking from literature. There is a need for larger high-quality studies with explicit description of patient groups and technique, sound methodology and uniform scoring and outcome measures.
- Changes in microfracture depth or diameter do not affect repair tissue quality in OCDT in the goat. Using water jet cutting could provide a more standardized treatment, but the "hydrochipper" is yet to be developed further into a clinically usable device.
- It is imperative to design a patient specific treatment algorithm. This can also guide future research and treatment with careful consideration of size, structural nature of a defect, previous treatment and patient characteristics.

References

1. Alic L, Haeck JC, Bol K, Klein S, van Tiel ST, Wielepolski PA, de Jong M, Niessen WJ, Bernsen M, Veenland JF. Facilitating tumor functional assessment by spatially relating 3D tumor histology and In Vivo MRI: Image registration approach. *PLoS One*. 2011;6:1–10.

2. Van Bergen CJ, Tuijthof GJ, Blankevoort L, Maas M, Kerkhoffs GM, Van Dijk CN. Computed tomography of the ankle in full plantar flexion: a reliable method for preoperative planning of arthroscopic access to osteochondral defects of the talus. *Arthroscopy*. 2012;28:985–992.

3. van Bergen CJ, Tuijthof GJ, Blankevoort L, Maas M, Kerkhoffs GM, van Dijk CN. Computed tomography of the ankle in full plantar flexion: a reliable method for preoperative planning of arthroscopic access to osteochondral defects of the talus. *Arthroscopy*. 2012;28:985–992.

4. Brittberg M, Winalski CS. Evaluation of cartilage injuries and repair. *J Bone Jt. Surg Am*. 2003;85–A Suppl:58–69.

5. Cernohorsky P, Kok AC, Bruin DM de, Brandt MJ, Faber DJ, Tuijthof GJ, Kerkhoffs GM, Strackee SD, van Leeuwen TG. Comparison of optical coherence tomography and histopathology in quantitative assessment of goat talus articular cartilage. *Acta Orthop*. 2015;86:257–263.

6. Cher WL, Utturkar GM, Spritzer CE, Nunley JA, DeFrate LE, Collins AT. An analysis of changes in in vivo cartilage thickness of the healthy ankle following dynamic activity. *J. Biomech*. 2016;49:3026–3030.

7. Choi WJ, Park KK, Kim BS, Lee JW. Osteochondral lesion of the talus: is there a critical defect size for poor outcome? *Am J Sport. Med*. 2009;37:1974–1980.

8. Christensen BB, Foldager CB, Jensen J, Jensen NC, Lind M. Poor osteochondral repair by a biomimetic collagen scaffold: 1- to 3-year clinical and radiological follow-up. *Knee Surg. Sports Traumatol. Arthrosc*. 2016;24:2380–2387.

9. Chu CR, Izzo NJ, Irrgang JJ, Ferretti M, Studer RK. Clinical diagnosis of potentially treatable early articular cartilage degeneration using optical coherence tomography. *J. Biomed. Opt*. 2007;12:51703.

10. Chu CR, Szczodry M, Bruno S. Animal models for cartilage regeneration and repair. *Tissue Eng Part B Rev*. 2010;16:105–115.

11. Dahmen J, Lambers KT, Reilingh ML, Bergen CJ Van. No superior treatment for primary osteochondral defects of the talus. *Knee Surgery, Sport. Traumatol. Arthrosc*. 2017.

12. Doral MN, Bilge O, Batmaz G, Donmez G, Turhan E, Demirel M, Atay OA, Uzumcugil A, Atesok K, Kaya D. Treatment of osteochondral lesions of the talus with microfracture technique and postoperative hyaluronan injection. *Knee Surg. Sports Traumatol. Arthrosc*. 2012;20:1398–1403.

13. den Dunnen S, Dankelman J, Kerkhoffs GM, Tuijthof G. Colliding jets provide depth control for water jetting in bone tissue. *J. Mech. Behav. Biomed. Mater*. 2017;72:219–228.

14. den Dunnen S, Mulder L, Kerkhoffs GM, Dankelman J, Tuijthof GJ. Waterjet drilling in porcine bone: the effect of the nozzle diameter and bone architecture on the hole dimensions. *J. Mech. Behav. Biomed. Mater*. 2013;27:84–93.

15. Eldracher M, Orth P, Cucchiarini M, Pape D, Madry H. Small Subchondral Drill Holes Improve Marrow Stimulation of Articular Cartilage Defects. *Am. J. Sports Med*. 2014;42:2741–2750.

16. Frehner F, Benthien JP. Microfracture: State of the Art in Cartilage Surgery? *Cartilage*. 2017:194760351770095.

17. Gelse K, Olk A, Eichhorn S, Swoboda B, Schoene M, Raum K. Quantitative ultrasound biomicroscopy for the analysis of healthy and repair cartilage tissues. *Eur. Cells Mater*. 2010;19:58–71.

18. Gormeli G, Karakaplan M, Gormeli CA, Sarikaya B, Elmali N, Ersoy Y. Clinical Effects of Platelet-Rich Plasma and Hyaluronic Acid as an Additional Therapy for Talar Osteochondral Lesions Treated with Microfracture Surgery: A Prospective Randomized Clinical Trial. *Foot ankle Int*. 2015;36:891–900.

19. Grassi W, Lamanna G, Farina A, Cervini C. Sonographic imaging of normal and osteoarthritic cartilage. *Semin Arthritis Rheum*. 1999;6:398–403.

20. Guney A, Akar M, Karaman I, Oner M, Guney B. Clinical outcomes of platelet rich plasma (PRP) as an adjunct to microfracture surgery in osteochondral lesions of the talus. *Knee Surg. Sports Traumatol. Arthrosc*. 2015;23:2384–2389.

21. Hattori K, Ikeuchi K, Morita Y, Takakura Y. Quantitative ultrasonic assessment for detecting microscopic cartilage damage in osteoarthritis. *Arthritis Res Ther*. 2005;7:R38-46.

22. Hauselmann HJ, Jakob RP, Levine D. ICRS Cartilage Injury Evaluation Package. *ICRS Cartil. Inj. Eval. Packag.* 2000:1–16.

23. Hoemann C, Kandel R, Roberts S, Saris DB, Creemers L, Mainil-varlet P, Méthot S, Hollander AP, Buschmann MD. (ICRS) Recommended Guidelines for Studies in Animal Models and Clinical Trials. *Cartilage*. 2011;2:153–172.

24. Jones A, Regan M, Ledingham J, Pattrick M, Manhire A, Doherty M. Importance of placement of intra-articular steroid injections. *BMJ*. 1993;307:1329–30.

25. Jung HG, Carag JA V, Park JY, Kim TH, Moon SG. Role of arthroscopic microfracture for cystic type osteochondral lesions of the talus with radiographic enhanced MRI support. *Knee Surgery, Sport. Traumatol. Arthrosc*. 2011;19:858–862.

26. Keen HI, Conaghan PG. Usefulness of ultrasound in osteoarthritis. *Rheum Dis Clin North Am*. 2009;35:503–519.

27. Khosla S, Thiele R, Baumhauer JF. Ultrasound guidance for intra-articular injections of the foot and ankle. *Foot ankle Int*. 2009;30:886–890.

28. Kraaij G, Tuijthof GJ, Dankelman J, Nelissen RG, Valstar ER. Waterjet cutting of periprosthetic interface tissue in loosened hip prostheses: an in vitro feasibility study. *Med. Eng. Phys.* 2015;37:245–250.

29. Kuroki H, Nakagawa Y, Mori K, Kobayashi M, Nakamura S, Nishitani K, Shirai T, Nakamura T. Ultrasound properties of articular cartilage immediately after osteochondral grafting surgery: In cases of traumatic cartilage lesions and osteonecrosis. *Knee Surgery, Sport. Traumatol. Arthrosc*. 2009;17:11–18.

30. Lee K, Bai L, Yoon T. Second-Look Arthroscopic Findings and Clinical Outcomes After Microfracture for Osteochondral Lesions of the Talus. *Am. J. Sports Med.* 2010.

31. Looze CA, Capo J, Ryan MK, Begly JP, Chapman C, Swanson D, Singh BC, Strauss EJ. Evaluation and Management of Osteochondral Lesions of the Talus. *Cartilage*. 2017;8:19–30.

32. Lorenz KJ, Kresz A, Maier H. [Hydrodissection for tonsillectomy. Results of a pilot study--intraoperative blood loss, postoperative pain symptoms and risk of secondary hemorrhage]. *HNO*. 2005;53:423–427.

33. Lötjönen P, Julkunen P, Tiitu V, Jurvelin JS, Töyräs J. Ultrasound speed varies in articular cartilage under indentation loading. *IEEE Trans. Ultrason. Ferroelectr. Freq. Control*. 2011;58:2772–2780.

34. Mannicke N, Schone M, Oelze M, Raum K. Articular cartilage degeneration classification by means of high-frequency ultrasound. *Osteoarthr. Cartil*. 2014;22:1577–1582.

35. Marlovits S, Singer P, Zeller P, Mandl I, Haller J, Trattnig S. Magnetic resonance observation of cartilage repair tissue (MOCART) for the evaluation of autologous chondrocyte transplantation: Determination of interobserver variability and correlation to clinical outcome after 2 years. *Eur. J. Radiol*. 2006;57:16–23.

36. Mei-Dan O, Carmont MR, Laver L, Mann G, Maffulli N, Nyska M. Platelet-rich plasma or hyaluronate in the management of osteochondral lesions of the talus. *Am. J. Sports Med*. 2012;40:534–541.

37. Te Moller NC, Pitkänen M, Sarin JK, Väänänen S, Liukkonen J, Afara IO, Puhakka PH, Brommer H, Niemelä T, Tulamo R-M, Argüelles Capilla D, Töyräs J. Semi-automated ICRS scoring of equine articular cartilage lesions in optical coherence tomography images. *Equine Vet. J*. 2016:1–7.

38. O'Driscoll SW, Marx RG, Beaton DE, Miura Y, Gallay SH, Fitzsimmons JS. Validation of a simple histological-histochemical cartilage scoring system. *Tissue Eng*. 2001;7:313–320.

39. O'Loughlin PF, Heyworth BE, Kennedy JG, Loughlin PF, Heyworth BE, Kennedy JG, Loughlin PF, Heyworth BE. Current concepts in the diagnosis and treatment of osteochondral lesions of the ankle. *Am. J. Sports Med*. 2010;38:392–404.

40. O'Malley MJ, Chu CR. Arthroscopic optical coherence tomography in diagnosis of early arthritis. *Minim. Invasive Surg*. 2011;2011.

41. Orth P, Duffner J, Zurakowski D, Cucchiarini M, Madry H. Small-Diameter Awls Improve Articular Cartilage Repair After Microfracture Treatment in a Translational Animal Model. *Am. J. Sports Med*. 2016;44:209–219.

42. Orth P, Peifer C, Goebel L, Cucchiarini M, Madry H. Comprehensive analysis of translational osteochondral repair: Focus on the histological assessment. *Prog. Histochem. Cytochem*. 2015;50:19–36.

43. Pan Y, Li Z, Xie T, Chu CR. Hand-held arthroscopic optical coherence tomography for in vivo high-resolution imaging of articular cartilage. *J. Biomed. Opt*. 2003;8:648–54.

44. Park H-W, Lee K-B. Comparison of chondral versus osteochondral lesions of the talus after arthroscopic microfracture. *Knee Surg. Sports Traumatol. Arthrosc*. 2015;23:860–867.

45. Pinski JM, Boakye LA, Murawski CD, Hannon CP, Ross KA, Kennedy JG. Low Level of Evidence and Methodologic Quality of??Clinical Outcome Studies on Cartilage Repair of??the??Ankle. *Arthroscopy*. 2016;32:214–222.

46. Rutgers M, van Pelt MJP, Dhert WJ, Creemers LB, Saris DB. Evaluation of histological scoring systems for tissue-engineered, repaired and osteoarthritic cartilage. *Osteoarthr. Cartil*. 2010;18:12–23.

47. Saxena A, Eakin C. Articular talar injuries in athletes: results of microfracture and autogenous bone graft. *Am J Sport. Med*. 2007;35:1680–1687.

48. Schone M, Schulz RM, Tzschatzsch H, Varga P, Raum K. Ultrasound palpation for fast in-situ quantification of articular cartilage stiffness, thickness and relaxation capacity. *Biomech. Model. Mechanobiol*. 2017;16:1171–1185.

49. Shang X-L, Tao H-Y, Chen S-Y, Li Y-X, Hua Y-H. Clinical and MRI outcomes of HA injection following arthroscopic microfracture for osteochondral lesions of the talus. *Knee Surg. Sports Traumatol. Arthrosc*. 2016;24:1243–1249.

50. Shapiro F, Koide S, Glimcher MJ. Cell origin and differentiation in the repair of full-thickness defects of articular cartilage. *J Bone Jt. Surg Am*. 1993;75:532–553.

51. Smith GD, Taylor J, Almqvist KF, Erggelet C, Knutsen G, Garcia Portabella M, Smith T, Richardson JB, Portabella MG, Smith T, Richardson JB. Arthroscopic assessment of cartilage repair: a validation study of 2 scoring systems. *Arthroscopy*. 2005;21:1462–1467.

52. Stanish WD, McCormack R, Forriol F, Mohtadi N, Pelet S, Desnoyers J, Restrepo A, Shive MS. Novel scaffold-based BST-CarGel treatment results in superior cartilage repair compared with microfracture in a randomized controlled trial. *J. Bone Joint Surg. Am*. 2013;95:1640–1650.

53. Steadman JR, Rodkey WG, Rodrigo JJ. Microfracture: surgical technique and rehabilitation to treat chondral defects. *Clin Orthop Relat Res*. 2001:S362-9.

54. Vila Y Rico J, Dalmau A, Chaques FJ, Asuncion J. Treatment of Osteochondral Lesions of the Talus With Bone Marrow Stimulation and Chitosan-Glycerol Phosphate/Blood Implants (BST-CarGel). *Arthrosc. Tech.* 2015;4:e663-7.

55. Vollmer CM, Dixon E, Sahajpal A, Cattral MS, Grant DR, Gallinger S, Taylor BR, Greig PD. Water-jet dissection for parenchymal division during hepatectomy. *HPB (Oxford).* 2006;8:377–385.

174

Appendix 9A.1
Adapted imaging protocol for ultrasound examination of (osteo-)chondral defects in the talus.

Ultrasound settings
High-resolution ultrasound is able to detect cartilage and underlying bony disruptions. Appropriate settings are required for optimal imaging. *Table 9.A1* displays the settings used in our protocol.

Table 9A.1. Ultrasound settings

Parameter	Setting
Frequency	17 MHz
Depth	3.0 cm
Gain	49%
Frame rate	High
Frames per second	30
Dynamic range	70 dB
Persistence	2
Clarity	High

Positioning
Plantar flexion of the foot is vital for imaging the maximal talar surface due to over-projection of the tibia. At the start of the examination the foot is placed in maximal plantar flexion using the following technique (*Fig. 9A.1*). The patient is seated on the examination bench with the knee flexed and the dorsum of the foot completely flat on the bench. The patient is moved backwards on the examination bench (or the foot is moved forward) while keeping the dorsum of the foot flat on the table

Figure 9A.1. Optimal positioning for ultrasound examination of OCDT
Left: Patient sitting on examination bench with knee flexed and foot with plantar surface on the table.
Right: Patient moved backwards on the examination bench while keeping plantar surface of the foot on the table.

(*Fig. 9A.1*). The foot will be in maximal plantar flexion when the patixent cannot move further backwards while keeping his/her foot flat on the examination bench. One can consider using weights on the toes or sitting on the toes (as is done in knee examination tests) to ensure maximal plantar flexion.

Structured examination

The observer should perform a scan of the talus in a consistent and standardized manner using landmarks for guidance. We recommend performing two motions (*Fig. 9A.2, centre*).

The first motion starts at the medial ankle with the probe placed perpendicular on the foot on the deltoid ligament. The joint line is positioned in the centre of the probe, visualizing the tibial rim and the proximal surface of the talus at all times while moving the probe to lateral (*Figure 9A.2, right*). The lateral rim is reached where the lateral malleolus begins and when the anterior talofibular ligament is visualized.

The probe is then moved distally to perform the second motion back to medial in order to display the more distal surface of the talus that might not have been visible during the first motion (*Figure 9A, left*). The main landmarks here are the frontal cartilaginous rim of the talus, the transition of the talar neck to the body and the prominence on the medial part of the talus.
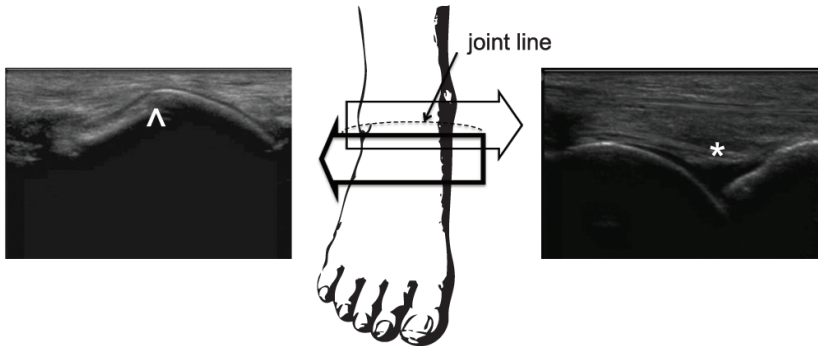

Figure 9A.2. Structured ultrasound examination of the talar surface with landmarks.
Centre: showing the two motions during the exam, medial to lateral and back. *Right:* Ultrasound image of the proximal sweep with the joint line (*) centred in the image. *Left:* Ultrasound image of the distal sweep showing the more distal articular cartilage up to its frontal rim (^). *Ti: tibia; ta=talus*

Recording (osteo)chondral defects.

When a (osteo)chondral defect is detected, several characteristics can be noted.

<u>Location</u>

To identify the location of a (osteo)chondral defect, the talus can be divided into three zones (*Fig. 9A.3*). This can be done in two ways: either by using a coronal overview of the talus and dividing this image into three equal zones, or by using the ankle tendons as an anatomical reference as used in previous literature [4]. The medial zone was defined by the anterior deltoid ligament medially and the lateral border of the tibialis anterior tendon; the central zone by the tibialis anterior and the medial border of the extensor digitorum longus tendon; the lateral zone by the extensor digitorum longus and the anterior talofibular ligament.
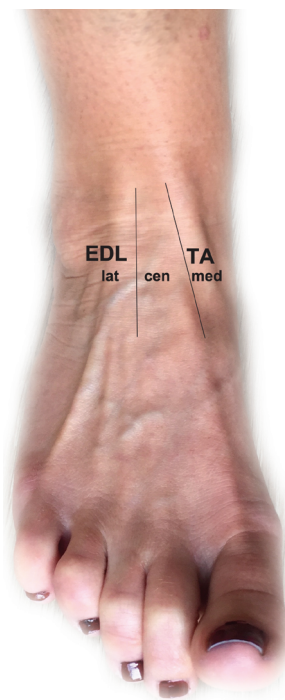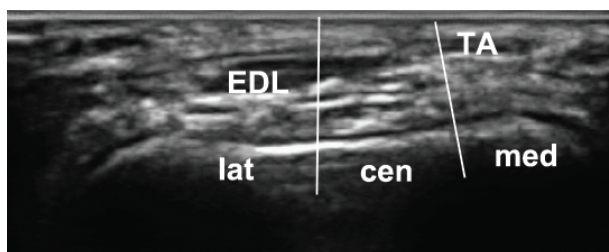

Figure 9A.3. three zones used to identify the location of the defects on ultrasound.

Top: using a coronal ultrasound overview to determine in which third of the talus the defect is located. *Right:* using ankle tendons as landmarks. The medial zone defined by the anterior deltoid ligament medially and the lateral border of the tibialis anterior. The central zone by the lateral border of the tibialis anterior and the medial border of the extensor digitorum longus tendon. The lateral zone by the lateral border of the extensor digitorum longus tendon and the anterior talofibular ligament. *TA: tiabialis anterior; EDL: extensor digitorum longus; lat: lateral zone; cen: central zone; med: medial zone.*
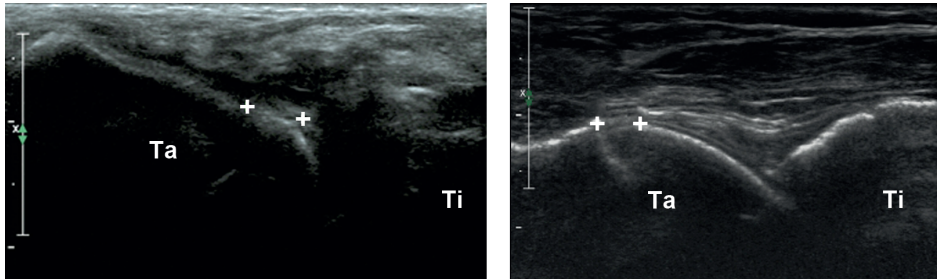
Figure 9A.4. Different aspects of a chondral defect, *left*, and an osteochondral defect, *right*. Disruptions within the defect are visible within the marked area.

Nature of the lesion

The defect should be categorized into an osteochondral or solely chondral lesion based on characteristics previously described [2] (*Fig 9A.4*). Irregularities in the hypoechoic, generally homogenous, cartilage layer suggest a chondral defect (*Fig. 9A.4, left*), while concurrent disruption of the hyperechoic bone-cartilage interface is a sign of an osteochondral defect (*Fig. 9A.4, right*).

Size

Coronal and sagittal measurements can be taken and recorded together with the location and lesion characteristics. Based on previous research both chondral and osteochondral defects as small as 3 mm should be detectable reliably [1, 3, 4].

Postoperative imaging of cartilage repair tissue

Future research will have to determine the feasibility for ultrasound imaging of postoperative cartilage repair tissue, before a guideline for such imaging can be composed.

References

1. Disler DG, Raymond E, May DA, Wayne JS, McCauley TR. Articular Cartilage Defects: In Vitro Evaluation of Accuracy and Interobserver Reliability for Detection and Grading with US1. *Radiology*. 2000;215:846–851.

2. Kok AC, Terra MP, Muller S, Askeland C, van Dijk CN, Kerkhoffs GMMJ, Tuijthof GJM. Feasibility of ultrasound imaging of osteochondral defects inthe ankle: A clinical pilot study. *Ultrasound Med. Biol.* 2014;40:2530–2536.

3. Mathiesen O, Konradsen L, Torp-Pedersen S, Jorgensen U, Jørgensen U. Ultrasonography and articular cartilage defects in the knee: an in vitro evaluation of the accuracy of cartilage thickness and defect size assessment. *Knee Surg Sport. Traumatol Arthrosc*. 2004;12:440–443.

4. Tuijthof GJM, Kok AC, Terra MP, Aaftink JFA, Streekstra GJ, van Dijk CN, Kerkhoffs GMMJ. Sensitivity and specificity of ultrasound in detecting (osteo)chondral defects: A cadaveric study. *Ultrasound Med. Biol.* 2013;39:1368–1375.

ENGLISH AND DUTCH SUMMARY
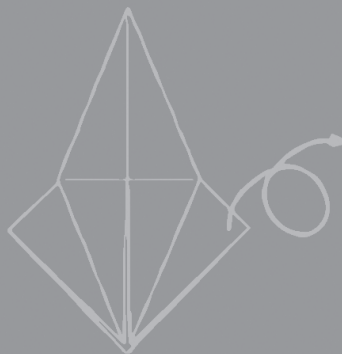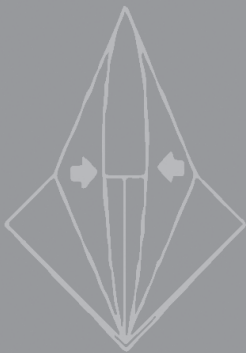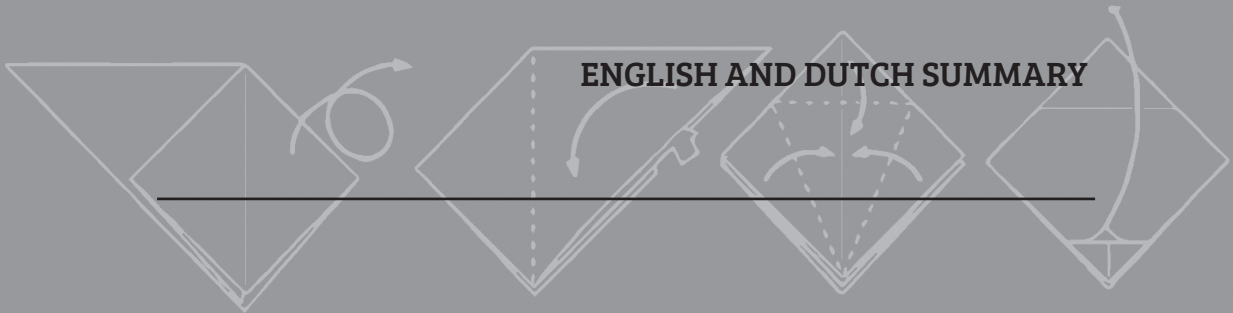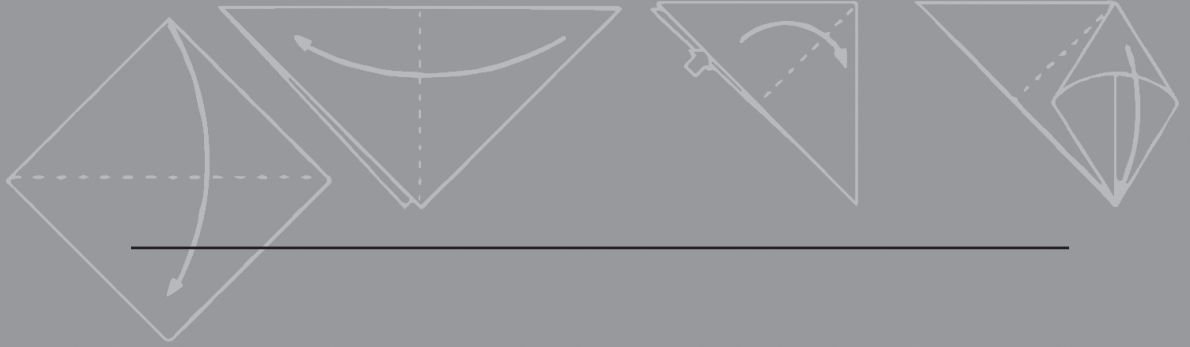
English summary

Background

An osteochondral defect of the talus (OCDT) is a lesion of the cartilage and the underlying subchondral bone of a joint causing deep ankle pain, swelling, ankle instability and locking. In due time these OCDT can progress to ankle joint osteo-arthritis with prolonged symptoms of pain and loss of joint function. The complex structure of hyaline cartilage has limited self-healing capacities and complicated healing mechanisms. Extensive knowledge of the cartilage repair process is essential to understand why treatments might be successful and to enable their further development. This thesis addresses a number of challenges in imaging, staging and treatment techniques that contribute significantly to our understanding of cartilage repair and the optimization of diagnostics and treatment of OCDT in the ankle.

Part I: Optimizing pre-clinical imaging

In-depth understanding of the cartilage healing process starts with pre-clinical research. We need reproducible morphologic, quantitative and qualitative data that is comparable over time to understand the effect of treatment techniques on cartilage repair. However, there is no true consensus on the preferred assessment modalities yet yet.

Chapter 2: Macroscopic cartilage repair tissue assessment using the ICRS compared to histological assessment for talar osteochondral defects treated with microfracture.

Currently, it is unclear whether macroscopic scoring during arthroscopy can achieve reliable assessment of cartilage repair tissue. We used 32 samples from an OCDT goat model to evaluate whether assessment of repair cartilage quality using macroscopic scoring (ICRS score) was comparable to the golden standard: histological scoring (O'Driscoll score). The average scores were similar, but the interobserver correlation for the ICRS score was poor and the correlation of the average total ICRS score and the O'Driscoll score was not significant. This lack of correlation might be related to the samples not displaying the entire range of possible histological outcome, but also due to the fact that the ICRS is a semi-quantitative score that only uses superficial morphological data. Possibly the accuracy can be improved by more elaborate or automated assessment.

Chapter 3: Comparison of optical coherence tomography and histopathology in quantitative assessment of goat talus articular cartilage

We explored the use of Optical Coherence Tomography (OCT) as an alternative to histology and arthroscopic assessment in a similar model as presented in *Chapter 2*. A representative histological slice was compared to the corresponding OCT image.

The ICC for histology and OCT matches on cartilage thickness were near-perfect for healthy cartilage, but less for repair tissue area and surface roughness. Differences were attributable to wrinkling of the histological slices, inaccuracy of the assumed refractive index and difficulty to achieve accurate matching of the exact location of histology and OCT slices. Possible future improvements include better co-localisation of OCT and histological slices using 3D histology and using 3D arthroscopic OCT *in vivo*.

Part II: Optimizing clinical imaging

For OCDT imaging in clinical practice both MRI and CT show good to excellent sensitivity and specificity. However, these modalities have disadvantages for use in more extensive follow-up of cartilage repair mechanisms in patients. Studies in osteoarthritis and rheumatology research have shown that ultrasound enables imaging of bone erosion and pathological changes in cartilage, making it a possible alternative for longitudinal follow-up of patients with an anterior or centrally located OCDT.

Chapter 4: Sensitivity and specificity of ultrasound in detecting (osteo)chondral defects: a cadaveric study. We first determined the accuracy of ultrasound for detection of OCDT in a cadaveric study using ten fresh formerly frozen human cadaver ankles with arthroscopically created osteochondral and chondral defects. Ultrasound exams by two blinded observers were compared to CT and photographs. Overall sensitivity was 96% for observer 1 and 92% for observer 2, with chondral defects being more difficult to detect. The specificity for both observers was 100%. Defect measurements were accurate, with 68% and 79% of the defect sizes within relevant limits of agreement (20.2 ± 1.0 mm).

Chapter 5: feasibility of ultrasound imaging of osteochondral defects in the ankle: a clinical pilot study. Eight patients with a CT confirmed anterior or central OCDT were imaged by an experienced musculoskeletal radiologist. Nine additional patients who did not have an OCDT in the anterior talar dome served as negative controls. Five OCDT were detected with ultrasound. Six negative control patients were also

diagnosed by ultrasound as negative. Two of the false-positive ultrasound diagnoses were described as chondral lesions, which we were unable to objectify with the CT scans. Similar to CT, ultrasound revealed typical morphologic OCDT features, such as cortex irregularities, cartilage disruptions, displaced fragments (Loomer grade IV) and cysts with a fibrous roof (Loomer grade V). Ultrasound could also be a useful future tool in the pre-operative planning to determine whether a lesion can be treated using anterior arthroscopy without the need of an additional plantar CT scan. Future research will consider ultrasound for post-operative follow up, using 3D tracked imaging enabling read-back and one-on-one location retrieval between different exams.

Another future application involves more invasive ultrasound imaging of acoustic properties of cartilage and using cartilage stiffness and relaxation times to detect microscopic changes and *in vivo* biomechanical testing.

Part III: Optimizing treatment
Studies on the effect of the actual execution of treatment techniques are scarce. In part III of this thesis we critically examine the technique of two widely used, less invasive treatments to understand whether changes in the technique performance could optimize results.

Chapter 6: The optimal injection technique for the osteoarthritic ankle: A randomized, cross-over trial. This randomized cross-over patient study investigates the accuracy of two methods for intra-articular injection in 72 patients: with or without using the traction device that is commonly used for ankle arthroscopy. Both methods were used on each patient one month apart. The success rate was 76% for both techniques. Following the infiltration with traction, 41 patients (58%) experienced mainly moderate adverse events versus 39 patients (55%) without traction. No significant difference was found in the number of attempts to place the needle into the joint, experienced pain or patient preference for either technique. Considering the high failure rate, which is in correspondence with previous literature, it is advisable to use of imaging (traditional contrast-aided fluoroscopy or ultrasound) during injection using either technique, especially with severe osteoarthritis, anterior osteophytes or less experienced surgeons.

Chapter 7: Is technique performance a prognostic factor in bone marrow stimulation of the talus? This literature review includes six articles (198 patients) that present a technique description in their method section to discover whether differences

in technique performance are recorded and whether these influence outcome. The majority of included articles were retrospective case series with limited statistical analysis and a relatively small number of patients. Key elements were similar and in concordance with the original technique by Steadman et al: removal of unstable cartilage, hole depth variation between 2 and 4 mm until bleeding or fat droplets occurred, and a distance between the created holes of 3 to 4 mm.

Chapter 8: No effect of hole geometry in microfracture for talar osteochondral defects. Since there is little technique variation for microfracture in literature, we tested two hypotheses in an animal study: (1) holes that reach deeper into the bone marrow-filled trabecular bone allow for more hyaline-like repair; and (2) a larger number of holes with a smaller diameter result in more solid integration of the repair tissue, less need for new bone formation and higher fill of the defect. In eight goats an osteochondral defect was created in the talus and treated by drilling six 0.45 mm diameter holes in the defect 2 mm deep; in eight more goats, six 0.45 mm diameter holes were punctured to a depth of 4 mm. All contralateral defects were treated with three 1.1 mm diameter holes 3 mm deep, mimicking the clinical situation, as internal controls. Analysis after 24 weeks showed a statistically significant median difference between the treatment and control legs per goat per group in histological quality (modified O'Driscoll score). However, we found no clinically significant relationship between repair tissue quality and the depth or the size of microfracture holes compared to the controls. Safranin-O intensity on digital imaging and repair tissue volume on EPIC micro CT scans were also similar. We did witness a large variation in quality of repair tissue and defect fill within groups and goats, despite adequate sample size and standardized protocols. A possible improvement to the current rigid microfracture tools that create unstandardized and therefore variable distribution of holes could be using flexible arthroscopic water jet cutting creating several holes at once in a standardized pattern.

Conclusion

Based on the results of these studies presented in this thesis we conclude the following:

- There is need for a guideline outlining which imaging techniques and validated imaging scoring systems can be used in diagnostic assessment of OCDT and repair tissue after treatment. Such a scheme is already available for the knee in the form of the ICRS cartilage evaluation package. This could serve as an example for a similar package for the ankle.

- Advanced techniques that have proven useful in other fields can be considered for imaging OCDT repair to increase our understanding of the cartilage repair process. Optical Coherence Tomography for example can assess cartilage thickness and surface morphology without biopsy with good correlation with histology.
- Ultrasound imaging is feasible as a cheaper, less invasive alternative for extensive follow up for anterior and central OCDT. Future research will concentrate on its usefulness in clinical imaging of repair tissue and on quantitative ultrasonic assessment of cartilage quality.
- Intra-articular infiltration in the ankle benefits from imaging using either conventional fluoroscopy or ultrasound by decreasing the amount of unintended extra-articular injections.
- Detailed descriptions of the microfracture technique are often lacking from literature. There is a need for larger high-quality studies with explicit description of patient groups and technique, sound methodology and uniform scoring and outcome measures. Future studies should not only include precise information on their methods, but also data on possible prognostic factors (such as lesion size, patient related factors and postoperative regimen), use a sound methodology and uniform grading systems, and provide standardized outcome measurements.
- Changes in microfracture depth or diameter do not affect repair tissue quality in OCDT in the goat. Using water jet cutting could provide a more standardized treatment, but the "hydrochipper" is yet to be developed further into a clinically usable device.
- It is imperative to design a patient specific treatment algorithm. In our opinion OCDT treatment should not be differentiated for affected tissue, but by affected structural component and size. Also, the primary or secondary nature should be established and treated as a different entity. This can also guide future research and treatment with careful consideration of size, structural nature of a defect, previous treatment and patient characteristics. The challenge lies in defining if and where simple additives suffice, and where extensive reconstructive treatment is necessary.

Nederlandse samenvatting

Achtergrond en doel

Een osteochondraal defect van de talus (OCDT) is een letsel van kraakbeen en het onderliggende subchondrale bot. Het veroorzaakt diepe enkelpijn, zwelling, enkelinstabiliteit en slotklachten. Uiteindelijk kunnen deze OCDT zich ontwikkelen tot artrose met chronische symptomen van pijn en verlies van de gewrichtsfunctie. De complexe structuur van het hyalien kraakbeen maakt dat het een beperkte zelfhelende capaciteit heeft met complexe herstelmechanismen. Uitgebreide kennis van het kraakbeen herstelproces is essentieel om te begrijpen waarom behandelingen succesvol zouden kunnen zijn en hun verdere ontwikkeling mogelijk te maken. Dit proefschrift richt zich op een aantal uitdagingen in de beeldvorming, stadiering en behandeltechnieken die een belangrijke bijdrage leveren aan ons begrip van het herstel van kraakbeen en de optimalisatie van de diagnostiek en behandeling van OCDT in de enkel.

Deel I: Optimalisatie van preklinische beeldvorming

Diepgaande kennis van het genezingsproces van kraakbeen begint met preklinisch onderzoek. We moeten reproduceerbare morfologische, kwantitatieve en kwalitatieve gegevens verzamelen, die vergelijkbaar zijn over de tijd om het effect van de behandeltechnieken op het herstel van kraakbeen te begrijpen. Echter, er is nog geen echte consensus over de gouden standaard ten aanzien van de te gebruiken methoden.

Hoofdstuk 2: Macroscopische evaluatie van herstelweefsel middels de ICRS score vergeleken met histologische analyse bij osteochondraal defecten in de enkel behandeld met microfracture. Op dit moment is het onduidelijk of evaluatie op basis van macroscopische beoordeling vergelijkbaar kan zijn met histologie. We gebruikten 32 tali van een OCDT geitmodel om te evalueren of een macroscopische score (ICRS score) vergelijkbaar is met de gouden standaard: histologische scoring (O'Driscoll score). De gemiddelde macroscopische scores waren vergelijkbaar, maar de interobserver correlatie voor de ICRS score was slecht (50% met een κ van 0,4, p <0,001) en de correlatie tussen de gemiddelde totale ICRS score en de O'Driscoll score was niet significant. Dit gebrek aan correlatie kan verband houden met het feit dat de defecten niet het gehele bereik van het mogelijk histologisch resultaat tonen, maar ook doordat de ICRS een semi-kwantitatieve score is die alleen oppervlakkige morfologische gegevens gebruikt. Mogelijk kan de nauwkeurigheid worden verbeterd door een uitgebreidere of geautomatiseerde beoordeling.

Hoofdstuk 3: Vergelijking van optische coherentie tomografie en histologie voor kwantitatieve beoordeling van gewrichtskraakbeen in de geiten talus. In dit hoofdstuk maakten we gebruik van Optische Coherentie Tomografie (OCT) als alternatief voor histologie en arthroscopische beoordeling in een model vergelijkbaar met *Hoofdstuk 2*. Een histologische coupe werd vergeleken met een OCT beeld van dezelfde locatie. De ICC voor histologie en OCT voor kraakbeendikte waren bijna perfect voor gezond kraakbeen, maar minder bij herstelweefsel oppervlakte en oppervlakte gladheid. De gemeten verschillen zijn mede te wijten aan rimpels in de histologische coupes, de deels onbekende brekingsindex en een toch complexe bepaling van de exact gelijke locatie van de histologische en OCT coupes. Optimale co-lokalisatie met behulp van 3D histologie zou deze resultaten in de toekomst kunnen verbeteren, eventueel in combinatie met 3D arthroscopische OCT *in vivo*.

Deel II: Verbeteren van klinische beeldvorming

Voor de klinische praktijk hebben MRI en CT scans een goede tot uitstekende sensitiviteit en specificiteit. Echter, deze modaliteiten hebben een aantal nadelen indien ze overwogen worden voor meer uitgebreide follow-up in het kader van studie naar kraakbeen herstelmechanismen bij patiënten. Diverse studies naar artrose binnen de reumatologie hebben aangetoond dat echografie boterosie en pathologische veranderingen in kraakbeen kan laten zien. Dit proefschrift onderzoekt of echografie een mogelijk niet-invasief, dynamisch en financieel gunstig alternatief kan zijn binnen het longitudinaal follow-up onderzoek van patiënten met een anterieur of centraal gelegen OCDT.

Hoofdstuk 4: sensitiviteit en specificiteit van echografie bij het detecteren van (osteo-) chondraal defecten: een kadaver onderzoek. In tien *fresh frozen* menselijke kadaver enkels werden arthroscopisch osteochondraal en chondrale defecten gemaakt. Twee geblindeerde onderzoekers maakten echografische beelden, die werden vergeleken met CT scans en digitale foto's. De sensitiviteit bedroeg 96% voor onderzoeker 1 en 92% voor onderzoeker 2. De specificiteit bedroeg bij beiden 100%. Chondraal defecten waren moeilijker te detecteren. Grootte berekeningen waren accuraat: 68% en 79% van het defectafmetingen waren binnen de relevante grenzen van overeenkomst (20,2 ± 1,0 mm).

Hoofdstuk 5: haalbaarheid van echografische beeldvorming van osteochondraal defecten in de enkel: een klinische pilotstudie. Op basis van CT scans werden acht patiënten geïncludeerd met een anterieure of centrale OCDT, welke potentieel zichtbaar zou kunnen zijn op echografie. Negen extra patiënten zonder OCDT

dienen als negatieve controles. Een ervaren radioloog beoordeelde de aanwezigheid of afwezigheid van een OCDT op basis van 2D echografie beelden, welke werden vergeleken met het beeld op CT. Vijf van de acht eventueel detecteerbare defecten werden gedetecteerd met echografie. Zes van negen negatieve controlepatiënten werden door middel van echografie als negatief gediagnosticeerd. Twee van de valspositieve diagnoses werden beschreven als chondrale laesies, welke niet te objectiveren waren met de CT-scans. Echografie toonde typische morfologische kenmerken vergelijkbaar met CT, bijvoorbeeld cortex onregelmatigheden en losse fragmenten. Kraakbeen verstoringen, evenals Loomer graad IV (losliggend fragment) en graad V (cyste met een fibreuze bedekking), waren ook zichtbaar. Ook zou echografie een handig hulpmiddel kunnen zijn in de preoperatieve planning om te bepalen of een letsel kan worden behandeld met behulp van anterieure artroscopie zonder de noodzaak van een extra plantair flexie CT-scan. Toekomstig onderzoek zal moeten bepalen in welke mate veranderingen in kraakbeen herstelweefsel zichtbaar is met echografie, voordat we dit overwegen voor postoperatieve follow-up. Het gebruik van 3D-tracked imaging kan hierbij een belangrijke bijdrage leveren door read back opties en een-op-een locatieherkenning tussen onderzoeken op verschillende tijdstippen. Een andere toekomstige toepassing omvat echografisch akoestisch onderzoek naar kraakbeenstijfheid en relaxatietijden, waardoor *in vivo* biomechanische eigenschappen kunnen worden bestudeerd.

Deel III: Optimalisatie van de behandeling

Onderzoek naar de daadwerkelijke uitvoering van behandeltechnieken is schaars. In deel III van dit proefschrift kijken we kritisch naar de techniek van twee belangrijke behandelingen om te begrijpen of veranderingen in de techniek de resultaten kunnen verbeteren.

Hoofdstuk 6: optimale injectietechniek voor de enkel met artrose: een gerandomiseerd cross-over onderzoek. In dit hoofdstuk wordt een patiëntenonderzoek gepresenteerd met 72 patiënten om de nauwkeurigheid van twee infiltratiemethoden te vergelijken: met of zonder behulp van een tractie instrument dat gewoonlijk wordt gebruikt voor enkelartroscopie. Iedere patiënt werd met beide methoden behandeld met een maand tussenpose. De positie van de injectie werd gecontroleerd onder röntgendoorlichting. Het succespercentage was 76% voor beide technieken. Er was geen significant verschil tussen beide technieken in een hoeveelheid repositiepogingen van de naald, ervaren pijn of techniekvoorkeur. De aanzienlijke hoeveelheid extra-articulaire injecties, welke overeenkomt met eerdere literatuur, rechtvaardigt standaard controle van de naaldpositie met beeldvorming, conventionele röntgen

of echografie, in het bijzonder bij ernstige artrose, anterieure osteofyten of minder ervaren chirurgen.

Hoofdstuk 7: Is techniekuitvoering een voorspellende factor voor microfracture van de talus? Hoofdstuk 7 is een literatuurstudie van zes artikelen (198 patiënten) die een techniekomschrijving van microfracture in hun methodesectie hadden opgenomen om te constateren of er verschillen zijn en of deze invloed hebben op de uitkomst. De meerderheid waren retrospectieve case series met een beperkte statistische analyse en een relatief klein aantal patiënten. De techniekbeschrijving was vaak vergelijkbaar met de techniek zoals beschreven in het oorspronkelijke artikel door Steadman et al.: debridement van instabiel kraakbeen, microfracture diepte tussen de 2 en 4 mm tot zich puntbloedingen of vetdruppeltjes voordeden, en een afstand tussen de gecreëerde gaten van 3-4 mm. De resultaten zijn vergelijkbaar met vorige algemene reviews. Derhalve lijkt variatie in techniek, zoals deze momenteel in de literatuur wordt beschreven, niet van invloed op de uitkomst van microfracture voor OCDT.

Hoofdstuk 8: Geen effect van variatie in geometrie van microfacture bij de behandeling van osteochondraal defecten in de geiten talus. Deze studie onderzoekt twee mogelijke aanpassingen van de microfracturetechniek in een geitenmodel: (1) gaten die dieper in het trabeculaire bot reiken produceren meer hyalien kraakbeen herstelweefsel; en (2) een groter aantal gaten met een kleinere diameter leidt tot stevigere integratie van weefselherstel, minder nieuwe botvorming en hogere vulling van het defect. Hiervoor werden bilateraal osteochondraal defecten gemaakt bij 16 geiten. In acht geiten werd één defect behandeld met microfracture met zes gaten van 0,45 mm diameter van 2 mm diep; in de overige acht geiten werden zes 0,45 mm diameter gaten gemaakt tot een diepte van 4 mm. Alle contralaterale defecten werden behandeld met drie 1,1 mm diameter gaten 3 mm diep, om de huidige klinische situatie na te bootsen als interne controles. Analyse na 24 weken toonde geen klinisch significante relatie tussen herstelweefselkwaliteit en de diepte of diameter van microfracture gaten bij histologie (O'Driscoll histologische score), Safranine-O-intensiteit of herstelweefselvolume op de EPIC micro CT scans. Wel zagen wel grote variatie in de kwaliteit van reparatieweefsel en opvulling binnen de groepen en ook binnen de geiten, ondanks voldoende sample size en gestandaardiseerde protocollen.

Een mogelijke verbetering ligt in het huidige rigide microfracture instrumentarium, dat een niet gestandaardiseerde en dus variabele verdeling van de gaten creëert. Een toekomstige optie is het gebruik maken van flexibel arthroscopisch waterstraal

snijden, waardoor meerdere gaten tegelijkertijd in een gestandaardiseerd patroon worden gevormd.

Conclusie

Op basis van de resultaten van de studies in dit proefschrift hebben we het volgende kunnen concluderen:

- Momenteel is er geen richtlijn voor beeldvorming van kraakbeen herstelweefsel en scoringssystemen. Een gevalideerde leidraad voor beeldvorming en gevalideerde scoringssystemen voor de diagnostiek en de postoperatieve fase is daarom nodig.
- Geavanceerde technieken die op andere gebieden nuttig zijn gebleken moeten overwogen worden in het kader van onderzoek om ons begrip van het kraakbeen herstelproces van OCDT in de enkel te vergroten. Optical Coherence Tomografie bijvoorbeeld kan kraakbeendikte en oppervlaktemorfologie beoordelen zonder biopsie met een goede correlatie met histologie.
- Echografische beeldvorming is een goedkoop, minder invasief alternatief voor intensieve follow-up van anterieure en centrale OCDT. Toekomstig onderzoek zal zich concentreren op het nut hiervan in de klinische beeldvorming van weefselherstel en kwantitatieve echografie van kraakbeenkwaliteit.
- Intra-articulaire infiltratie in de enkel is gebaat bij beeldvorming door middel van conventionele röntgendoorlichting of echografie om het aantal onbedoeld extra-articulaire injecties te verkleinen.
- Gedetailleerde beschrijvingen van de microfracture techniek ontbreken vaak in de literatuur. Toekomstige studies ten aanzien van de behandeltechnieken dienen niet alleen nauwkeurige informatie over hun techniek en methoden te bevatten, maar ook gegevens te verschaffen over mogelijke prognostische factoren, gebruik te maken van een degelijke methodologie en uniforme scoringssystemen en gestandaardiseerde uitkomstmaten.
- Veranderingen in microfracture diepte of diameter hebben geen invloed op de kwaliteit van het kraakbeen herstelweefsel van OCDT in de geit. Het gebruik van waterstraalsnijden kan bijdragen aan een gestandaardiseerde behandeling, maar de "hydrochipper" moet nog worden verder ontwikkeld worden tot een klinisch apparaat.
- De behandeling van OCDT dient te gebeuren met een zorgvuldige afweging van de grootte en het structurele karakter van een defect, eerder ondergane behandelingen en kenmerken van de patiënt.
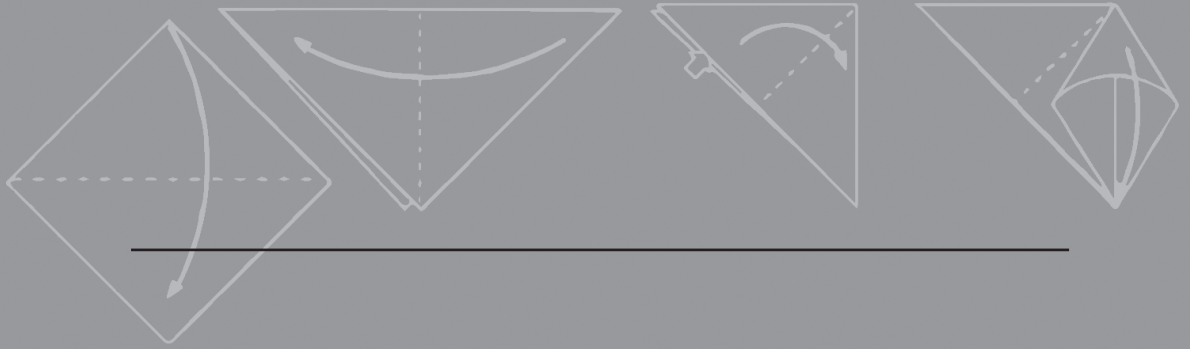
ADDENDUM

DANKWOORD
CURRICULUM VITAE AND PHD PORTFOLIO
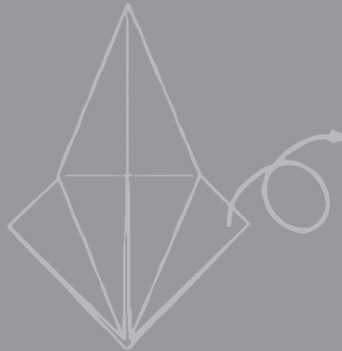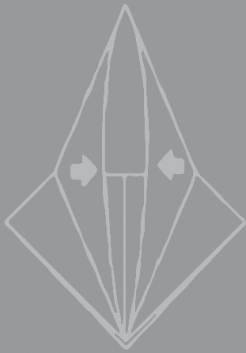
DANKWOORD

Gabrielle, jij breekt ijzer met handen. Wat een respect heb ik voor jouw doorzettingsvermogen en kritische blik. Soms met harde hand, maar altijd met een visie. Je bent eigenhandig verantwoordelijk voor één van mijn grootste wapenfeiten van deze periode: aandacht voor details, waardoor ik dat (figuurlijke) keukenschort steeds minder nodig heb. Ik hoop in de toekomst iets terug te geven voor al je onmisbare input in de afgelopen periode.

Gino, ik ben je dankbaar voor je aanstekelijke enthousiasme vanaf dat eerste gesprek op de poli, waar ik kwam vragen of ik onderzoek mocht komen doen. Stiekem zijn we toch al een hoop jaren en life events verder, maar ik kom nog steeds iedere keer *supercharged* uit zo'n gesprek met jou. Dank voor je geduld, je interesse en je voorbeeld. Allora, forza!

Beste Prof. van Dijk, beste Niek, ook u ken ik al zo lang als dat ik de orthopedie ken. Dank voor de mogelijkheid om bij de ORCA twee jaar onderzoek te doen. Het is de begin geweest van een prachtige tijd en mijn keuze voor de orthopedie. Hoe kan het ook anders. Dank voor de waardevolle aanwijzingen voor mijn wetenschappelijke carriere en de coulance voor het schrille contrast in onze motorische vaardigheden op de squashbaan.

Lieve mede cubicle en G4-genoten met wie ik het gebrek aan daglicht mocht delen over de jaren heen: altijd adrem binnen en buiten de wetenschap met een onnavolgbaar uithoudingsvermogen voor het sociale programma. Ondanks al mijn gereis tussen de VU, ACTA, het Erasmus, TU Delft en de kelder van de Fysiologie was het fijn om aan te kunnen schuiven bij de gezellige basis daar. Leendert, dank voor je inhoudelijk advies. Lieve Inger, wat waren die statistiek sessies op je kamer goed en ontzettend gezellig. Ik ben jaloers op iedereen die nu ergens anders bij je binnen mag lopen. Stagestudenten, Juri, Johan, Daniel, dank voor jullie tijd en hulp.

TU Delft! Nooit durven dromen dat ik nog zoveel met fietsenmakers zou mogen optrekken na mijn switch van Bouwkunde naar de Geneeskunst. Ik ken nergens anders zoveel mensen die ogenschijnlijk onoverkomelijke tegenslagen simpelweg herdefiniëren tot een hobbeltje in de weg. Steven, je rustige positiviteit is een feestje om mee samen te werken. Ik hoop dat je snel weer vol kan genieten van alles en een killer van een verdediging neer kan zetten. Nazli, my savior for everything with a motherboard: you rock. I am so going to miss you and your superpowers... Marjon, Bente, Reinier, dank voor al jullie hulp.

Dank aan alle mensen vanuit andere specialismen met wie ik het genoegen heb gehad om onderzoek mee te doen, zowel binnen als buiten het AMC. Maaike, wat waren we blij om jou aan boord te hebben. Mario, Geert, Iwan dank voor alle know how. Klaas, Paul, en Ger, het is niet heel 3R van me, maar ik zou graag langer onderzoek met jullie hebben gedaan. Wellicht ooit nog een 3^e ronde? Dames en heren van de ACTA, menig zonsop- en ondergang heb ik versleten in jullie prachtige lab uitkijkend over Amsterdam. Dank dat jullie deze orthopedie dame van die andere universiteit tijdelijk hebben geadopteerd.

My supervisors at SINTEF, Toril, Christian and Sebastien, and all the other boys and girls there, Marta, Palli, Sinara, Inger: my time in Norway was one of the best foreign experiences I've had. Everything about you was just so relaxed and positive. Tusend takk og jeg savner deg!

Pap. De dag dat jij je met het ochtendgloren bij het dieren OK complex gemeld hebt om een dagje met je dochter mee te opereren, was echt een van de leukste dagen van mijn onderzoekstijd. Ik ben jullie zo dankbaar dat ik altijd mag komen aanwaaien met wie dan ook, wanneer dan ook, voor hoe lang dan ook. En mam, je bent mijn voorbeeld voor hoe je als vrouw onvoorwaardelijk lief, begaan én sterk kunt zijn.

Last but not least, Roy. Je houdt deze dame met je eerlijke en soms ongezouten mening met beide benen op de grond. Oprecht begaan, maar je laat me vrij in mijn keuzes. En dat kan niet altijd makkelijk zijn geweest. Dit boekje is ook zeker een deel jouw bloed, zweet en tranen: dank voor het om 01u00 's nachts ophalen na een dag kadavervoeten echoën, OK foto's maken, tirades over publicatie frustraties aanhoren en eindeloos kaftontwerpen reviewen. Mijn liefste, ik kijk zo uit naar al die mooie grote (en kleine) avonturen in onze toekomst. Ik houd van je om duizend redenen.

CURRICULUM VITAE AND PHD PORTFOLIO
Personal Information
Name   **Aimée-Claire Kok-Pigge**

Education
08/2010	**M.D.**
09/2003 – 08/2010	**Master of Science Medicine**
	University of Amsterdam
	Additional Courses: Medical ethics, public health and peace,
	European integration, conflict dynamics
04/2008 - 05/2008	**French language and medical French course**
	Alliance Française, Paris, France
09/2002 – 07/2003	**Bachelor architecture** (not completed)
	Technical University Delft
09/2001 – 12/2001	**Italian language and European art history**
	Scuola Leonardo da Vinci, Firenze, Italy
09/1995 – 07/2001	**Secondary school**
	Gemeentelijk Gymnasium, Hilversum

Experience
09/2017 – present	**Resident (AIOS) Orthopaedic Surgery**
	Amphia ziekenhuis, Breda
01/2017 – 08/2017	**Resident (AIOS) Orthopaedic Surgery**
	Academical Medical Centre (AMC), Amsterdam
07/2015 – 12/2016	**Resident (AIOS) Orthopaedic Surgery**
	Tergooi ziekenhuizen, Hilversum
04/2014 – 06/2015	**Resident (AIOS) Orthopaedic Surgery**
	Academical Medical Centre (AMC), Amsterdam
09/2012 – 03/2014	**Resident (AIOS) Orthopaedic Surgery** at the Department of
	General Surgery, Rode Kruis Ziekenhuis, Beverwijk
09/2010 – 08/2012	**PhD fellow** at the Department of Orthopaedic Surgery
	Academical Medical Centre (AMC), Amsterdam

Memberships
2016 – present	**AOSpine** member
2015 – present	**De Jonge Specialist (Dutch medical resident organisation)**
	Platform Future & Innovation: taskforce health care finance,
	annual congress organization.
2015 – present	**Dutch Society for Arthroscopy (NVA)** member

2014 – present	**Dutch Association for Orthopaedic Residents (VOCA)** member
2010 – present	**Dutch Orthopaedic Association (NOV)** Taskforce Renewal of the health care evaluation agenda (2017)
2005 – 2007	**International Federation of Medical Student Associations (IFMSA)** Coordinator of clinical clerkships for foreign students

Scientific experience

2016	**AIOS Upgrade (annual national resident congress)**, Zwolle Course organisation
02/2012 – 04/2012	**SINTEF Science and Technology,** Trondheim, Norway Three-month research scholarship to explore the feasibility of ultrasound for the imaging of osteochondral defects
2010, 2011	**Amsterdam Foot and Ankle Course,** AMC Amsterdam Course organisation
2010, 2011	**Knee Arthroplasty Course,** AMC Amsterdam Course organisation
2009, 2010	**Injection accuracy with the use of a traction device in hyaluronic acid injections in the ankle** Department of Orthopaedic Surgery, AMC Amsterdam with A.G.H. Witteveen, M.D. PhD
2006	**Towards an ultrasounds atlas of the mouse for follow up of pathological processes** Department of Cell Biology and Histology, AMC Amsterdam with C.J.F. van Noorden, M.D. PhD
2006	**IFMSA symposium on Child abuse,** AMC Amsterdam Course organisation
2005	**Evaluation of screening of asymptomatic patients with hypertrophic cardiomyopathy** Department of Clinical Genetics, AMC Amsterdam with I. Cristiaans M.D. PhD

Courses and diplomas

2017	**Medical Business Masterclass,** MB, Amsterdam
	Value Based Health Care, Value in Care, Amsterdam
2016	**AOSpine Principles Course—Spinal Trauma,** Amsterdam
	Affordability and quality of health care, Elevate, online course
	Shoulder arthroscopy course, NVA, Utrecht
	Young orthopaedic surgeons' shoulder course, Rotterdam
2015	**Knee arthroscopy course,** NVA, Utrecht
	International knee arthroscopy course, München, Germany
2014	**TIAS summer academy: an update in healthcare management**
	TIAS Medical Business School, Tilburg
	Radiation hygiene for medical specialists, level 4A
	Boerhaave Institute, Leiden
2013	**AO Principles of fracture management course,** Leeds, U.K.
2012	**Advanced Trauma Life Support, ALSG** (renewed 2016)
	Emergency Management of Severe Burns, Hilversum
	Muscoluskeletal Ultrasound Imaging Course
	Nationaal Trainingscentrum Echografie, Weesp
2007	**Advanced Medical Assistance Course** including AED use
	AMC Amsterdam (renewed 2014)

PhD training: courses

2011	**Practical biostatistics course,** AMC Amsterdam
	Basic course legislation and organization for clinical researchers, AMC Amsterdam (renewed 05/2015)
	Laboratory course for animals (animal research permit, art. 9)
	St. Radboud University, Nijmegen
2010	**Systematic reviews course,** AMC Amsterdam
	Developing a cochrane systematic review, AMC Amsterdam
	AMC world of science, AMC Amsterdam

Podium presentations

10/2017	**Spuiten of slikken – advances in cartilage repair treatments** Amphia Ziekenhuis, Breda
08/2014	**Pitch Imaging osteochondral defects using ultrasound** Design of medical devices Conference - Europe, TU Delft
04/2014	**Current concepts of bone marrow simulation: current evidence and future prospects** (invited lecture) Ankle Foot Associates (AFAS-ESSKA) International Congress, Prague, Czech Republic
09/2013	**No effect of hole geometry in microfracture for talar osteochondral defects** Society for Arthroscopy and Joint Surgery (AGA) congress, Wiesbaden, Germany
02/2013	**No effect of hole geometry in microfracture for talar osteochondral defects** Dutch Orthopaedic Association (NOV) congress, Amsterdam
10/2012	**Sensitivity and specificity of ultrasound in detecting (osteo) chondral defects: a cadaveric study** European Orthopaedic Research Society (EORS) congress, Amsterdam
05/2011	**Depth-related differences in mesenchymal stem cell concentration** Master class Prof. Dr. R. Jaenisch on innovative stem cell research
11/2011	**Lecture on animal studies in cartilage repair research** Minor Arthroscopy, Biomechanical Engineering, TU Delft

Parameters of esteem: scholarschips

2011	**Anna Fonds travel grant,** Anna Fonds/NOREF **Yggdrasil young guest and doctoral researchers' annual scholarships**, Research Counsel Norway
2010	**Personal research scholarship,** Rene Marti Keunig-Eckhart Foundation

Publications

2017 Backes Y., Hellemons M., Kienhorst L., <u>Kok A.C.</u>, de Laat P. **Arbeidsvoor-waarden: waar heb ik recht op (on resident agreements)** *De Jonge Specialist Magazine 2017 3:8*

2016 <u>Kok A.C.</u>, Kienhorst L., Hellemons M., de Laat P., Backes Y. **Wat kost een AIOS (on the costs of resident training)** *De Jonge Specialist Magazine 2016 3:22*

2015 Natenstedt J., <u>Kok A.C.</u>, Dankelman J., Tuijthof G.J.M. **What quantitative mechanical loading stimulates in vitro cultivation best?** *J Experimental Orthopaedics 2015 2:15*

   <u>Kok A.C.</u>, van Bergen C.J.A., Tuijthof G.J.M., Klinkenbijl M.N., van Noorden C.J.F., Kerkhoffs G.M.M.J. **Macroscopic ICRS poorly correlates with O'Driscoll histological cartilage repair assessment in a goat model.** *Clin Res Foot Ankle 2015 3:173.*

   Cernohorsky P., <u>Kok A.C.</u>, Bruin D.M., Brandt M.J., Faber D.J., Tuijthof G.J.M., Kerkhoffs G.M.M.J. Strackee S.D., van Leeuwen T.G. **Comparison of optical coherence tomography and histopathology in quantitative assessment of goat talus articular cartilage.** *Acta Orthop. 2015 Apr;86(2):257-63.*

2014 <u>Kok A.C.</u>, Terra M.P., Muller S., Askeland A., van Dijk C.N., Kerkhoffs G.M.M.J., Tuijthof G.J.M., **Clinical note: feasibility of ultrasound imaging of osteochondral defects in the ankle, a clinical pilot study.** *Ultrasound Med Biol. 2014 Oct;40(10):2530-6.*

2013 Witteveen A., <u>Kok A.C.</u>, Sierevelt I.N., Kerkhoffs G.M.M.J., van Dijk C.N. **The optimal injection technique for the osteoarthritic ankle: A randomized, cross-over trial.** *Foot Ankle Surg. 2013 Dec;19(4):283-288.*

   <u>Kok A.C.</u>, Tuijthof G.J.M., den Dunnen S., van Tiel J., Siebelt M., Everts V., van Dijk C.N., Kerkhoffs G.M.M.J., **No effect of hole geometry in microfracture for talar osteochondral defects.** *Clin Orthop Relat Res 2013 Aug; 471(8).*

   Tuijthof G.J., <u>Kok A.C.</u>, Terra M.P., Aaftink J.F., Streekstra G.J., van Dijk C.N., Kerkhoffs G.M.M.J. **Sensitivity and specificity of ultrasound in detecting (osteo)chondral defects: a cadaveric study**. *Ultrasound Med Biol. 2013 Aug;39(8):1368-75.*

2012 <u>Kok A.C.</u>, den Dunnen S., Tuijthof G.J.M., van Dijk C.N., Kerkhoffs G.M.M.J. **Is technique performance a prognostic factor in bone marrow stimulation of the talus?** *J Foot Ankle Surg. 2012 Nov;51(6):777-82.*

   Wiegerinck J.I., <u>Kok A.C.</u>, van Dijk C.N. **Surgical Treatment of Chronic Retrocalcaneal Bursitis: A Systematic Review.** *Arthroscopy*, 2012 Feb;28(2):283-93.

Miscellaneous
Foreign languages
English, Dutch and German: fluent
French and Italian: conversant

Interests
Orthopaedic surgery (Upper Extremity, Spine, Oncology).
Medical business management (e.g. taskforces on same day admission, EMR intro-
duction, various courses).
Conflict dynamics, European integration, cultural differences.

Leisure activities
Sports: endurance sports (triathlon), motorcycling, hiking.
Travel and cooking.
Volunteer and neighbourhood coordinator for Burennetwerk Amsterdam.